Energy Island Baltic Sea

Metocean Assessment

Part A: Description and Verification of Data Basis

Report
IO Number 4500092960

2024-02-07

Prepared for Energinet Eltransmission A/S

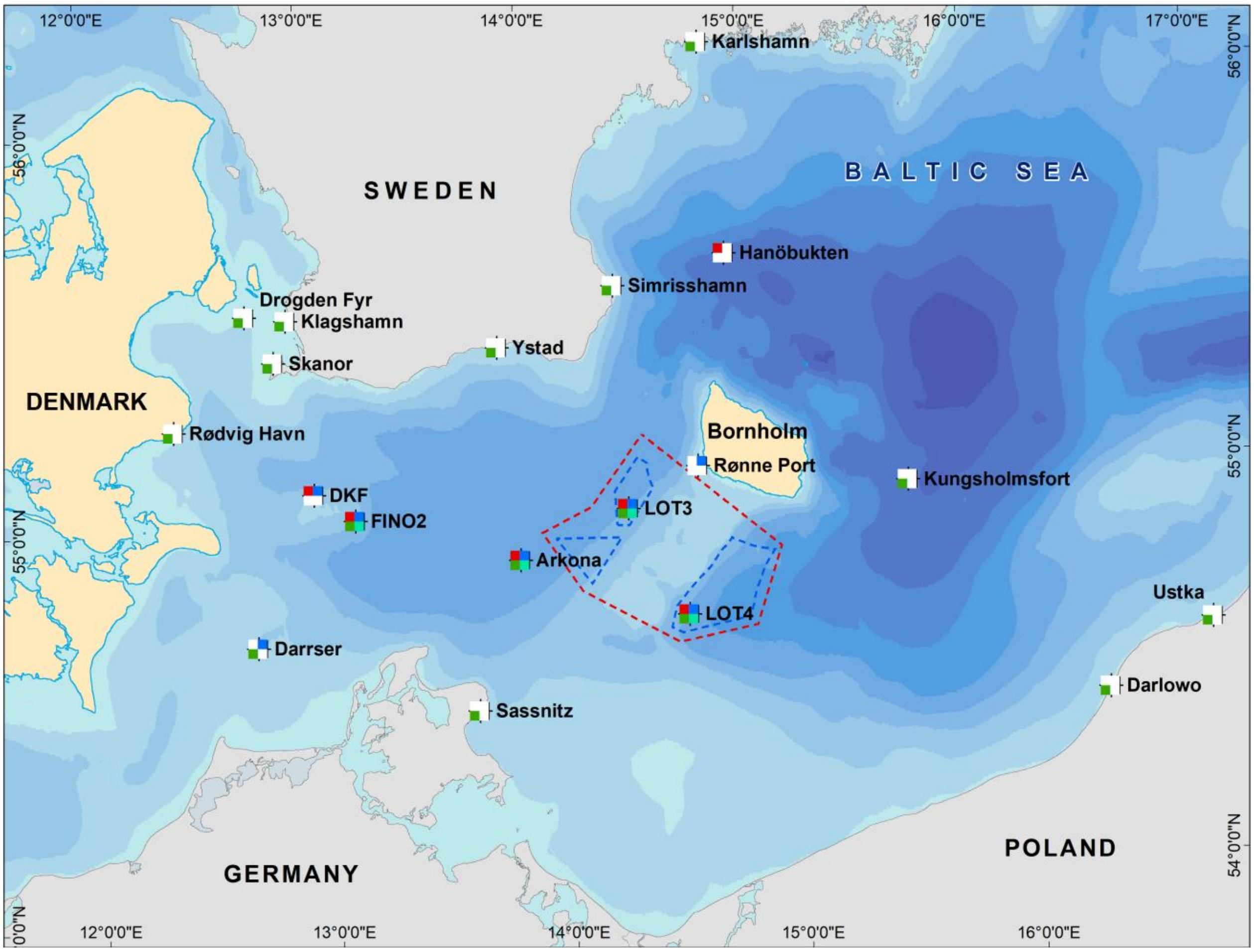

Energy Island Baltic Sea

Metocean Assessment
Part A: Description and Verification of Data Basis

Report
IO Number 4500092960

Prepared for:	Energinet Eltransmission A/S
Represented by	Mr Kim Parsberg Jakobsen

Front page: Stations with measurements used on the verification of the models. Same legend as Figure 0.1

Contact person:	Morten Rugbjerg, mnr@dhigroup.com, +45 45 16 94 18
Project Manager:	Morten Rugbjerg
Quality Supervisor:	Jacob Berg Jørgensen
Author:	Arief Rullyanto and Ole Svenstrup Petersen
Project No.:	11829021
Approved by:	Jacob Berg Jørgensen
Approval date:	2024-02-07
Revision:	Final 1.2 (incorporating comments to final 1.1 report from client)
Classification:	Confidential
File name:	11829021_DHI_EIBS_Metocean_PartA_Description_and_verification_of_data_basis

DHI A/S • Agern Allé 5 • • DK-2970 Hørsholm • Denmark
Telephone: +45 4516 9200 • dhi@dhigroup.com • www.dhigroup.com • Company Reg. No.: 36466871

Contents

Figures

Tables

Appendices

Nomenclature

Variable	Abbreviation	Unit
Atmosphere		
Wind speed @ 10 m height	WS_{10}	m/s
Wind direction @ 10 m height	WD_{10}	°N (clockwise from)
Air pressure @ mean sea level	P_{MSL}	hPa
Air temperature @ 2 m height	$T_{air,2m}$	°C
Relative humidity @ 2 m height	RH_{2m}	-
Downward solar radiation flux	DSWR	W/m^2
Ocean		
Water level	WL	mMSL
Current speed	CS	m/s
Current direction	CD	°N (clockwise to)
Water temperature	T_{sea}	°C
Water salinity	Salinity	PSU
Waves		
Significant wave height	H_{m0}	m
Peak wave period	T_p	s
Mean wave period	T_{01}	s
Zero-crossing wave period	T_{02}	s
Peak wave direction	PWD	°N (clockwise from)
Mean wave direction	MWD	°N (clockwise from)
Direction standard deviation	DSD	°

Definitions	
Coordinate System	WGS84 EPSG 4326 (unless specified differently)
Direction	Clockwise from North Wind: °N coming from Current: °N going to Waves: °N coming from
Time	Times are relative to UTC
Vertical Datum	MSL (unless specified differently)

Abbreviations	
2D	2-dimensional
3D	3-dimensional
ADCP	Acoustic Doppler Current Profiler
AFDW	Ash-Free Dry Weight
AME	Average Mean Error
AO	Arctic Oscillation
BSH	Bundesamt für Seeschifffahrt und Hydrographie
CC	Correlation Coefficient
CEM	Coastal Engineering Manual, Meteorology and Wave Climate
CFSR	Climate Forecast System Reanalysis
CMEMS	Copernicus Marine Environment Monitoring Service
DA	Data Assimilation
DEA	Danish Energy Agency
DKBS	Danish Waters and Baltic Sea
DKF	Danish Krieger's Flak
DNV	Det Norske Veritas
DNVGL	Det Norske Veritas Germanischer Lloyd
ECMWF	European Centre for Medium-Range Weather Forecasts
EIBS	Energy Island Baltic Sea
EMODnet	The European Marine Observation and Data Network
EnKF	Ensemble Kalman Filter
ERA5	ECMWF Re-analysis v5
EV	Explained Variance
FINO2	Forschungsplattformen in Nord- und Ostsee No 2
FEED	Front-End Engineering Design
GHRC	Global Hydrology Resource Center
GWM	Global Wave Model
HD	Hydrodynamic
HRFC	High Resolution Full Climatology
IEC	International Electrotechnical Commission
IOW	Leibniz Institute for Baltic Sea Research
ISO	International Organization for Standardization
LiDAR	Light Detection and Ranging
LIS	Lightning Imaging Sensor

Abbreviations	
HRFC	High Resolution Full Climatology
IPCC	Intergovernmental Panel on Climate Change
LRFC	Low Resolution Full Climatology
mMSL	Metres above Mean Sea Level
MOOD	MetoOcean-On-Demand
MSL	Mean Sea Level
NAO	North Atlantic Oscillation
NASA	National Aeronautics and Space Administration
NCEP	National Center for Environmental Prediction
NORA3	3 km Norwegian reanalysis
OI	Optimal Interpolation
OTD	Optical Transient Detector
OWF	Offshore Wind Farm
PR	Peak Ratio
PSU	Practical Salinity Unit
QQ	Quantile-Quantile
RMSE	Root Mean Square Error
SCAND	Scandinavian pattern
SLP	Sea Level Pressure
SLR	Sea Level Rise
SI	Scatter Index
SW	Spectral Wave
UTC	Coordinated Universal Time
WAM	WAve Model
WGS84	World Geodetic System 1984
WMO	World Meteorological Organisation

Revision

Version	Date	Revision log
Draft 0.1	23 August 2023	Draft version for client review
Final 1.0	17 November 2023	Final version incorporating comment to draft report from client
Final 1.1	20 December 2023	Final version incorporating comment to final 1.0 report from client
Final 1.2	7 February 2024	Final version incorporating comment to final 1.1 report from client

Executive Summary

Energinet Eltransmission A/S (Energinet) commissioned DHI A/S (DHI) to carry out a metocean site conditions assessment that shall serve as a basis for Front-End Engineering and Design (FEED) of two offshore wind farms named Energy Island Baltic Sea (EIBS) to be located to the southwest of Bornholm in the Baltic Sea. This report presents the metocean study made by DHI.

The results of the metocean study consist of three reports: a metocean data basis report (Part A), a metocean data analysis report (Part B), and a hindcast revalidation note. Additionally, a metocean hindcast database is provided.

The present Part A report covers the description and the verification of the data basis established by hindcast modelling (including models and comparisons of these with measurements), which will be applied in the metocean data analysis (Part B). All measurement locations together with the location of EIBS are shown in Figure 0.1.

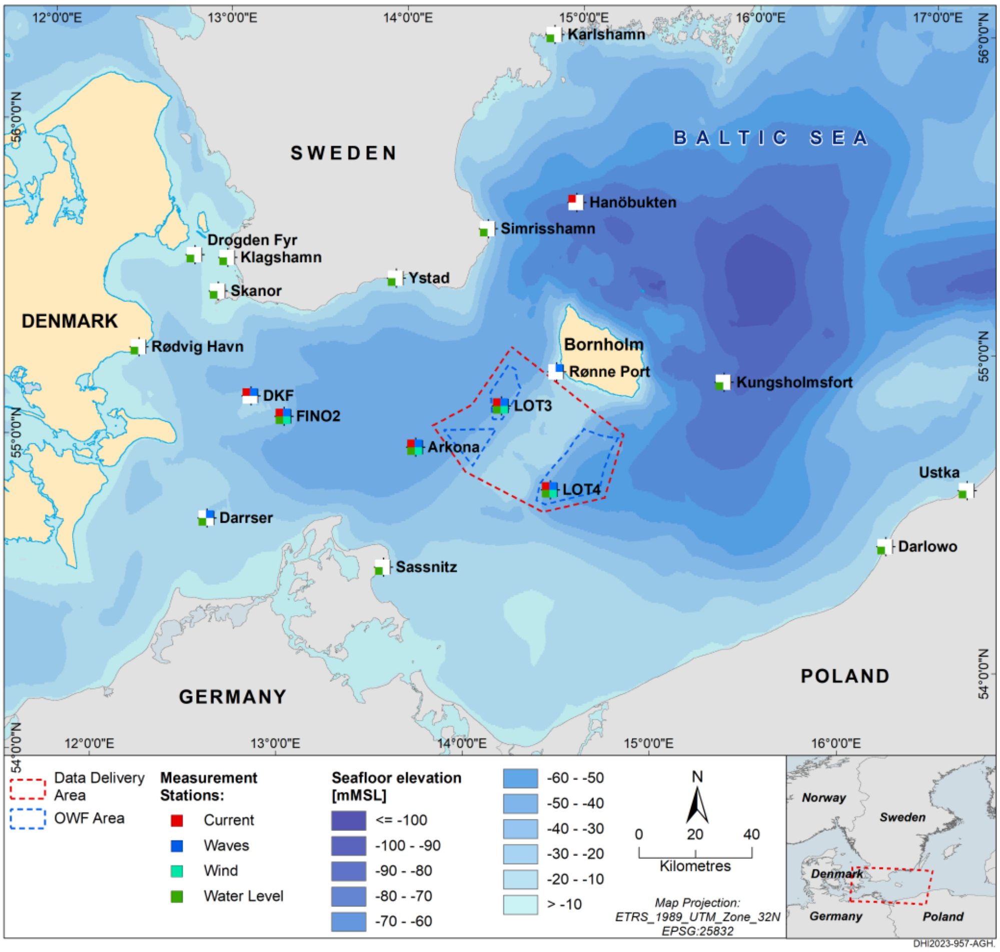

Figure 0.1 **Location of the Energy Island Baltic Sea, the related offshore wind farm development area, and the measurement stations considered.**

All model data were prepared for the 44-year period 1979-2022 except for the 3D hydrodynamic model data, which was prepared for the 25-year period 1998-2022.

Bathymetric data basis

Bathymetric data from three sources were used: local survey data from Energinet, data from the Geodatastyrelsen, and EMODnet data for areas where the two previous sources were not available.

Wind data basis

Wind data from the Norwegian reanalysis (NORA3) meteorological model dataset were used, both for the wind analyses and for the forcing of the wave hindcast model. For the hydrodynamic model, a combination of the CFSR global atmospheric dataset (1997-2010) and StormGeo North European downscaled winds (2010 – present) was used, as this is consistent with the forcing used for DHI's 3D hydrodynamic model DKBS from which boundary conditions have been obtained.

NORA3 is a high-resolution 3 km atmospheric dynamic downscaling of the state-of-the-art reanalysis data, called ERA5, from European Centre for Medium-Range Weather Forecasts (ECMWF). The NORA3 dataset was validated against measurements from the local EIBS SeaWatch Wind LiDAR Buoys (LOT3 and LOT4) and against FINO2 and Arkona stations, showing a very good agreement between model and measurements.

CFSR is the global atmospheric reanalysis wind dataset from NOAA, which has been applied in numerous metocean studies in the Baltic area. The StormGeo is a 0.1 degree downscaled dataset produced by StormGeo which has been used by DHI from 2010 onwards to force our Baltic current models. The StormGeo is a downscaled dataset based on ECMWF.

Water level data basis

Hindcast water level data was extracted from the DHI North Europe regional model ($HD_{NE\text{-}ERA5}$) covering northeast Europe. These data were established by numerical modelling using DHI’s MIKE 21 Flow Model FM and validated against regional measurements. Additionally, comparisons were made at Tejn and Rønne harbours, both on the island of Bornholm, showing a good agreement between model and measurements.

Current data basis

A dedicated 3D hydrodynamic model, HD_{EIBS}; with a high-resolution mesh in the OWF area (see Figure 0.1) was set up and calibrated using measurements from the OWF area and from several other stations in the Baltic Sea.

The vertical resolution in the 3D model is 1 m (max) in sigma-layers down to -20 m water depth and 2 m in the z-layers below. At the boundaries, the model was forced by data from DHI’s DKBS 3D model, and the same meteorological forcing as used for the DKBS model was applied for consistency.

Wave data basis

A dedicated spectral wave model (SW_{EIBS}) with a high-resolution mesh in the OWF area was set up and calibrated to establish a validated and long-term wave data basis at the EIBS site applicable for the assessment of normal and extreme wave conditions.

The calibration of the wave model focussed on the measurements from the OWFs but included also several other measurements from the Baltic Sea.

Basis for other atmospheric parameters

In addition to wind and surface pressure data, time series data of air temperature and humidity were extracted from the NORA3 dataset, while the solar radiation was extracted from the CFSR dataset. Finally, lightning data was obtained from the LIS/OTD Gridded Climatology dataset from NASA [1].

Basis for other oceanographic parameters

In addition to current data, sea temperature, salinity and water density data were extracted from HD_{EIBS}.

Furthermore, a marine growth assessment has been included.

Climate change and sea level rise assessment

An assessment of the sea level rise at the EIBS OWFs and of other possible climate change impacts has been undertaken and is presented.

Metocean hindcast database

A metocean hindcast database was developed for EIBS consisting of three sets of data:

- Model data at the 6 analysis points (within the EIBS OWFs), which are analysed in Part B of the present study [2].
- Model data from the wave model and from the 2D and 3D HD models covering the red polygon in Figure 0.1.
- All measurements applied in the model calibration and validation in the present report.

The provided atmospheric, wave and ocean variables are listed in Table 0.1. All data were provided to Energinet in MIKE dfs file formats. The dfs files can be read using either the Python MikeIO[1] or the DHI-MATLAB-Toolbox[2] open-source libraries available at GitHub.

---

[1] https://github.com/DHI/mikeio
[2] https://github.com/DHI/DHI-MATLAB-Toolbox

Table 0.1 Summary of the provided EIBS metocean database
Atmosphere and wave data are provided for the period 1979-2022 (44 years) and ocean data for the period 1998-2022 (25 years). All data provided with a time step of 1 hour.

Category	Variable	Abbrev.	Unit
Atmosphere			
Dataset: NORA3 Rep. avg. period: 1 hour	Pressure @ mean sea level#	P_{MSL}	hPa
	Wind speed @ 10 m height#	WS10	m/s
	Wind direction @ 10 m height#	WD10	°N (coming
	Air temperature @ 2 m height#	$T_{air,2m}$	°C
	Relative humidity @ 2 m height#	RH	-
Ocean (HD 3D)	**Surface, mid-depth, near-bed**		
Dataset: HD_{EIBS}	Current speed	CS	m/s
	Current direction	CD	°N (clockwise
	Salinity	Sal	PSU
	Seawater temperature	T_{sea}	°C
Ocean (HD 2D)			
Dataset: $HD_{NE-ERA5}$	Water level	WL	mMSL
Waves (SW)	**Total, wind-sea, and swell**		
Dataset: SW_{EIBS} Rep. avg. period: 2 hours	Significant wave height	H_{m0}	m
	Maximum wave height*#	H_{max}	m
	Maximum wave crest height*#	C_{max}	m
	Peak wave period	T_p	s
	Energy wave period#	T_{-10}	s
	Zero-crossing wave period	T_{02}	s
	Peak wave direction	PWD	°N (clockwise)
	Mean wave direction	MWD	°N (clockwise)
	Direction standard deviation	DSD	°

*: Not split into total, wind-sea and swell
#: Only provided for the 6 analysis points (see Part B report)

1 Introduction

This study provides detailed metocean conditions to use in the Front-End Engineering and Design (FEED) for the two offshore wind farms (OWFs) named Energy Island Baltic Sea located in the area to the southwest of the Danish Island of Bornholm in the Baltic Sea. The study consists of three reports: a metocean data basis (Part A) which is the present report, a metocean data analysis (Part B) [2], and a hindcast revalidation note [3]. Additionally, a metocean hindcast database is provided.

Energinet Eltransmission A/S (Energinet) was instructed by the Danish Energy Agency (DEA) to initiate site investigations, including a metocean conditions assessment, for offshore wind farms in an area to the southwest of Bornholm in the Baltic Sea (see Figure 0.1). Based on this, Energinet commissioned DHI A/S (DHI) to provide a detailed metocean site condition assessment study for use in FEED as described in “CONSULTANCY CONTRACT REGARDING SITE METOCEAN CONDITIONS ASSESSMENT FOR OFFSHORE WIND FARMS – BALTIC SEA” signed 7 March 2023.

The study consists of several deliverables:

- Part A: Description and Verification of Data Basis (this report)
- Part B: Data Analyses and Results [2]
- Summary presentation (PowerPoint)
- Long-term hindcast data (digital time series)
- Measurement data (digital time series)
- Hindcast revalidation note [3]

In the present Part A report, the metocean data basis is described, and the data verified in the following sections:

- Bathymetry (Section 2)
- Wind (Section 0)
- Water Level (Section 4)
- Currents, Temperature and Salinity (Section 5)
- Waves (Section 6)
- Other Atmospheric Conditions (Section 6.4)
- Other Oceanographic Conditions (Section 8)
- Climate Change (Section 0)

The study refers to the following common practices and guidelines:

- DNV-RP-C205 [4]
- IEC 61400-3-1 [5]

2 Bathymetry

This section describes the general bathymetry, or seabed levels, in the Baltic Sea and the EIBS site followed by an evaluation of the relevant bathymetric data sources, their alignment and vertical datum, leading to a consistent and accurate bathymetric dataset applicable for the hydrodynamic and wave hindcast modelling activities of this project.

2.1 General seabed levels

The Baltic Sea area is a glacial formation with depths ranging from very shallow areas down to about 440 m in Gotland Deep. The entrance to the Baltic Sea is through the Danish Straits, connecting to the Baltic Sea to Kattegat Sea and the North Sea (Atlantic Ocean). Around the project site at Bornholm, the bathymetry is dominated by the Rønne Bank, which separates the Arkona Basin to the west and the Bornholm Basin and the Pomeranian Bay to the East. The two channels to the North and South of Bornholm constitute the main entrance to the Baltic Proper.

2.2 Bathymetric data sources

The model domain has been selected to provide the optimal location for model boundaries for the 3D HD model (see Section 5) and the wave model (see Section 6). Boundary data are, in general, extracted from DHI's Baltic Sea 3D model archive, DKBS. These bathymetry data are a merging of (in prioritised sequence) locally surveyed data, the Danish Geodatastyrelsen's 50 m gridded survey[3] and data from EMODnet[5]. See Table 2.1 and Figure 2.1.

Table 2.1 Bathymetry datasets used for the Energy Island Baltic Sea models.

Dataset	Spatial resolution	Source	Datum[4]
Local survey	5 m	Energinet	DTU21
Danmarks Dybdemodel	50 m	Geodatastyrelsen	LAT/DVR90
EMODnet	100 m	Various[5]	MSL

[3] Danmarks Dybdemodel, 50 m opløsning (gst.dk)
[4] The difference between vertical datums in the Baltic is less than 0.1 m., so we have not made any adjustment of depth
[5] EMODnet Map Viewer (europa.eu)

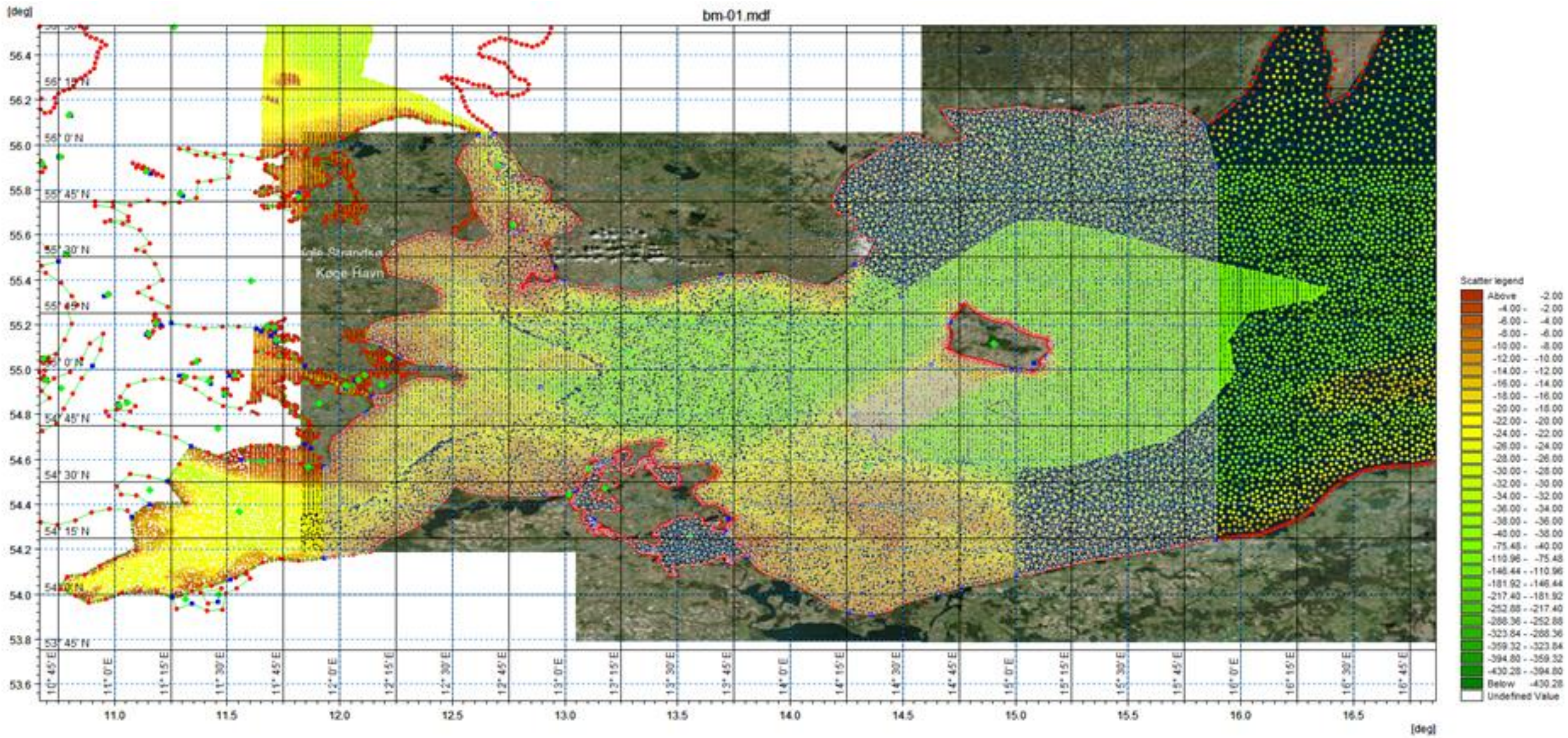

Figure 2.1 Bathymetry data used for the Energy Island Baltic Sea model mesh.

3 Wind

Atmospheric data used as forcing of the spectral wave (SW) model and for extreme value analysis was adopted from the 3 km Norwegian reanalysis dataset (NORA3).

NORA3 is a high-resolution atmospheric dynamic downscaling of the state-of-the-art reanalysis data from European Centre for Medium-Range Weather Forecasts (ECMWF), called ERA5. The NORA3 dataset is described and validated against measurements from the local EIBS SeaWatch Wind LiDAR Buoys (LOT3 and LOT4) and the FINO2 and Arkona.

Atmospheric forcing applied for the 2D HD and 3D HD models are described in Sections 4 and 5 respectively.

3.1 General wind characteristics

The wind climatic conditions in the Baltic Sea region are heavily influenced by key atmospheric teleconnection patterns of the Northern Hemisphere and European-Atlantic sectors, with a particular focus on the North Atlantic Oscillation (NAO), Arctic Oscillation (AO), and Scandinavian pattern (SCAND).

Notably, the NAO plays a central role around the southern part of the Baltic Sea. The NAO index is calculated based on the sea level pressure (SLP) difference between Lisbon, Portugal, and Stykkisholmur, Iceland. During the positive phase of the NAO, winter brings stronger than usual westerly winds sweeping across northern Europe. Conversely, the negative phase leads to weaker westerly winds, making way for the occurrence of easterly winds in the region.

In general, the wind speed in the study area experiences a relatively calm period from April to August, while November to February is considered the windy period.

3.2 Wind measurements

Wind measurement data used for local validation of the NORA3 data (see Section 3.3.1) are listed in Table 3.1 and their location is illustrated in Figure 3.1. Local measurements (LOT3 and LOT4) were available at several elevations from 4 mMSL (anemometer) and from 30 - 270 mMSL at total 11 heights (LiDAR) during 2021-11-21 to 2022-11-21 (12 months) [6].

Table 3.1 Details of wind measurement stations
Measurements applied in this study.

Station Name	Longitude [°E]	Latitude [°N]	Measurement Height [mMSL]	Data coverage	Instrument type	Model	Owner / Surveyor
LOT3	14.3556	54.9948	4 (anemometer) 30, 40, 60, 90, 100, 120, 150, 180, 200, 240, 270 (Lidar)	2021-11-21 – 2022-11-21	Anemometer and Lidar Buoy	Gill Windsonic M ZephIR ZX300	Energinet / FUGRO
LOT4	14.5882	54.7170	4 (anemometer) 30, 40, 60, 90, 100, 120, 150, 180, 200, 240, 270 (Lidar)	2021-11-21 – 2022-11-21	Anemometer and Lidar Buoy	Gill Windsonic M ZephIR ZX300	Energinet / FUGRO
FINO 2	13.1541	55.0070	32	2011-05-05 – 2020-09-12	Anemometer	-	BSH
Arkona	13.8667	54.8833	10	2002-02-28 – 2017-12-31	-	-	BSH

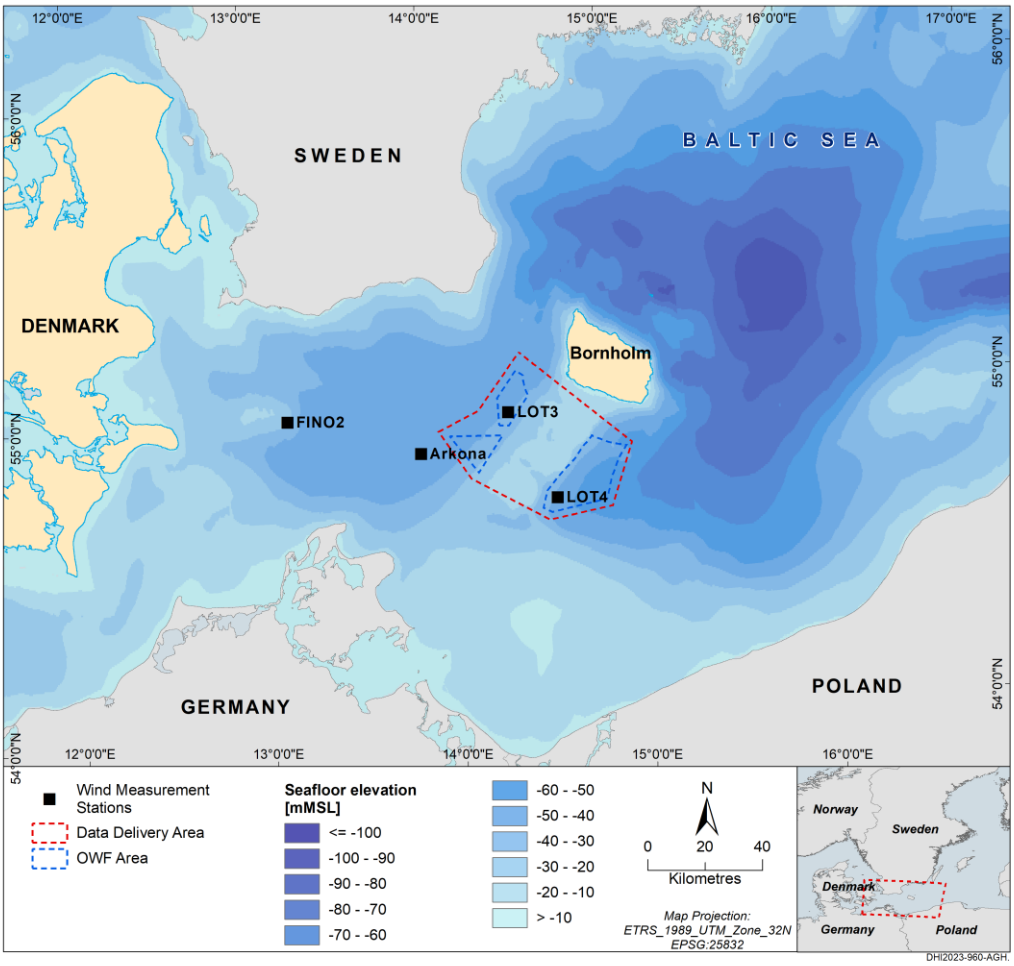

Figure 3.1 Location of wind measurements
Measurements applied in this study.

The wind measurements at the EIBS site, measured by the SeaWatch Wind Lidar Buoys [6] (i.e., LOT3 and LOT4), were quality controlled by the data surveyor (i.e., FUGRO) and checked by DHI before use. A similar process was done for the Arkona and FINO2 datasets, recorded by BSH (Bundesamt für Seeschifffahrt und Hydrographie, Germany).

3.2.1 Wind profile (height conversion)

Wind speed at various heights above sea may be required for design purposes and for comparison of hindcast model data against measurements.

This section describes common wind profiles and compares them to the local measurements to arrive at a recommended profile and height conversion factors for normal and extreme wind speeds.

The literature provides several guidelines for describing the vertical wind speed profile. The most common are the Frøya, power and log profiles.

Frøya profile

Assuming neutrally stable atmospheric conditions, the vertical and temporal distribution of wind speed during storm conditions can be described by the Frøya profile. The Frøya profile is described as follows, in [4] and [7]:

$$U(\mathrm{T,z}) = U_0\left(1 + \mathrm{C}\ \ln\frac{z}{H}\right).\left[1 - 0.41 \cdot I_U(z) \cdot \ln\left({}^{T}/_{T_0}\right)\right] \quad \textbf{(3.1)}$$

- $U(\mathrm{T,z})$ is the mean wind speed [m/s] with averaging period T<T_0 = 3600 s at height z [mMSL]
- U_0 the 1-hour mean wind speed [m/s] at the reference elevation H = 10 m above sea level
- C a dimensionally dependent coefficient equal to $0.0573 \cdot (1 + 0.148U_0)^{1/2}$ for H = 10 m
- I_U a dimensionally dependent value for the turbulence intensity of wind speed, given by

$$I_U = 0.06 \cdot (1 + 0.043 \cdot U_0) \cdot \left({}^{z}/_{H}\right)^{-0.22}$$

- T_0 is the reference time averaging interval of 3600 s

Log profile

The wind profile of the atmospheric boundary layer (surface to around 100m in neutral conditions) is generally logarithmic in nature and is often approximated using the log wind profile equation that accounts for surface roughness and atmospheric stability. However, for neutral conditions, the atmospheric stability term drops out and the profile simplifies to:

$$U_z = U_r \cdot log(z/z_0)/log(r/z_0) \quad \textbf{(3.2)}$$

where, U_z is the wind speed at height z, U_r is the wind speed at height r, and z_0 is the surface roughness length (in meters) (0.0001 for open sea without waves, and 0.0001 – 0.01 for open sea with waves [4], or using the wind speed dependent Charnock relation in [5]).

Power profile

The power law relationship is often used as a substitute for the log wind profile when surface roughness (and/or stability information) is not available. The power profile is defined as:

$$U_z = U_r \cdot (z/r)^{\alpha} \qquad \textbf{(3.3)}$$

where, U_z is the wind speed at height z, U_r is the wind speed at height r, and α is the power law exponent (typically 0.11 for extremes [8] and 0.14 in normal conditions [5]).

Recommended wind profile

The vertical shear naturally fluctuates significantly over time due to the varying state and stability of the atmosphere, and thus, the shear at individual profiles sometimes deviates substantially from the mean shear.

Figure 3.2 shows comparisons of the theoretical wind profiles and the wind measurements up to a height of 120 m at LOT3 and LOT4 for all wind speeds (top) (using α = 0.08) and for $WS_{10,10\text{-}min}$ > 20 m/s (bottom) (using α = 0.10). The Frøya profile gives higher ratios (between U_z and U_r)) for very extreme wind speeds, which may be because the Frøya profile was developed and validated for wind conditions off the Norwegian coast.

The distribution of the shear coefficient (α) is presented in Figure 3.3. Estimations of α were made for each time step by applying a power law between two heights. For all wind speeds (from a height of 4 to 30 m), the mean α is 0.082. For $WS_{10,10\text{-}min}$ > 15 m/s (from a height of 30 to 100 m), the mean α is 0.103.

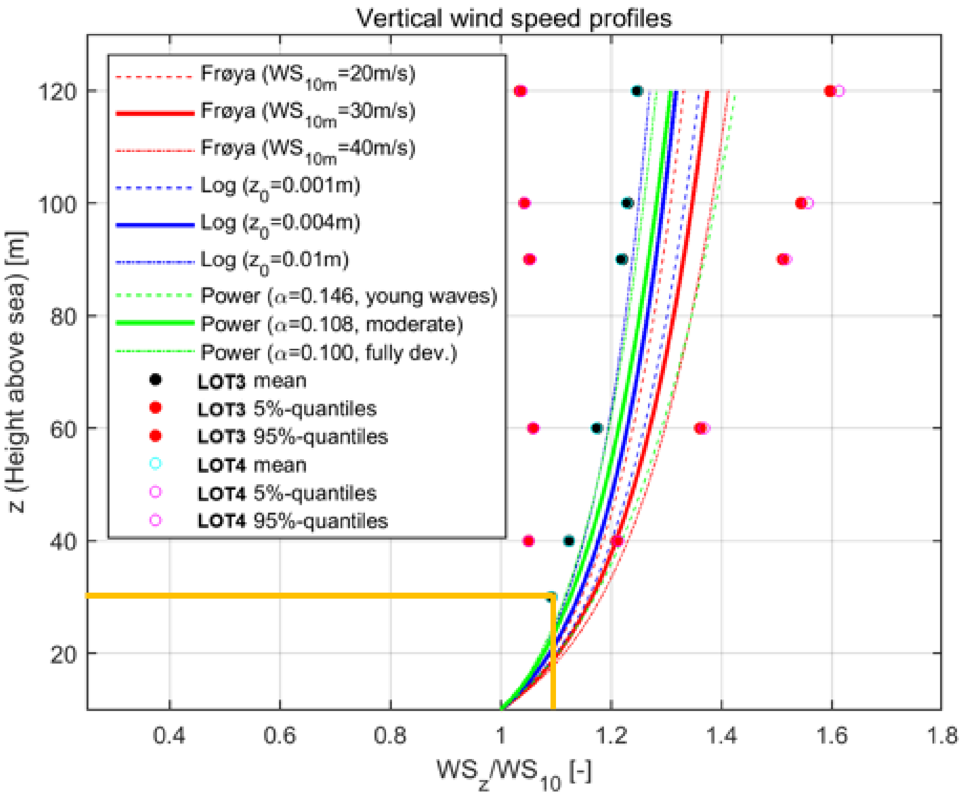

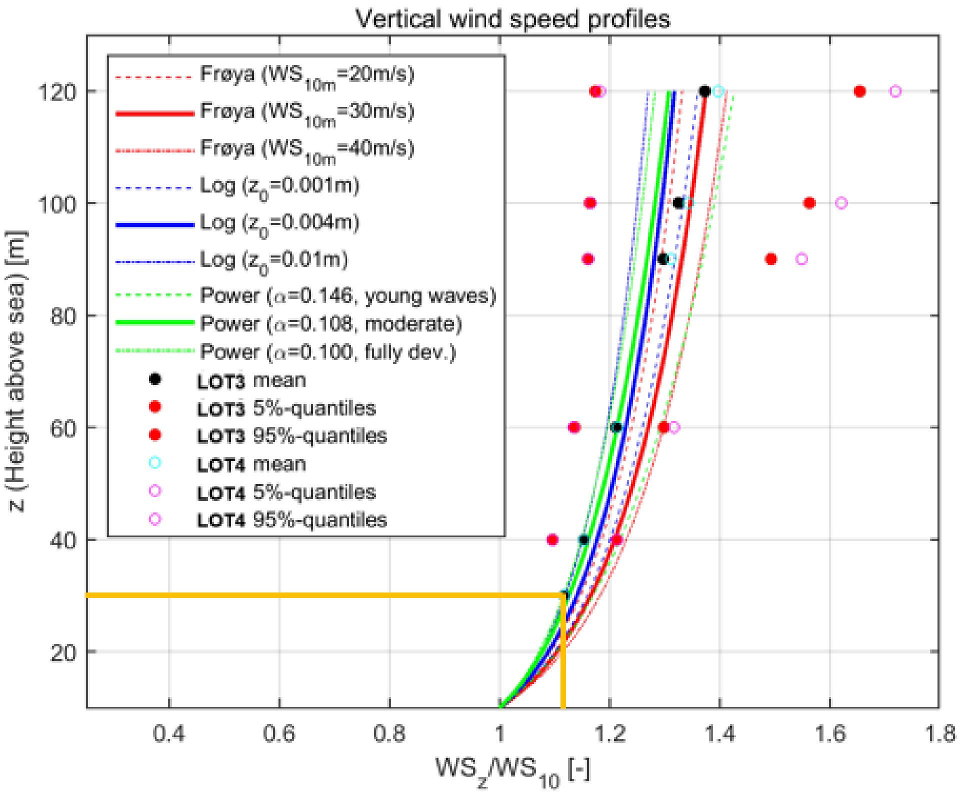

Figure 3.2 Comparison of theoretical wind speed profiles and measurements at LOT3 and LOT4
Top: All measured wind speeds (using α = 0.08);
Bottom: Measured $WS_{10,10\text{-min}}$ >15 m/s (using α = 0.10).

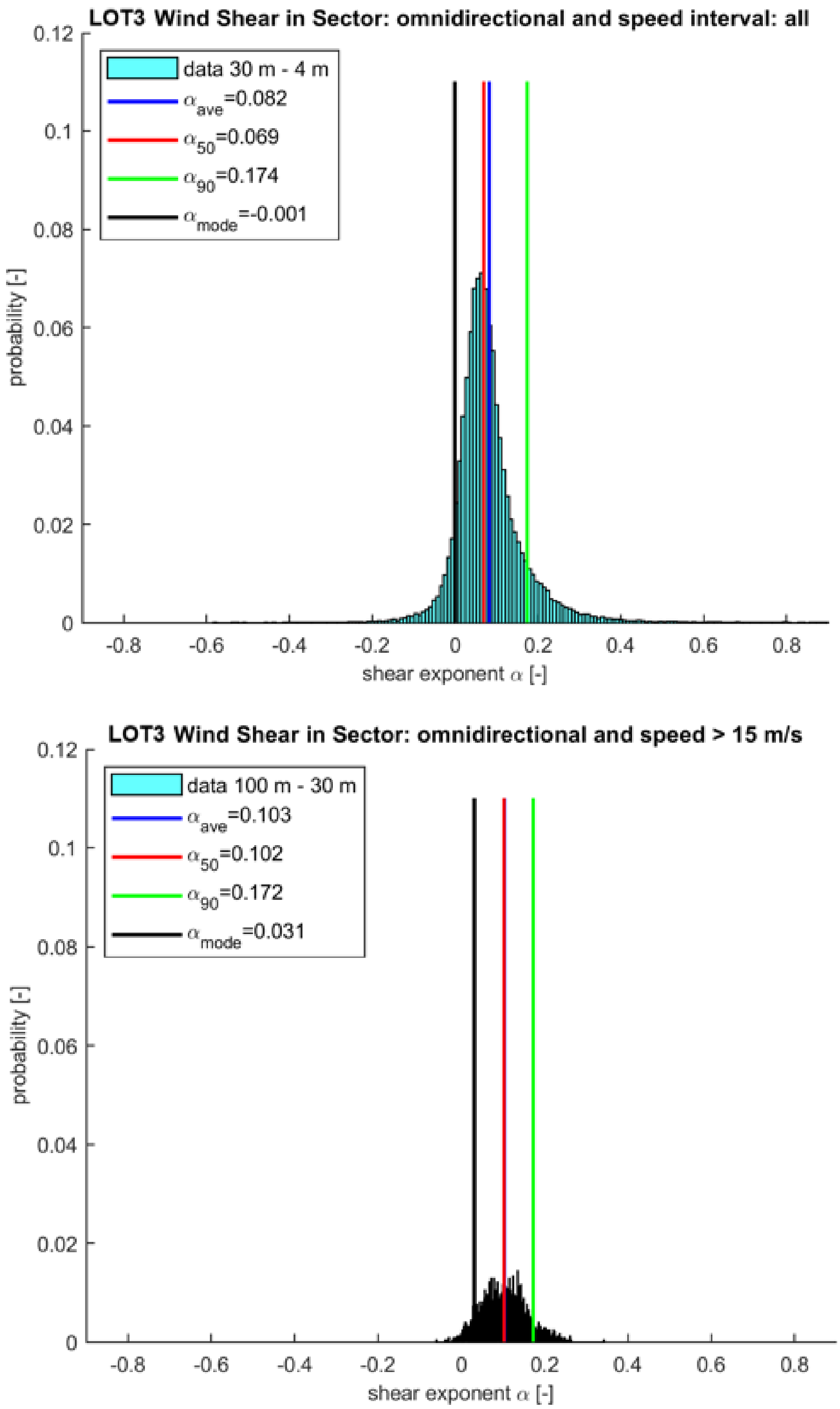

Figure 3.3 **Distribution of omnidirectional wind shear coefficient (α) at LOT3**
Calculated with power law fit to the 10-min wind speed from height 4-30 m, all wind speeds (top) and 30-100 m, and wind speed > 15 m/s (bottom).

3.2.2 Wind averaging (temporal conversion)

Wind speed of various averaging periods may be required for design purposes and for comparison of hindcast model data against measurements.

This section describes common factors for conversion between various wind averaging periods, and compares them to the local measurements, to arrive at recommended temporal conversion factors for extreme wind speeds.

Common temporal conversion factors

Table 3.2 lists common temporal conversion factors to convert between various averaging periods of extreme wind speeds. The factors are developed specifically for storm conditions, i.e., to represent the strongest sample wind speed (fx 10-min) within 1 hour. For example, if a 10-min extreme wind speed is 1.1 times the 1 h extreme wind speed, this means that the strongest wind speed in 6 samples of 10-min duration is expected to be 1.1 times the average for all 6 samples (= the 1 h mean). Thus, the factors are not applicable to convert time series of wind speeds (as this would increase the mean value).

The factors are adopted from IEC [5], CEM [9], WMO [10], and DNV/ISO [4] ([7] Frøya, see Eq. (3.1)). The CEM factors are given as equations relative to the 1 h mean, Eq. (3.4).

$$
\begin{aligned}
{U_t}/{U_{3600}} &= 1.277 + 0.296 \cdot tanh\left(0.9 \cdot \log10\left(\frac{45}{t}\right)\right), \text{ for } 1 < t < 3{,}600 \\
{U_t}/{U_{3600}} &= 1.5334 - 0.15 \cdot \log10(t), \text{ for } 3{,}600 < t < 36{,}000
\end{aligned}
\quad (3.4)
$$

The IEC [5], CEM [9], and WMO [10] factors are independent of wind speed (fixed surface roughness). Hence, when using a wind speed independent vertical profile (such as the power profile), the factors become independent of height. The WMO factors are recommended specifically for tropical cyclones.

The DNV/ISO [4] [7] (Frøya) factors consider the variation in turbulence intensity as function of speed and height, and therefore, four examples using 20, 30, and 40 m/s wind speed at 10 and 30 m height, respectively, are shown for Frøya.

The table shows that Frøya gives higher conversion factors than the other references, especially for the very extreme wind speeds and short temporal scales (note that Frøya is dependent on the wind speed and height above sea).

Table 3.2 Common temporal conversion factors of extreme wind speed
Factors are for conversion from 1 h to other averaging periods.

Reference	Remark	3 h	2 h	1 h	10-min	1-min	3-s
DNV [4], ISO [7] (Frøya)	20m/s, 10m height	-	-	1.00	1.08	1.19	1.32
	30m/s, 10m height	-	-	1.00	1.10	1.23	1.40
	40m/s, 10m height	-	-	1.00	1.12	1.27	1.47
	40m/s, 30m height	-	-	1.00	1.09	1.22	1.37
IEC[1,3] [5]	All speeds/heights	0.95	0.97	1.00	1.05	-	-
CEM [9]	All speeds/heights	0.93	0.95	1.00	1.05	1.24	1.51
WMO[2] [10]	All speeds/heights	-	-	1.00	1.03	1.11	1.30

[1] Converted from being relative to the 10-min value to being relative to the 1 h value.
[2] WMO is recommended specifically for tropical cyclones.
[3] The 2 h factor was obtained by interpolating between 3 h and 1 h.

Recommended temporal conversion factors

Figure 3.4 presents the maximum 10-min average vs. the 1 h average wind speed measured at LOT3 together with the IEC [5] and DNV/ISO [4] [7] (Frøya) temporal conversion factors.

The figure demonstrates that IEC provides a good fit to the measurements on average when considering the strongest wind speeds (> 15 m/s), while Frøya appears to overestimate the temporal conversion. Table 3.2 shows that the IEC factors are roughly in between the CEM [9] and WMO [10] factors when considering the range of 2 h to 10-min.

In conclusion, it is recommended to adopt the IEC factors for converting between averaging times of extreme wind speed within the range of 2 h and 10-min, i.e., a factor of 1.05 to convert from 1 h to 10-min average duration of extreme wind speeds. A more cautious/conservative approach would be to adopt the Frøya profile for temporal conversion of extreme wind speeds.

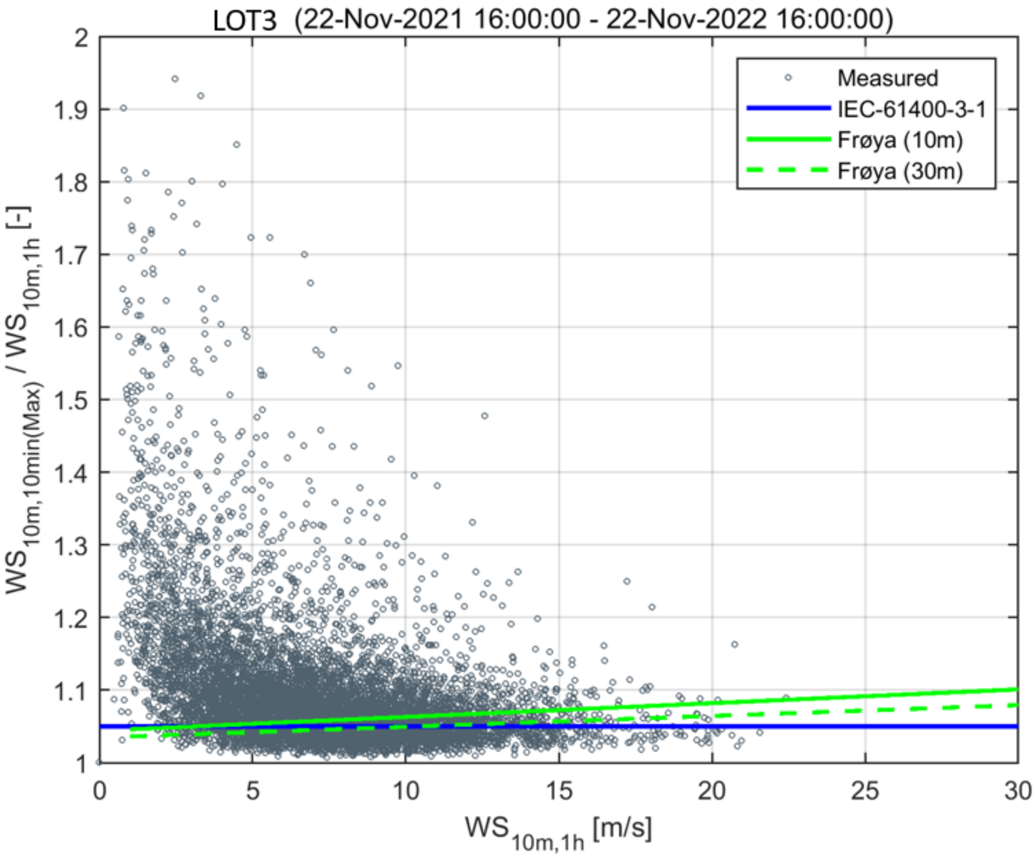

Figure 3.4 Ratio of temporal average of wind speed at LOT3
y-axis is the ratio of 10-min wind speed and 1 h wind speed, and x-axis is the 1 h wind speed.

3.3 Hindcast wind data

3.3.1 NORA3

The NORA3[6] atmospheric dataset provided by The Norwegian Meteorological Institute is derived through high-resolution atmospheric dynamic downscaling of the advanced ERA5 reanalysis dataset from the ECMWF [11]. The NORA3 model receives boundary values from ERA5 at 6-hour intervals, while storing hourly output data (with some outputs saved every third hour). The NORA3 model domain covers nearly the entire northern portion of the Atlantic Ocean, with a horizontal resolution of 3x3 km and 65 vertical layers of the atmosphere.

Averaging period of the NORA3 dataset

The averaging period is relevant when comparing various sources of data (e.g., models and measurements (peaks)), when considering operational conditions (weather windows), and for design purposes (extreme values).

For (in-situ) measurements, the averaging period is the duration of time across which each recording is averaged; this is typically 10 min for wind measurements.

The output of numerical (hindcast/reanalysis) models represents an average of an area (grid cell) rather than a point, at a given point in time, and is not

[6] NORA3 | MARINE.MET.NO

inherently associated with any averaging period. Further, there may be physical phenomena that the model does not describe or resolve adequately.

As such, one may expect the measurements to exhibit more variability (at high frequencies) compared to model data, or, reversibly, that the model data is somewhat ‘smoothed’ in time compared to measurements. The degree of ‘smoothing’ would depend on a combination of model type, forcing and grid.

To support validation of model data and application for operational and design purposes, a representative averaging period of the model data is assessed by comparing the magnitude and slope of the frequency power spectra of the model data to that of measurements averaged with various time windows. Such an analysis illustrates the energy density (variability) of the time series signals at frequencies up to the Nyquist frequency (two times the sampling frequency of the data, i.e., up to 2 h for model data saved 1-hourly).

Figure 3.5 shows a frequency power spectrum of wind speed from NORA3 and measurements (LiDAR) at LOT3. A clear distinction between the NORA3 model spectrum, the 30 min and 1 h averaged time series spectra of the measurement is difficult to observe. To be conservative the NORA3 wind is chosen to represent 1h averages (for both LOT3 and LOT4). For a 3 km spatial resolution time series, 1h-average can seem large. According to Table 3.2 it corresponds to approximately 3%.and hence can be considered as an unbiased uncertainty.

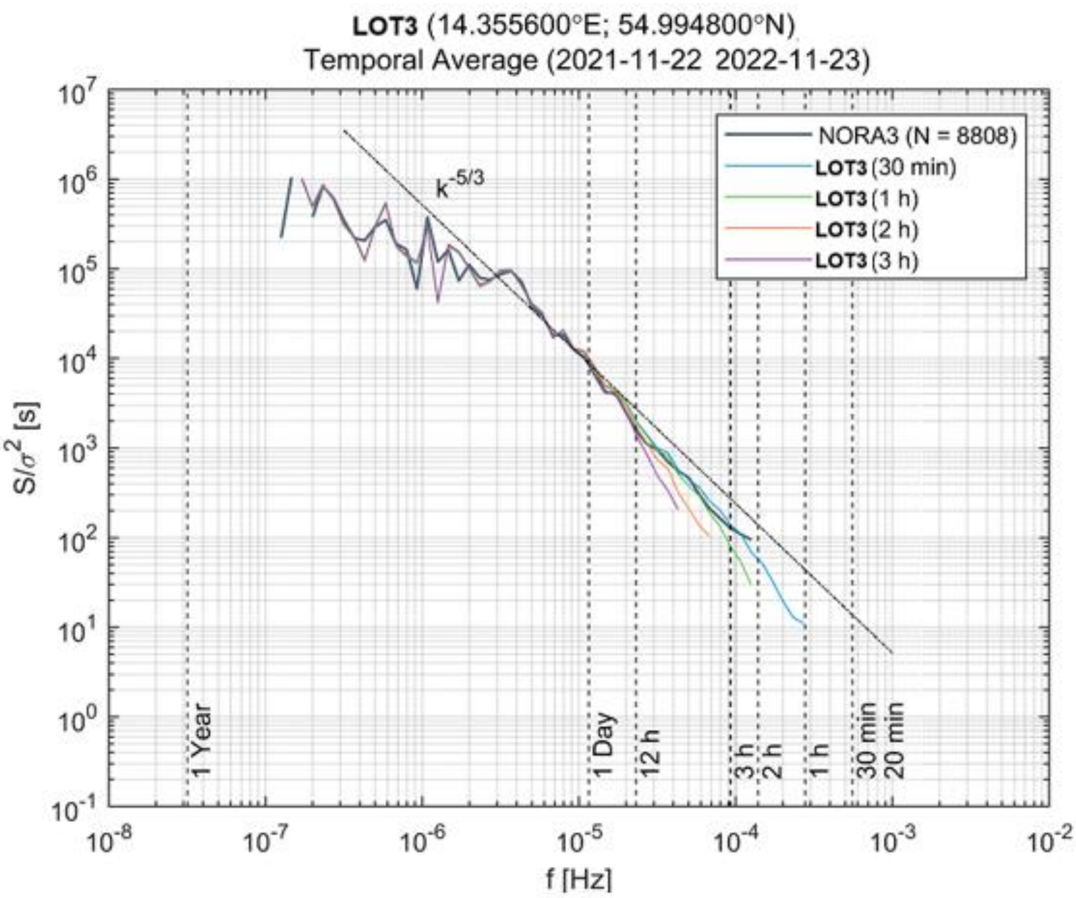

Figure 3.5 Frequency power spectrum of wind speed at 10 m at LOT3

3.3.2 Validation of NORA3 wind

The NORA3 dataset was validated against the measurements recorded by the Fugro floating LiDAR (LOT3 and LOT4) at the EIBS site, and by BSH at FINO2 and Arkona stations.

The measured wind speed (from Lidar at 30 m) was converted to 10 mMSL following the approach in Section 3.2.1 (power profile with α = 0.08 as recommended for normal (average) wind conditions).

Figure 3.6 to Figure 3.9 present comparisons of measured and NORA3 data in terms of time series, scatter plots and wind roses. The figures demonstrate a very good agreement between the datasets regarding both wind speed and direction.

In summary, the NORA3 data exhibits a high correlation with local measurements and is deemed highly reliable as a wind forcing input for spectral wave model (see Section 6), resulting in expectedly precise predictions of waves at the EIBS site.

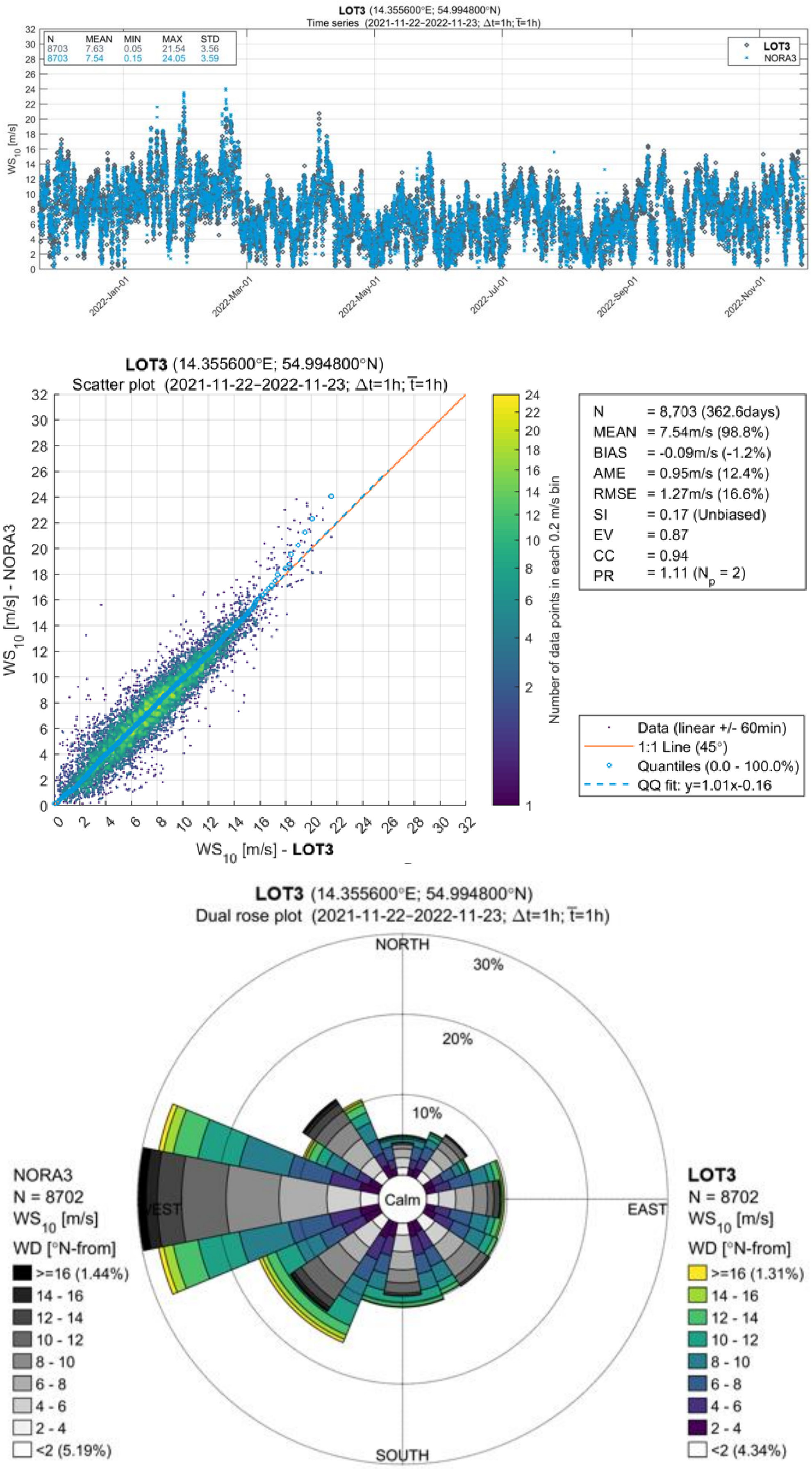

Figure 3.6 **Comparison of NORA3 wind against and measured wind at 10 m at LOT3**
Scatter plot (top) and dual rose plot (bottom).

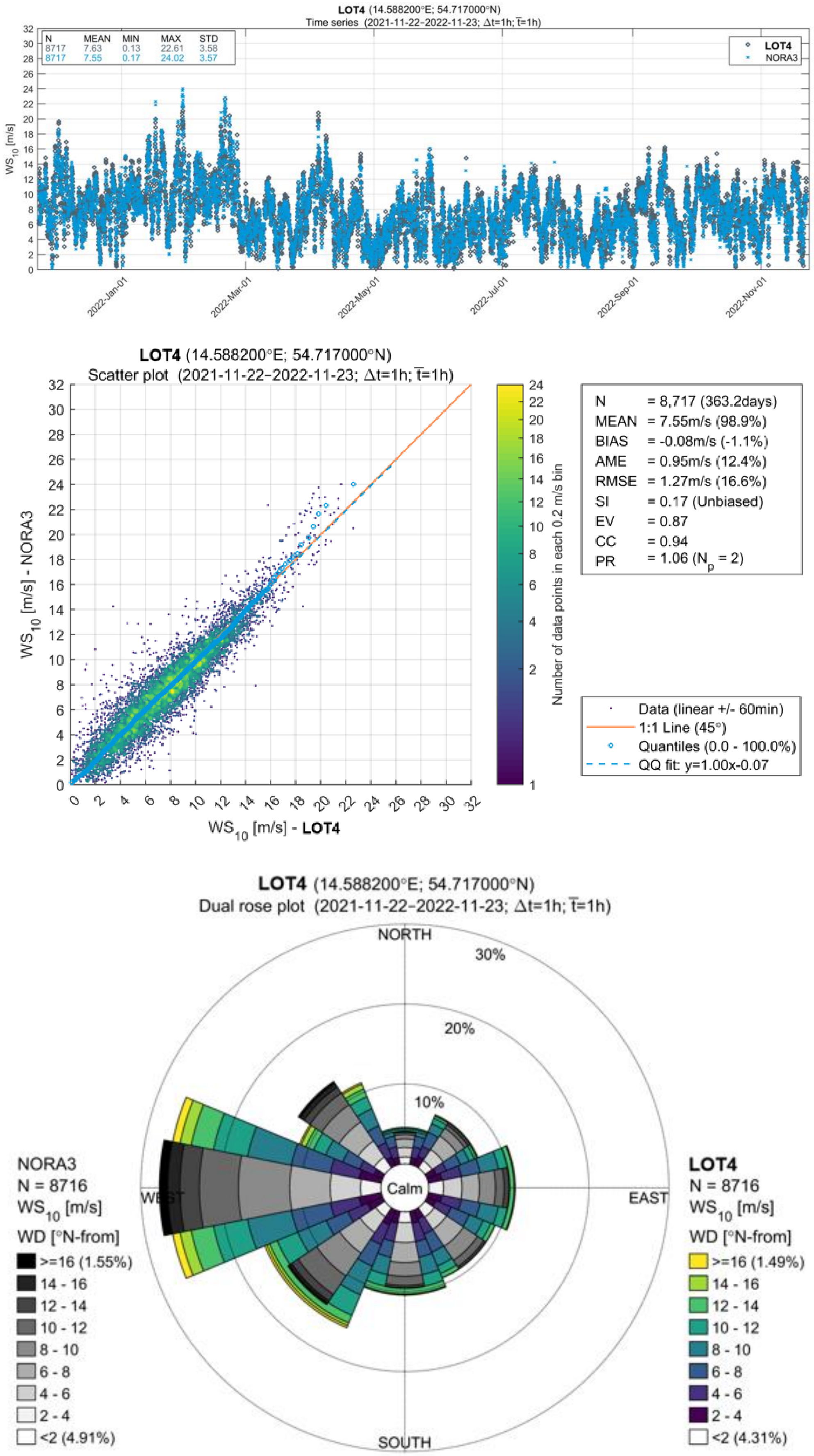

Figure 3.7 Comparison of NORA3 wind against measured wind at 10 m at LOT4
Scatter plot (top) and dual rose plot (bottom).

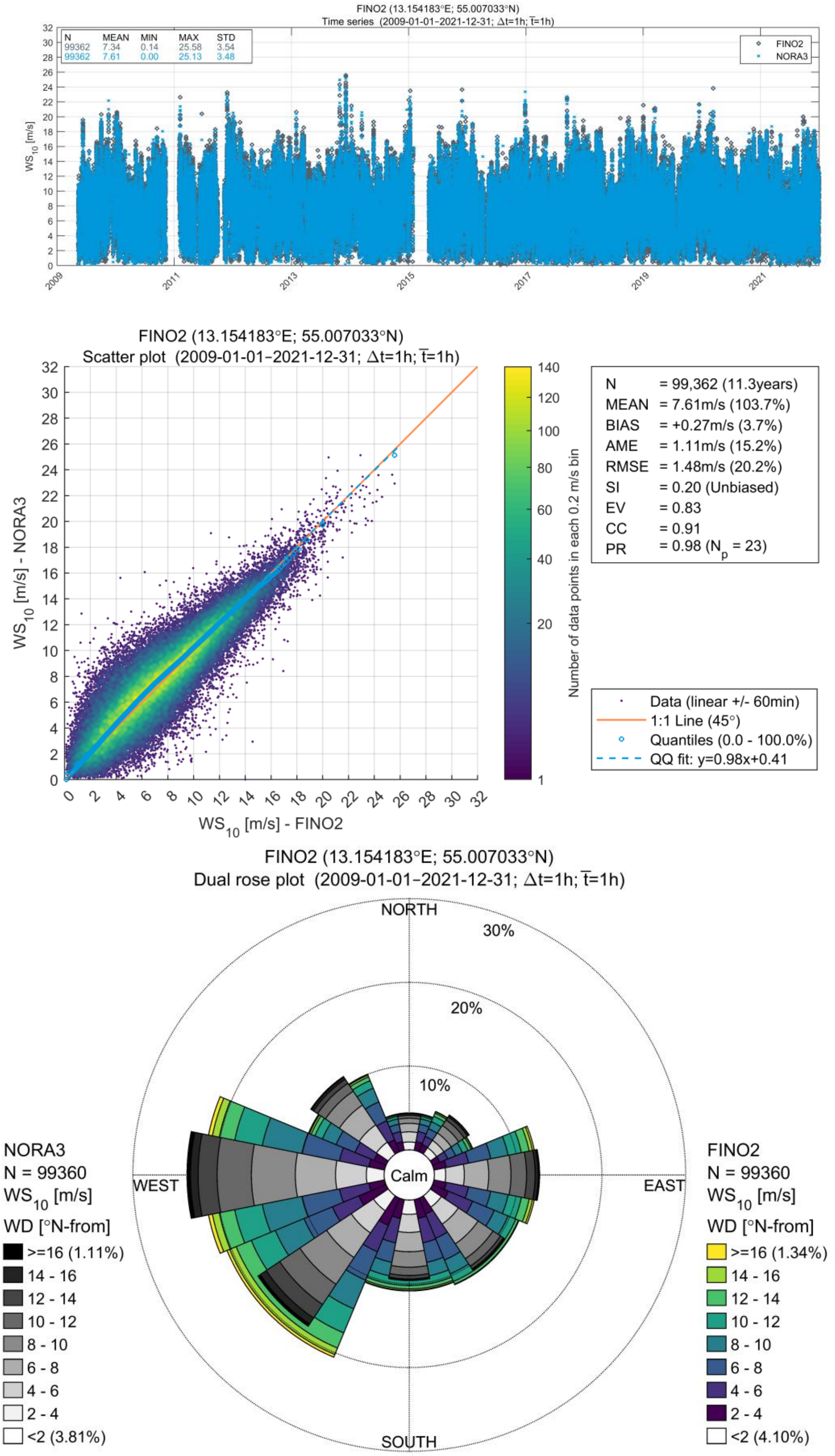

Figure 3.8 **Comparison of NORA3 wind against and measured wind at 10 m at FINO2**
Scatter plot (top) and dual rose plot (bottom).

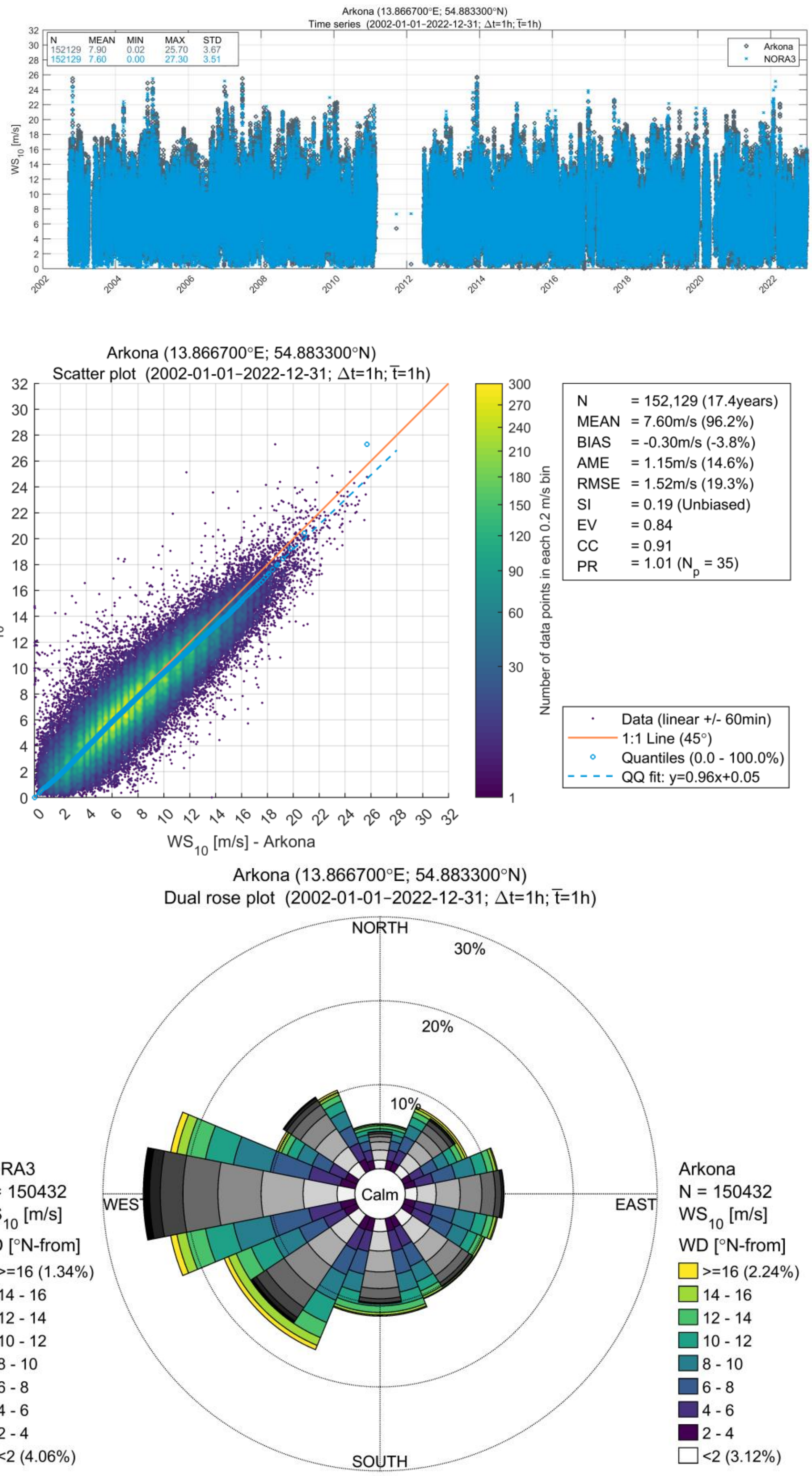

Figure 3.9 **Comparison of NORA3 wind against and measured wind at 10 m at Arkona**
Scatter plot (top) and dual rose plot (bottom).

4 Water Levels

Hindcast water level data was established from the DHI North Europe regional model ($HD_{NE-ERA5}$) covering northeast Europe. These data were established by numerical modelling using DHI's MIKE 21 Flow Model FM and validated against regional measurements.

4.1 General water level characteristics

The Baltic Sea is a microtidal estuary with a semi-diurnal tide of only 10-20 cm in amplitude. It is one of the largest estuaries in the world with a large surface and is connected to the oceans via the narrow Danish Straits. The bathymetry and the orientation give a relatively complicated response to passing low-pressure systems, that may induce surges up to several meters of height. Critical situations may arise, for example, when westerly storms push water in from the North Sea and into the Bay of Botnia[7]. As the storm center travels eastward, wind may change to northerly and easterly, which in combination with the constriction by the Danish Straits, can create a high surge in the southern Baltic[8].

4.2 Water level measurements

Water level measurements from selected institutions around the Baltic have been used to validate and force the water level model in this study. Table 4.1 and Figure 4.1 show the stations used. All the data are from governmental institutions who are responsible for QA of the data.

Table 4.1 Water level measurements
Data considered in this study.

Station	Lon. E	Lat. N	Period
Tejn	55.25	14.83	200501-202305
Darlowo	54.44	16.38	202011-202305
Drogden	55.54	12.71	199203-202305
Gedser	54.57	11.93	199203-202305
Rodvig	55.25	12.37	199108-202305
Ronne	55.1	14.68	199402-202305
SassnitzTG	54.51	13.64	201401-202304
Simrishamn	55.56	14.36	198206-202305
Skanor	55.42	12.83	199202-202305
Ustka	54.59	16.85	200503-202305
Ystad2	55.42	13.83	201907-202305

[7] Kai Bellinghausen 1 , Birgit Hünicke 1 , and Eduardo Zorita (2023). Short-term prediction of extreme sea-level at the Baltic Sea coast by Random Forests. Natural Hazards and Earth Systems, https://doi.org/10.5194/nhess-2023-21Preprint
[8] Wolski, Tomasz & Wiśniewski, Bernard. (2021). Characteristics and Long-Term Variability of Occurrences of Storm Surges in the Baltic Sea. Atmosphere. 12. 1679. 10.3390/atmos12121679.

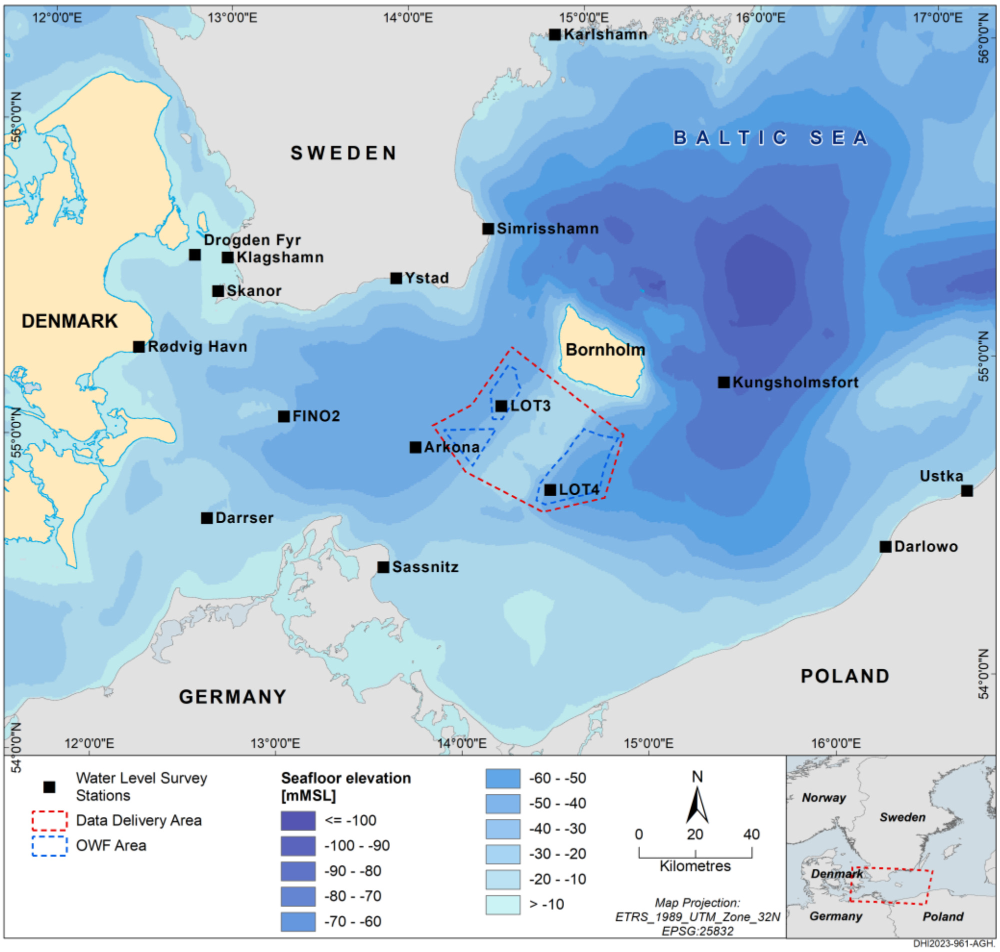

Figure 4.1 Location of water level measurements
Data considered in this study.

4.3 Hindcast water level data

4.3.1 North Europe HD ERA5 Model ($HD_{NE-ERA5}$)

DHI's two-dimensional North Europe regional hydrodynamic model ($HD_{NE-ERA5}$) simulates water levels and depth-averaged current data established through numerical modelling using the MIKE 21 Flow Model FM, with its 2022 version.

'The $HD_{NE-ERA5}$ model domain extends from the deep water beyond the continental shelf and encompasses the shelf-seas of north-western Europe, including the Irish and Celtic Sea, the English Channel, the North Sea, and the Baltic Sea.

$HD_{NE-ERA5}$ is based on an unstructured flexible mesh with refined mesh in shallow areas and covers the period 1979-01-01 to 2022-12-31.

The model includes tide (boundaries extracted from DHI's Global Tide Model), and surge forced by wind and air pressure from the ERA5 atmospheric model.

Table 4.2 summarises the $HD_{NE-ERA5}$ model configuration. The setup is based on an extensive calibration/validation process against available WL measurements within the model domain.

Table 4.2 Overview of DHI's $HD_{NE\text{-}ERA5}$ model setup parameters

Setting	$HD_{NE\text{-}DA}$
Mesh resolution	~2.5 km to 30 km
Simulation period	1979-15-01 – 2022-31-12 (43 years)
Basic equations	Hydrodynamic module - 2D (depth-integrated)
Time step	30 min
Density	Barotropic
Eddy viscosity	Smagorinsky formulation with a constant value of 0.28
Bed resistance	Depth-dependent Manning map: • < 30 m: 38 $m^{1/3}/s$ • 30-100 m: 42 $m^{1/3}/s$ • > 100 m: 45 $m^{1/3}/s$
Wind forcing	ERA5 (wind field at 10 mMSL and atmospheric pressure at MSL, variable in time)
Wind drag	$C_A = 1.255 \cdot 10^{-3}$, $C_B = 2.425 \cdot 10^{-3}$, $W_A = 7\ m/s$, $W_B = 25\ m/s$ (Empirical parameters used to calculate the drag coefficient of air)
Bathymetry	EMODnet version 2020
Tidal potential	Included: 11 constituents (M2, O1, S1, K2, N2, K1, P1, Q1, MF, MM, SSA)
Boundary conditions	Tidal boundaries extracted from DHI's Global Tidal Model with surge forced by wind and air pressure from the Climate Forecast System Reanalysis (ERA5) atmospheric model.
Data Assimilation	1993-2022
River discharge	Not included (considered to have an insignificant influence on the water level and current in a 2D regional model where no baroclinic conditions were included)

4.3.2 Output specifications

The output from $HD_{NE\text{-}ERA5}$ is summarised in Table 4.3. It includes water level (WL) relative to mean-sea-level, depth-averaged current speed (CS), and depth-averaged current direction (CD), which are saved for each model mesh element at intervals of 0.5 hours. However, only the water levels are applied in the present study.

Table 4.3 Model output parameters from $HD_{NE\text{-}ERA5}$

Parameter Name	Symbol	Unit	Temporal resolution (h)
Water level	WL	mMSL	0.5
Depth average current speed	CS	m/s	0.5
Depth average current direction	CD	°N (going-to)	0.5

4.3.3 Validation of water level

The $HD_{NE\text{-}ERA5}$ has been validated for the general area in about 20 stations, with good results. Generally, the scatter indices fall below 0.3, and the peak ratio is between 0.95 and 1.05. This report includes validation for the four stations most relevant for the EIBS, Tejn harbour, Rønne port, LOT3 and LOT4, as shown below in Figure 4.2 to Figure 4.11.

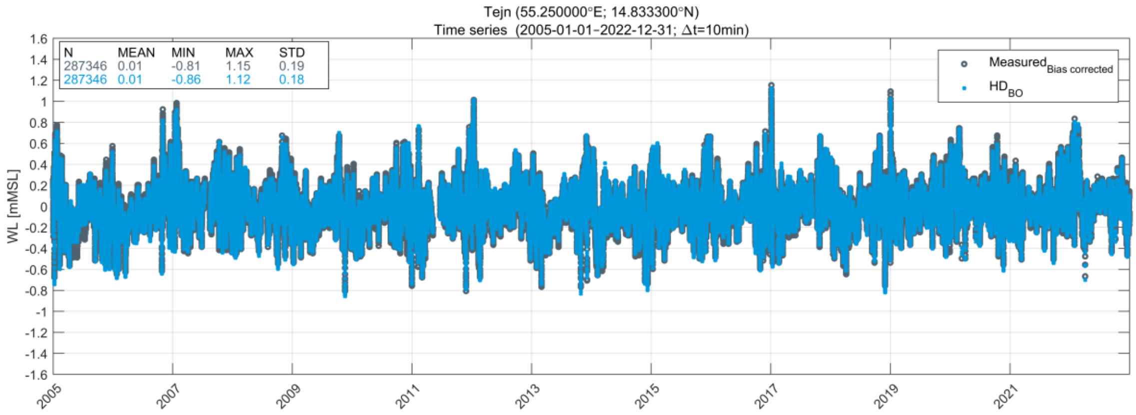

Figure 4.2 Time series of modelled and observed water levels at Tejn harbour

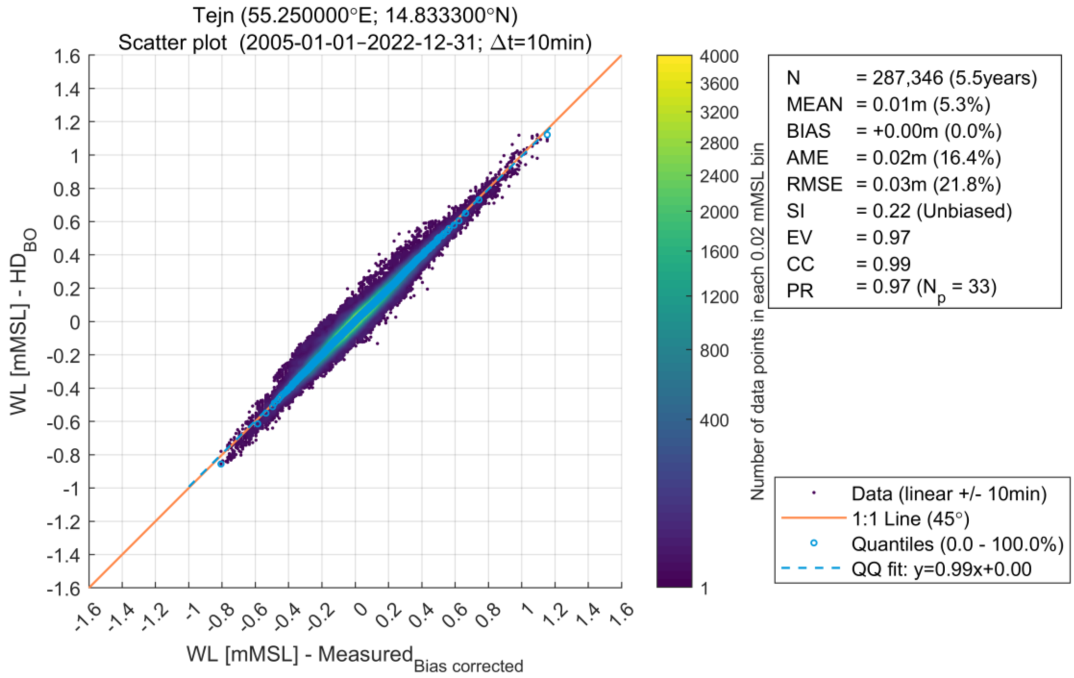

Figure 4.3 Scatter diagram of observed and modelled water level variations at Tejn harbour

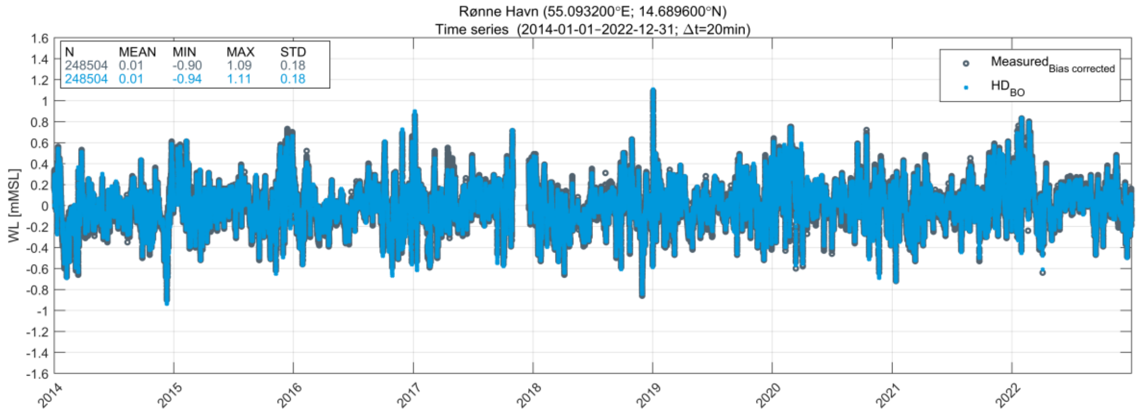

Figure 4.4 Time series of observed and modelled water level variations at Rønne port

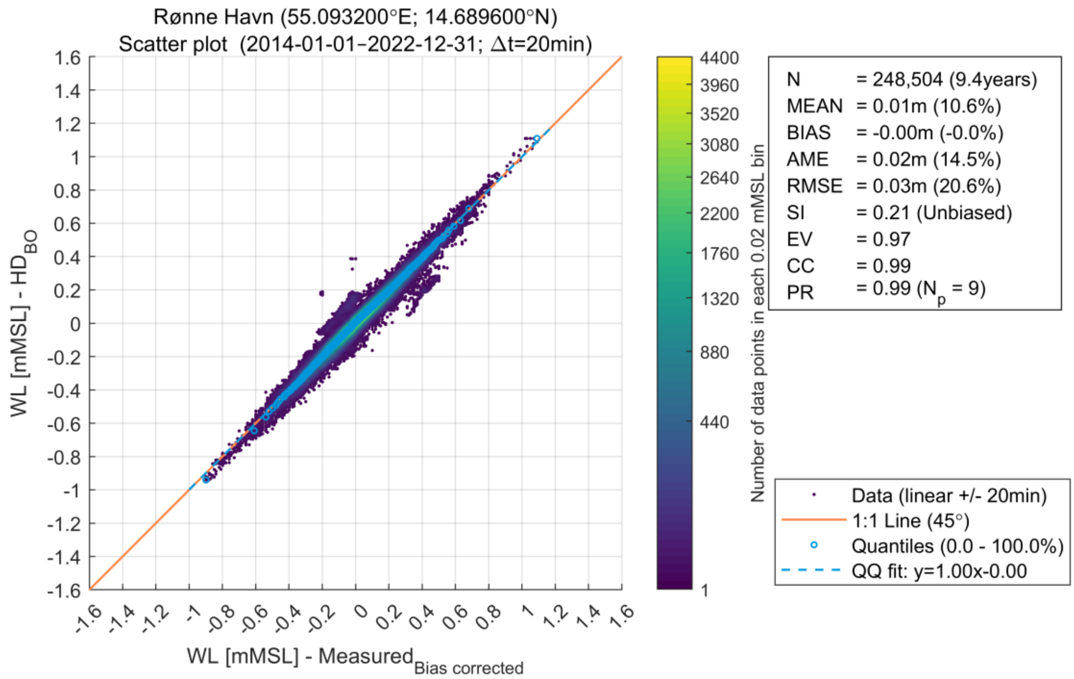

Figure 4.5 Scatter diagram of observed and modelled water level variations at Rønne port

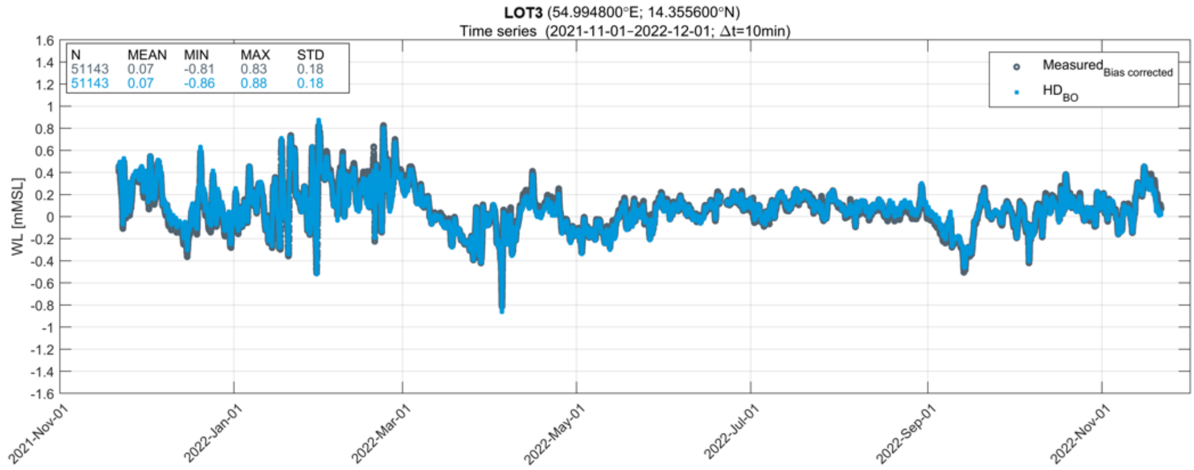

Figure 4.6 **Time series of modelled and observed water levels at LOT3 (2021-11-01 - 2022-12-01)**

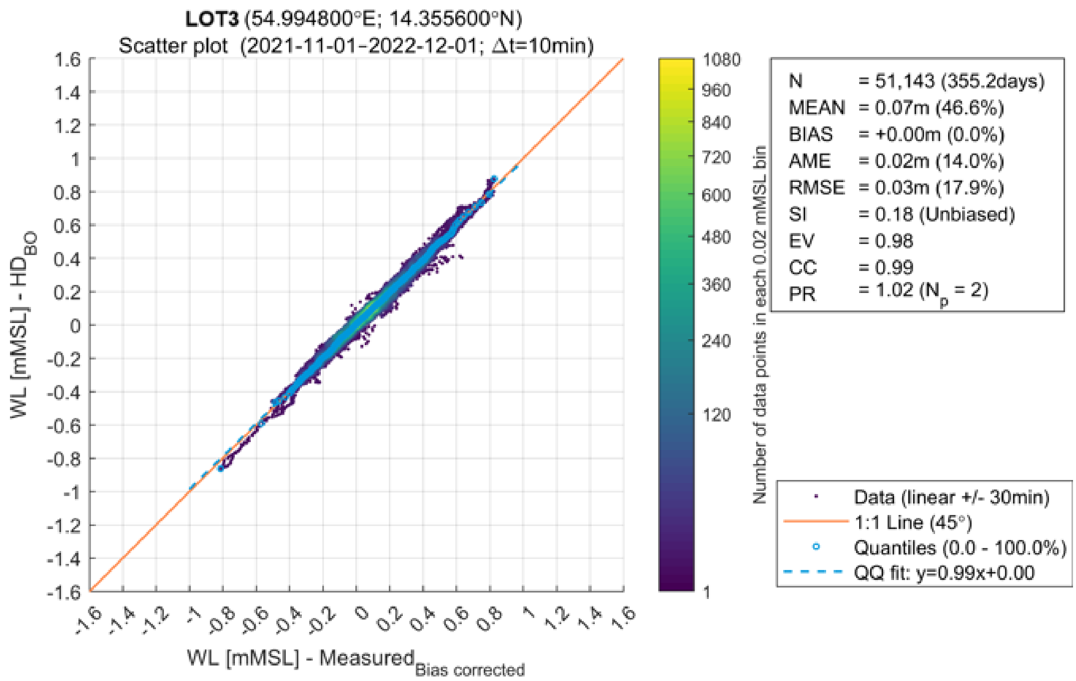

Figure 4.7 **Scatter diagram of observed and modelled water level variations at LOT3 (2021-11-01 - 2022-12-01)**

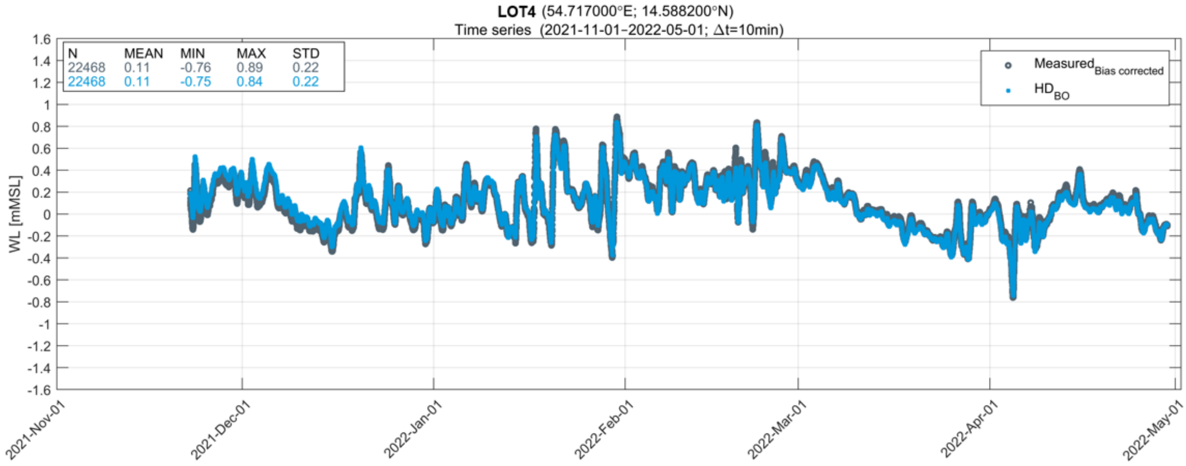

Figure 4.8 Time series of modelled and observed water levels at LOT4 (2021-11-01 - 2022-05-01)

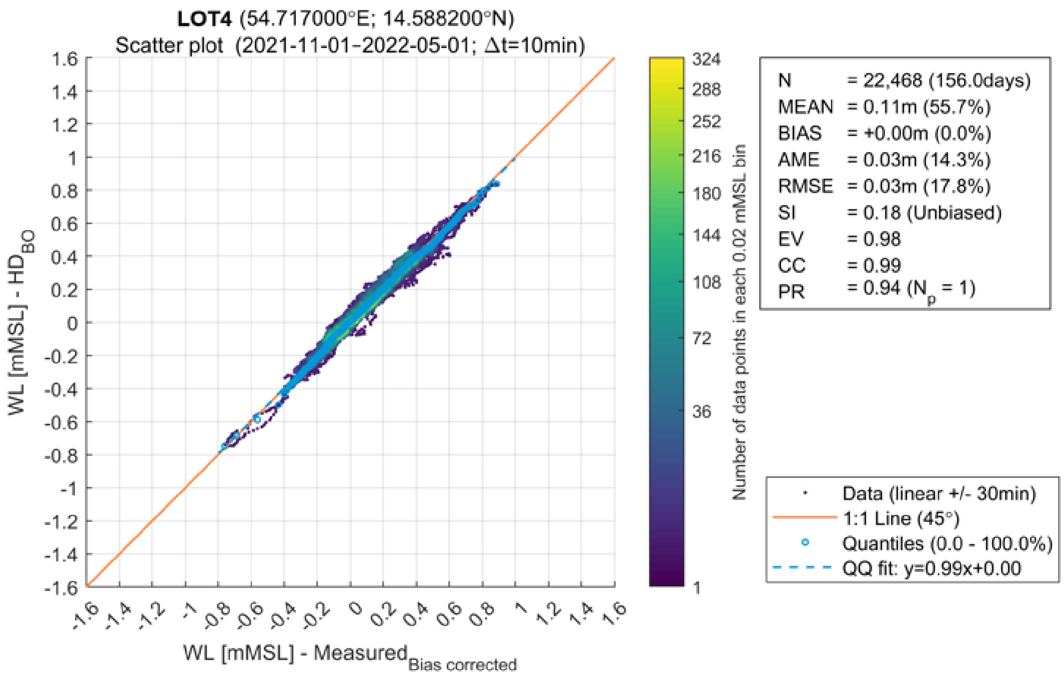

Figure 4.9 Scatter diagram of observed and modelled water level variations at LOT4 (2021-11-01 - 2022-05-01)

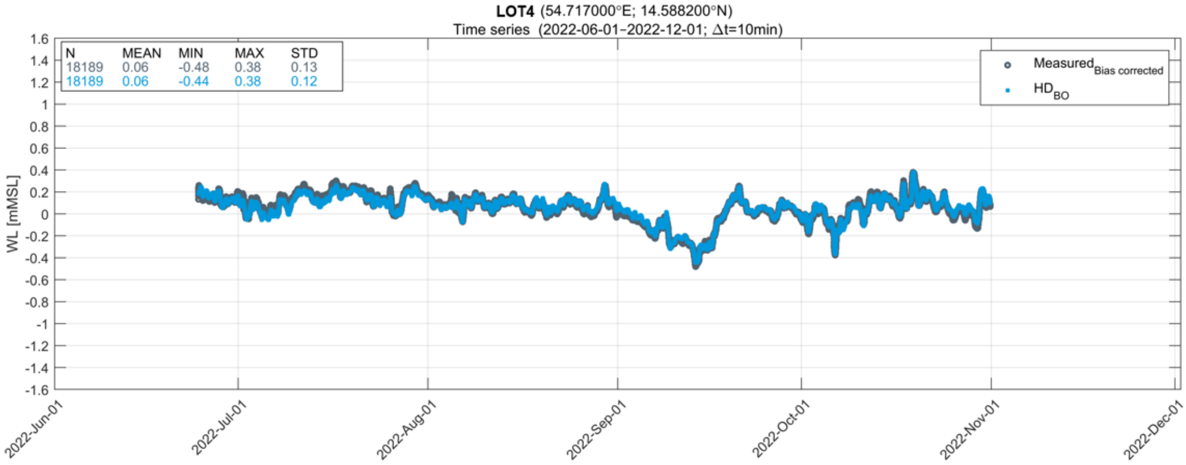

Figure 4.10 Time series of modelled and observed water levels at LOT4 (2021-11-01 - 2022-05-01)

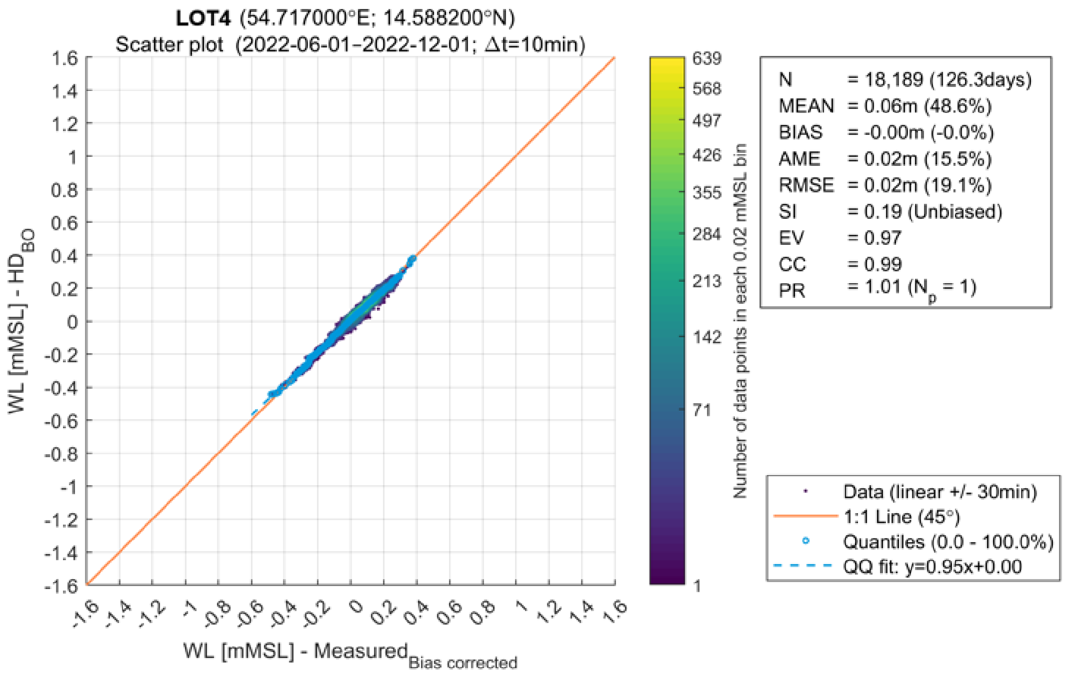

Figure 4.11 Scatter diagram of observed and modelled water level variations at LOT4 (2021-11-01 - 2022-05-01)

5 Current, Temperature and Salinity

This section presents a general overview of the current, seawater temperature and salinity conditions at EIBS and presents the measurements and the hindcast current data from HD_{EIBS}.

5.1 General current characteristics

EIBS is located at Rønne Bank, which separates the Arkona Basin and the Bornholm Basin and is situated at the entrance to the Baltic Proper, as shown in Figure 5.1.

The Baltic Sea is the world's largest estuary, where the general circulation is governed by outflowing fresh water draining a large part of Northeastern Europe through the Danish Belts, and a compensating saline inflow from the Kattegat Sea and North Sea [12] [13]. This leads to a general salinity gradient from the Bay of Botnia towards the Danish Belts, with salinity in the Baltic Proper varying around 8-12 PSU at the surface, to 25 PSU in the deepest basins.

The water exchange is relatively dynamic, with a continuous freshwater outflow from rivers in the surface layers, while the renewal of the deep saline water masses occurs intermittently by major Baltic inflows [14] [15]. These are events occurring typically 1-2 times per year where the meteorological conditions, typically passing North Atlantic low-pressure systems, create events where a large volume of saline water can flow in from the Kattegat Sea. These denser water masses will eventually come to rest in the deepest parts of the Baltic Sea, where they are slowly mixed vertically due to turbulence. Inflows from Kattegat Sea typically come into the Arkona Basin past Kriegers Flak and may continue past Rønne Bank into the Bornholm Basin and beyond [16].

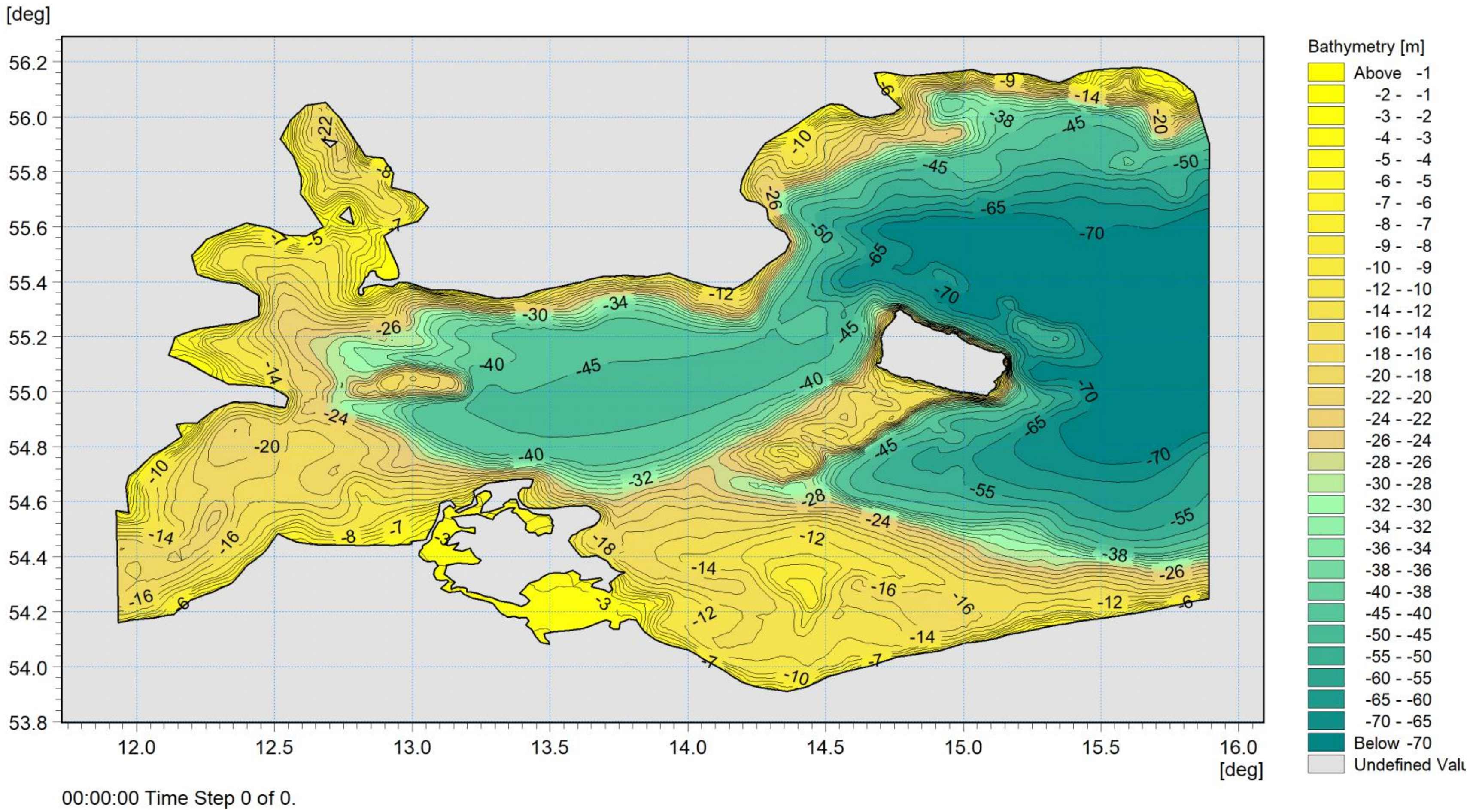

Figure 5.1 Bathymetry of the Arkona and Bornholm Basins of the Baltic Sea (from EIBS 3D model)

Schematics of the large-scale circulation in the Baltic Sea are presented in Figure 5.2, showing the outflow of fresh or brackish water from the major North European rivers in the surface and the compensating inflow of denser waters from Kattegat Sea and the North Sea in the deeper layers [17]. The figure also depicts how the dense water inflow follows the deep trenches and channels on its eastward way. The surface layers are continuously mixed with the denser bottom water via turbulence and entrainment, such that a gradient with increasing salinity is established from the Bay of Botnia towards the Danish Straits [18].

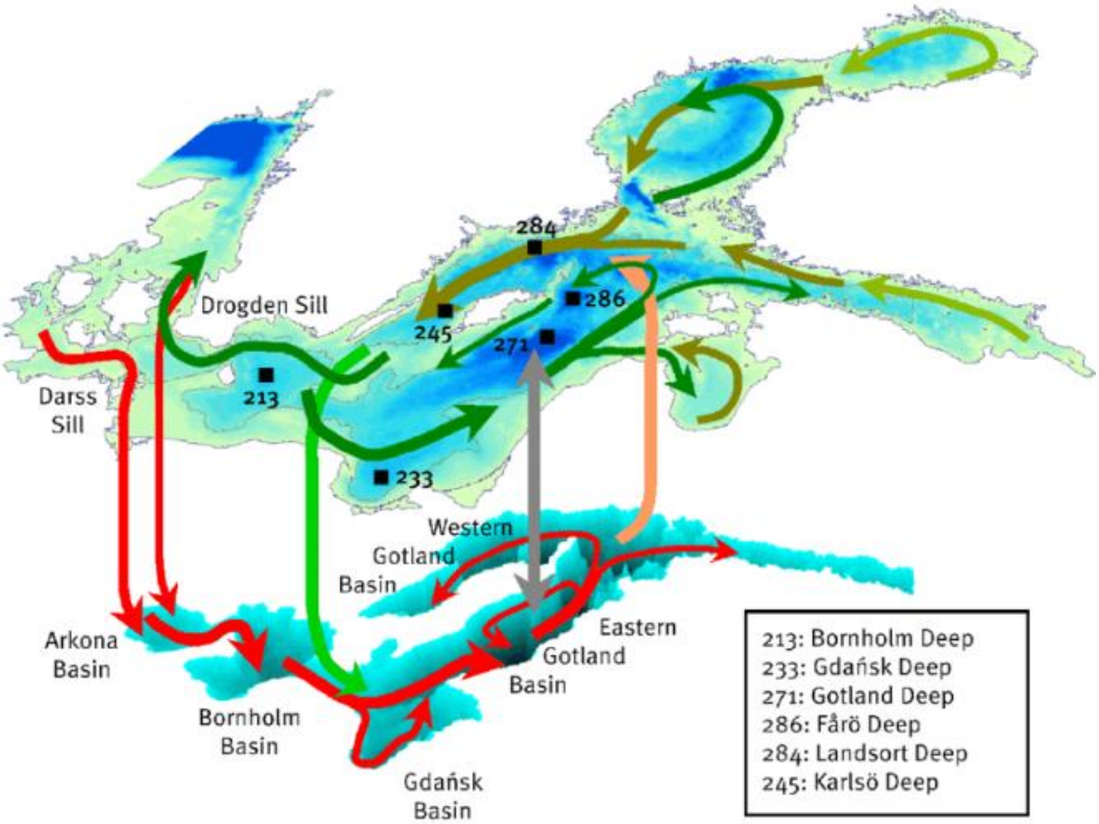

Figure 5.2 General circulation in Baltic Sea [19]
Green and red arrows denote the surface and bottom layer circulation, respectively. The light green and beige arrows show entrainment, and the grey arrows denote diffusion. Numbers are standard hydrographic stations of Leibniz Institute for Baltic Sea Research (IOW) long-term observations.

5.2 Current measurements

Measurements of currents are important for validation of the 3D hydrodynamic model used in this study. There are a few long-term stations with current profile measurements at several depths: At the FINO2 mast and at the Arkona buoy. In addition, a measurement buoy was deployed at the Krieger's Flak and at two stations at the western and eastern side of the EIBS area, LOT3 and LOT4 [6], see Figure 5.3 and Table 5.1.

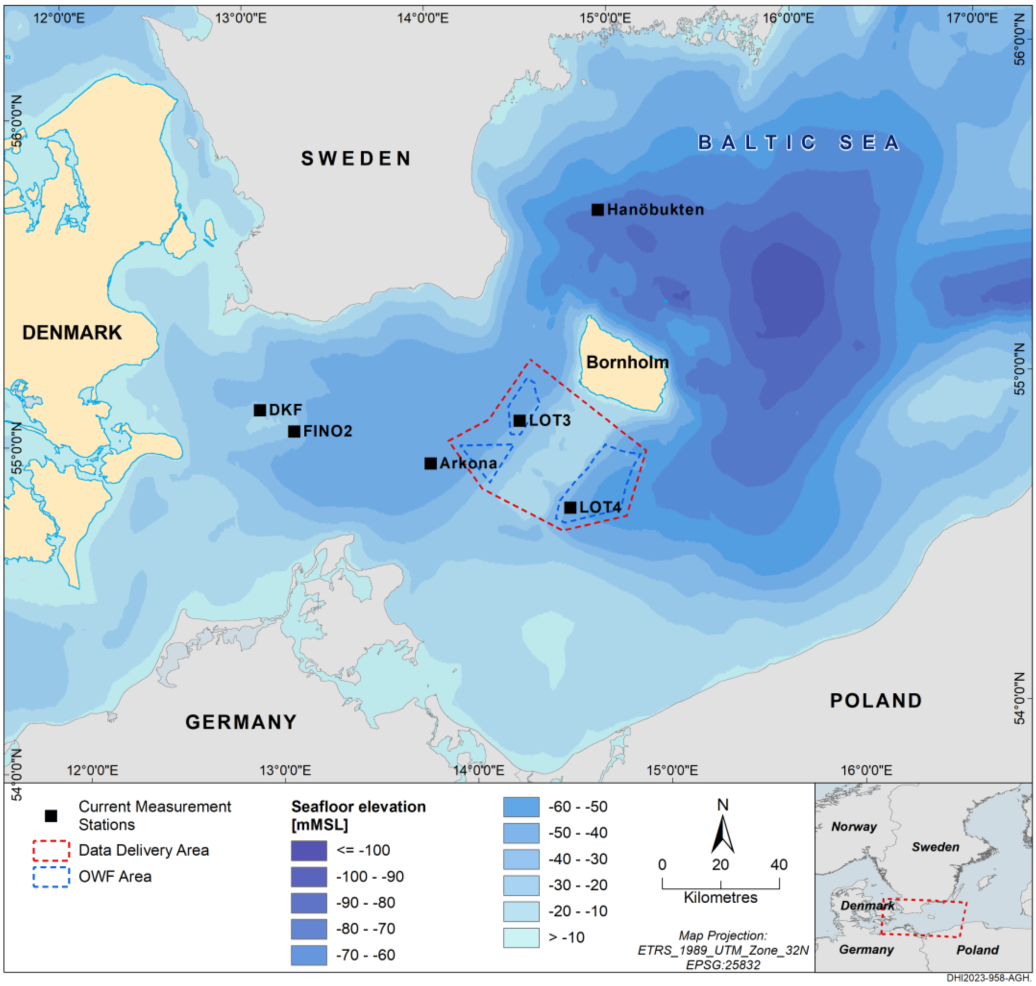

Figure 5.3 Location of local current measurements
Data applied in this study.

Table 5.1 Stations with current measurements
Data applied in this study.

Station Name	Longitude [°E]	Latitude [°N]	Depth [mMSL]	Availability period	Parameters	Owner / Surveyor
Energy Island Buoy 3	54.9948	14.3556	39.8	Nov 2021 – 2023.08.21	1m intervals in depth range 1m to 39m	Energinet
Energy Island 3 Upward	54.9948	14.3556	39.8	Mar 2022 – Jun 2022	1m intervals in range 4m to 42m above seabed	Energinet
Energy Island Buoy 4	54.7170	14.5882	42.3	Nov 2021 - 2023.08.21	1m intervals in depth range 1m to 41m	Energinet
Energy Island 4 Upward	54.7170	14.5882	42.3	Jan 2022 – Jun 2022	1m intervals in range 4m to 44m above seabed	Energinet
Kriegers Flak (DKF)	55.0790	12.9781	21.0	Mar 2020 - May 2022	Surface	Vattenfall
Arkona	54.8833	13.8667	45.0	Sep 2002 - 2023.08.21	2m intervals in range 4m to 42m above seabed	BSH
FINO2	55.0083	13.1542	25.0	Jan 2015 – Dec 2022	1m intervals in depth range 2m to 20m	BSH

The two project measurement sites were equipped with two instruments each, one downward-looking ADCP mounted on the Lidar buoy, and one bottom-mounted ADCP. Comparing the two instruments, an indication that the downward-looking ADCP gives consistently higher currents speeds than the bottom mounted was observed. It is suspected by this study that this may be due to the wave induced motion of the floating buoy, which may give a higher noise level and potentially a positive bias of the currents. The quality assurance by this study of the other sites did not find any issues.

5.3 Temperature and salinity

Temperature and salinity were measured at three (3) locations as indicated in Table 5.2. The measurements in general cover the depth reasonably well to catch the dynamics of vertical stratification. The sampling frequency, however, is not sufficient to resolve potential internal waves that typically have frequencies lower than 0.01 HZ (about 3 min periods).

Table 5.2 Temperature and salinity measurements

Station Name	Longitude [°E]	Latitude [°N]	Depth [mMSL]	Availability period	Parameters	Owner / Surveyor
Energy Island Buoy LOT4	54.717	14.5882	42.3	Nov 2021 – 2023.08.21 per 10min	T and S in 4 depths from 9m-33m and surface	Energinet/ Fugro
FINO2	55.0083	13.1542	25.0	Jan 2015 – Jul 2021 per 10min	T at surface and every 2m in 11 depths from 2m – 20m	BSH
Arkona	54.8833	13.8667	45.0	Sep 2002 – 2023.08.21 per 10min	T and S in 5 depths: 40m, 25m, 7m, 5m (T only) and 2m (T only)	BSH

5.4 EIBS 3D Model setup

The currents in the EIBS area were modelled and established using DHI's general marine modelling framework, MIKE 3[9]. This is a general hydrostatic 3-dimensional ocean model, based on the shallow water equations and density effects from temperature and salinity. The model uses a 2-equation turbulence model for viscosity and mixing. The model is generally forced by tides and surges, wind and atmospheric pressure, freshwater inflow and uses a dynamic atmospheric heat exchange module with radiant and latent heat transfer.

The numerical solution uses a flexible triangulated mesh and a combined sigma-z vertical discretization, enabling an efficient use of the spatial resolution. The model uses a spherical coordinate system and uses a semi explicit numerical explicit solution method.

The main modelling results are full 3D fields of the primary parameters, i.e., currents, temperature and salinity, typically saved every 1-3 hours, the frequency being dependent on the specific parameter.

5.4.1 Bathymetry

The model domain was selected to provide the optimal location for model boundaries. Boundary data were in general extracted from DHI's Baltic Sea model 3D archive, DKBS [20].

[9] MIKE 3 Documentation (mikepoweredbydhi.help)

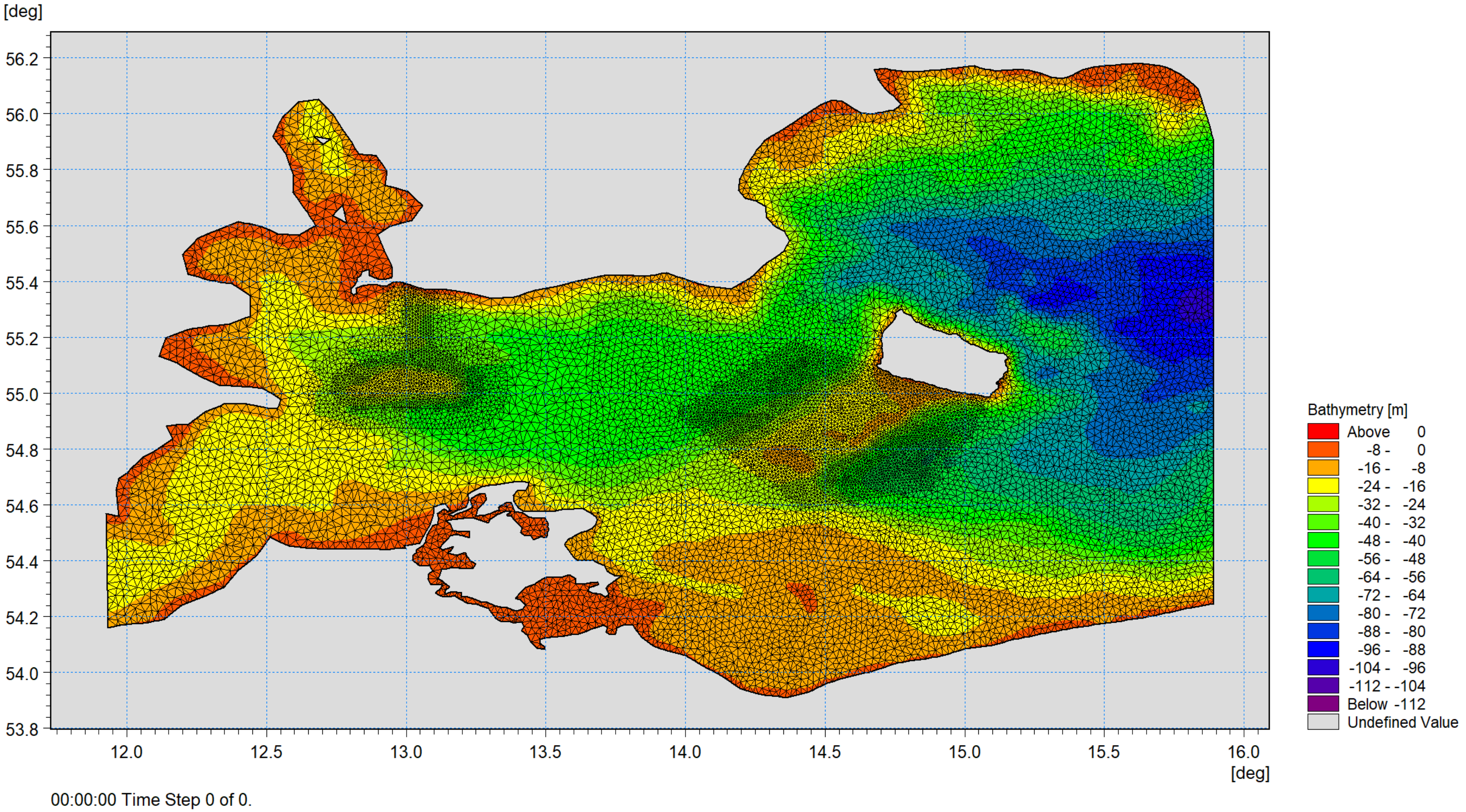

Figure 5.4 Layout of model domain and mesh for the EIBS 3D model, HD_{EIBS}

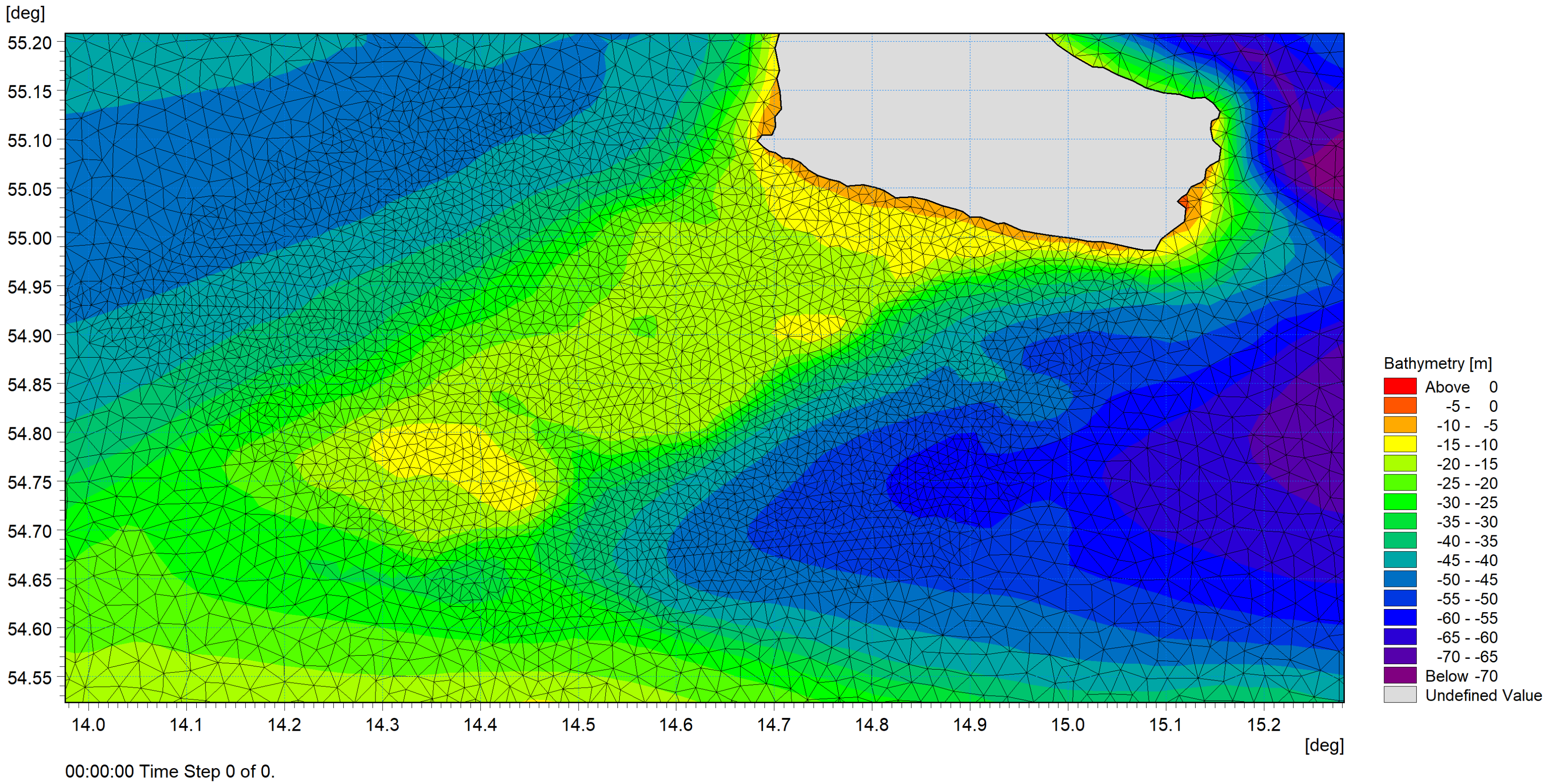

Figure 5.5 **Detail of the model mesh around the EIBS development**

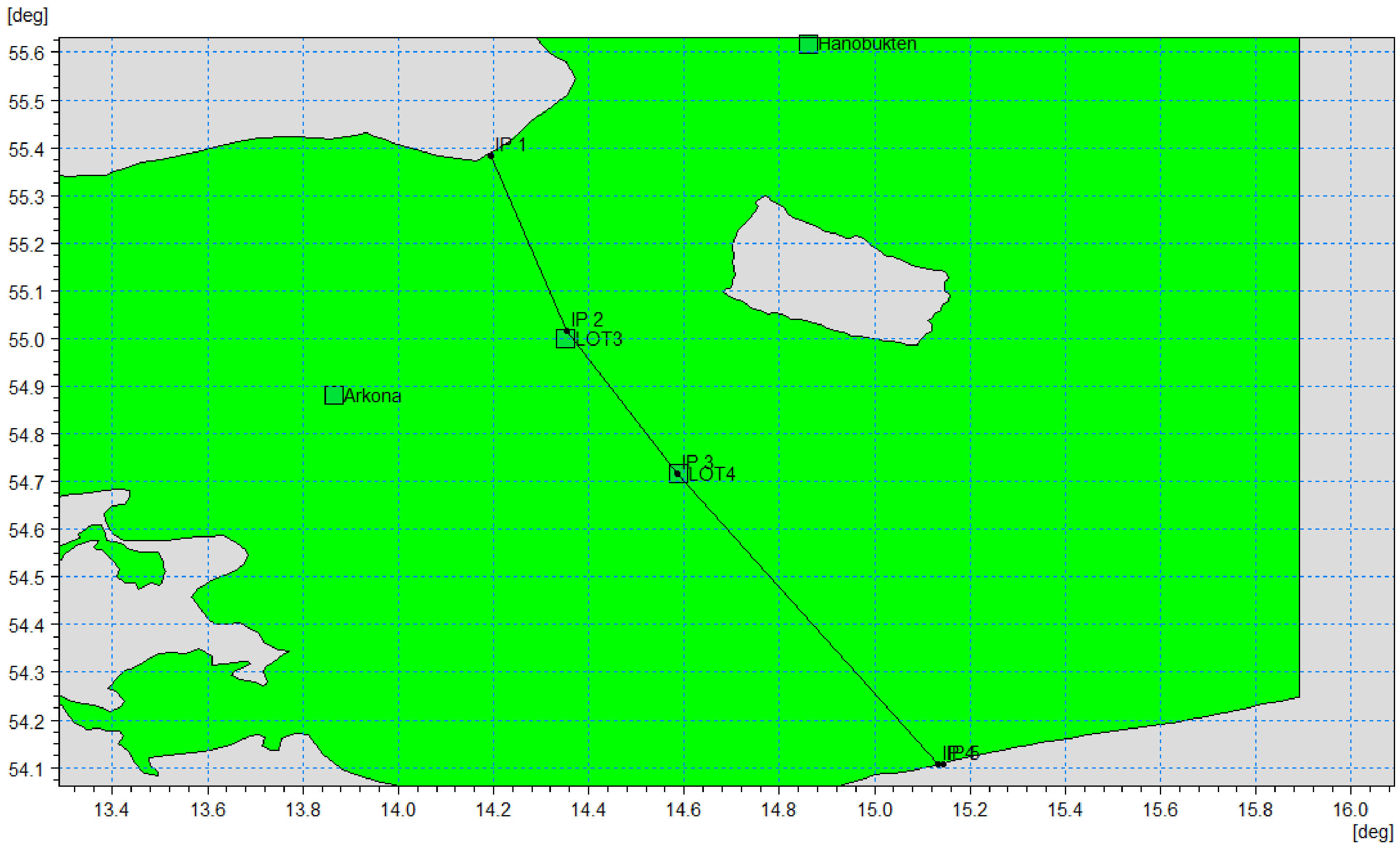

Figure 5.6 **Transect line going from Skåne across Rønne Bank (LOT3 and LOT4) to Pomeranian Bay in Poland**

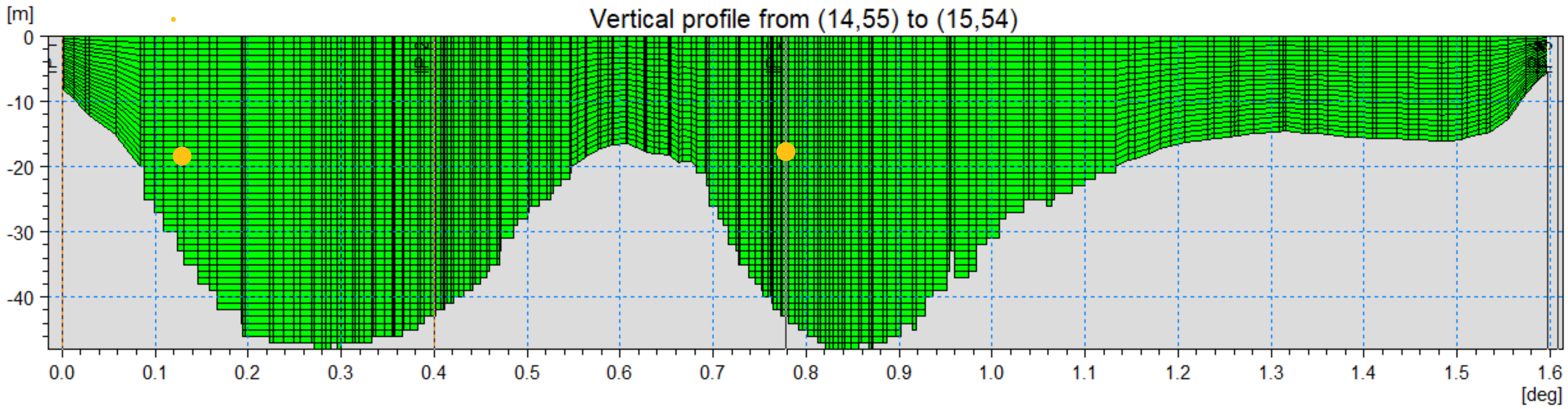

Figure 5.7 Vertical section from Skåne across Rønne Bank to Pomeranian Bay. The markers are at LOT3 (left) and LOT4

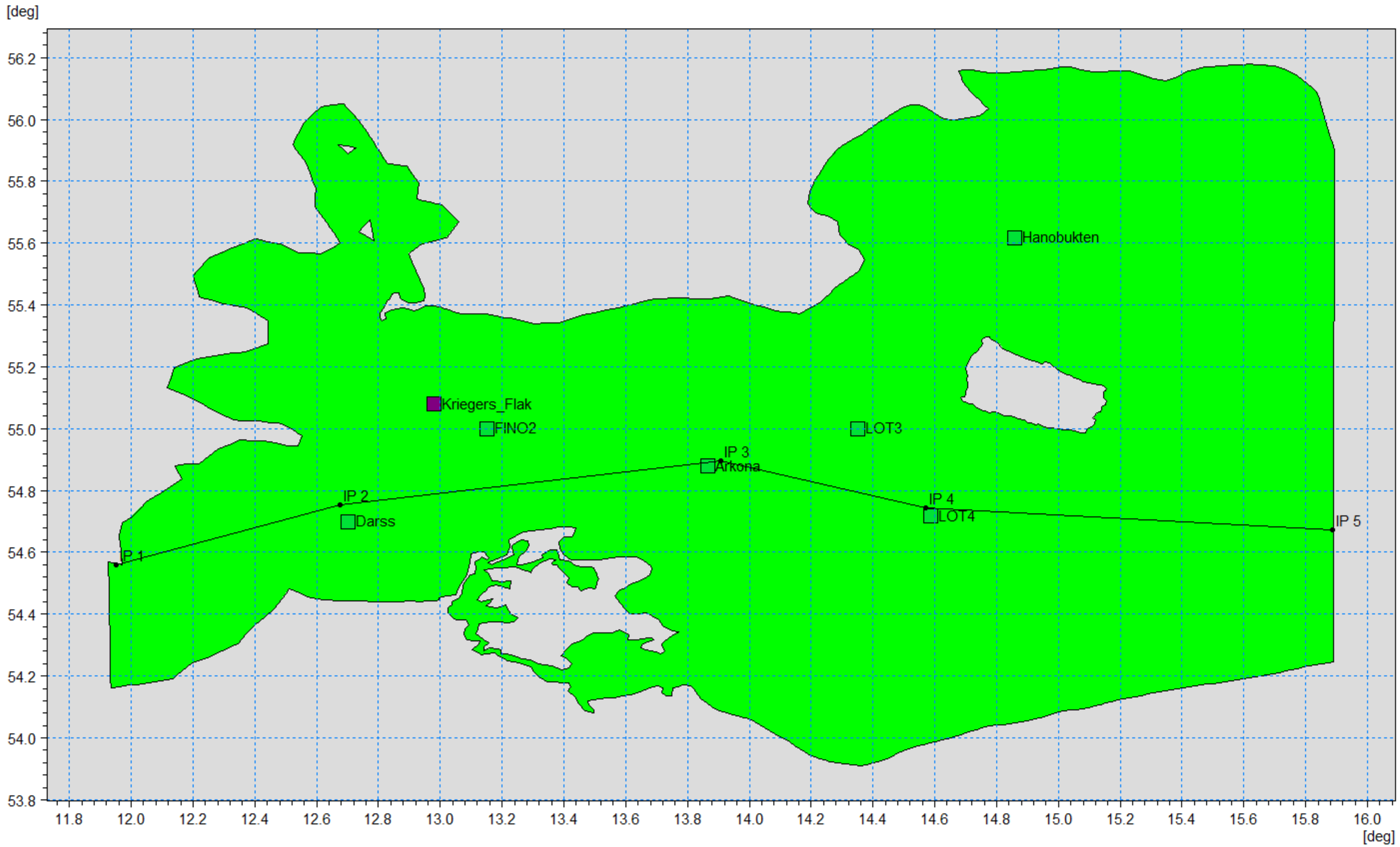

Figure 5.8 Transect line going from Gedser to central Baltic

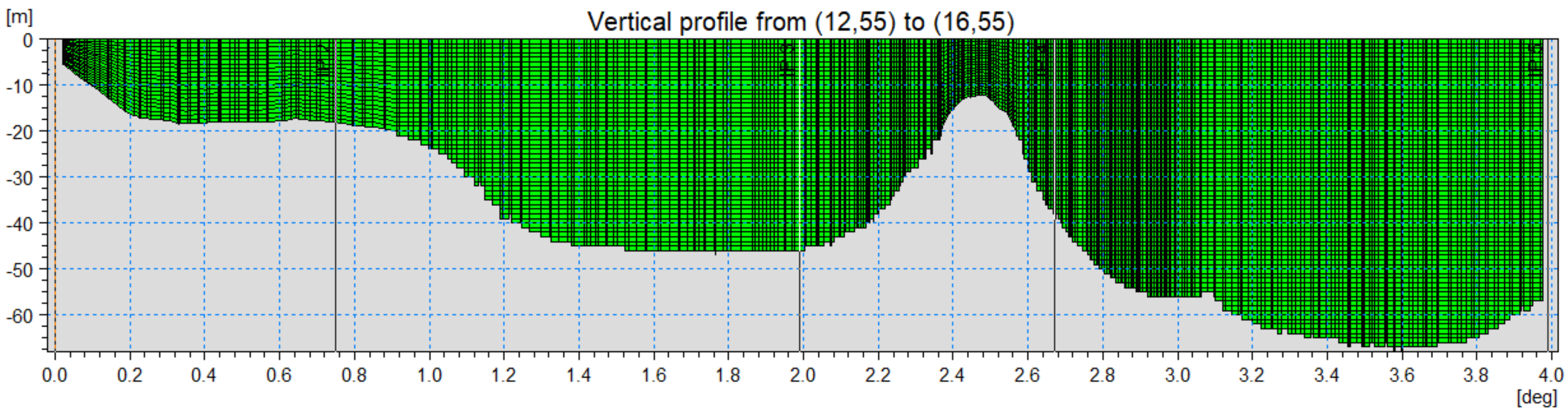

Figure 5.9 Vertical mesh along a transect from Gedser to central Baltic.

The model mesh is shown in Figure 5.4, Figure 5.5, Figure 5.7 and Figure 5.9. The mesh resolution in the OWF area is about 500 m, with increasing coarseness towards the model boundaries. The vertical resolution is maximum 1 m in the sigma-layers down to -20 m, varying in shallow waters as seen in Figure 5.9, and 2 m in the z-layers below. The final model mesh has been smoothed with a simple lowpass filter to even out small-scale rugosity.

5.4.2 Forcing and boundary data

The model was forced by wind and atmospheric conditions at the sea surface. Atmospheric data were sourced from a variety of models (see Table 5.3), basically using the same dataset as was used for the DKBS 3D model, in order to retain consistency. For detail of the DKBS 3D model see [20]. At the open lateral boundaries, the model uses water level variations, currents, and temperature and salinity variations. All are taken from the DKBS model archive. Fresh water inflow from the major rivers is also taken from the DKBS archive.

Table 5.3 Forcings and boundary conditions for HD_{EIBS} model

Dataset	Source	Parameters
Wind	CFSR[10] (1997-2010)	10, wind speed, East and North components
	StormGeo (2010-2023)	10m wind speed, East and North components
Atmospheric conditions	CFSR (1997-2010)	2m air temperature and clearness
Atmospheric conditions	StormGeo (2010-2023)	2m air temperature and clearness
Fresh water	DKBS	River discharge
Boundary conditions	DKBS	Elevations, currents, temperature and salinity

5.4.3 Model calibration

The model was calibrated using the year 2021 and 2022, as this is the period with the most current data available. The calibration data comprised water levels, current profiles, and temperature and salinity. The calibration was an iterative process where the most important model parameters were varied to get the best agreement with observations. Comparison was made with focus on the QQ scatter diagrams.

The most important model parameters are the mesh and resolution and the bed resistance, reflected in the bottom roughness. The final model parameters are summarised in Table 5.4.

[10] Climate Forecast System Reanalysis (CFSR) | Climate Data Guide (ucar.edu)

Table 5.4 HD_{EIBS} model parameters

Parameter	Comment
Bathymetry	Combined (see Table 2.1)
Horizontal resolution	~500m-5km Domain in EIBS about 600m to 1000m
Vertical resolution	20 σ-layers to -20 m, 2m z-levels below
Simulation period	1998-01-01 to 2022-12-31. Data stored at time step interval of 1 hour
Hydrodynamic	
Solution technique	High order
Density	Dependent on temperature and salinity
Bed roughness	Constant
Atmospheric forcing	Combined
Wind drag	Based on (Geernaert, 1990) [4]
Boundary conditions	Flather; Water levels and u-,v-velocity from DKBS
Data assimilation	None
Temperature/Salinity	
Dispersion	Vertical coef.: 0.05 Horizontal coef.: 0.01
Atmospheric heat exchange	CFSR data and StormGeo
Boundary conditions	DKBS
Turbulence	Smagorinsky horizontal, κ-epsilon vertical
Fresh water sources	Salinity 0 PSU; Temperature 10º C
Output	1-hourly 3D fields of eastward and northward water velocity 1-hourly 3D fields of temperature and salinity Time series in selected points with higher frequency

5.5 Hindcast current data – 3D data

5.5.1 Sensitivity studies

The setting up of the 3D current model is an iterative process where model domain, resolution and model parameters are varied to optimise the agreement with observations. Here, the year 2021 was mainly used as the model year, focusing on the stations LOT3 and LOT4, FINO2 and Arkona (see Table 5.1). A formal sensitivity study has not been carried out as the mesh resolution is close to the highest feasible.

5.5.2 Validation of HD_{EIBS} currents

The HD_{EIBS} 3D model was validated using the relevant measurement stations. Shown below are selected validation plots from the main stations.

The two project stations, LOT3 and LOT4, were each equipped with two (2) ADCPs, one downward-looking, mounted on the floating Lidar buoy, and one upward-looking bottom-mounted Upward ADCP

LOT3

The LOT3 ADCP was located on the north side of the Rønne Bank in about 35m depth, basically on the edge of the channel connecting the Arkona Basin with the Bornholm Basin. The current direction roughly follows the direction of the channel. Compared to the water level or wave validation (see Section 4.3.3 and 6.3.4), results are more scattered when looking at the current time series. The distribution, however, is reasonably well represented, as seen in Figure 5.12 and Figure 5.15.

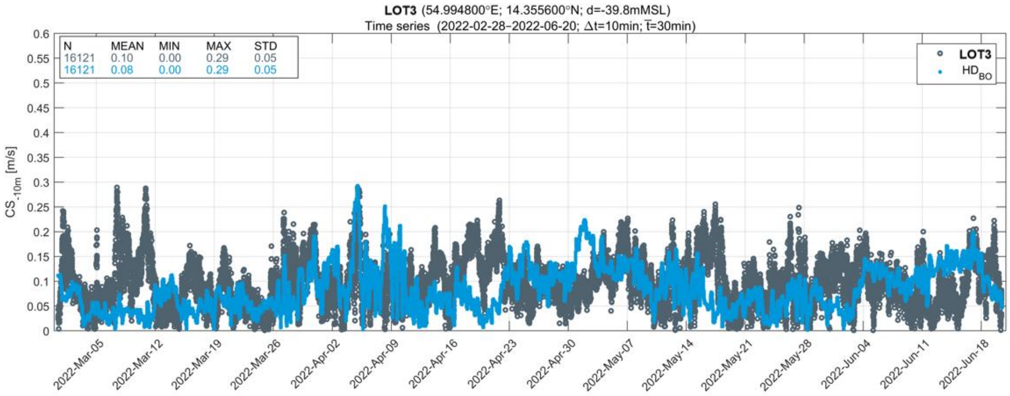

Figure 5.10 Time series of modelled and observed current speed at LOT3, 10 m depth
Observed data are from the Upward ADCP.

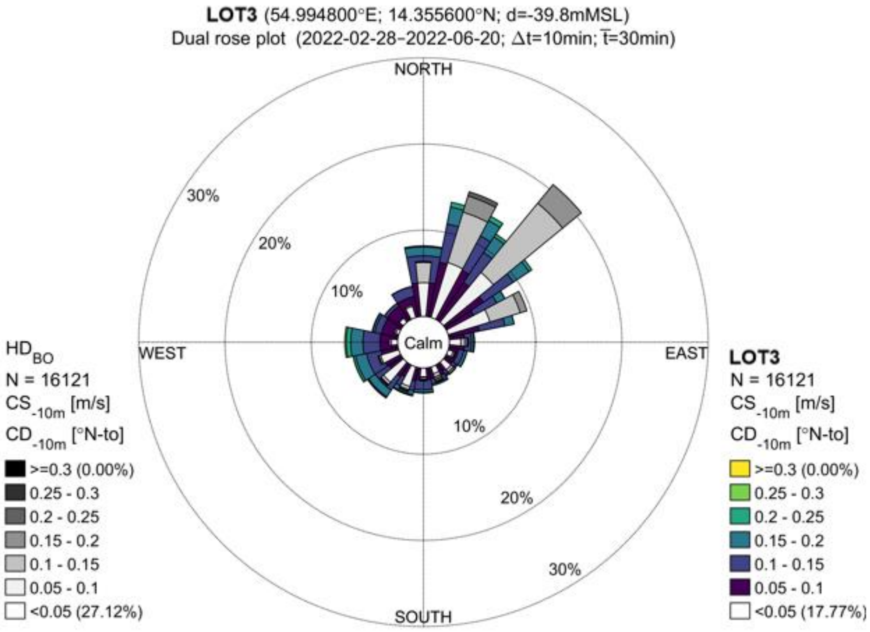

Figure 5.11 Current rose of modelled and observed currents from LOT3, 10 m depth
Observed data are from the Upward ADCP, Direction is “going to ºN”.

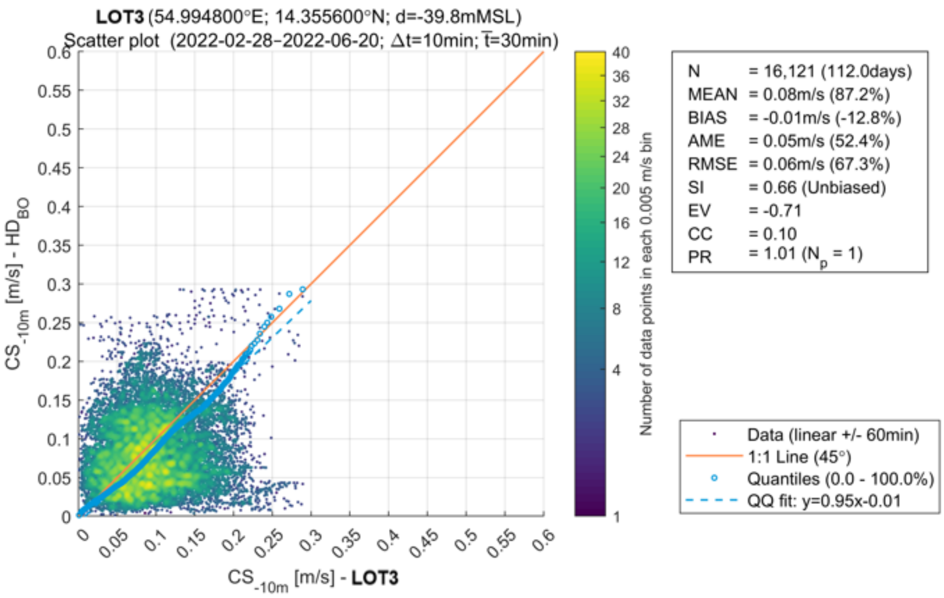

Figure 5.12 Scatter plot of observed and modelled current speed at LOT3, 10 m depth
Observed data are from the Upward ADCP. The plot shows the scatter points (colour indicates density), the QQ-line (blue circles) and fitted QQ line (dashed blue).

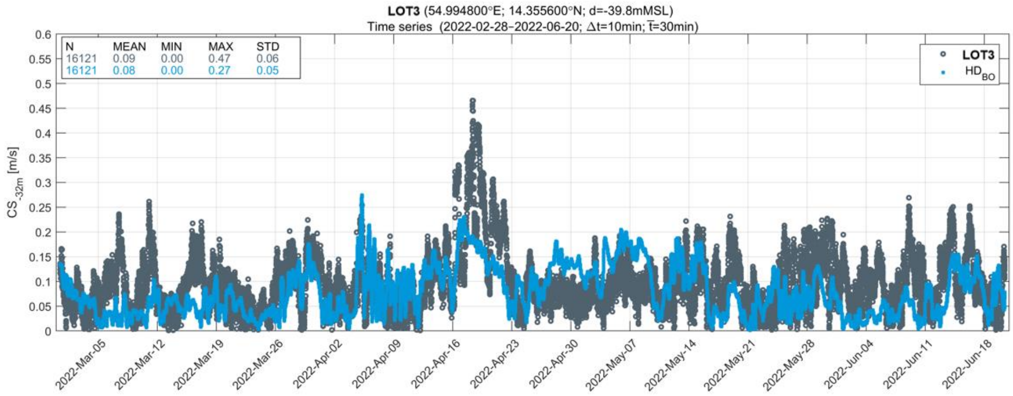

Figure 5.13 Time series of modelled and observed current speed at LOT3, 32 m depth
Observed data are from the Upward ADCP.

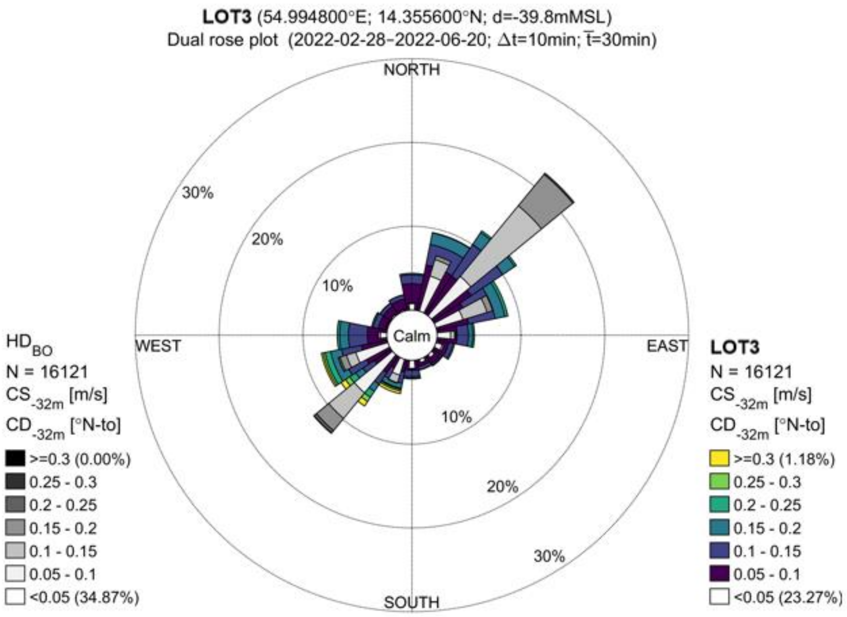

Figure 5.14 Current rose of modelled and observed currents from LOT3, 32 m depth
Observed data are from the Upward ADCP.

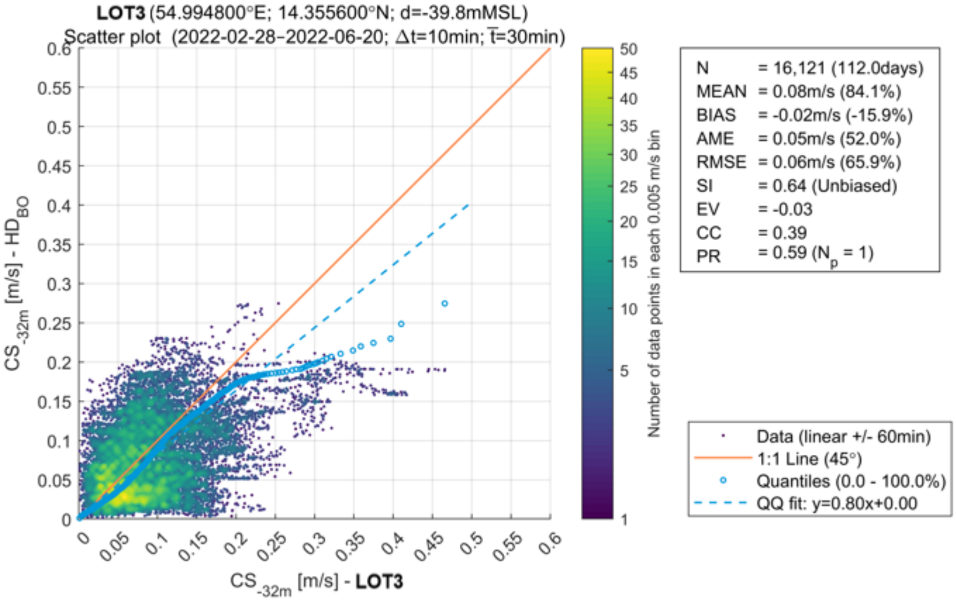

Figure 5.15 **Scatter plot of observed and modelled current speed at LOT3, 32 m depth**
Observed data are from the Upward ADCP.

LOT4

LOT4 is located on the south side of Rønne Bank on the edge of the Pomeranian Basin. The model results indicate that the currents in the area are relatively complex, being formed by the circulation in the Pomeranian Bay and the exchange between the Arkona Basin through the depression south of Rønne Bank. Looking at the observations, the surface currents are predominantly westward. The model validation indicates that currents generally have a low bias, about 10%-20%, especially during three events in January and February 2022, with a higher weight on westward currents.

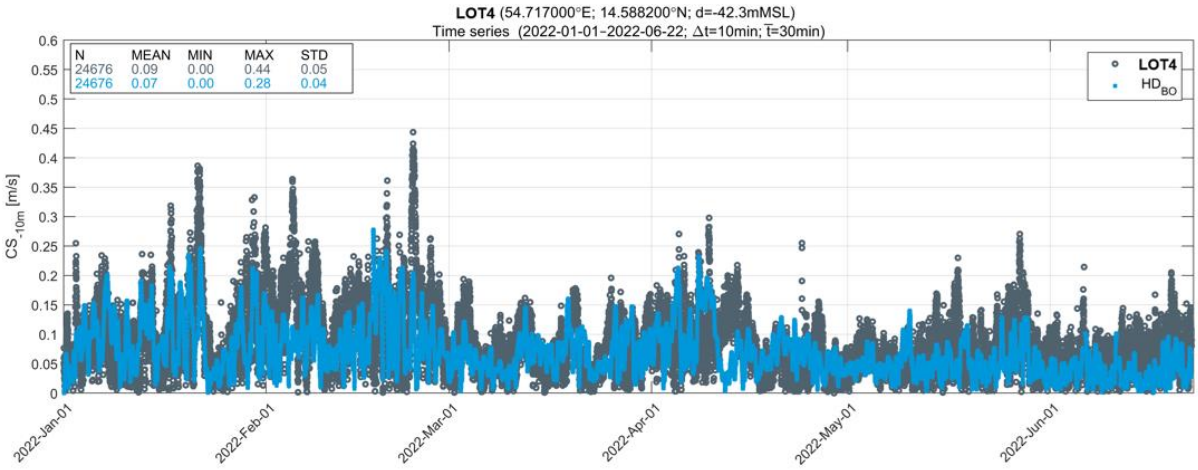

Figure 5.16 Time series of modelled and observed current speed at LOT4, 10 m depth
Observed data are from the Upward ADCP.

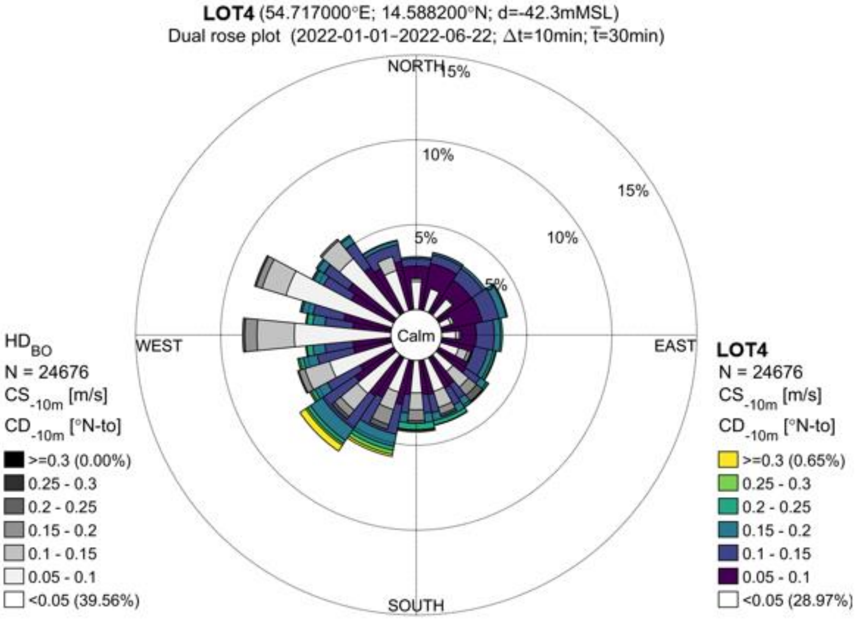

Figure 5.17 Current rose of modelled and observed currents from LOT4, 10 m depth
Observed data are from the Upward ADCP.

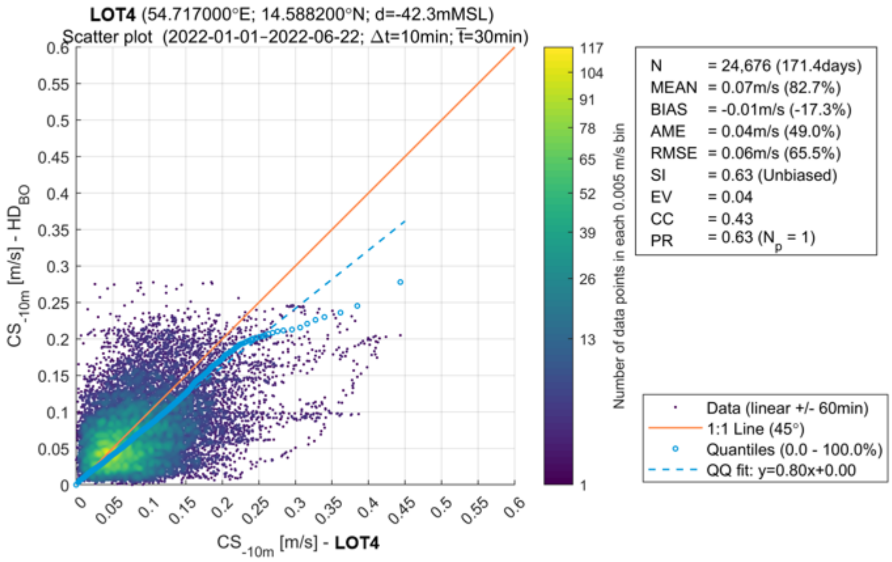

Figure 5.18 Scatter plot of observed and modelled current speed at LOT4, 10 m depth

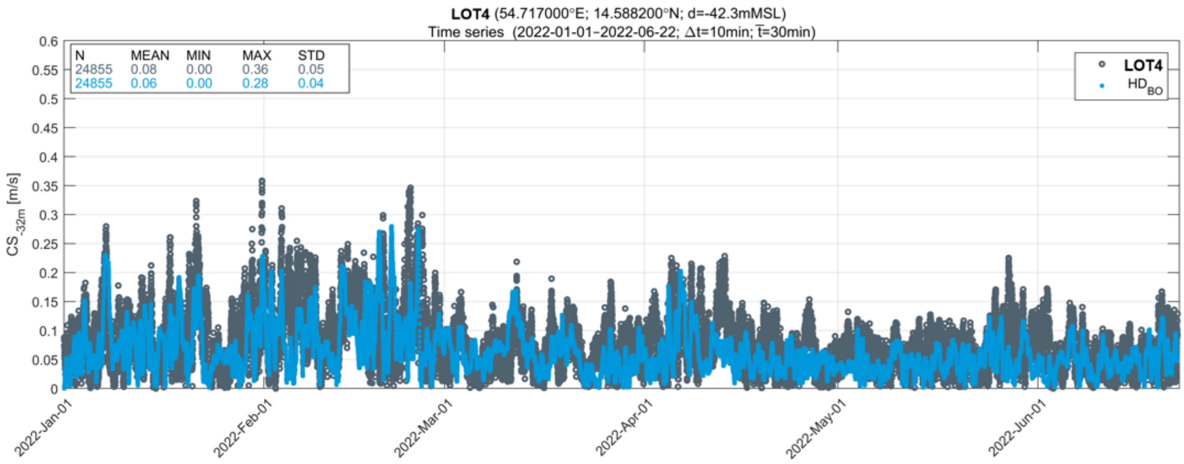

Figure 5.19 Time series of modelled and observed current speed at LOT4, 32 m depth
Observed data are from the Upward ADCP.

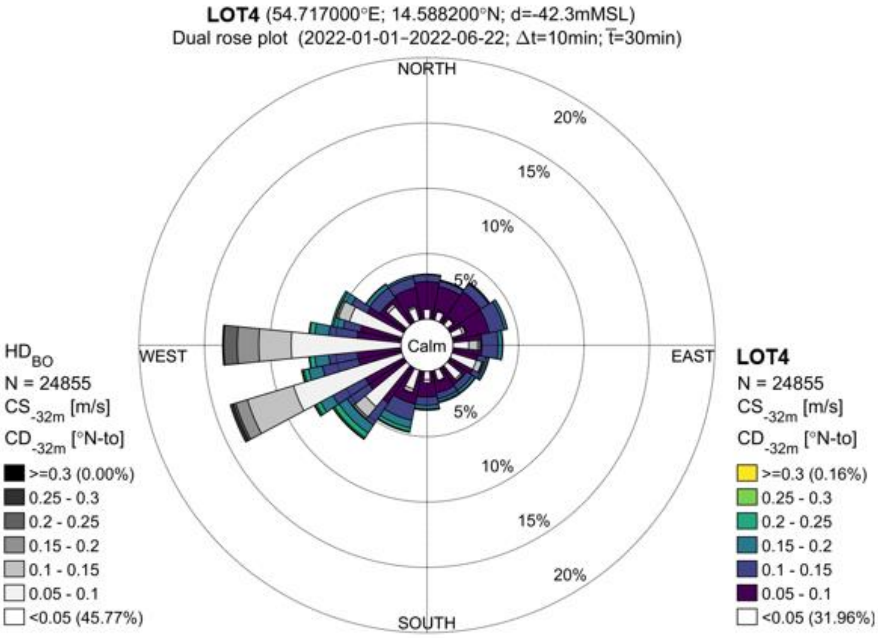

Figure 5.20 Current rose of modelled and observed currents from LOT4, 32 m depth
Observed data are from the Upward ADCP.

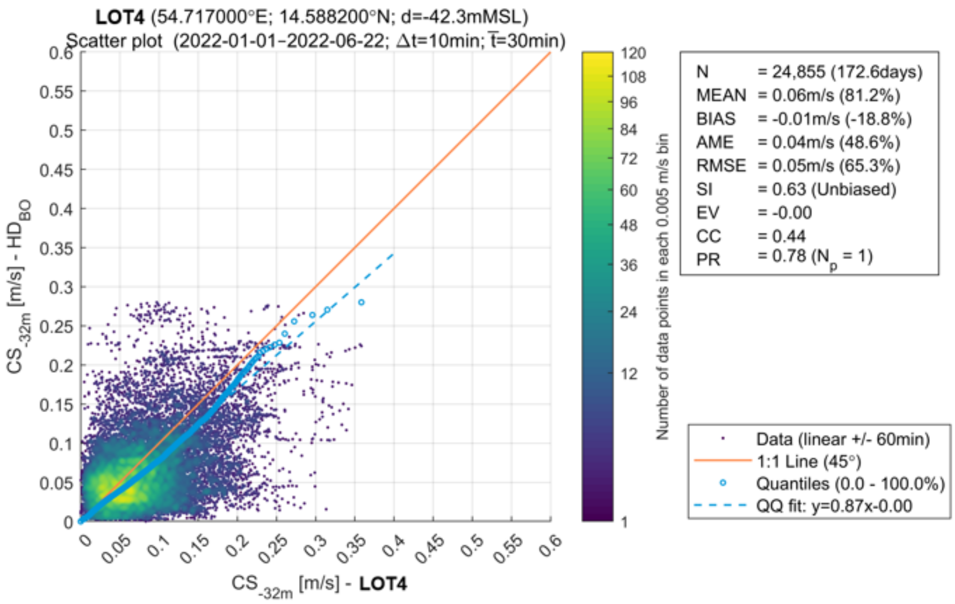

Figure 5.21 Scatter plot of observed and modelled current speed at LOT4, 32 m depth
Observed data are from the Upward ADCP.

Arkona Basin

The Arkona buoy is a long-term installation operated by Bundesamt für Seeschifffahrt und Hydrographie, Germany, since 2004 in the central part of the Arkona Basin. The buoy includes a current meter.

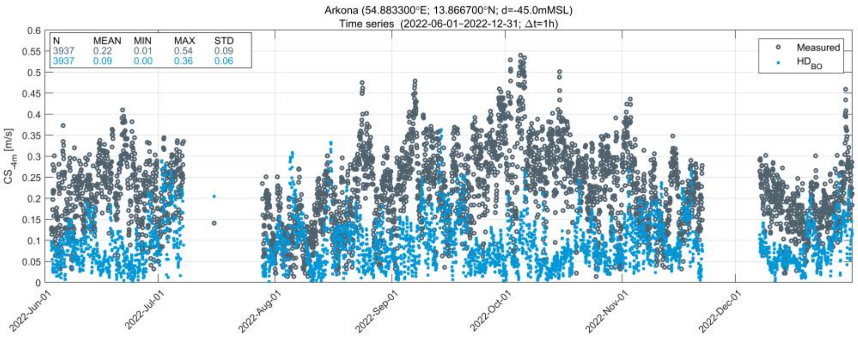

Figure 5.22 Time series of modelled and observed current speed at Arkona buoy, 4 m depth

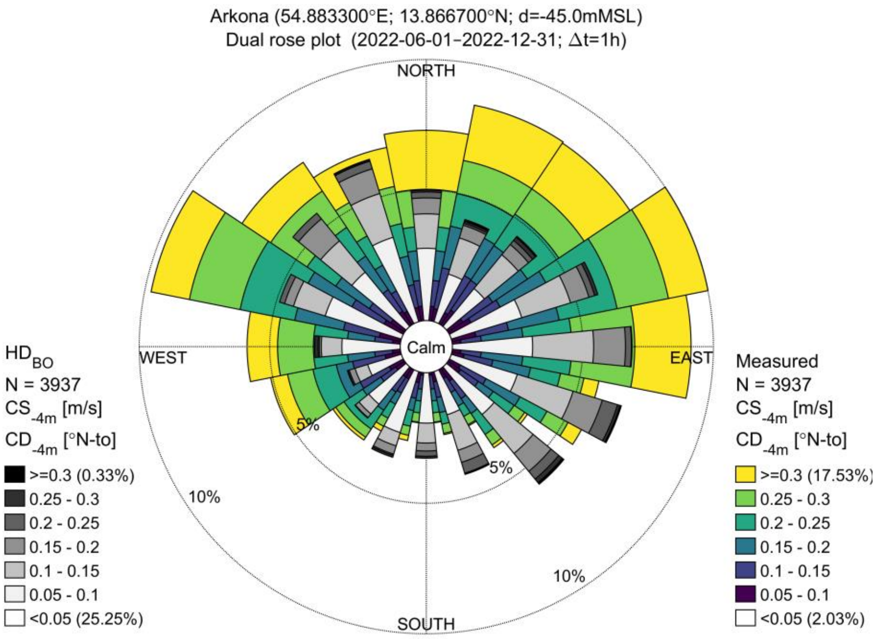

Figure 5.23 Current rose of modelled and observed currents from Arkona buoy at 4 m depth

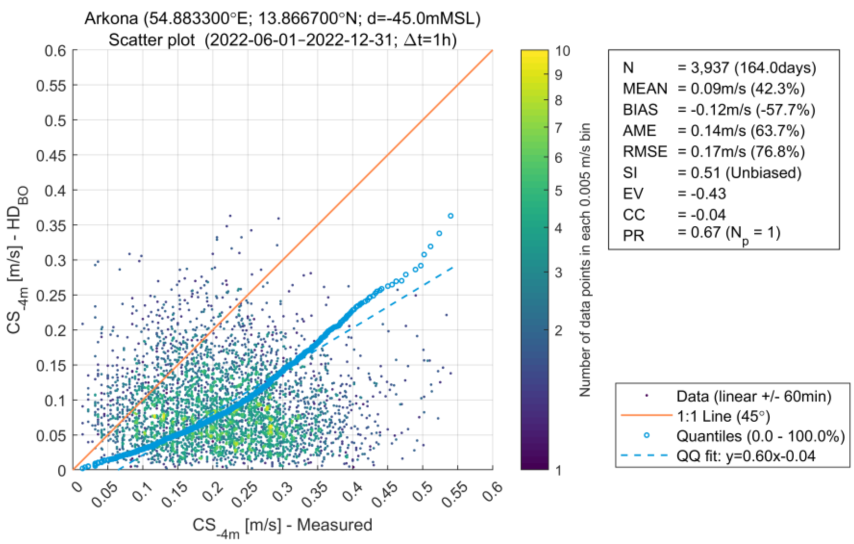

Figure 5.24 Scatter plot of observed and modelled current speed at Arkona buoy, 4 m depth

FINO2

FINO2 is a metmast located south of Kriegers Flak (see Figure 5.3), operated by Bundesamts für Seeschifffahrt und Hydrographie, Deutchland (BSH) for long-term. It is equipped with an ADCP current meter, data from which was made available to this study.

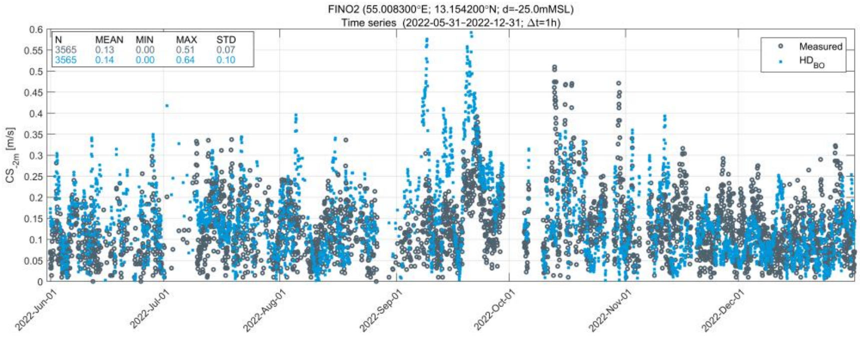

Figure 5.25 Time series of modelled and observed current speed at FINO2, 2 m depth

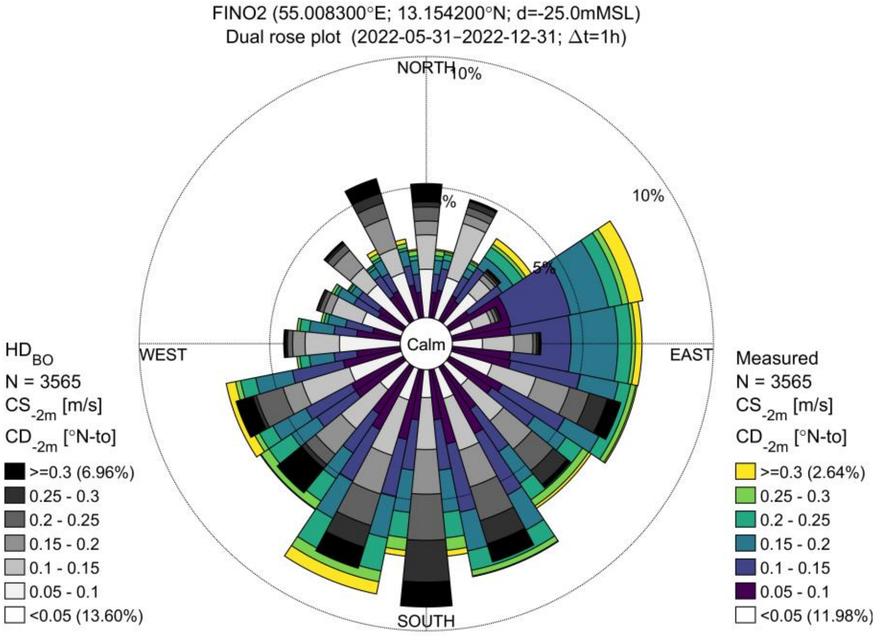

Figure 5.26 Current rose of modelled and observed currents from FINO2 at 2 m depth
Direction is “going to ºN”.

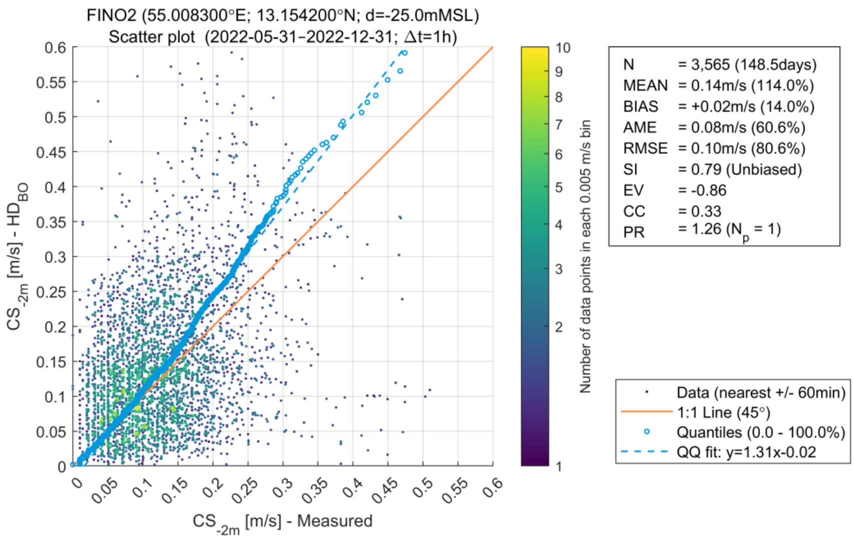

Figure 5.27 Scatter plot of observed and modelled current speed at FINO2, 2m depth

Kriegers Flak

Kriegers Flak, in this context, is a future windfarm site located at the confluence of the Danish, the Swedish and the German EEZs. At this site, an ADCP buoy has been deployed for a period of time (see Table 5.1).

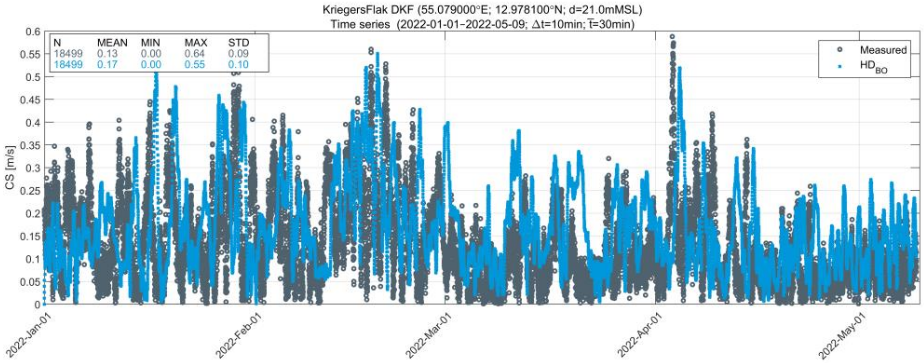

Figure 5.28 Time series of modelled and observed current speed at Kriegers Flak, 1 m depth

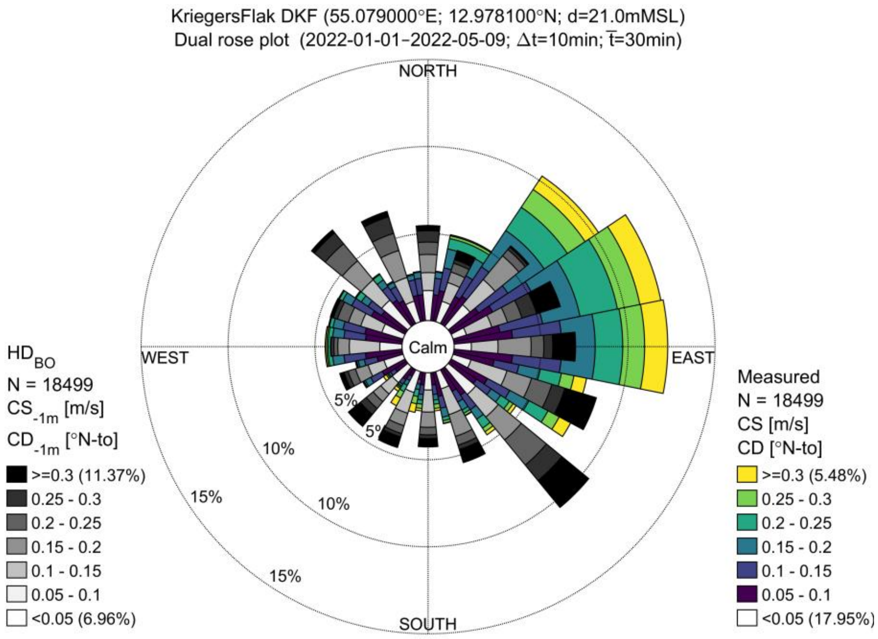

Figure 5.29 Current rose of modelled and observed currents from Kriegers Flak buoy at 1 m depth

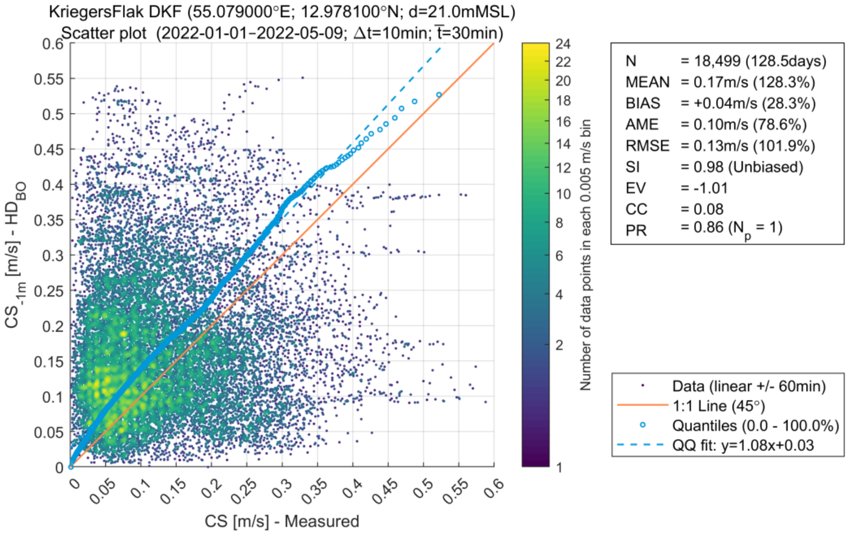

Figure 5.30 Scatter plot of observed and modelled current speed at Kriegers Flak, 1 m depth

5.5.3 Validation of extreme events

During the periods with measurements of currents, there were no significant extreme events. However, there were two events in the measured time series that are notable, as discussed below. The events are:

- At the LOT4 Station on 22 February 2022, where a 0.45 m/s current speed at 10 depth was measured
- At the LOT3 Station on 19 April 2022, where a 0.45 m/s current speed at 32 m depth was measured.

LOT4 in February 2022

The wind had been steadily coming from SW at around 10m/s and then turned through N, E and S with strong winds at about 20m/s. This induced a strong current across the Rønne Bank, as seen below in Figure 5.32.

LOT4 is located just south of Rønne Bank, and it seems that the model does not reach 0.45m/s measured at the site but does indicate currents up to about 0.7m/s (modelled) just North of the site. From the vertical sections it is seen that the vertical variation in current is changing across the section, but that the current profile is relatively constant above the halocline in 30 m-40 m depth during the event.

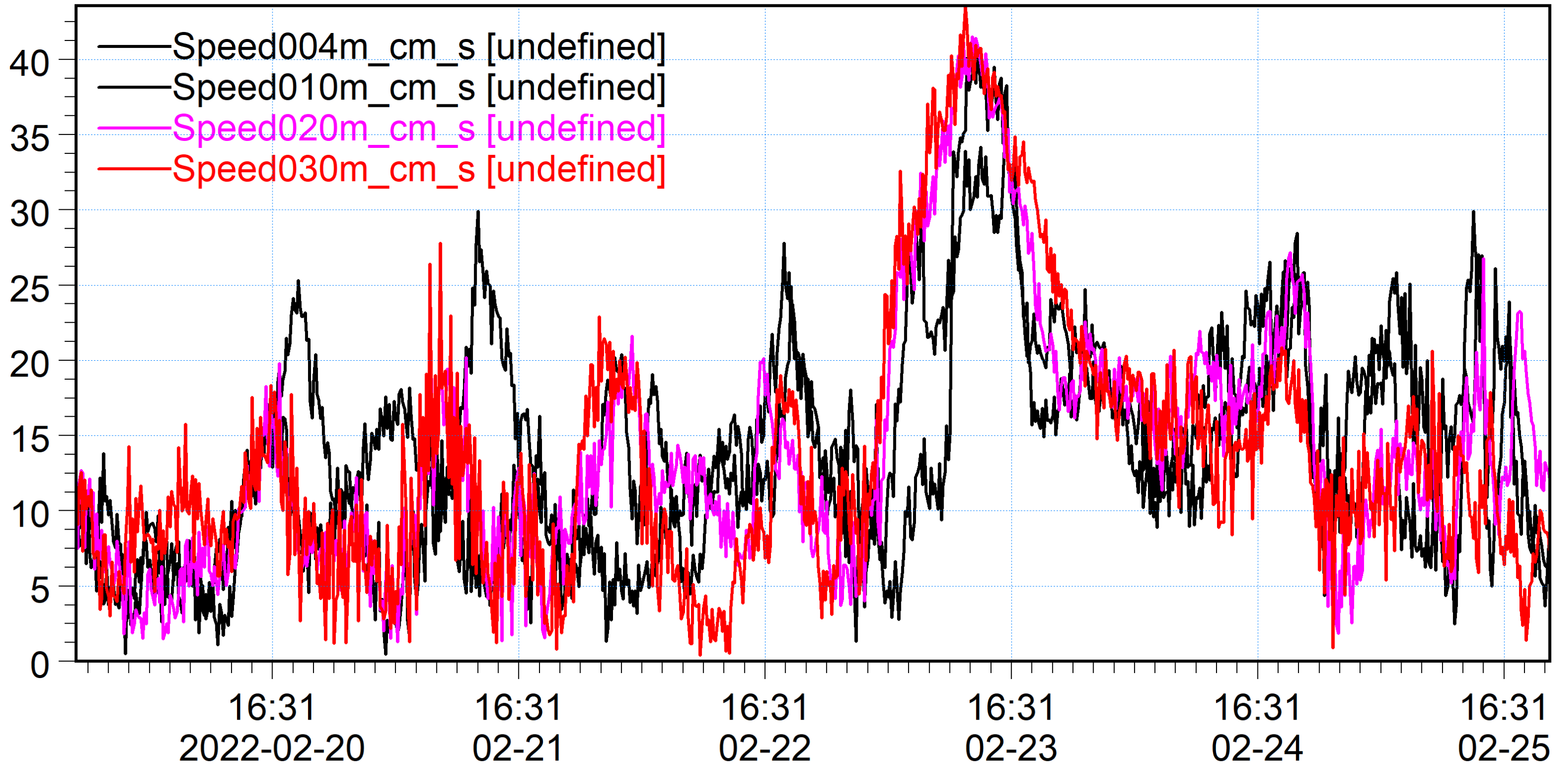

Figure 5.31 Zoom in on the measured current speed in four (4) depths at LOT4 during the February 22 event

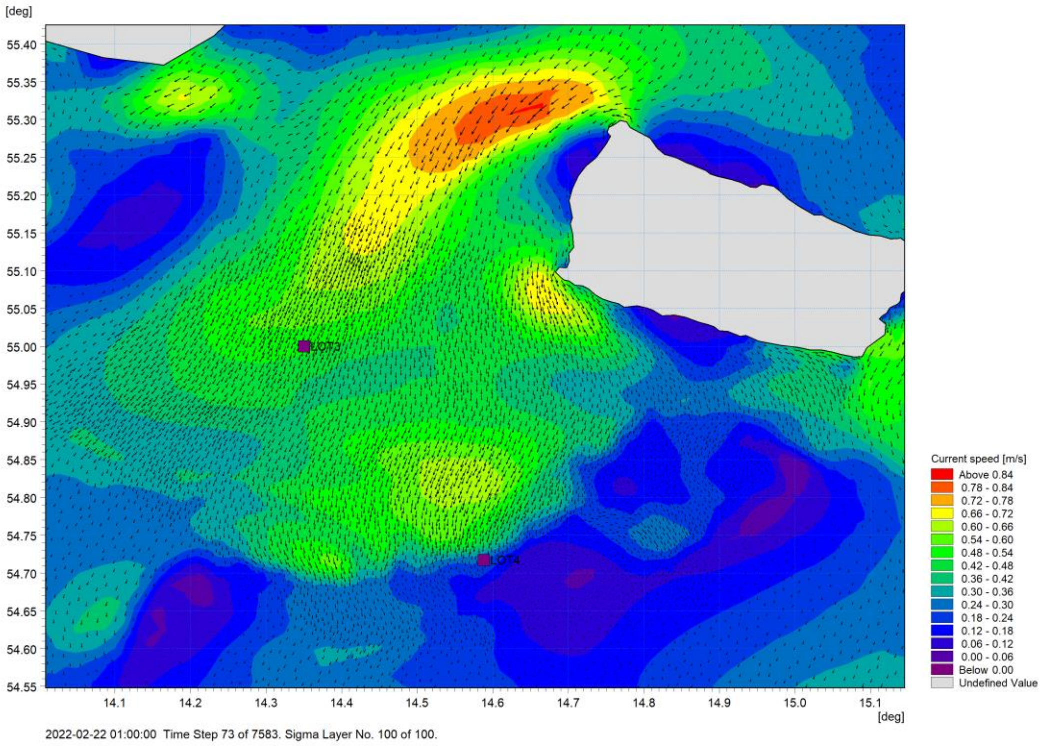

Figure 5.32 Map of surface currents during February 2022 event

The map indicates relatively strong currents across Rønne Bank. The LOT4 station is located in a strong gradient zone, where modelled currents reach 0.7 m/s (on 2 February 2022 at 01:00)

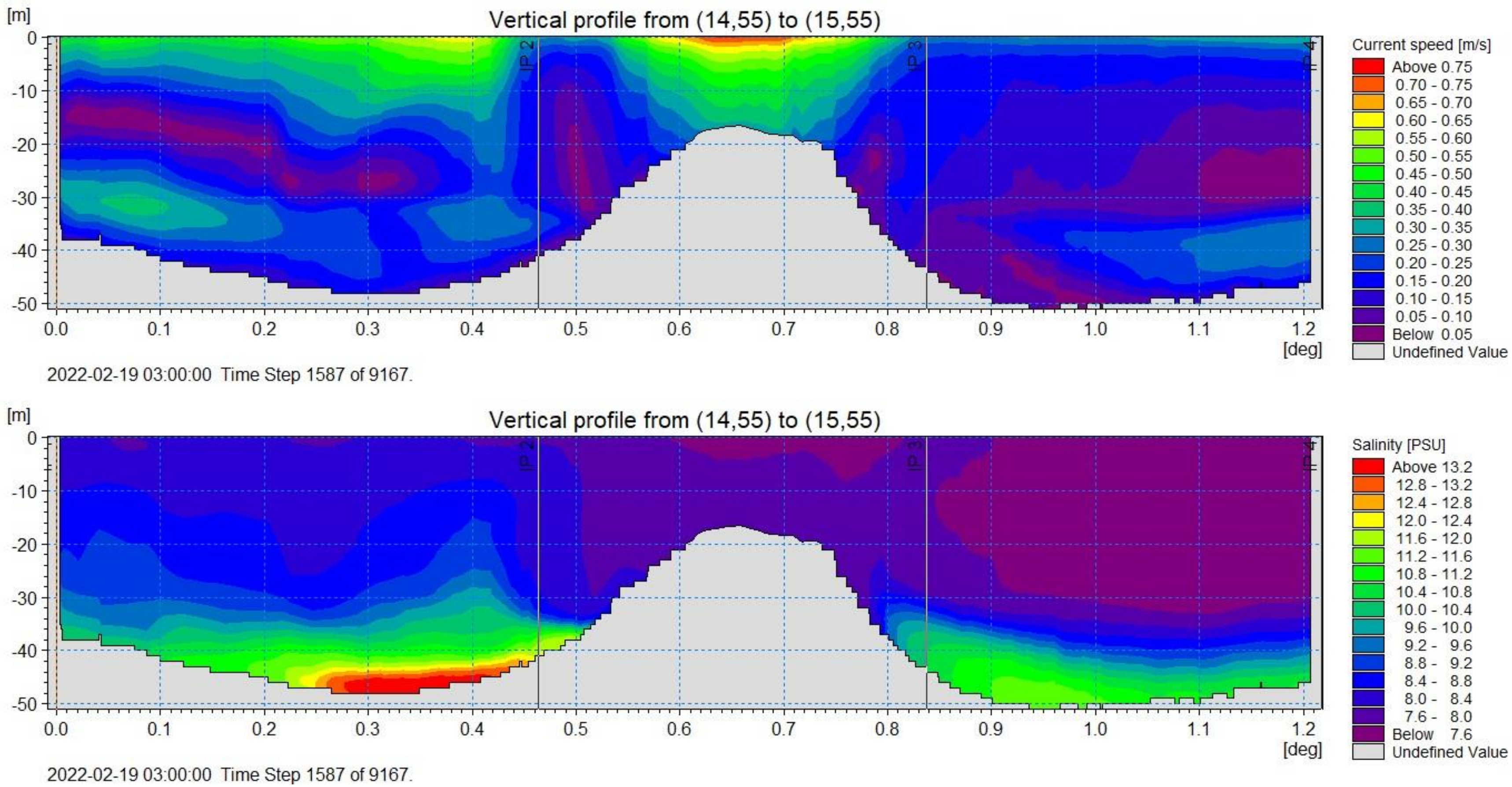

Figure 5.33 Vertical section with current speed (upper) and salinity (lower) from Skåne across Rønne Bank to Pomeranian Bay
The two vertical markers indicate LOT3 and LOT4.

LOT3 in April 2022

During late April 2022, the wind is from W about 10-15 m/s, turning over N to E. The surface currents at the site during the same period reach 0.4 m/s towards SW. From the map in Figure 5.35 it shows a relatively complex current system with strong currents in the channels north and south of the Rønne Bank. The vertical section indicates a relatively constant profile above the halocline at the two sites.

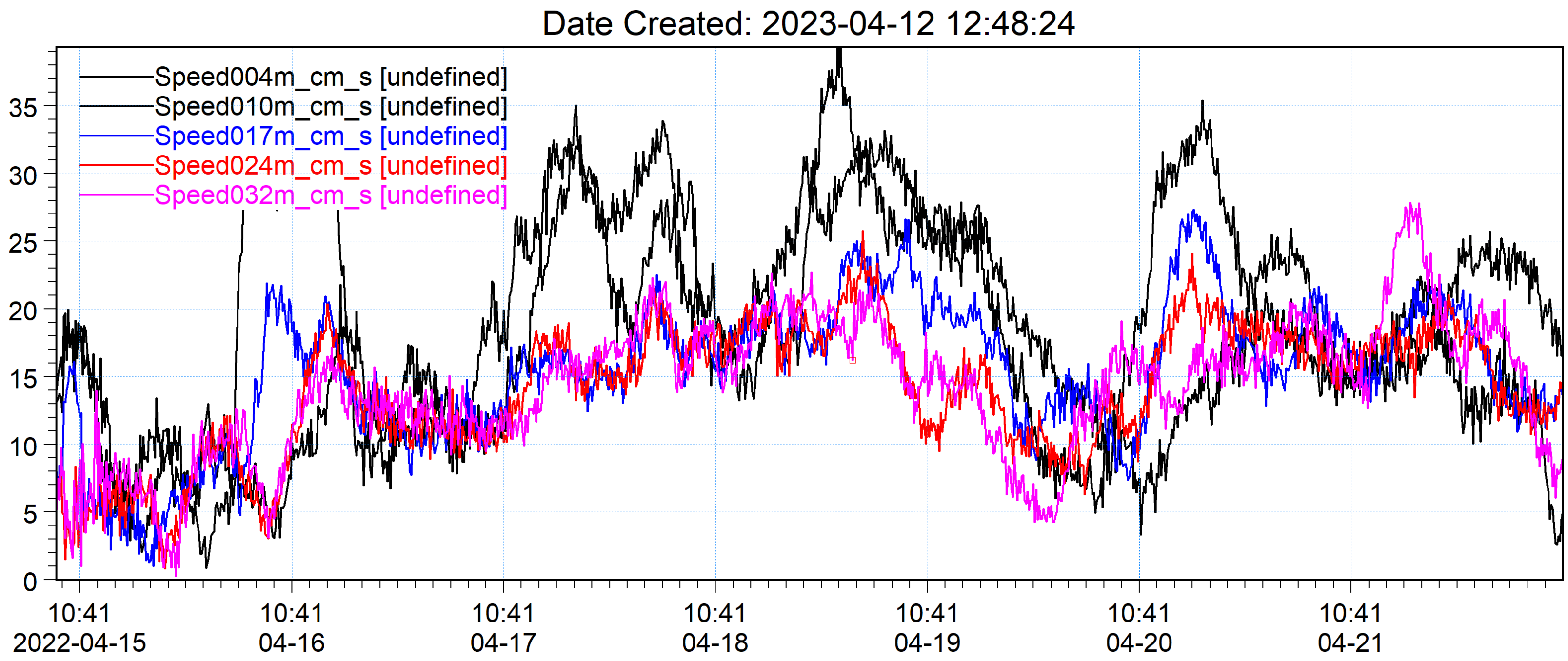

Figure 5.34 Measured current speed at LOT3 during late April 2022

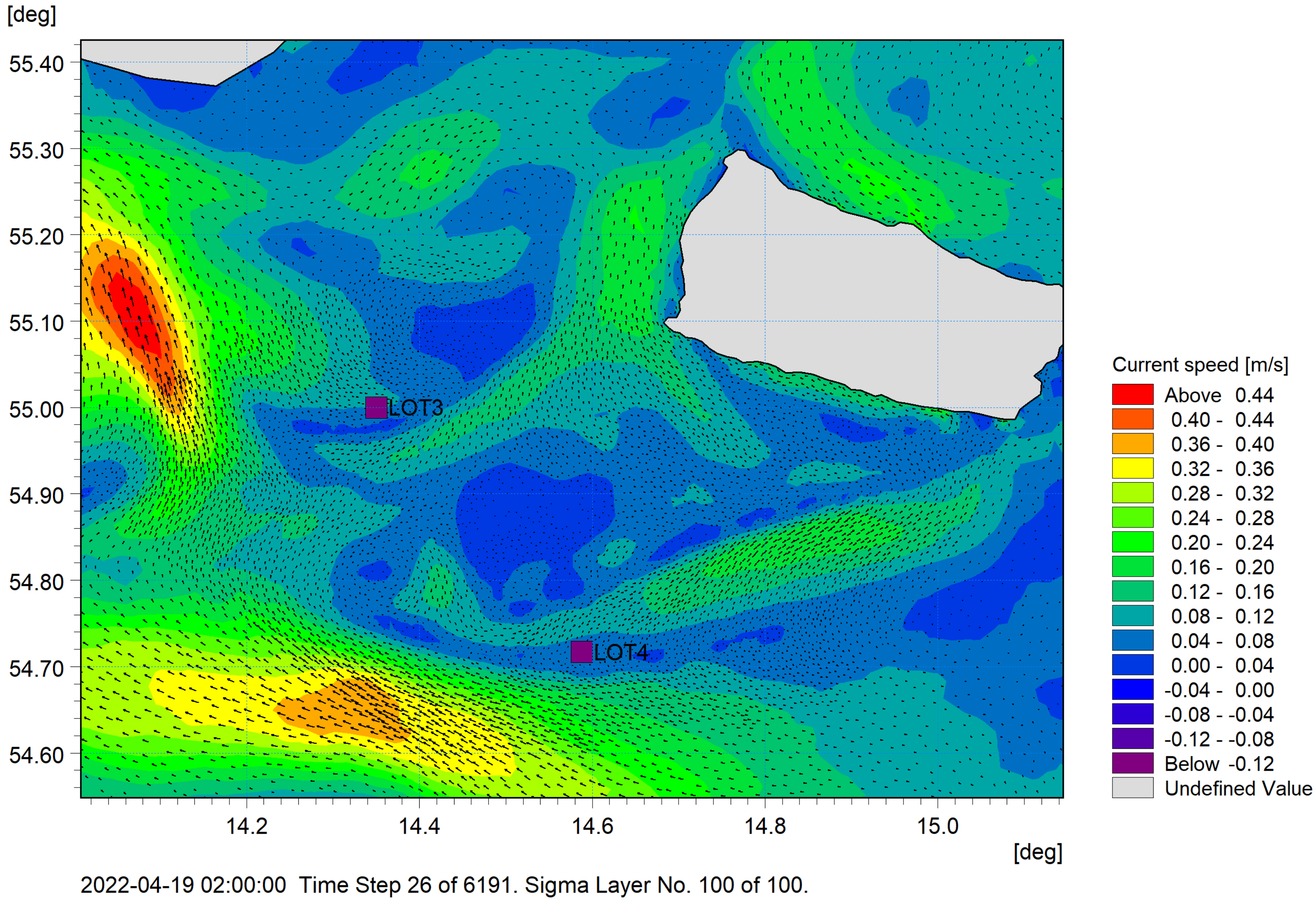

Figure 5.35 Map of surface current speed during the April 2022 event

LOT3 is located on the northern edge of the Rønne Bank.

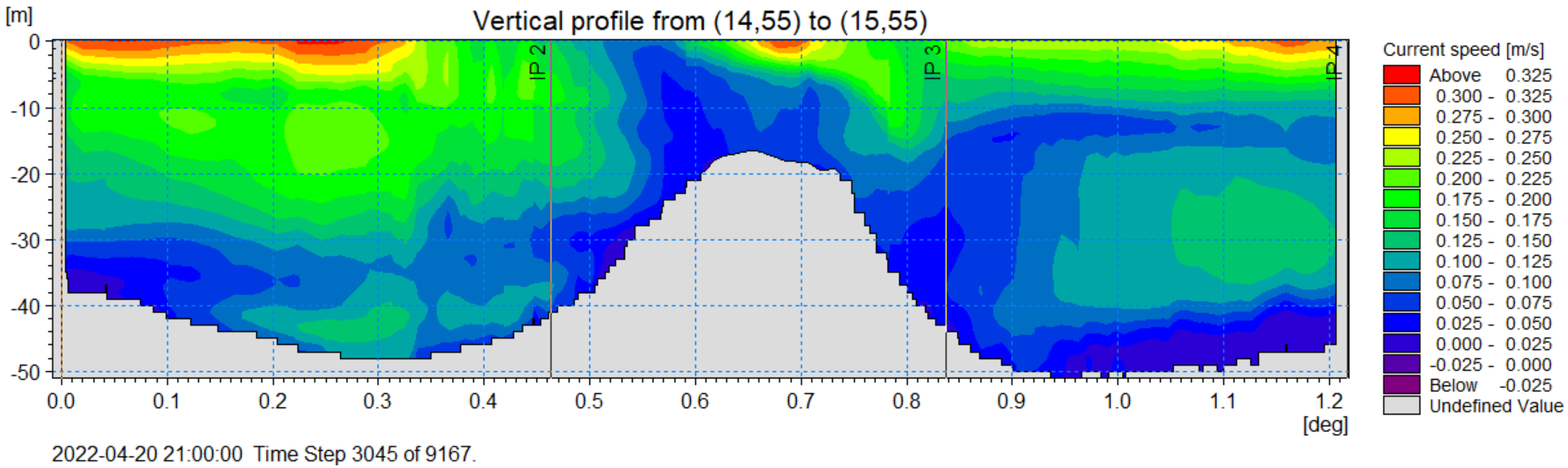

Figure 5.36 Vertical section of currents from Skåne across Rønne Bank to Pomeranian Bay
The vertical markers indicate LOT3 and LOT4.

5.6 Description of the vertical water column structure

In the Baltic Sea, the vertical structure of the water column has a significant influence on the currents and the circulation. The Baltic is nearly permanently stratified as a result of the inflow of freshwater from river runoff and dense salty water in exchange with the Kattegat Sea and North Sea. In the interest area, a few stations have profile measurements of temperature and salinity, enabling a validation of the model's representation of the water masses.

5.6.1 Current profiles

In Figure 5.37 and Figure 5.38 is shown the current profiles during the observed periods at LOT3 and LOT4. Profiles are shown for various percentiles, modelled and measured.

It is seen that the profiles are relatively constant with a narrow (about 5m) boundary layer near the seabed and for the observations, a layer near the surface where it appears to be affected by noise and sidelobes, such that data may not be accurate there. The modelled profiles display a variation close to a theoretical power-law profile and however generally a lower current than observed, especially for the higher percentiles.

In general, DHI recommends using the actual current profiles from the MIKE 3 hindcast. In the figures it is seen that the profiles appear relatively constant for median and 95% percentile currents. However, from the figures either a constant current profile or better the recommended DNV power-law profile will give a reasonable approximation. The current profile generally does not display any significant dynamic influence of the pycnocline '

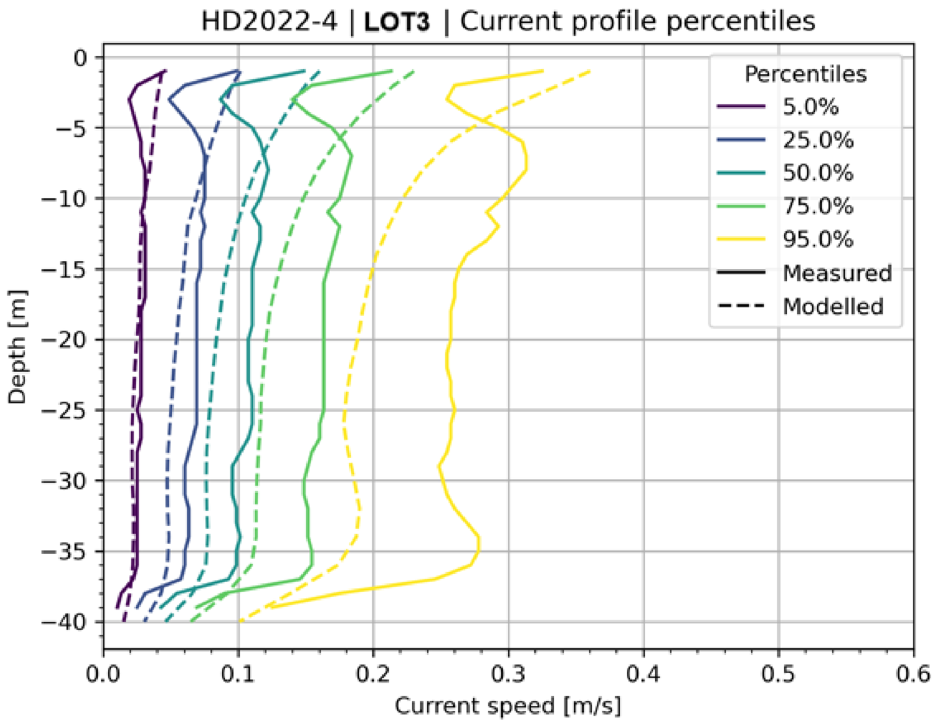

Figure 5.37 Measured and modelled current profile statistics at LOT3

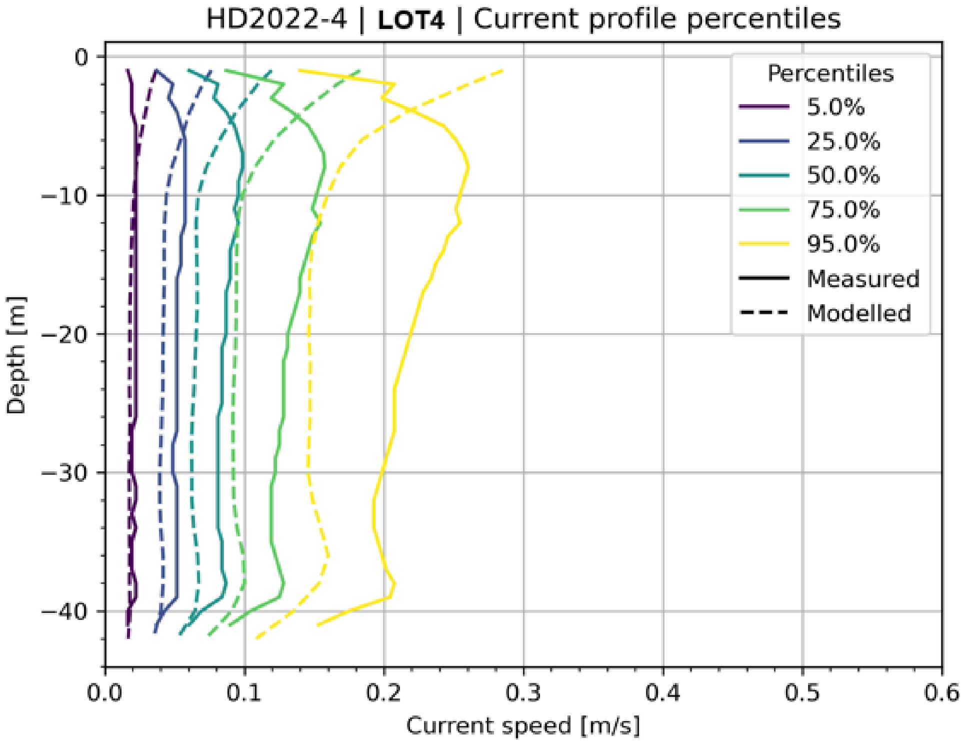

Figure 5.38 Measure and modelled current profile statistics at LOT4.

5.6.2 Pycnocline dynamics

In Figure 5.39 is shown the measured density in 4 levels at LOT4 during 2022 and in Figure 5.40 is shown a Houmoller plot (temperature contours in a time-depth axes) from LOT4 during 2022. The density variations in the upper layers at the site are mainly controlled by the temperature. The pycnocline at the site is seen to develop from April to November, mainly due to temperature differences (up to about 14 C in summer) as the dense saline bottom water stays in deeper basins (ref Burchard). The site is located on the SE side of Ronne Bank, thus the denser water tends to flow eastward only in the deepest part of the channels NW and SE of the site. The data indicate there is a gradual increase in density with a relatively weakly defined pycnocline deepening from 18m in June to 30m in September. The model results indicate that similarly a temperature induced weak pycnocline, typically in 10m depth during early summer and deepening during late summer and autumn. In Figure 5.41 is shown temperature profile statistics from 2021 and the profile on the day with the largest difference.

In It should be noted that there is not a significant footprint of the pycnocline in the current profiles at this site. The reason being that the pycnocline often stays in deeper basins and that due to the convergence through the Bornholm Channel, currents are relatively high.

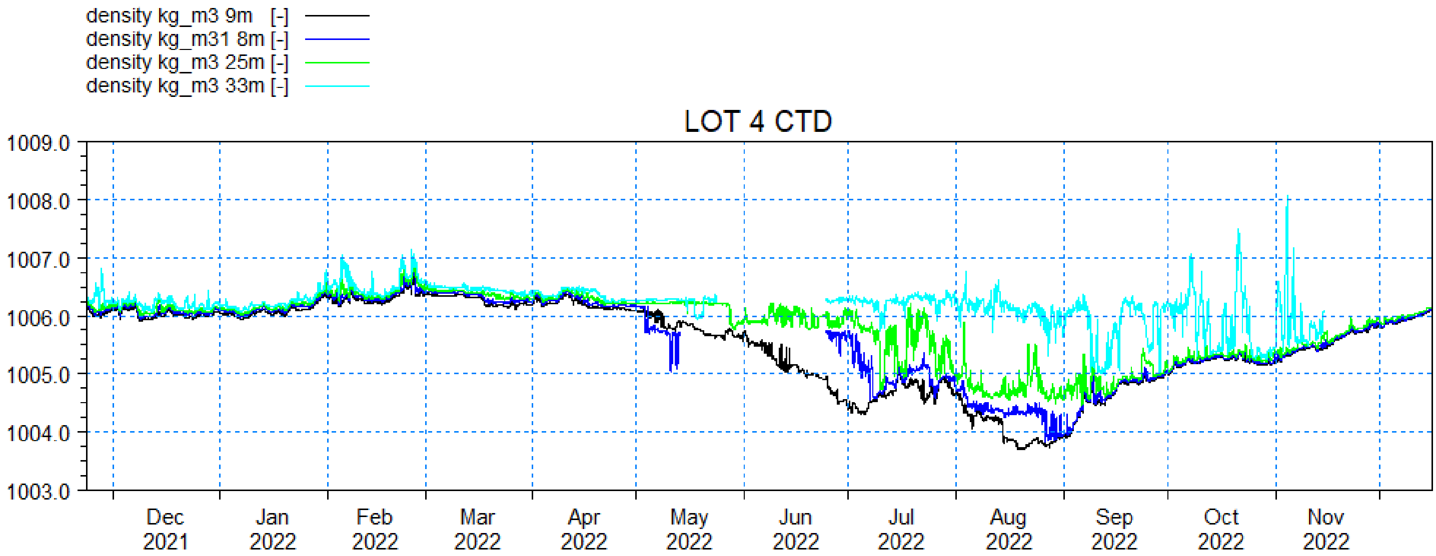

Figure 5.39 Timeseries of measured density at LOT4 at 4 depths

In Figure 5.42, time series of modelled and measured temperature at 4 different depths are shown. It is seen that the surface layers are following a seasonal variation. The upper 3 levels follow the same pattern and are in the same water mass inside the mixed layer, with some excursions, while the lowermost at 33 m has a distinctly different pattern, as this is immersed in the waters below the pycnocline.

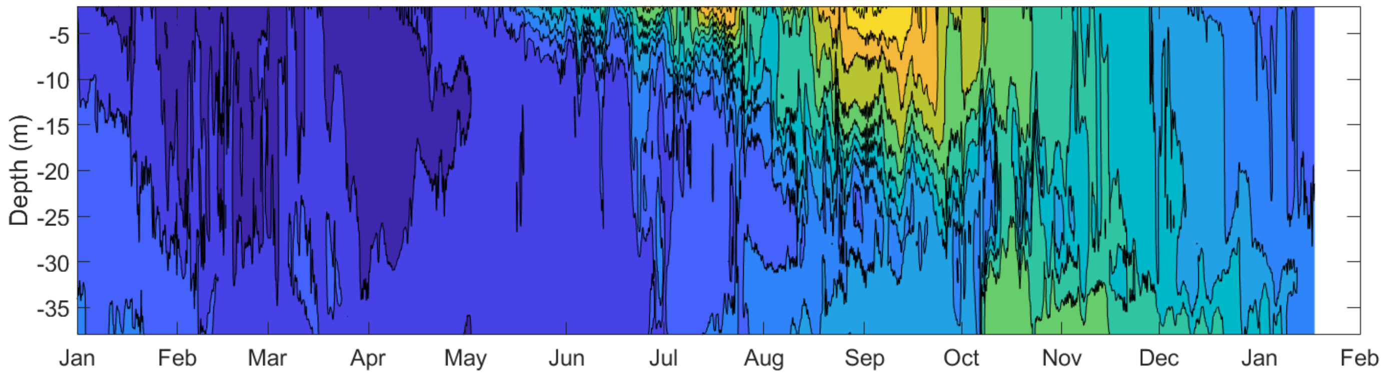

Figure 5.40 Houmoller plot of modelled temperature in LOT4 during 2022.

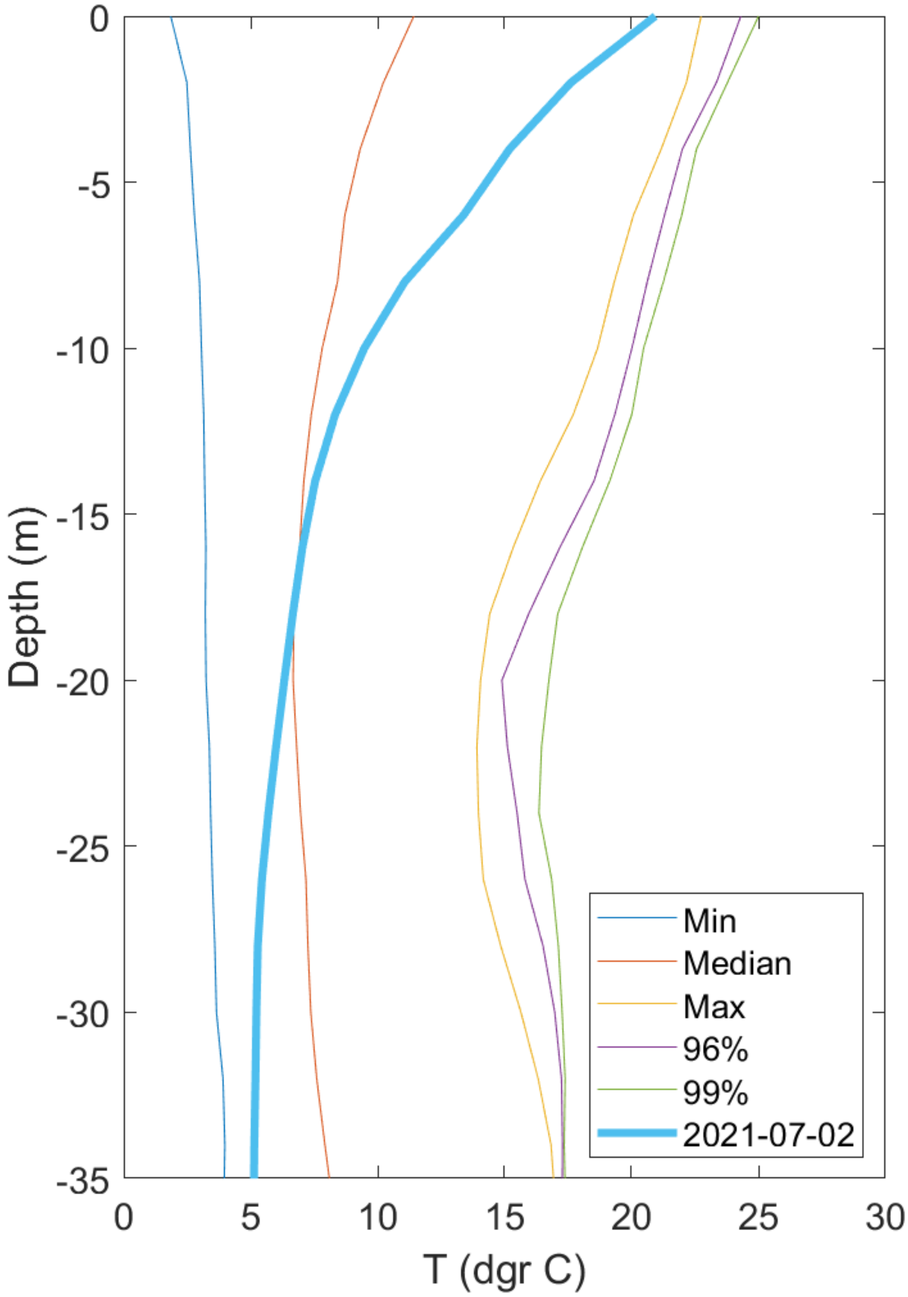

Figure 5.41 Temperature profile statistics at LOT4.
Also shown is the profile from the day with the largest temperature difference.

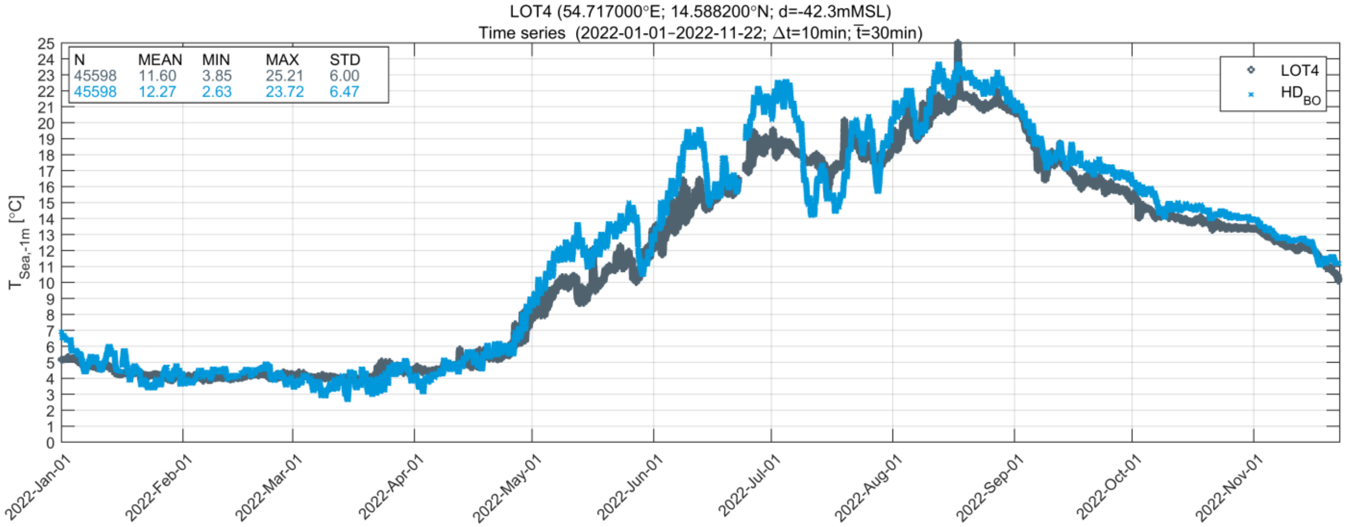
LOT4 (54.717000°E; 14.588200°N; d=-42.3mMSL)
Time series (2022-01-01–2022-11-22; Δt=10min; t̄=30min)
N MEAN MIN MAX STD
45598 11.60 3.85 25.21 6.00
45598 12.27 2.63 23.72 6.47
LOT4
HDBO
TSea,-1m [°C]
2022-Jan-01
2022-Feb-01
2022-Mar-01
2022-Apr-01
2022-May-01
2022-Jun-01
2022-Jul-01
2022-Aug-01
2022-Sep-01
2022-Oct-01
2022-Nov-01

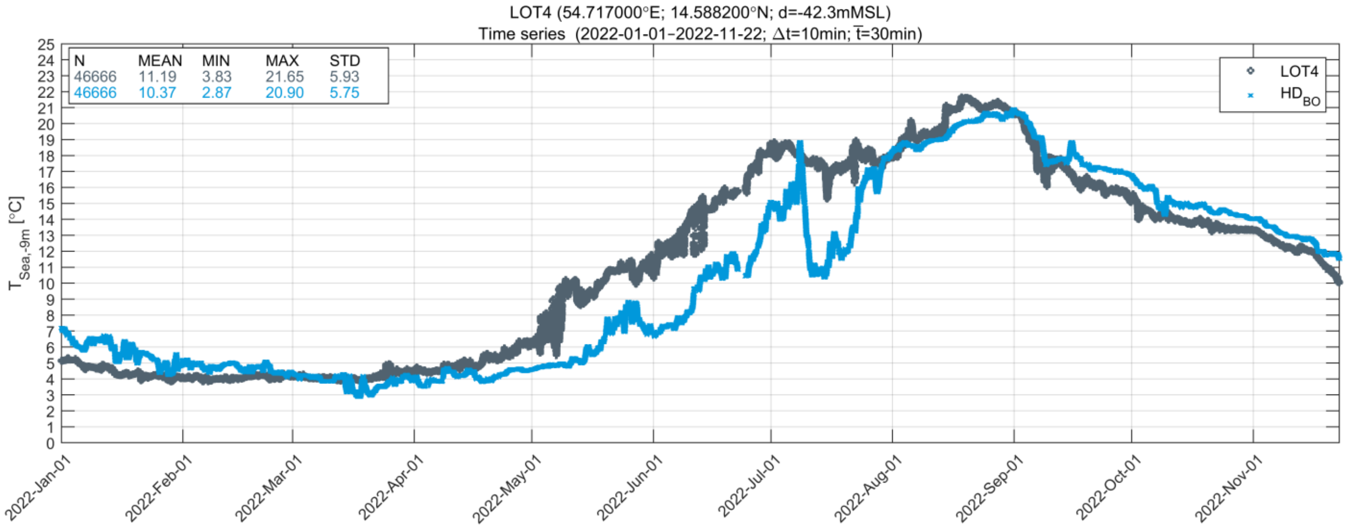
LOT4 (54.717000°E; 14.588200°N; d=-42.3mMSL)
Time series (2022-01-01–2022-11-22; Δt=10min; t̄=30min)
N MEAN MIN MAX STD
46666 11.19 3.83 21.65 5.93
46666 10.37 2.87 20.90 5.75
LOT4
HDBO
TSea,-9m [°C]
2022-Jan-01
2022-Feb-01
2022-Mar-01
2022-Apr-01
2022-May-01
2022-Jun-01
2022-Jul-01
2022-Aug-01
2022-Sep-01
2022-Oct-01
2022-Nov-01

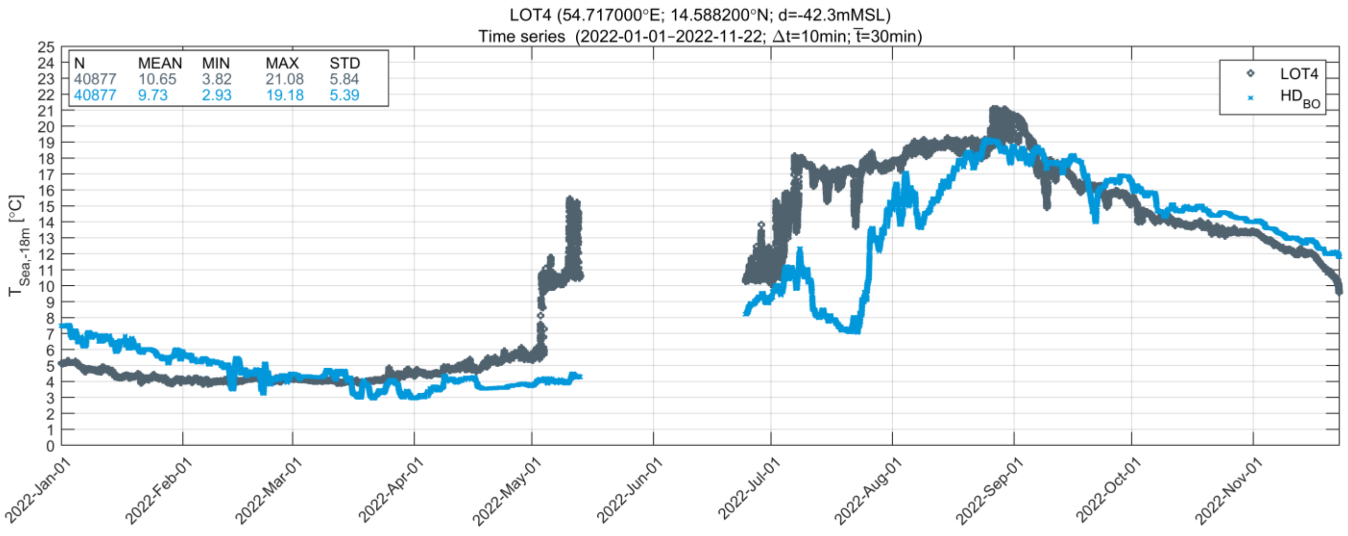
LOT4 (54.717000°E; 14.588200°N; d=-42.3mMSL)
Time series (2022-01-01-2022-11-22; Δt=10min; t̄=30min)
N MEAN MIN MAX STD
40877 10.65 3.82 21.08 5.84
40877 9.73 2.93 19.18 5.39
LOT4
HD BO
T Sea,-18m [°C]
2022-Jan-01
2022-Feb-01
2022-Mar-01
2022-Apr-01
2022-May-01
2022-Jun-01
2022-Jul-01
2022-Aug-01
2022-Sep-01
2022-Oct-01
2022-Nov-01

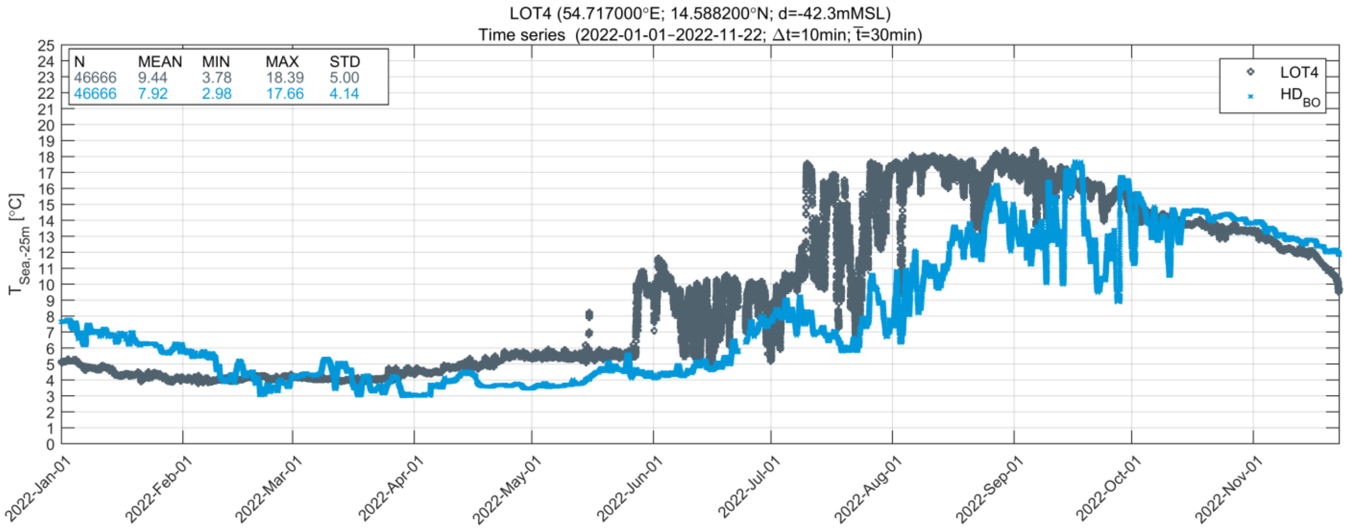
LOT4 (54.717000°E; 14.588200°N; d=-42.3mMSL)
Time series (2022-01-01-2022-11-22; Δt=10min; t̄=30min)
N MEAN MIN MAX STD
46666 9.44 3.78 18.39 5.00
46666 7.92 2.98 17.66 4.14
LOT4
HD BO
T Sea,-25m [°C]
2022-Jan-01
2022-Feb-01
2022-Mar-01
2022-Apr-01
2022-May-01
2022-Jun-01
2022-Jul-01
2022-Aug-01
2022-Sep-01
2022-Oct-01
2022-Nov-01

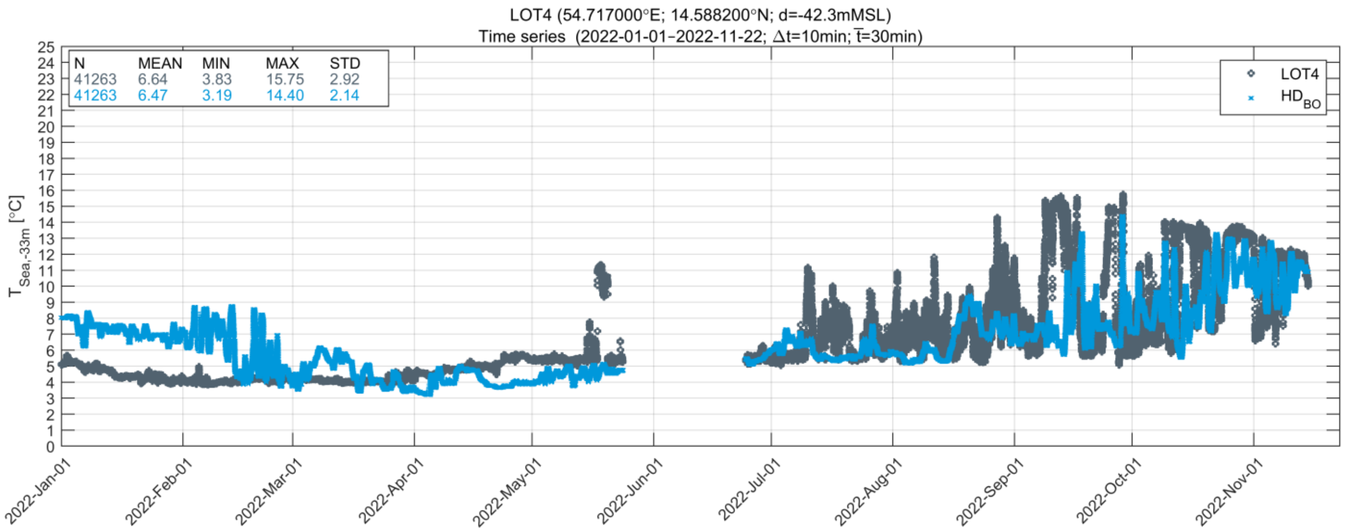

Figure 5.42 **Observed and modelled temperature at LOT4**
From top is shown surface, 9 m, 18 m, 25 m and 33 m.

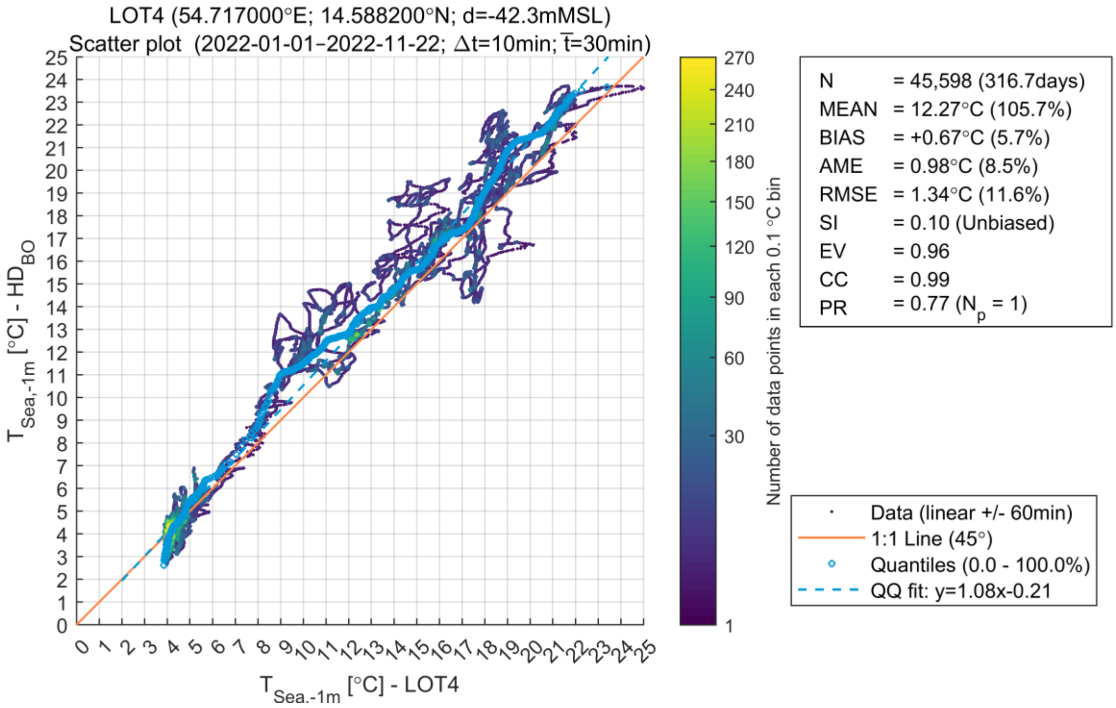

Figure 5.43 Scatter plot of observed and modelled temperature at LOT4 surface

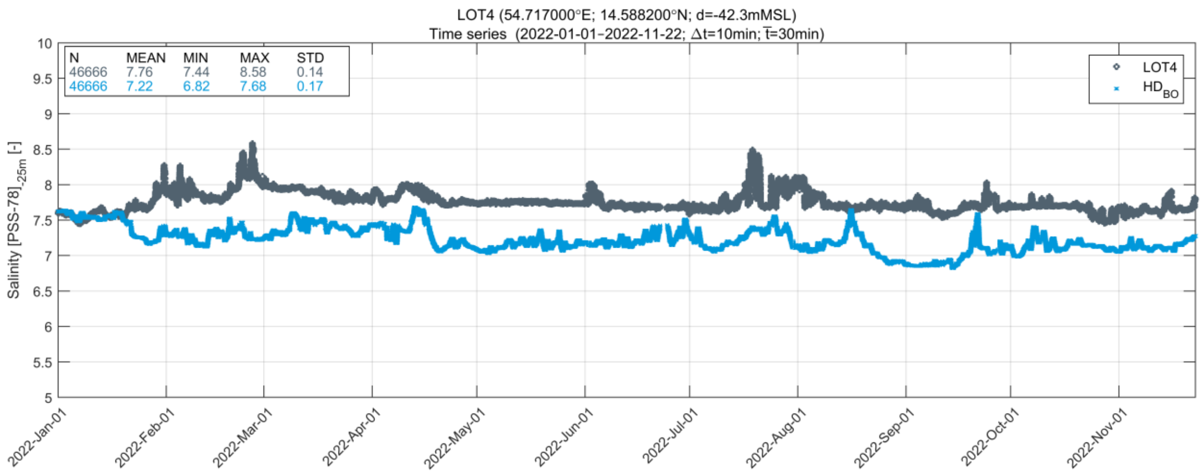

Figure 5.44 Observed and modelled salinity at LOT4, 25 m depth

Arkona

The Arkona Deep is situated at the entrance to the Baltic Proper, where a buoy with thermistors has been operated for long term. In the figures below is shown temperature variations in two depths at the buoy during 2021.

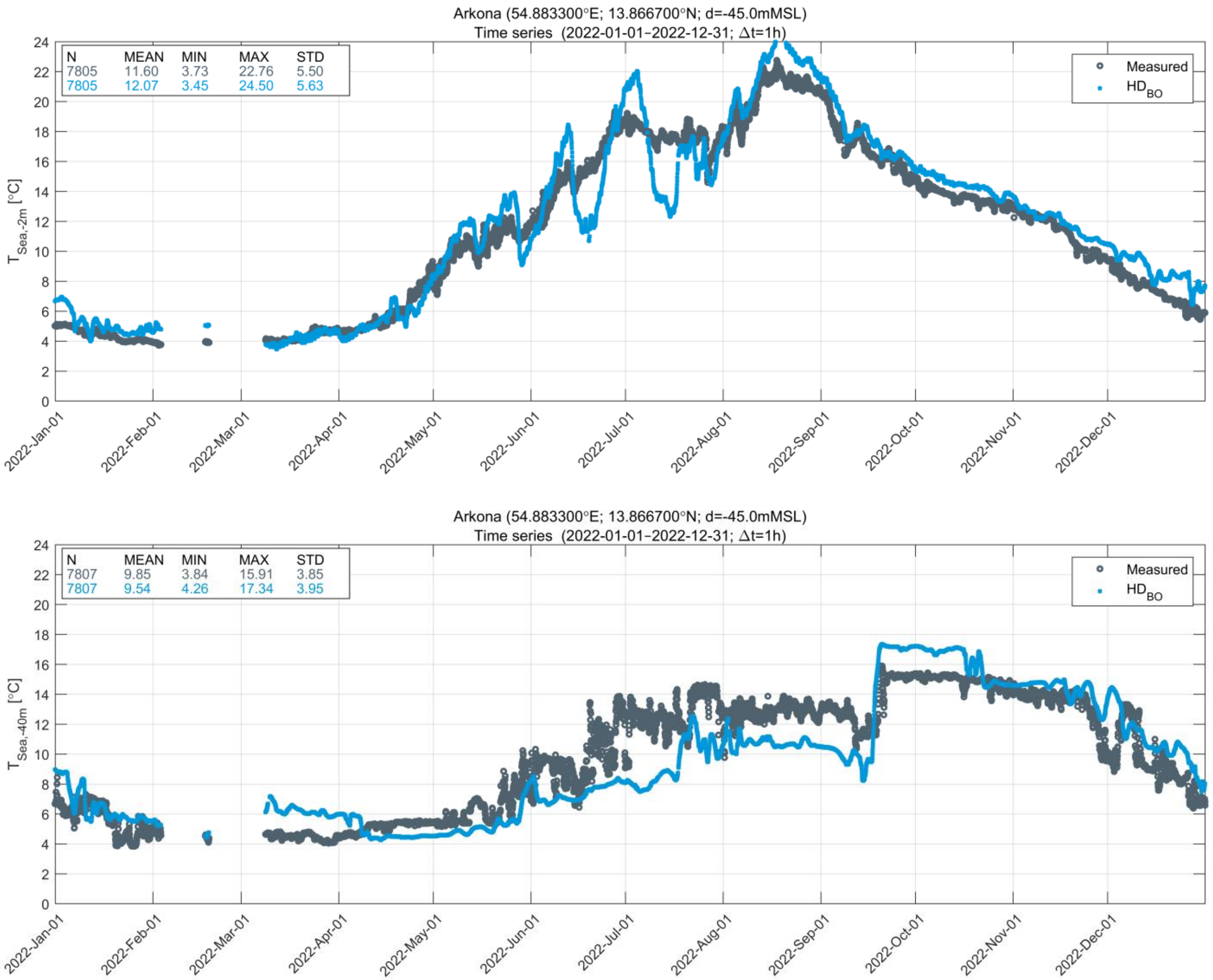

Figure 5.45 **Observed and modelled temperature at Arkona buoy**
From top: surface and 40m depth.

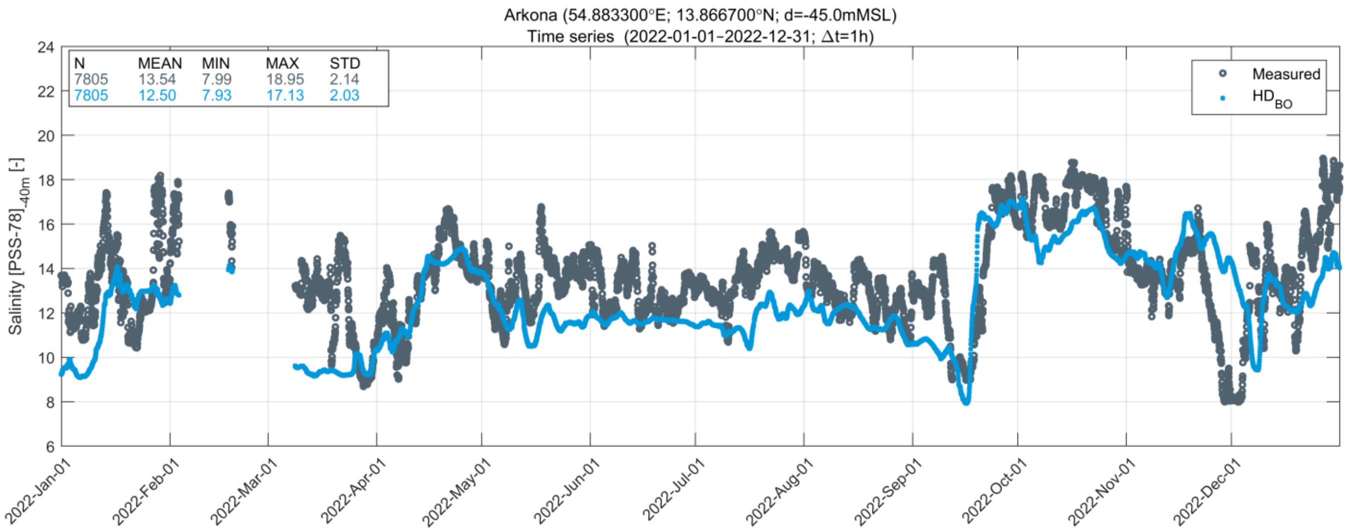

Figure 5.46 Observed and modelled salinity at Arkona buoy, 40 m depth

FINO2

In the figures below show temperature variations in two depths and salinity variations in one depth at the FINO2 mast during 2022.

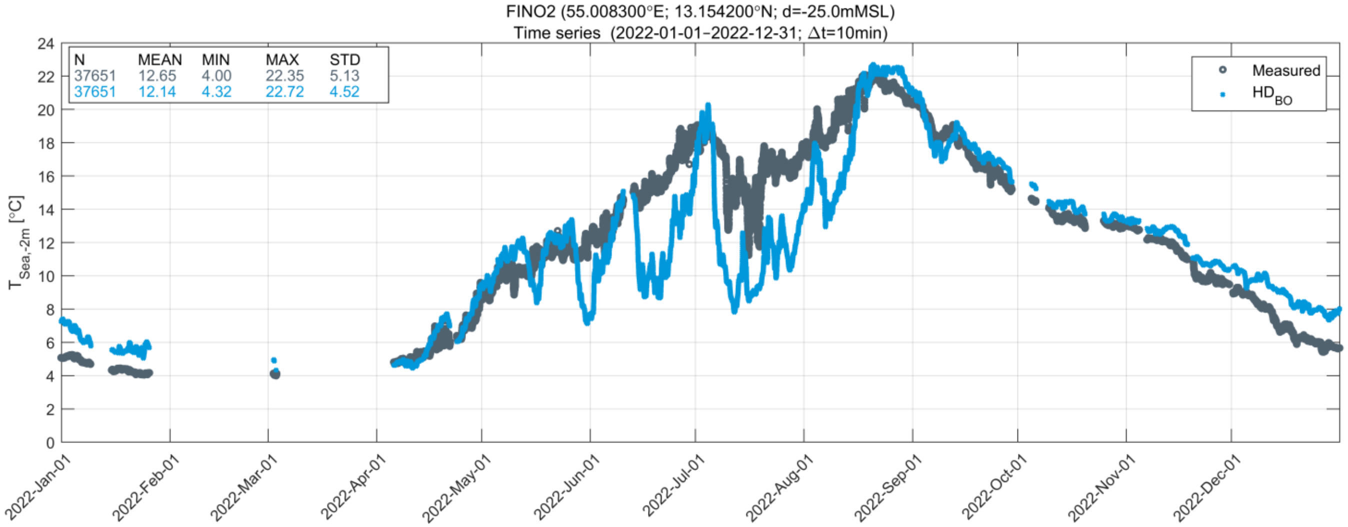

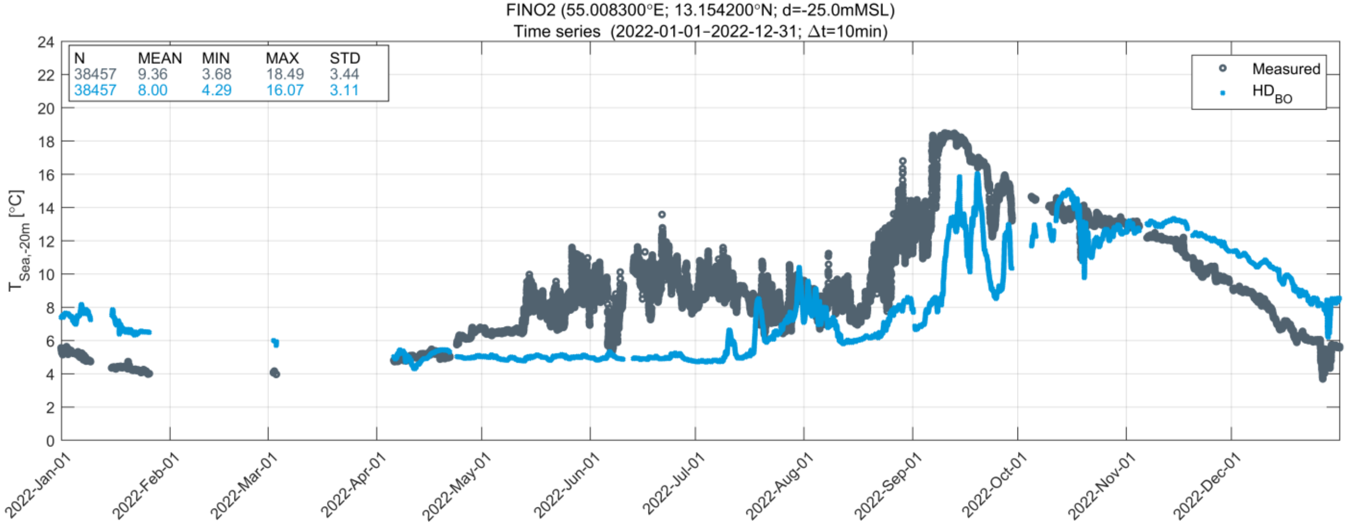

Figure 5.47 Observed and modelled temperature at FINO2 mast
From top: 2 m and 20 m depth

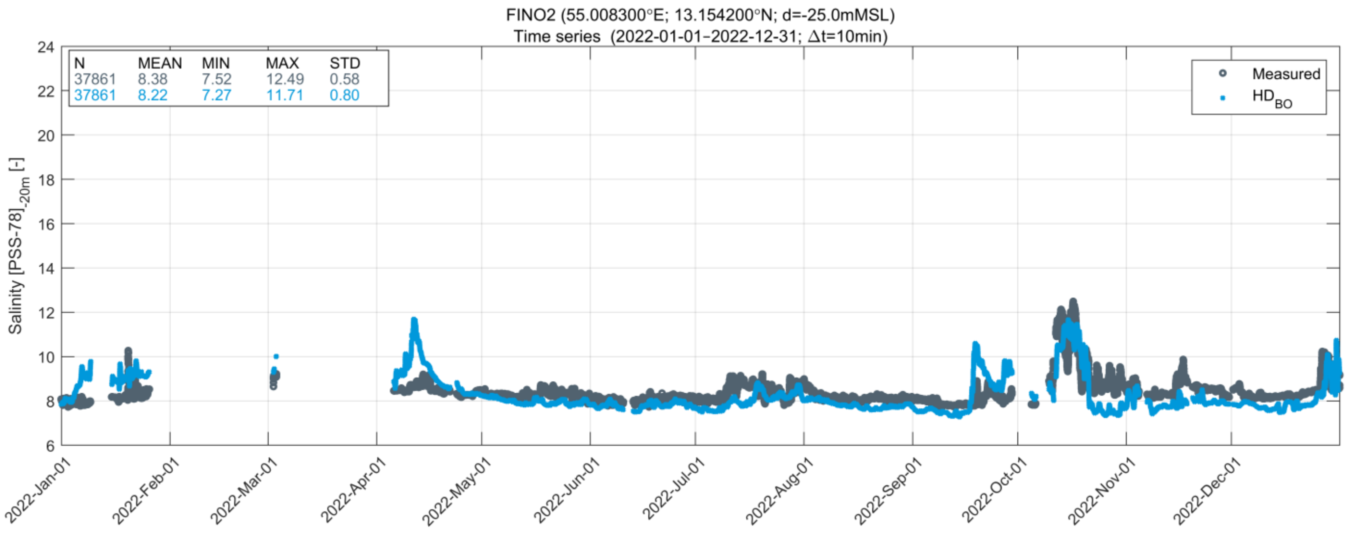

Figure 5.48 Observed and modelled salinity at FINO2 mast, 20 m depth

5.7 Validation summary

In summary, the validation has indicated that the HD_{EIBS} 3D model does represent a realistic picture of the current, temperature, and salinity around Rønne Bank. The validation indicates that there is uncertainty in the predictions and that there is a tendency for the currents in the deeper layers to be non-conservative i.e. underestimated.

To compensate for this uncertainty, based on the scatter plots shown earlier, DHI recommends the post-scaling factors as shown in Table 5.5.

Table 5.5 Post-scaling multiplication factors for current speeds

Depth	Factor
Surface	1.0
Mid-depth	1.25
Near-bed	1.1

6 Waves

This section presents a general overview of the Baltic Sea wave conditions and presents the wave measurements used to calibrate and validate the local spectral wave model (SW_{EIBS}) established to obtain a validated and long-term wave data basis at the EIBS site applicable for the assessment of normal and extreme wave conditions.

6.1 General wave characteristics

The wave climate of the Baltic Sea is characterised by the prevalence of short-period wind-generated waves. Due to its semi-enclosed nature and the existence of narrow straits linking it to the North Sea, the propagation of swell waves into the Baltic Sea basin is inhibited.

6.2 Wave measurements

The locations, water depths, etc., of measured wave parameters near or at the project site are summarised in Table 6.1.

The quality of the measurements at the project location recorded by LOT3 and LOT4 buoys was quality-controlled by FUGRO [6] and checked by DHI to remove any potential outliers or any irregularities in the data. The data from these have an averaging period of 1024 s, however, data was provided at a running average of 10 min intervals.

Measurements outside of the project area were assumed to be quality-checked by the different providers. Nevertheless, DHI investigated the measurement data to remove any spurious measurements (outliers or unexpected spikes). This is particularly important for the purpose of comparing the model results with the measurement data.

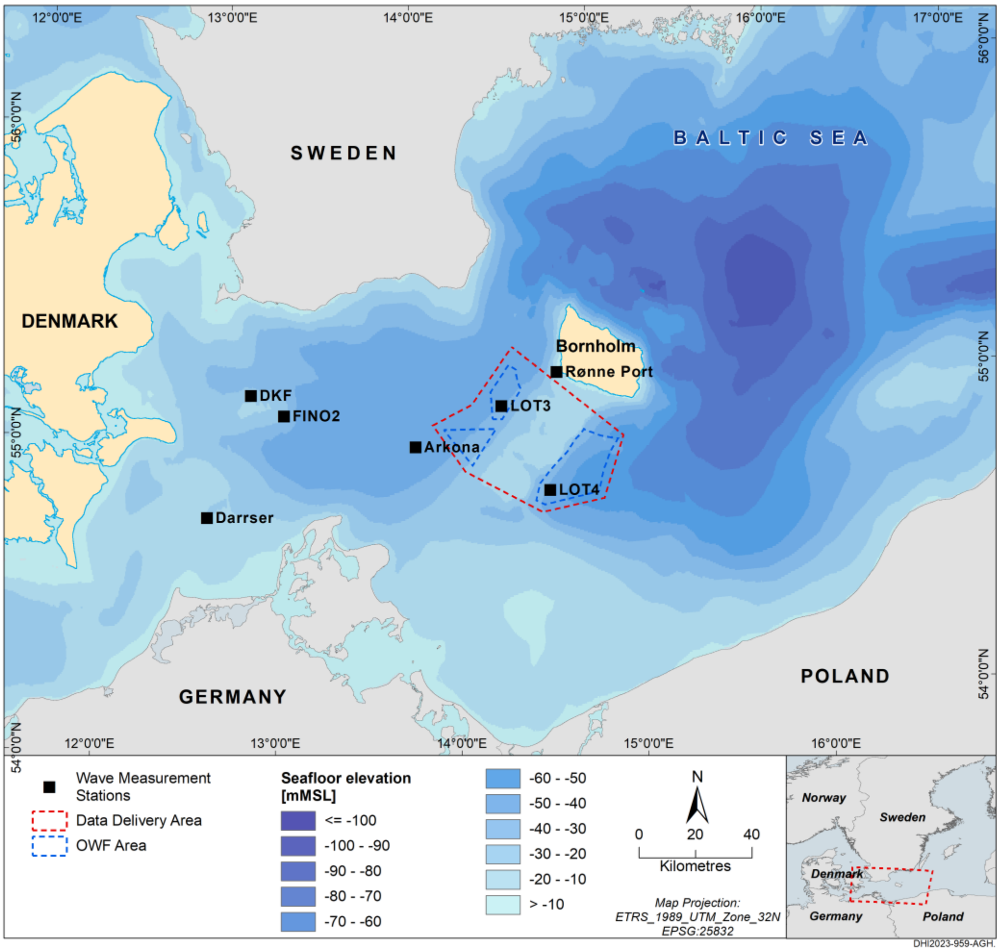

Figure 6.1 Location of wave measurements applied in the study

Table 6.1 Details of wave measurement stations

Station Name	Longitude [°E]	Latitude [°N]	Depth [mMSL]	Availability period	Instrument	Owner / Surveyor
LOT3	14.3556	54.9948	39.8	2021-11-21 – 2022-11-21	Wavesense 3	Energinet / Fugro
LOT4	14.5882	54.7170	42.3	2021-11-21 – 2022-11-21	Wavesense 3	Energinet / Fugro
FINO2	13.1541	55.0070	24.0	2011-05-05 – 2020-09-12	Datawell MkIII	BSH
Arkona	13.8667	54.8833	45.0	2002-02-28 – 2017-12-31	ODAS	BSH
Rønne Port	14.6739	55.0882	18.0	2021-11-25 – 2022-11-25	SW mini	Rønne Port
DKF	13.1541	55.0070	24.0	2011-05-05 – 2020-09-12	Datawell DWR4 and MkIII	Vattenfall / Fugro
Darrser	12.6890	54.6870	21.0	2003-07-02 – 2017-12-31	-	BSH

6.3 Hindcast wave data

The long-term wave data basis at the EIBS site was established through the set-up of a dedicated spectral wave model using DHI's MIKE 21 SW software.

6.3.1 MIKE 21 Spectral Wave FM (SW)

MIKE 21 SW is a state-of-the-art third-generation spectral wind-wave model developed by DHI. The model simulates growth, decay and transformation of wind-generated waves and swells in offshore and coastal areas. For more information on the MIKE 21 SW model, see [21] [22]. The latest available MIKE 21 SW release was used in this project: MIKE 21 SW 2022 Update 1.

6.3.2 Model Domain, SW_{EIBS}

A local spectral wave model (SW_{EIBS}) was established in this study, covering the domain shown in Figure 6.2. Bathymetry datasets used in this model are described in Section 2. The model has two open boundaries, located as shown in Figure 6.3. The wave model was forced by NORA3 wind and by boundary conditions from DHI's regional Northern Europe spectral wave model (SW_{NE}) [23]. The local wave model resolution increases from offshore towards the project site with a resolution of around ~3 km to about 500 m at the EIBS project site, as shown in Figure 6.3.

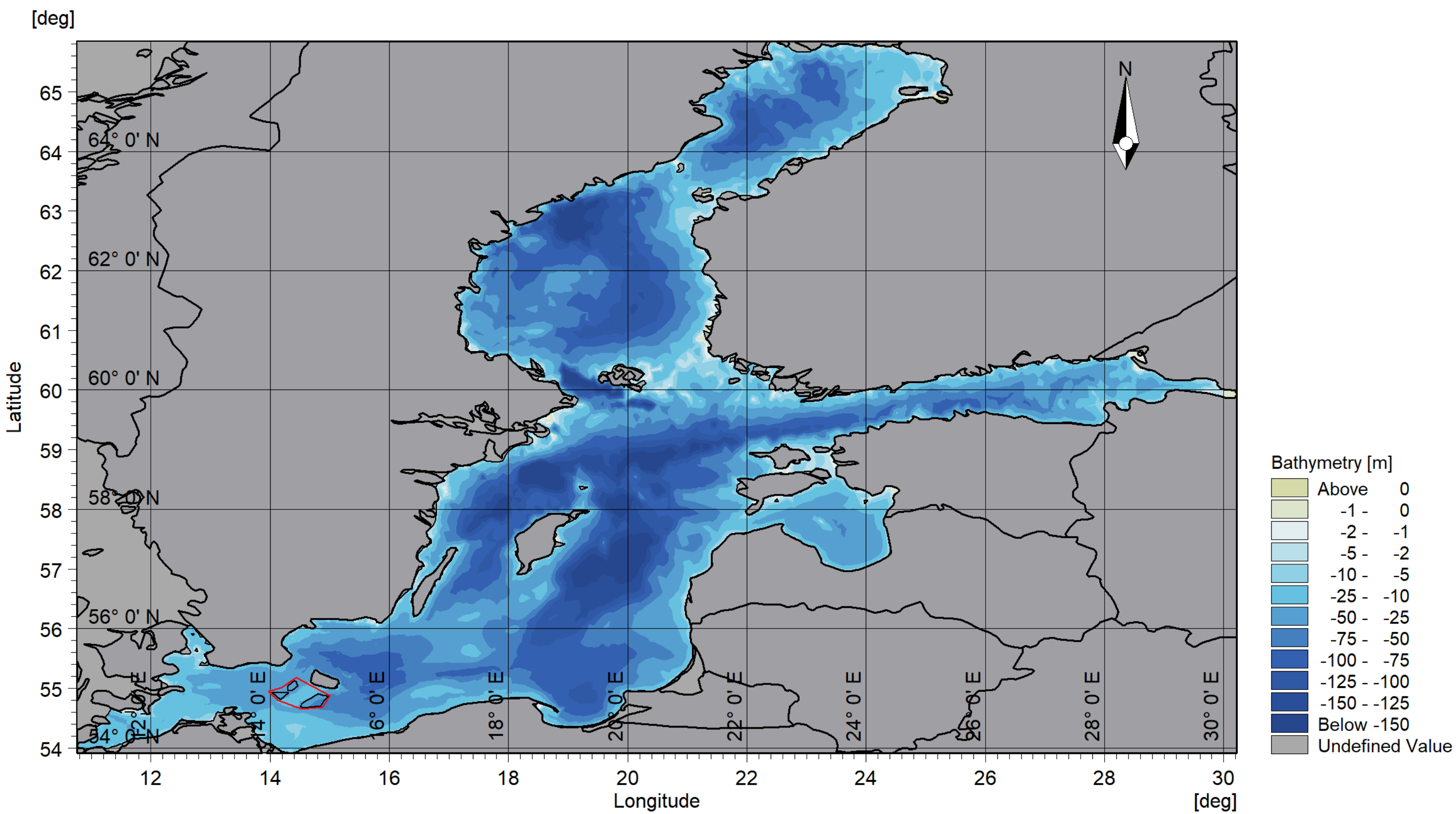

Figure 6.2 **SW_{EIBS} model domain and bathymetry**

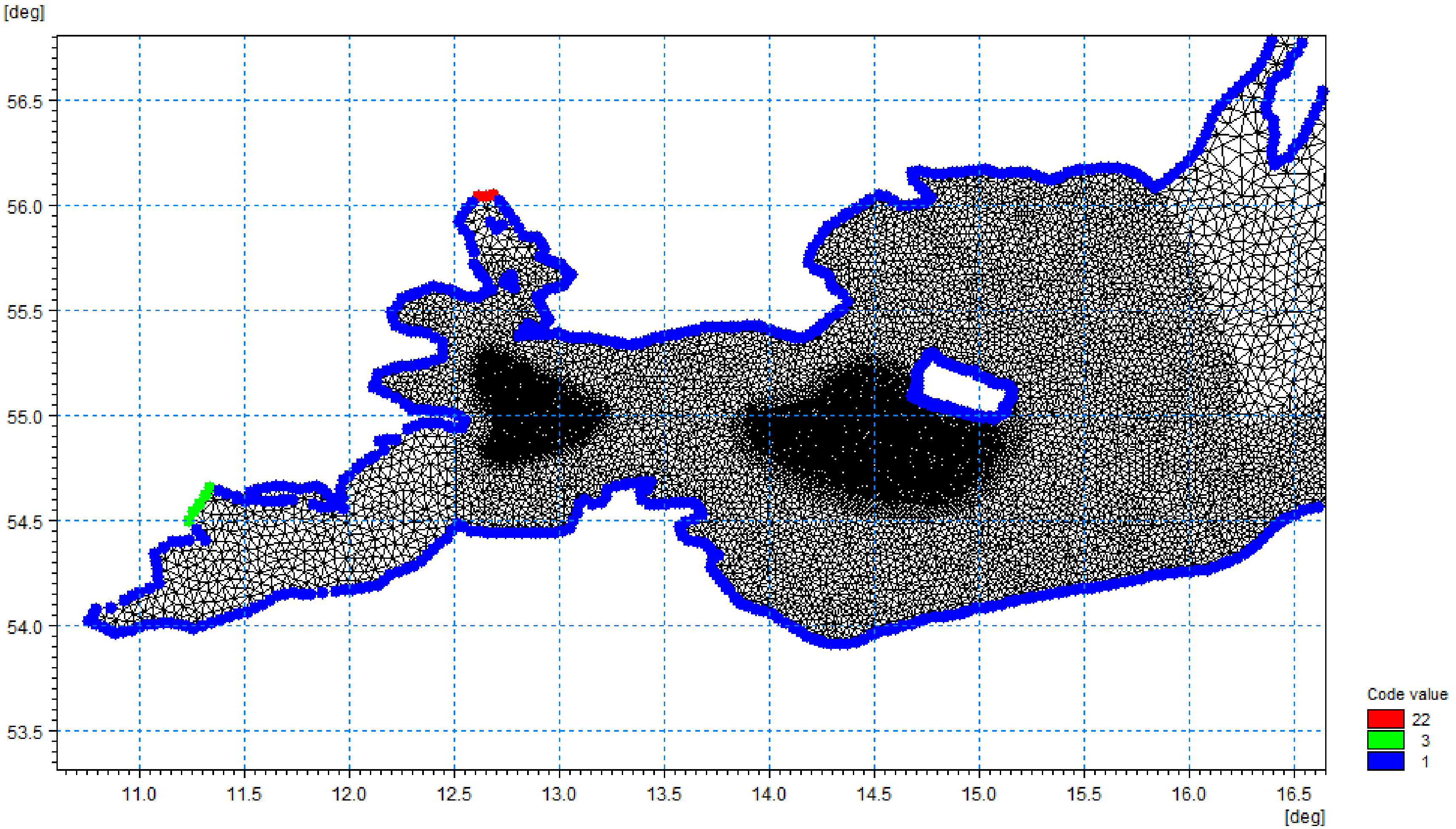

Figure 6.3 **SW_{EIBS} model mesh and boundaries**
Blue dots (code 1) indicate land boundary. Green (code 3) and red (code 22) indicate open boundaries.

6.3.3 Boundary conditions

The EIBS wave model, SW_{EIBS}, was forced by high-accuracy data from the existing DHI North Europe regional spectral wave model, SW_{NE}. Figure 6.4 shows the model domain, going from a resolution of ~16 km (in the North Atlantic) to about 5 km in the southern North Sea and the English Channel.

The SW_{NE} has been widely used with success in various projects in the North Sea, including major offshore wind farm projects as well as coastal infrastructure and oil and gas industry projects, and has been validated at several stations around the region [23].

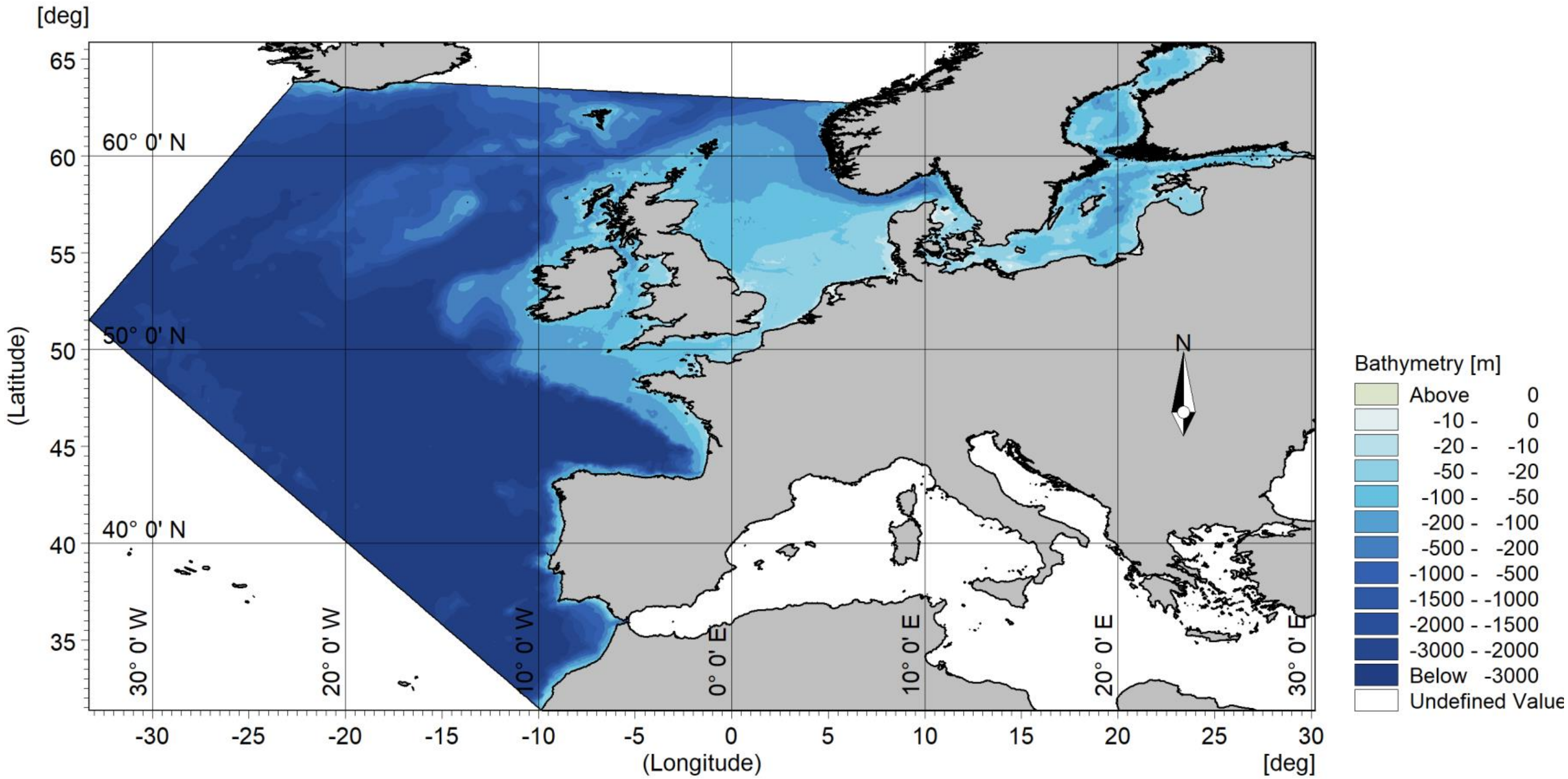

Figure 6.4 Domain of the DHI North Europe regional spectral wave model (SW_{NE})

6.3.4 Sensitivity studies

Model calibration

During the calibration phase of SW_{EIBS}, the sensitivity of model outputs to several model parameters (e.g., bed friction, wave breaking parameter) was assessed. Table 6.2 presents all parameters tested. In Section 6.3.5, Table 6.3 summarises the SW_{EIBS} model setup used for production of 44 years (1979-2022) of data.

Table 6.2 Parameters of SW_{EIBS} model tunned during calibration

Parameter	Value
Wave breaking	Included, Specified Gamma γ= [0.8, 0.9], Cdiss [1.7 – 2.3]
Formulation	WAM, Ardhuin
Bottom friction	Nikuradse: uniform (0.01, 0.02, 0.04), spatially varying (increased along the shallow area)
Air-sea interaction	Background Charnock: [0.0185, 0.062] (Coupled)
Wave age tunning parameter	[0.008 – 0.011]
Non-linear growth parameter	[1.2 – 1.4]

Mesh convergence

Mesh sensitivity tests were carried out by testing three different mesh resolutions encompassing the project site, including the cable corridor: 250, 500 and 1000 m (Figure 6.5), during five large storm events. The storm events were selected based on the regional long-term wave hindcast model result from SW_{NE}.

The five events selected were:

- 2017-09-13 to 2017-09-14
- 2013-12-05 to 2013-12-06
- 1999-12-03 to 1999-12-04
- 1983-01-18 to 1983-01-19
- 1981-11-24 to 1981-11-25

The comparison of the SW_{EIBS} wave model outputs (significant wave height, peak wave period and mean wave direction) is presented in Figure 6.7 to Figure 6.11. The changes of those wave parameters' output within the wind farm area (blue polygon in Figure 6.6) across three different mesh resolutions are insignificant. There are some changes when going from 1000 m to 500 m resolution around the shallow area on the west of the project area and negligible differences between the 500m and 250m. Hence, the 500 m model resolution was used for the production runs.

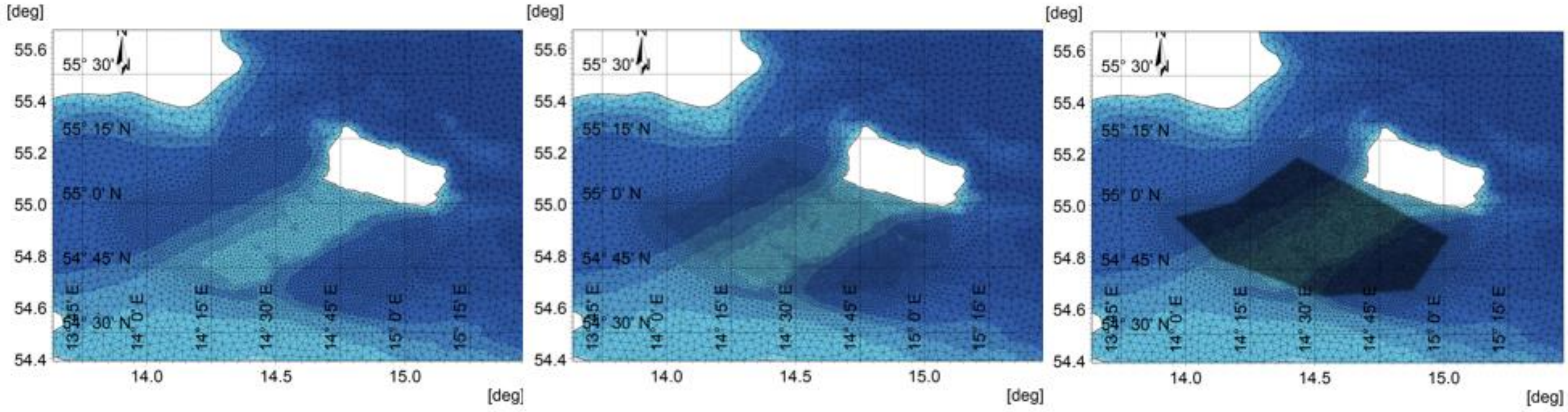

Figure 6.5 **SW_{EIBS} meshes used for the mesh convergence tests**
Resolutions of 1000 m (left), 500 m (middle) and 250 m (right).

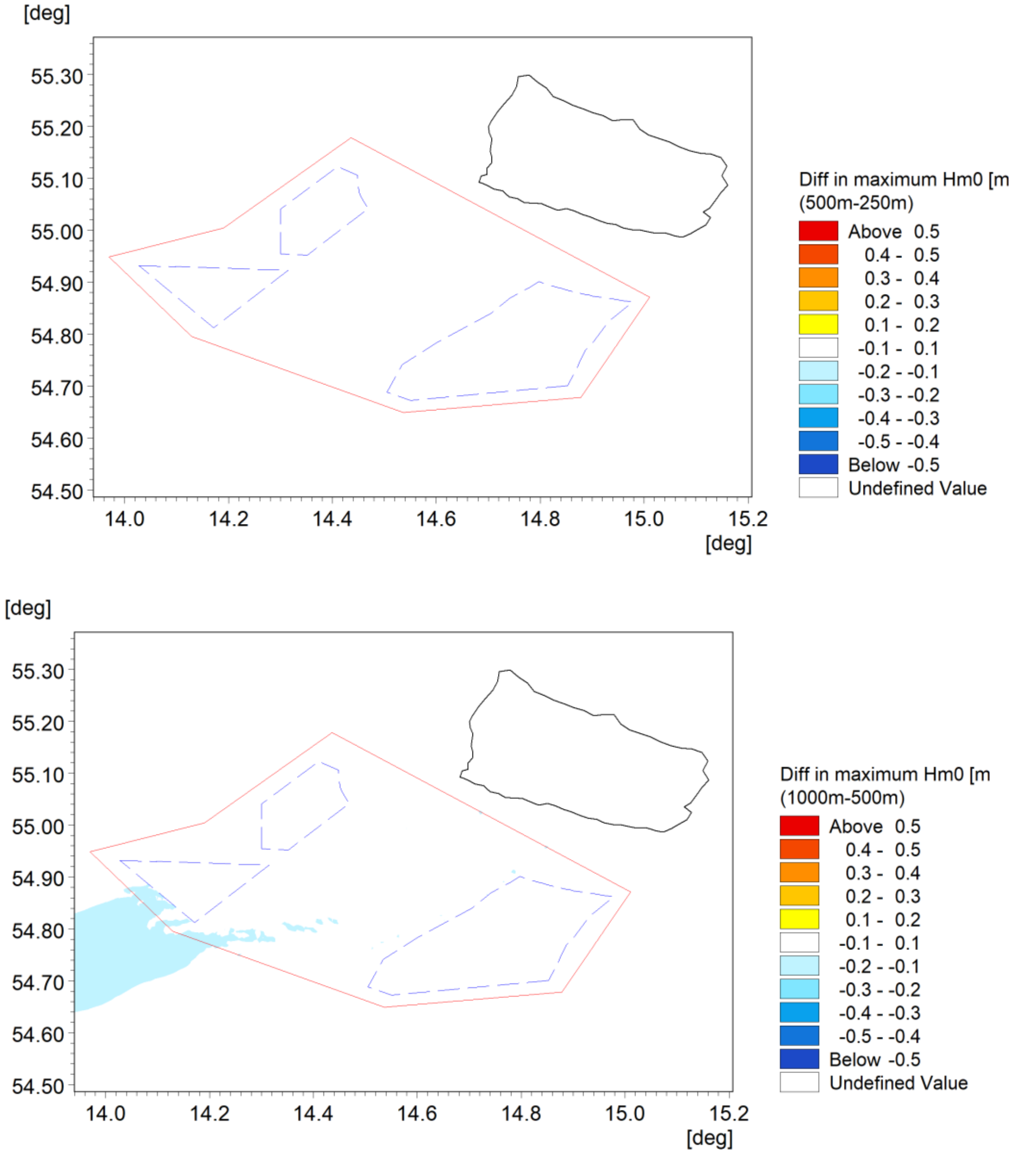

Figure 6.6 **Maps of difference of maximum H_{m0} of SW_{EIBS} during 2017 storm event for different mesh resolution**
500 m resolution – 250 m resolution (top), 1000 m resolution – 500 m (bottom).

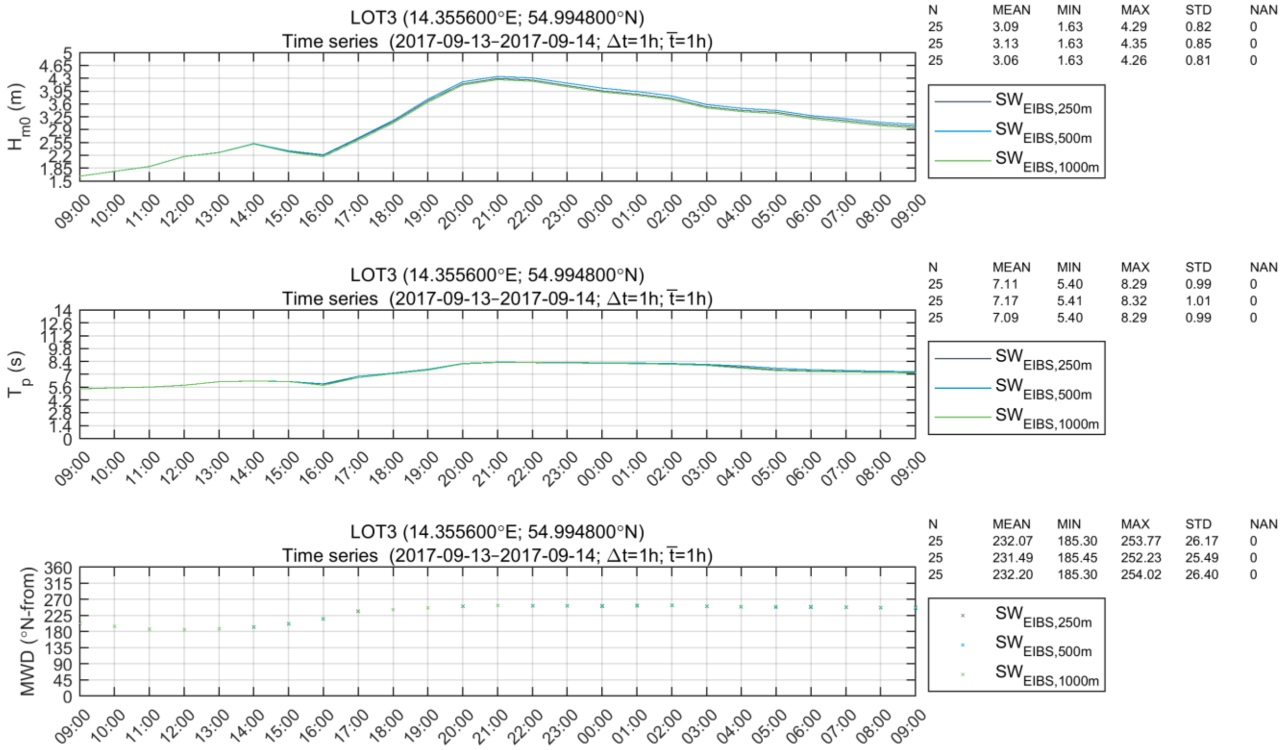

Figure 6.7 **Time series comparison of H_{m0}, T_p, and MWD for three different mesh resolutions of SW_{EIBS} at point LOT3 during 2017 storm event**

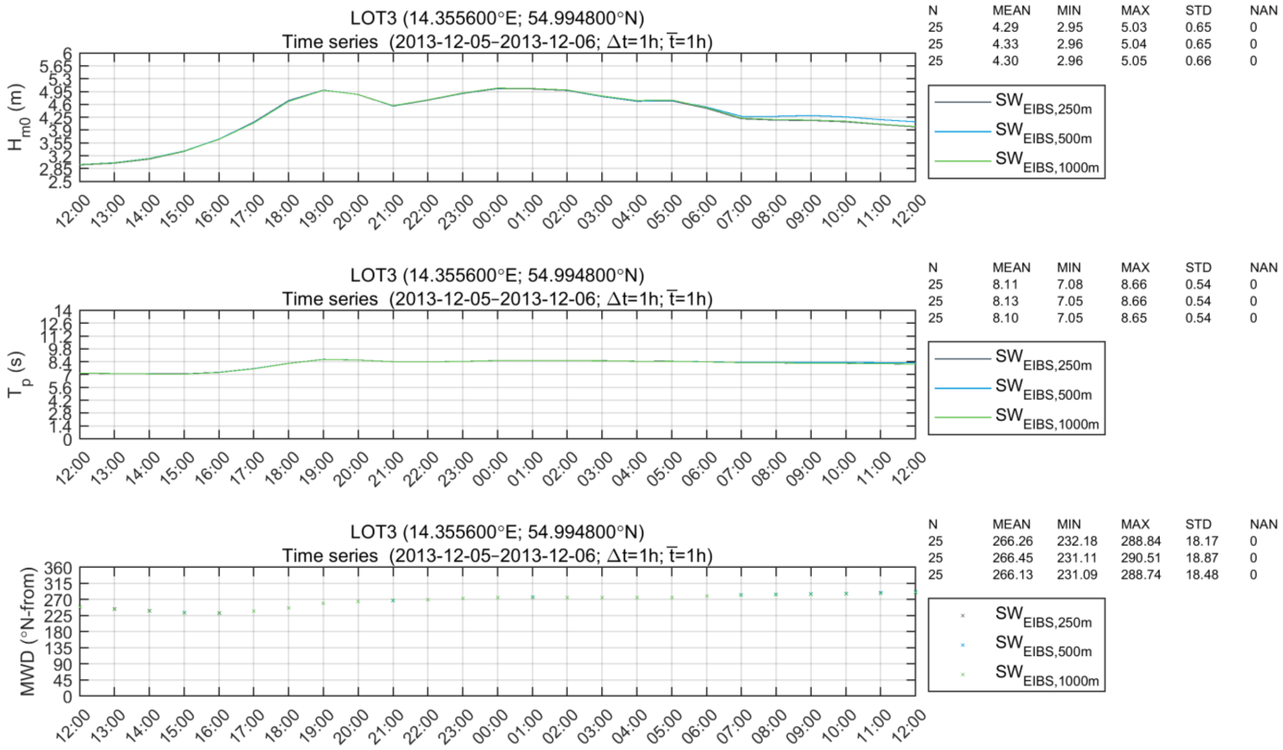

Figure 6.8 **Time series comparison of H_{m0}, T_p, and MWD for three different mesh resolutions of SW_{EIBS} at point LOT3 during 2013 storm event**

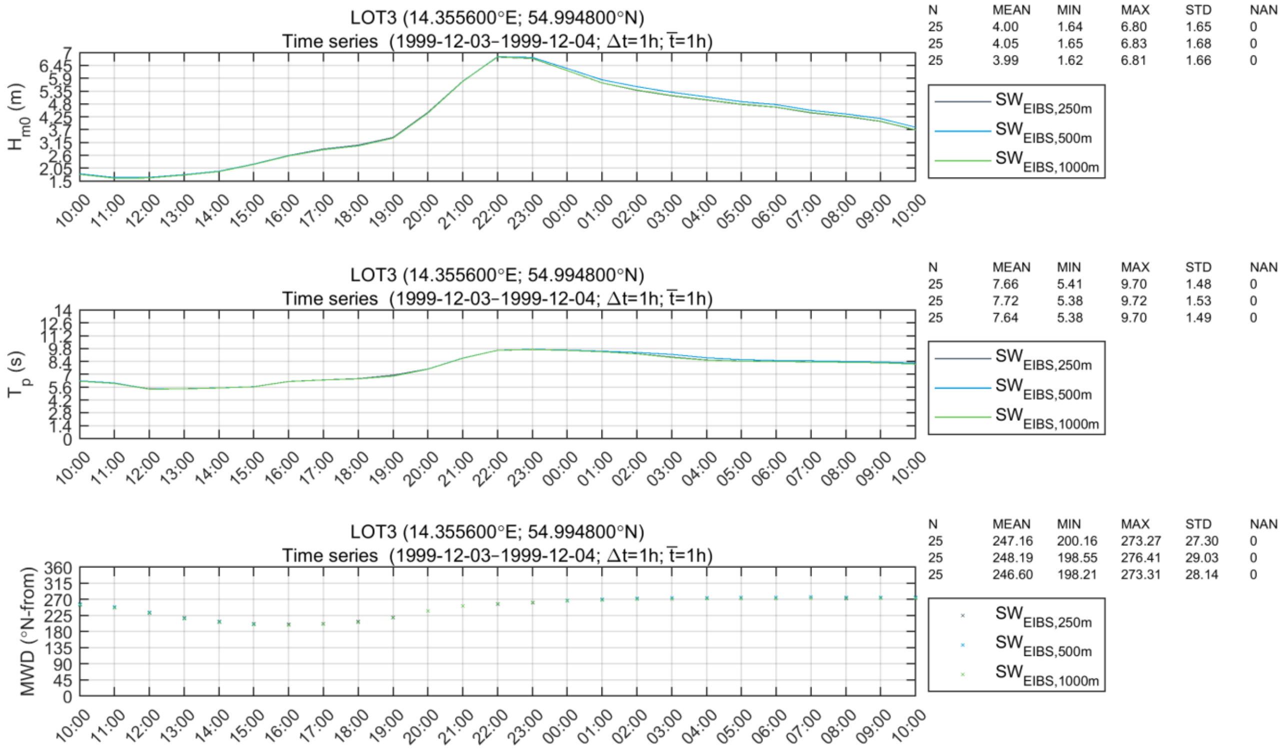

Figure 6.9 **Time series comparison of H_{m0}, T_p, and MWD for three different mesh resolutions of SW_{EIBS} at point LOT3 during 1999 storm event**

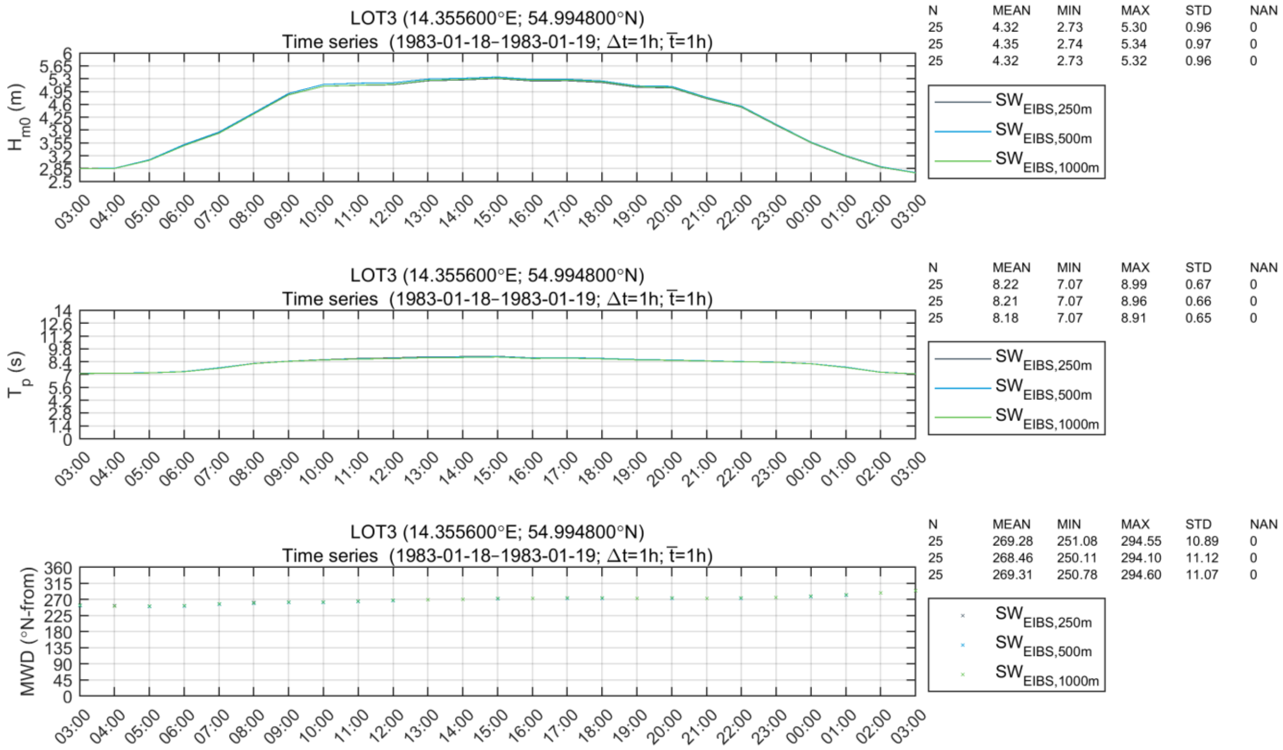

Figure 6.10 **Time series comparison of H_{m0}, T_p, and MWD for three different mesh resolutions of SW_{EIBS} at point LOT3 during 1983 storm event**

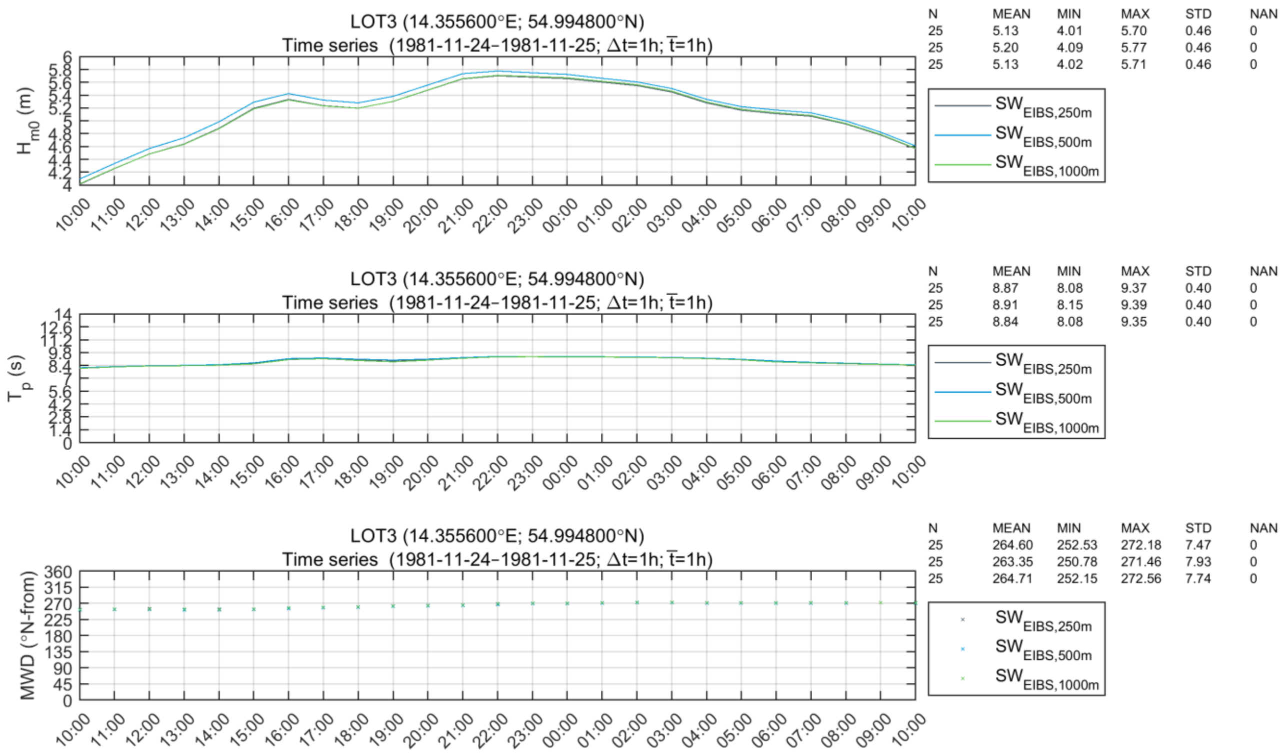

Figure 6.11 Time series comparison of H_{m0}, T_p, and MWD for three different mesh resolutions of SW_{EIBS} at point LOT3 during 1981 storm event

6.3.5 Model setup (SW_{EIBS})

The SW_{EIBS} model setup used for production of the 44 years (1979-2022) is summarised in Table 6.3.

Table 6.3 Specifications of SW_{EIBS} model settings
Final model setting of the local spectral wave model, SW_{EIBS}.

Setting	Value
Engine (version)	MIKE 21 Spectral Wave (SW) model (2022, Update 1)
Mesh resolution	Element size at EIBS OWF ~ 500m
Simulation period	1979-01-01 – 2022-12-31 (44 years), hourly output
Basic equations	Fully spectral in-stationary
Discretisation	37 frequencies (0.9 –17.4 s), 36 directions
Time step (adaptive)	0.01-90 s with a maximum time-step factor of 16
Water level	$HD_{NE\text{-}ERA5}$ (temporally and spatially varying)
Current conditions	$HD_{NE\text{-}ERA5}$ (temporally and spatially varying)
Wind forcing	NORA3
Air-sea interaction	Background Charnock (coupled and uncoupled)
Neutral winds	True (Varying in time and domain calculated from NORA3)
Correction of friction vel.	Cap value of 0.06
Air/water density ratio	Varying in time and domain calculated from NORA3
Energy transfer	Included, quadruplet-wave interaction (no triads)

Setting	Value
Wave breaking	Included, Specified Gamma, γ=0.9, α= 1
Bottom friction	Nikuradse, (spatially varying, 0.01 and 0.04)
Boundary conditions	Integrated parameter from SW_{NE}
Growth parameter	1.3
Wave age tunning param.	0.011
Output specifications	Integral wave parameters saved at all grid elements with a 1-hour min interval.

6.3.6 Output specifications

Model output was saved with a 1-hour interval and included the integral wave parameters listed in Table 6.4 at every mesh element in the model domain.

Each integral parameter was saved for the total sea state and for swell and wind-sea components, respectively. The wind-sea/swell partitioning was based on a wave-age criterion (see section 5.1 of [22]), where the swell components are defined as those components fulfilling:

$$\frac{U_{10}}{c}\cos(\theta - \theta_w) < 0.83$$

where U_{10} is the wind speed at 10 m above MSL, c is the phase speed, and θ and θ_w are the wave propagation and wind direction, respectively.

Table 6.4 Output specifications of SW_{EIBS}
Parameters are saved at all grid elements with 1 hour interval.

Parameter (total, wind-sea, and swell)	Abbreviation	Unit
Spectral significant wave height	H_{m0}	m
Maximum wave height	H_{max}	m
Peak wave period	T_p	s
Spectral mean wave period	T_{01}	s
Spectral zero-crossing wave period	T_{02}	s
Wave energy period	T_{m10}	s
Peak wave direction	PWD	°N (clockwise from)
Mean wave direction	MWD	°N (clockwise from)
Direction standard deviation	DSD	°

Averaging period of waves

The significant wave heights, H_{m0}, from the SW_{EIBS} model are essentially instantaneous 'snapshots' of the wave field that are saved at 1-hour time intervals from the model. The time scales resolved in the numerical models underpinning the hindcast data are affected by the spatial resolution and the wind forcing, and hence the data represents wave heights that are implicitly averaged over some time averaging period, T_{avg}. One may therefore expect measurements to exhibit higher variability compared to model data.

Correspondingly, the model data may be regarded as somewhat ‘smoothed’ (in space and time) compared to the observations. For practical applications such as extreme value assessment or load calculations (e.g., wave heights associated with extreme sea-states), appropriate accounting for the smoothed nature of the model data must be considered.

A frequently used approach for assessing the representative temporal scale (or smoothing) of the wave models is by comparing the power spectra of modelled wave heights with the power spectra of measurements that have been smoothed using various averaging windows (30-minutes, 60-minutes, 120-minutes, and 180-minutes). The spectral analysis was performed to the measured data sets from LOT4 as well as to their corresponding data sets from the SW_{EIBS}. The resulting frequency power spectra for H_{m0} are shown in Figure 6.12, where the frequency power spectra follow the 120-minute line the most closely. Therefore, for the purposes of this study, 120 minutes was adopted as the representative temporal averaging period of H_{m0} of the SW_{EIBS} model, i.e., T_{avg} = 120 minutes.

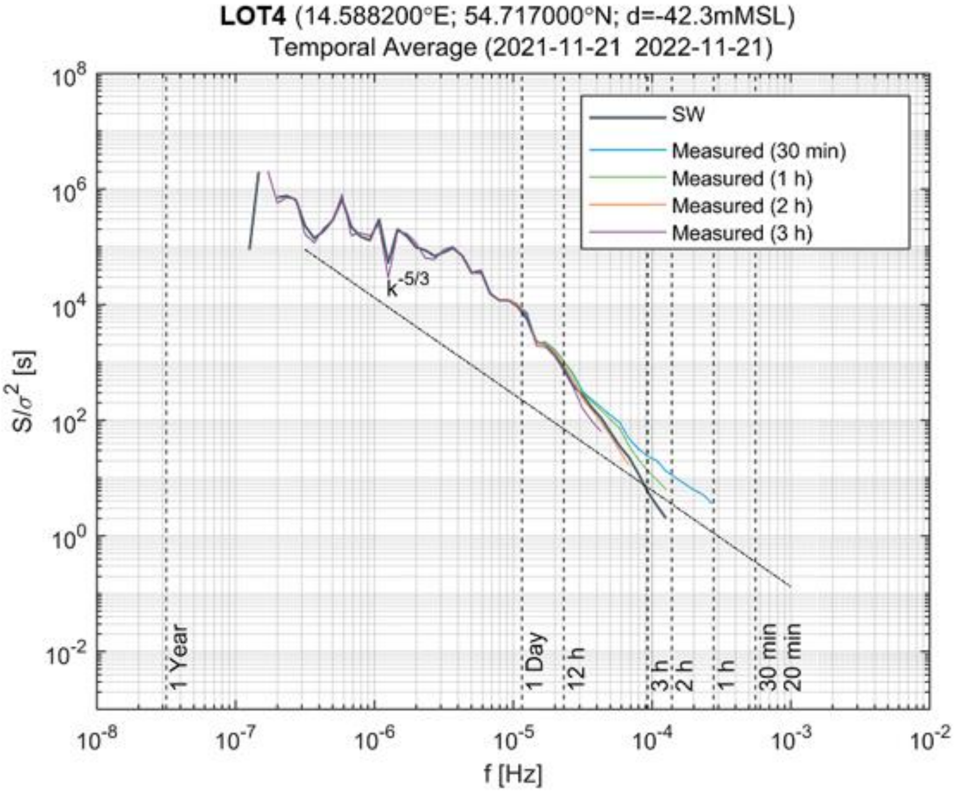

Figure 6.12 Frequency power spectra of H_{m0} at LOT4
Power spectra of H_{m0} from the SW_{EIBS} (black line), together with the 30-min, 1, 2 and 3-hour moving average window of the measurements (blue, green, orange, and purple lines respectively)

6.3.7 Validation of integral wave parameters

The results of the SW_{EIBS} wave model were validated against the full set of available wave measurements from the in-situ stations described in Section 2.1.4 and shown in Figure 6.1.

The performance of the wave model is presented in the time series plots, scatter plots and dual-rose plots (Figure 6.13 to Figure 6.34).

Overall, the model results show a good agreement with the measurements in terms of magnitude and direction.

The scatter plots between the model and the measurement show low bias and scatter index (SI), and cross correlation close to 1. The model is also able to capture the peak wave heights during extreme events, represented in the peak-to-peak ratio (PR) number being close to 1 (Table 6.5). Thus, the model can be applied without corrections for normal and extreme sea states. T_{02} is shown to compare well with measurements, particularly at LOT3 and LOT4, where the cut-off frequency from the instruments is known.

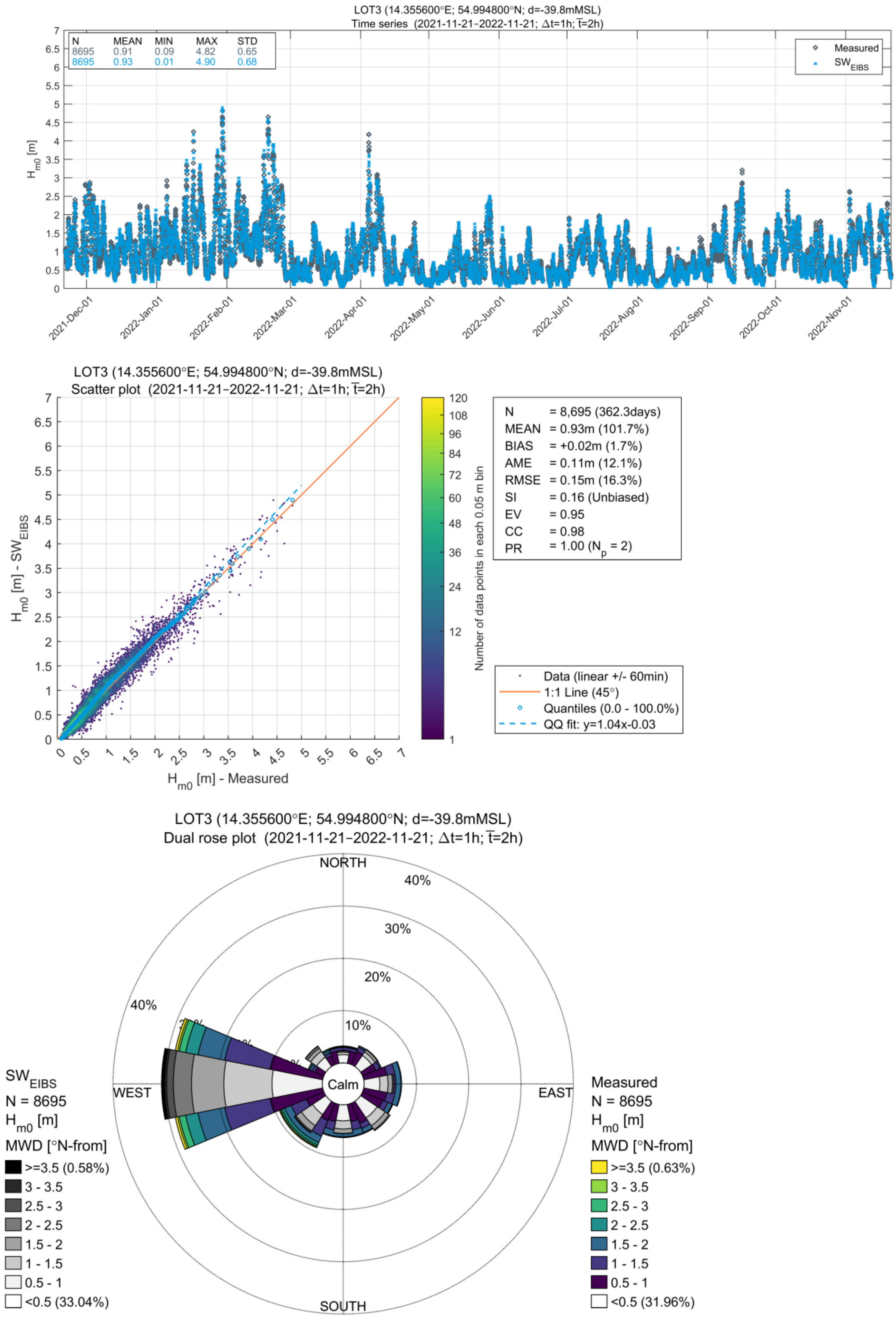

Figure 6.13 Comparison of measured and modelled H_{m0} at LOT3

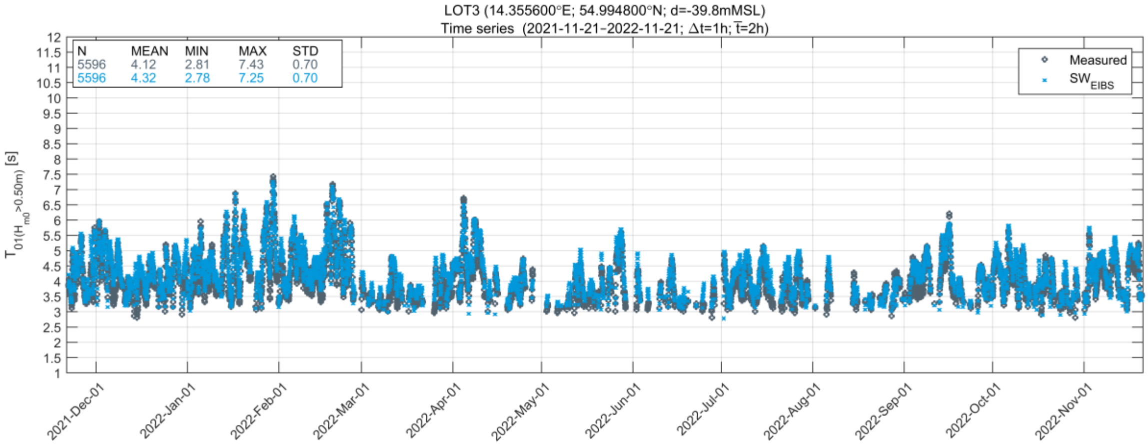

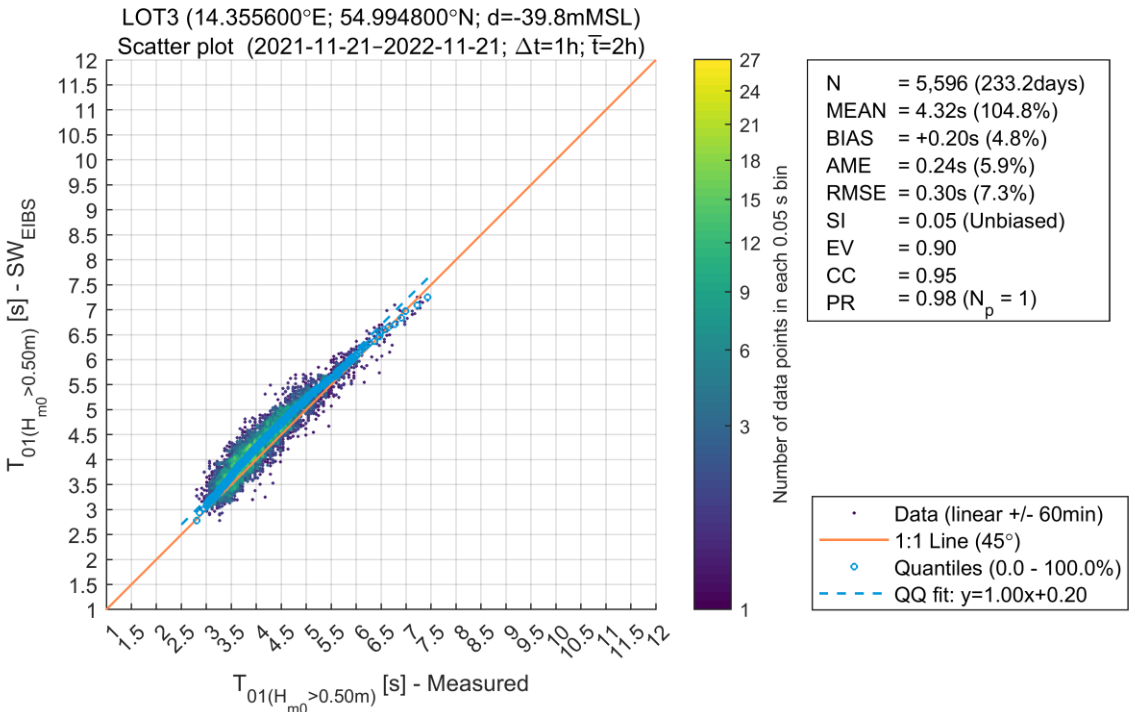

Figure 6.14 Comparison of measured and modelled T_{01} at LOT3

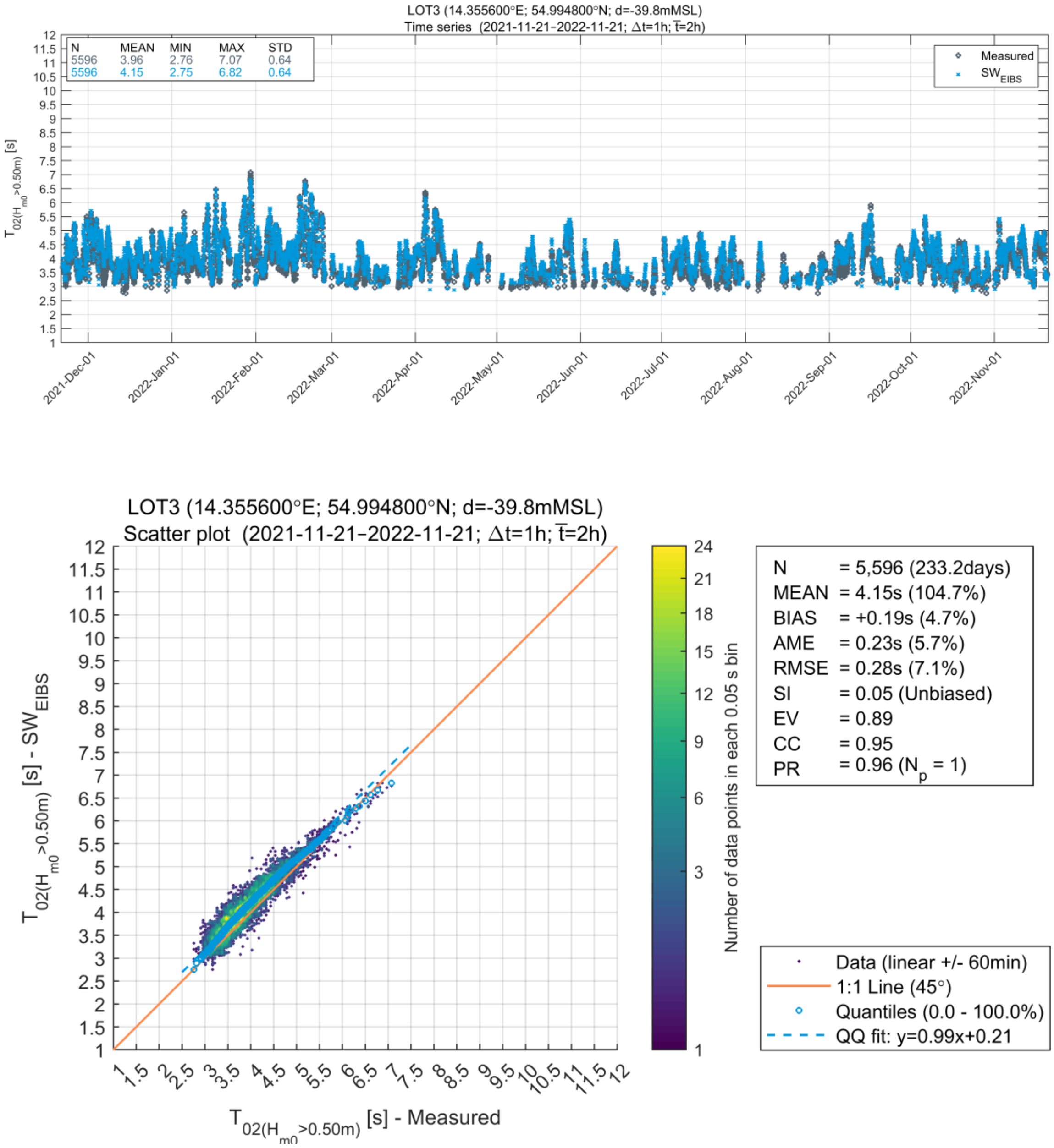

Figure 6.15 Comparison of measured and modelled T_{02} at LOT3

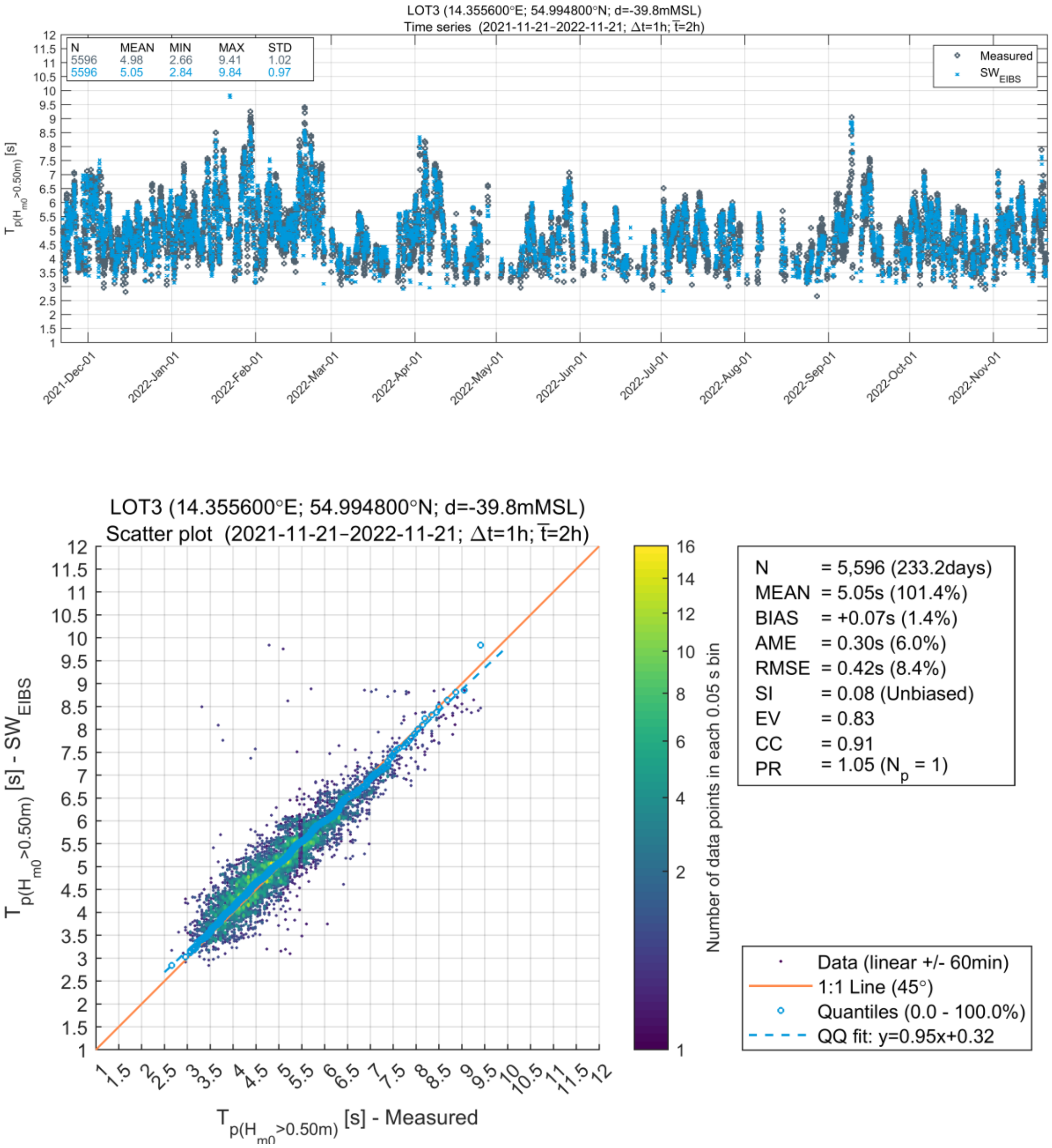

Figure 6.16 Comparison of measured and modelled T_p at LOT3

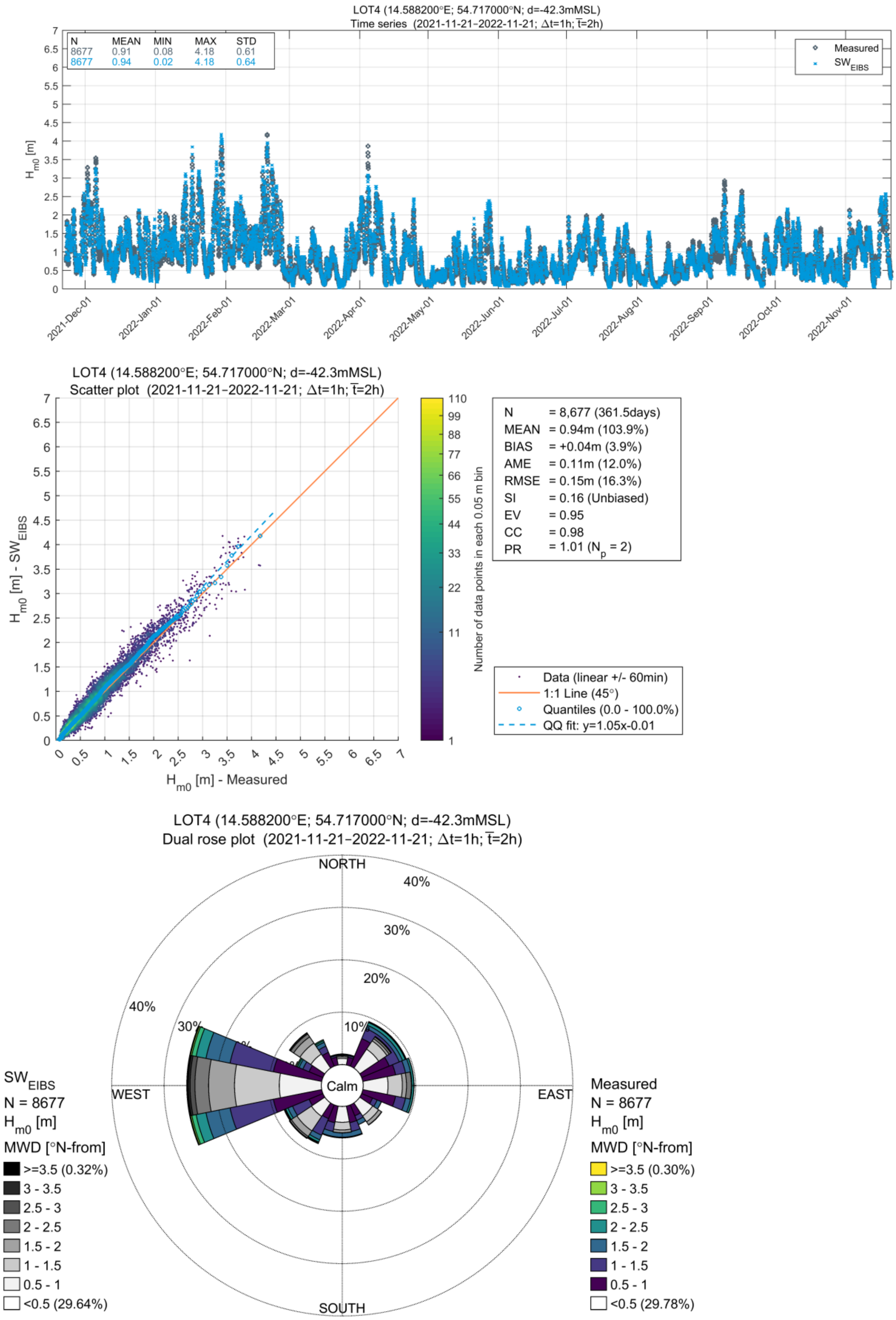

Figure 6.17 Comparison of measured and modelled H_{m0} at LOT4

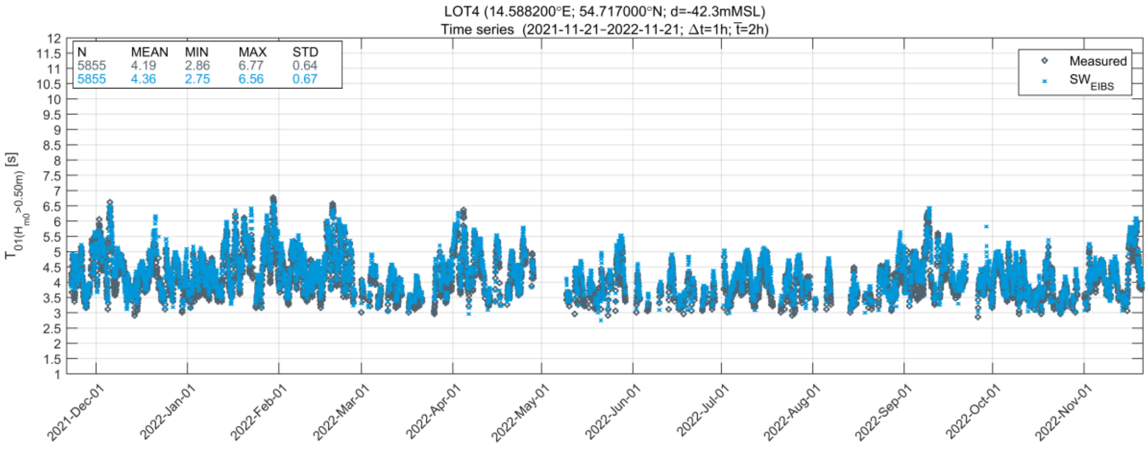

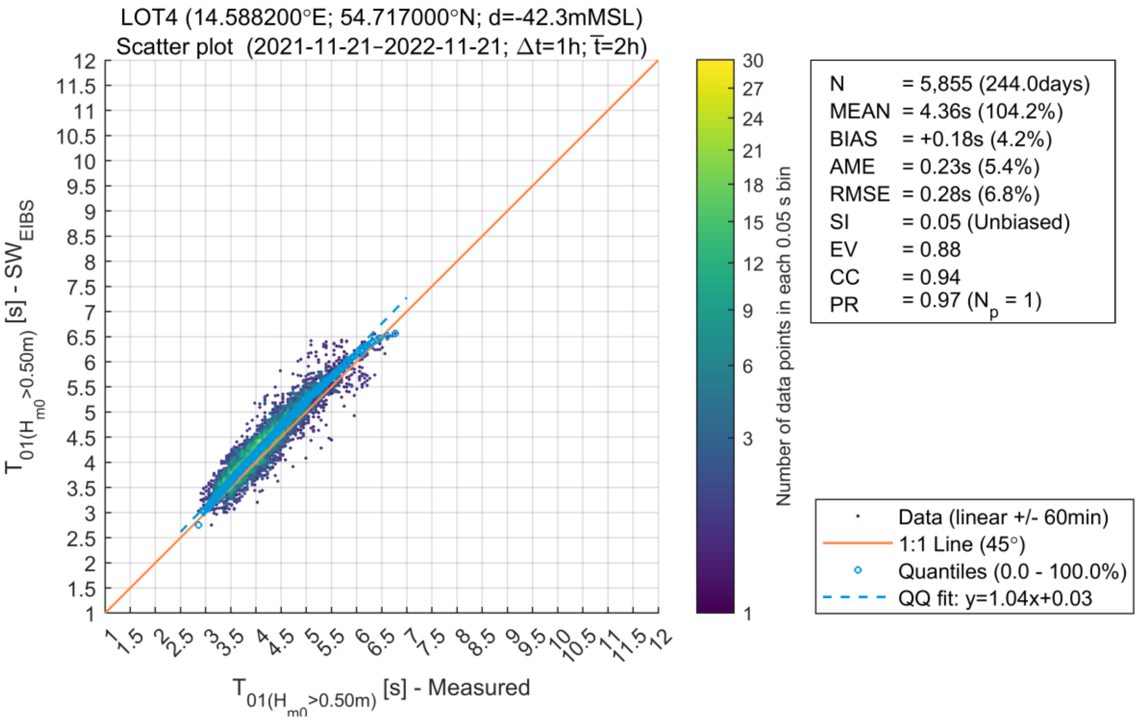

Figure 6.18 Comparison of measured and modelled T_{01} at LOT4

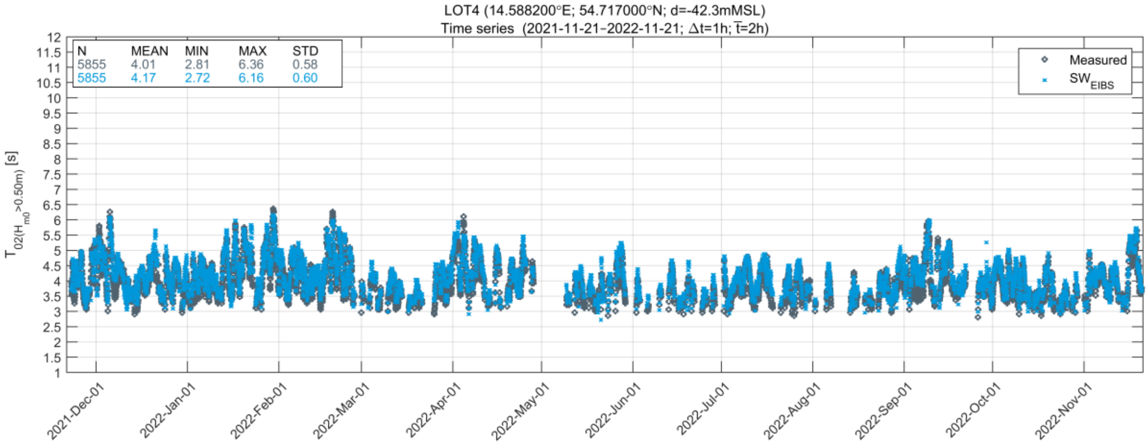

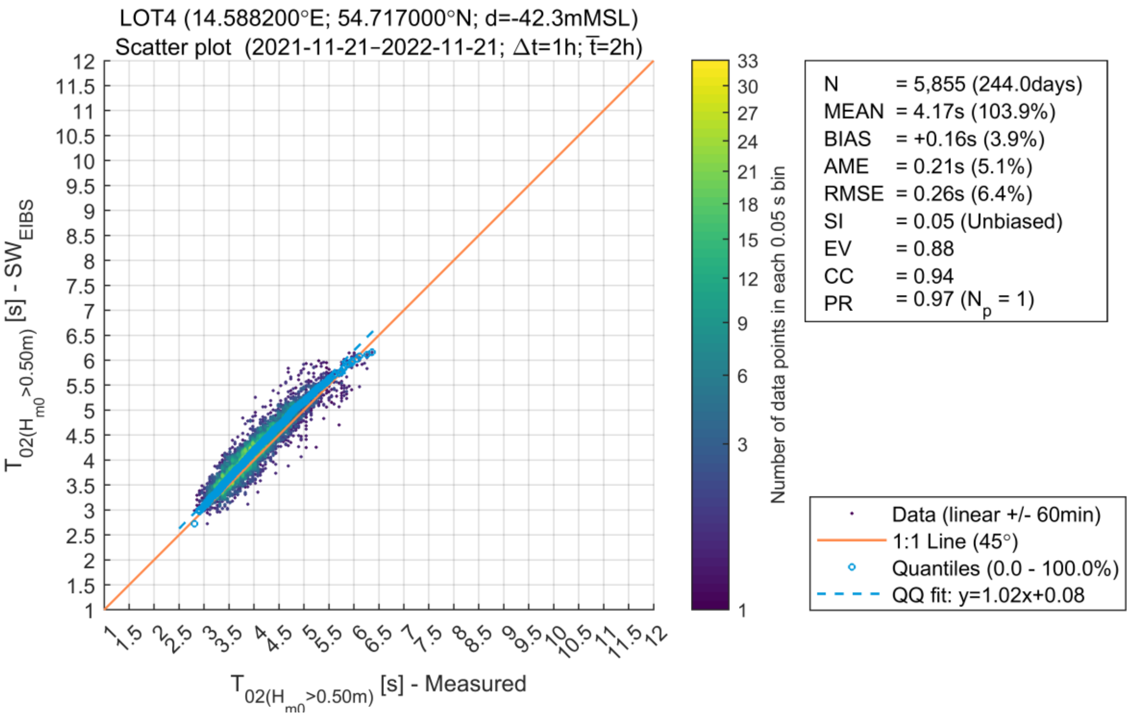

Figure 6.19 Comparison of measured and modelled T_{02} at LOT4

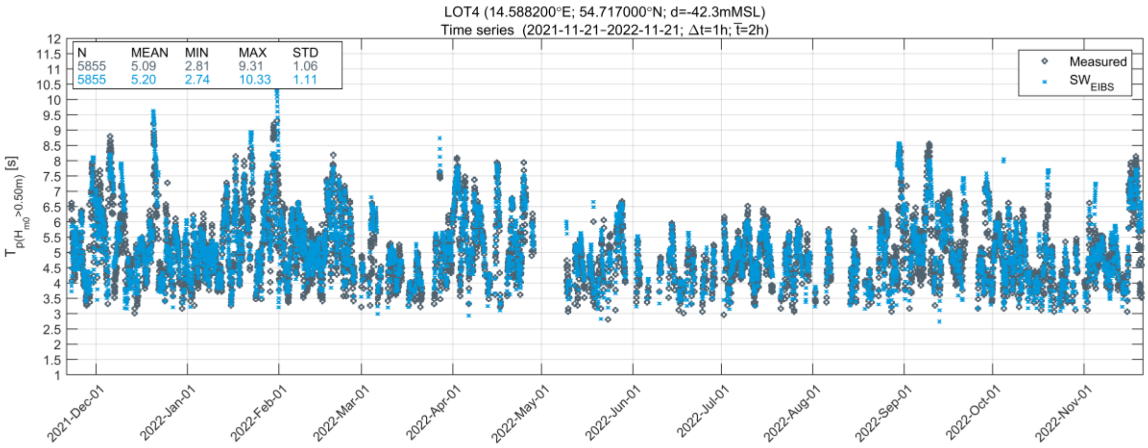

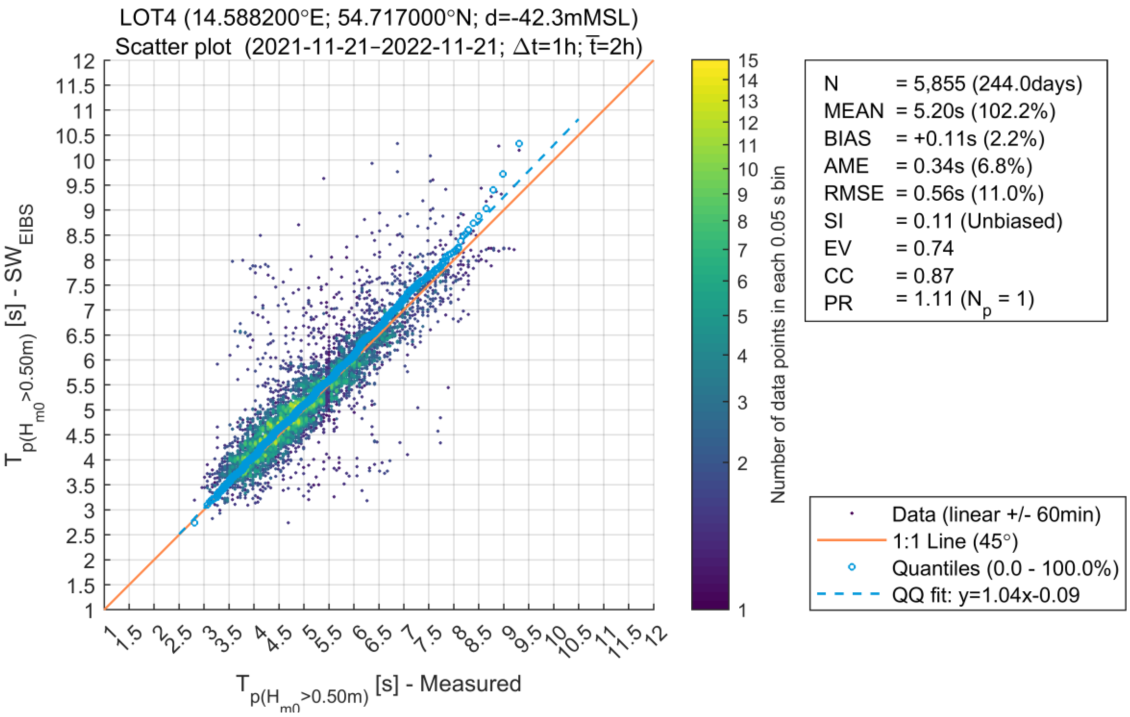

Figure 6.20 Comparison of measured and modelled T_p at LOT4

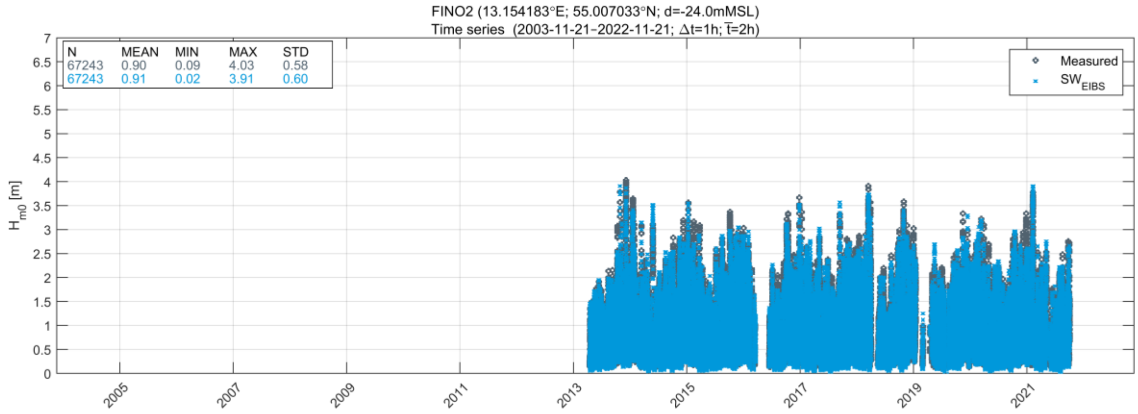

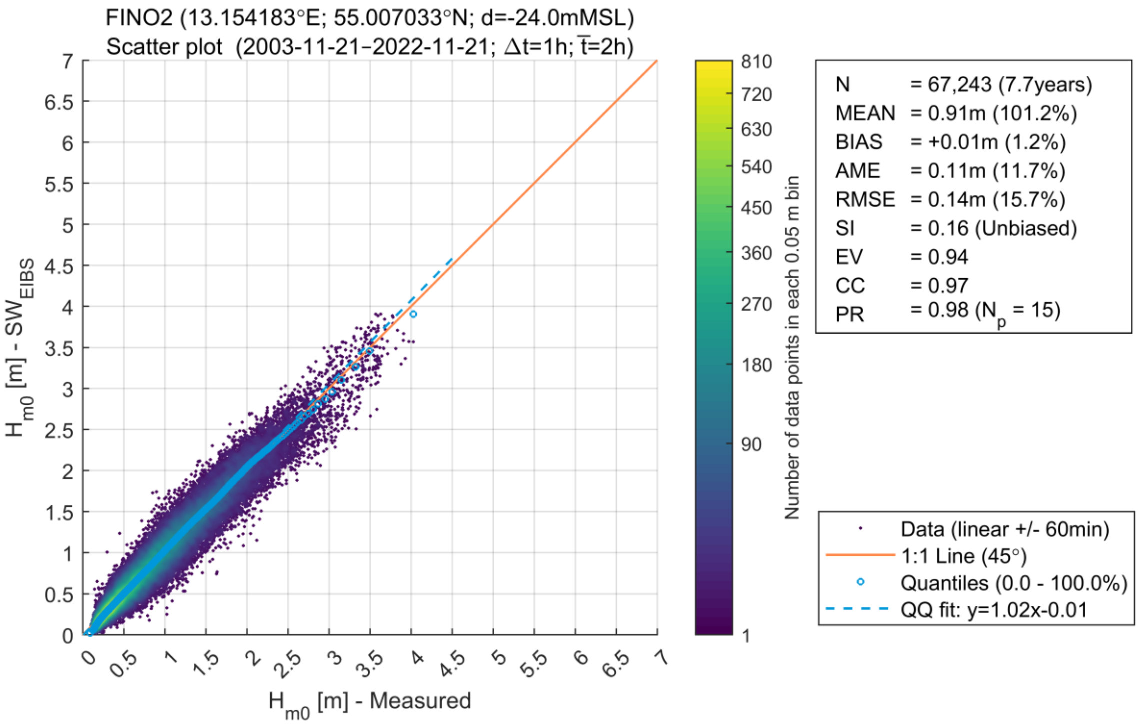

Figure 6.21 Comparison of measured and modelled H_{m0} at FINO2

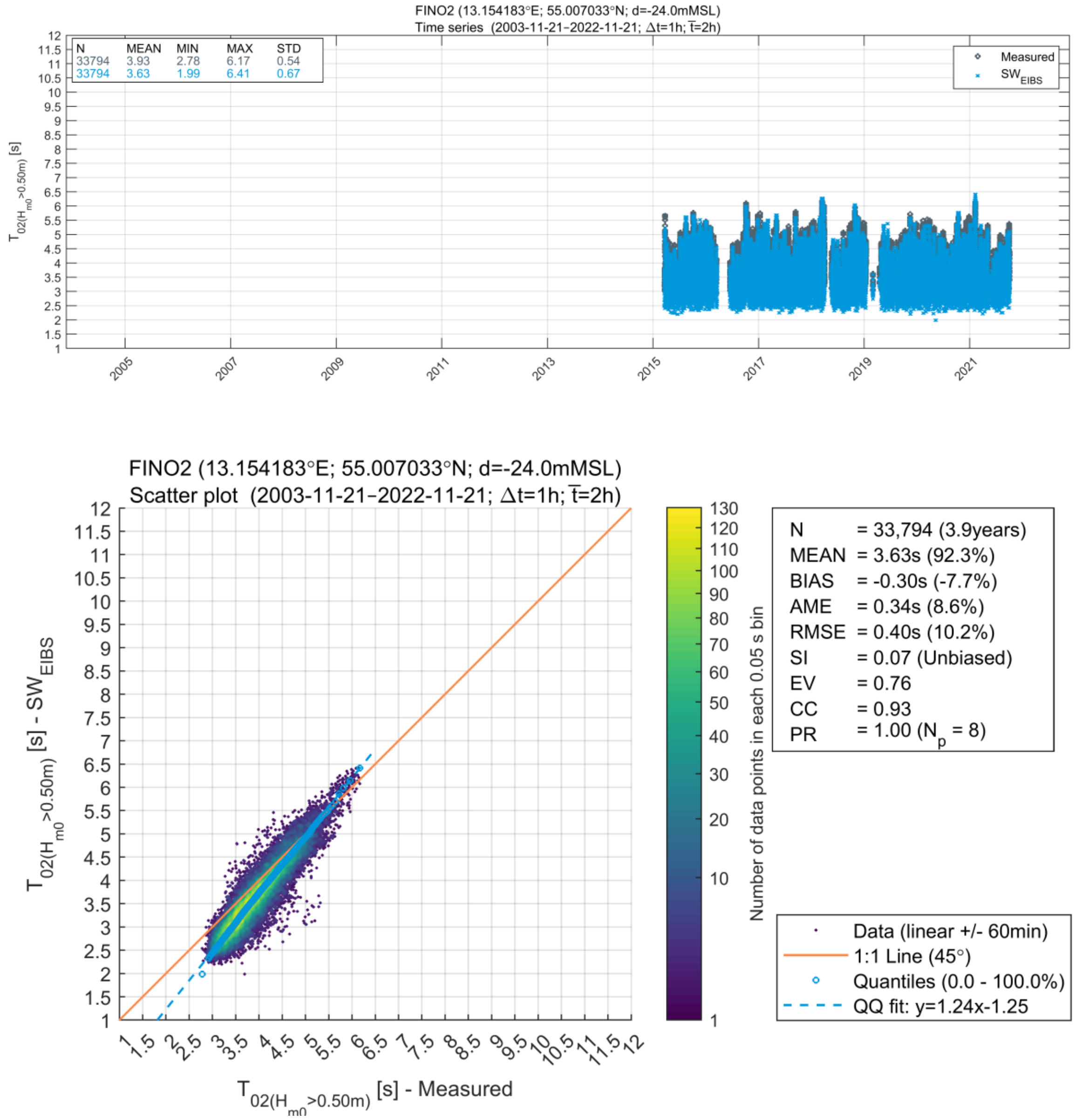

Figure 6.22 Comparison of measured and modelled T_{02} at FINO2

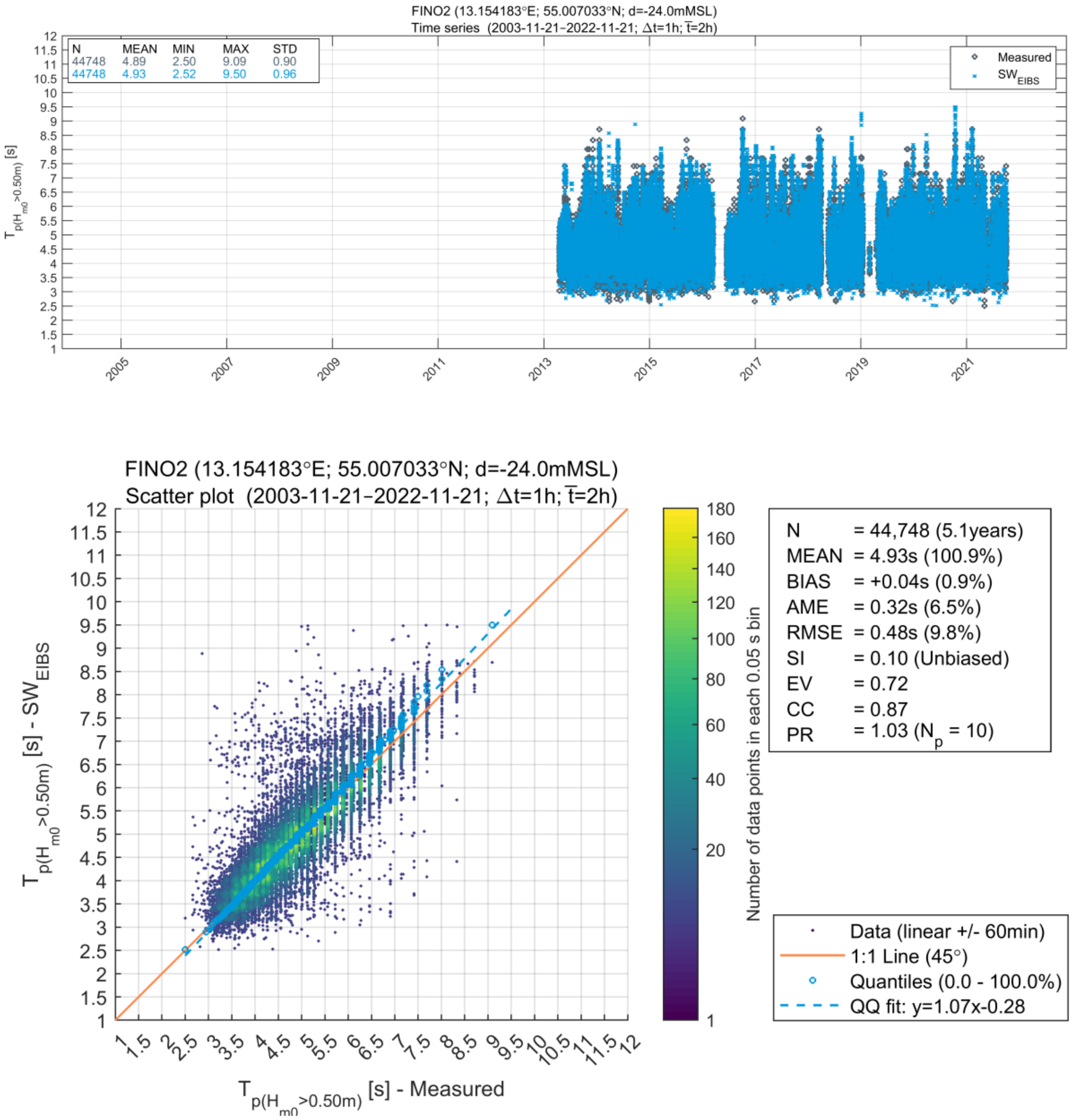

Figure 6.23 Comparison of measured and modelled T_p at FINO2

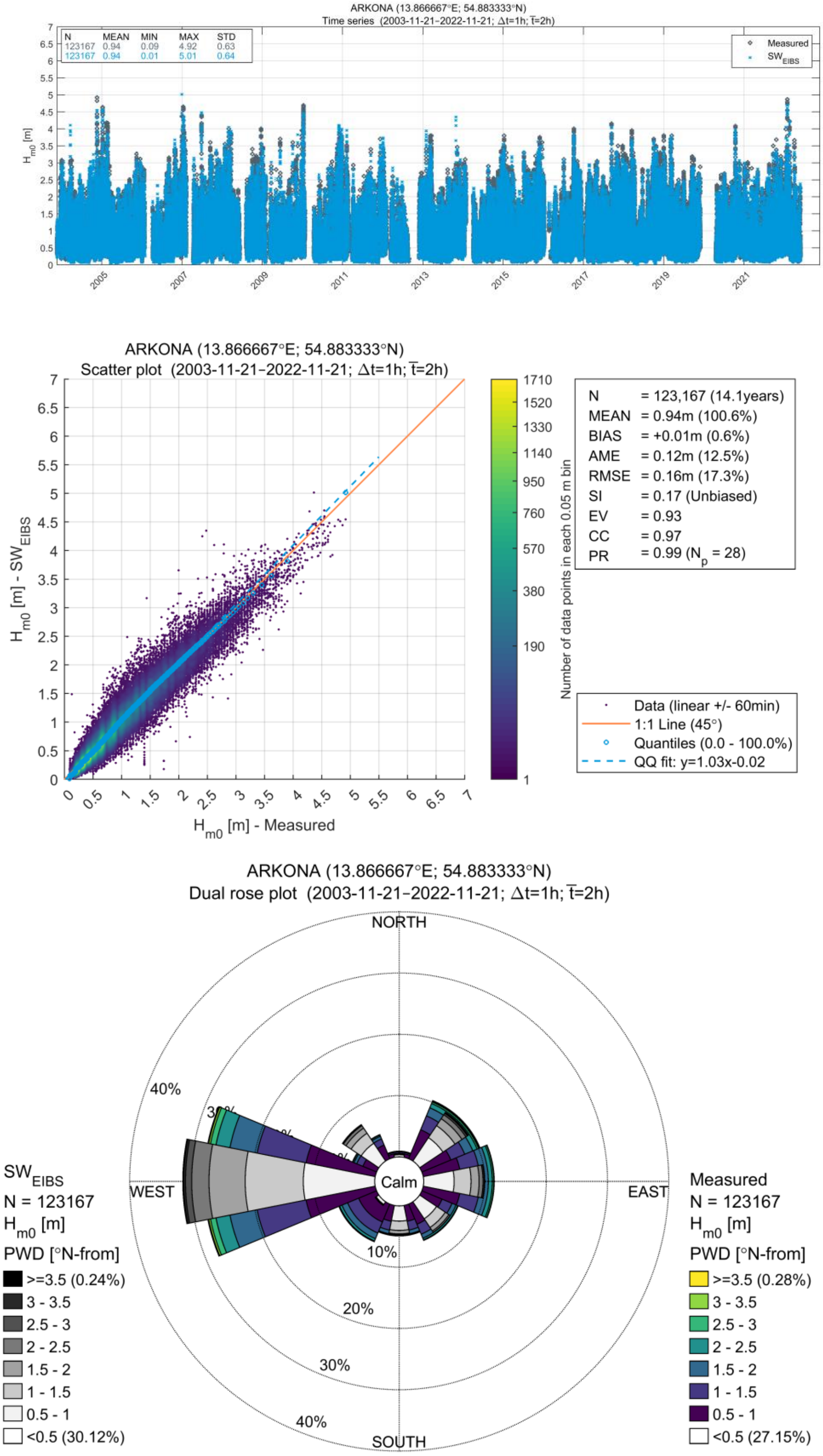

Figure 6.24 Comparison of measured and modelled H_{m0} at Arkona

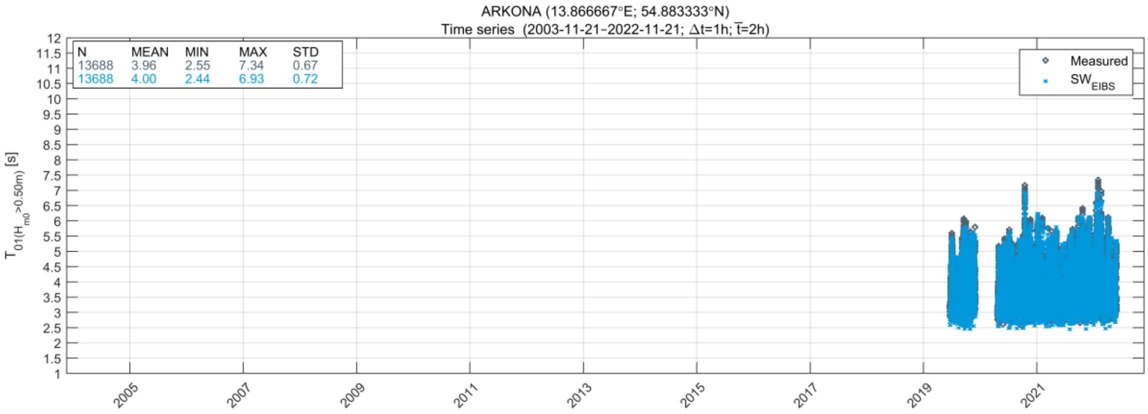

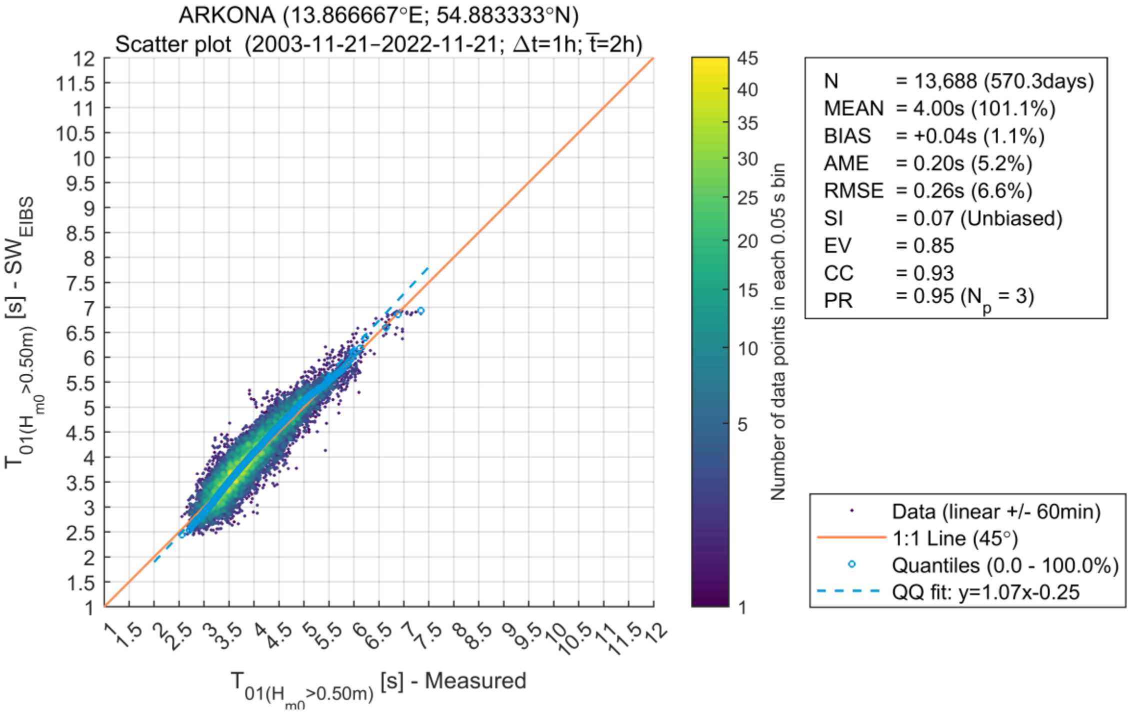

Figure 6.25 Comparison of measured and modelled T_{01} at Arkona

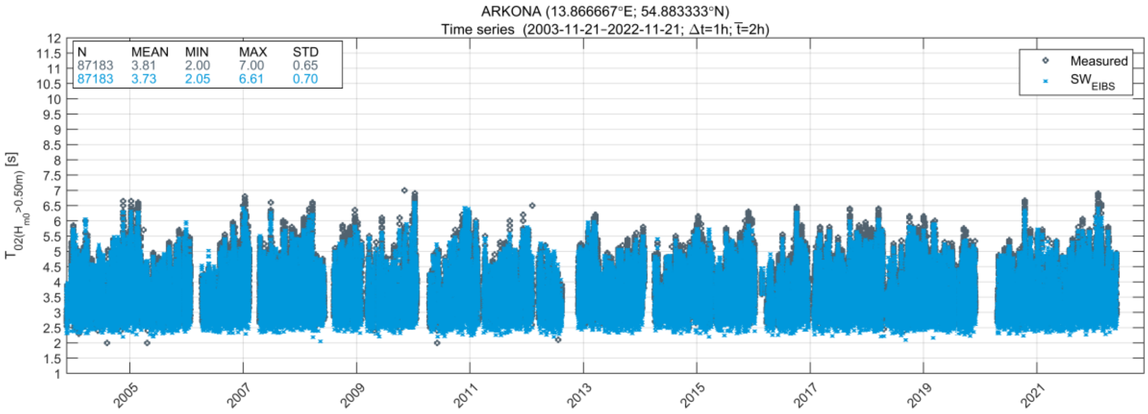

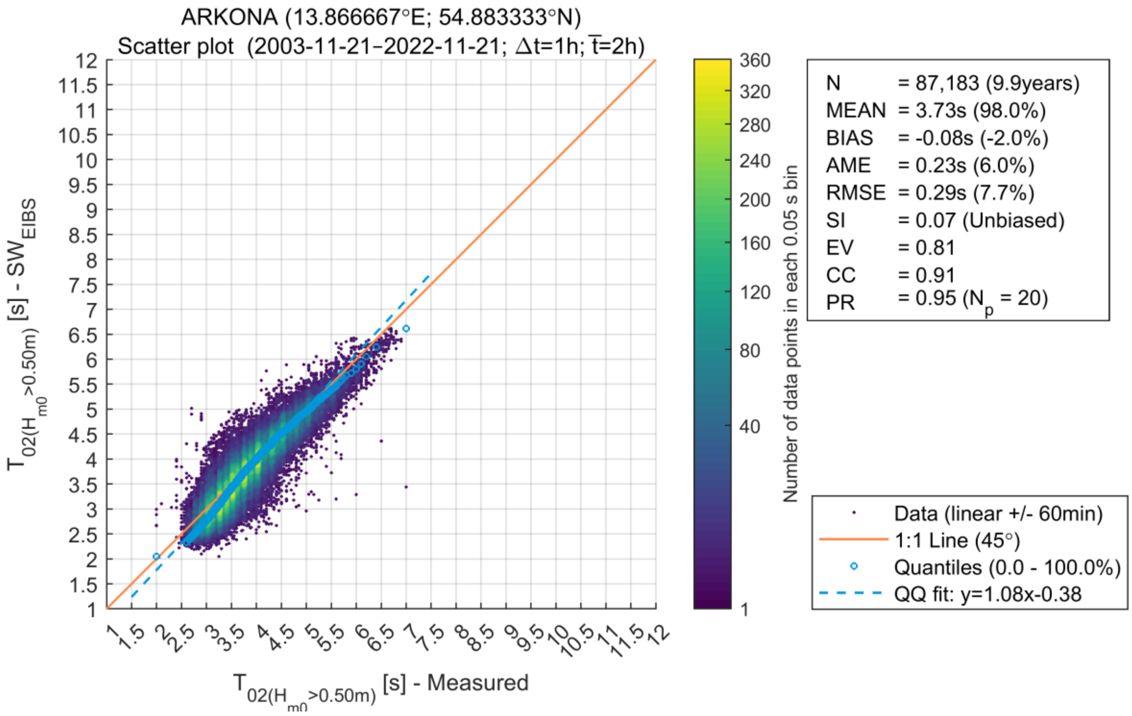

Figure 6.26 Comparison of measured and modelled T_{02} at Arkona

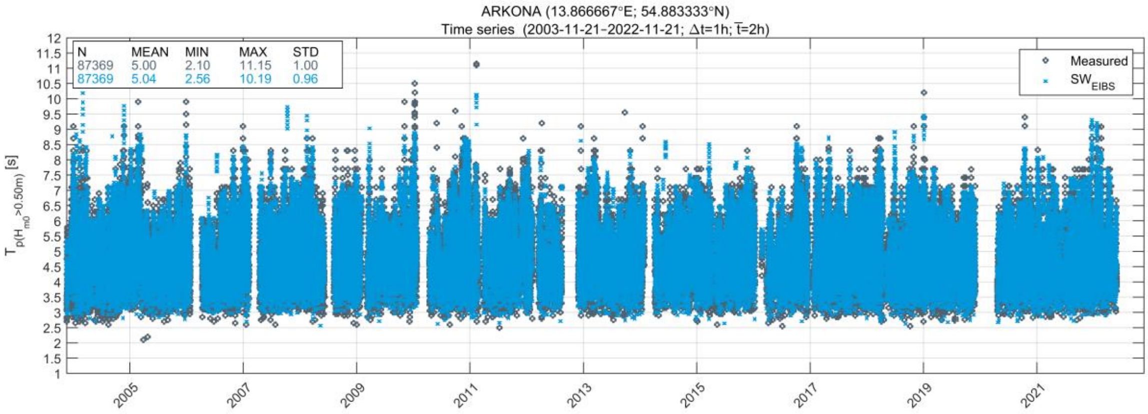

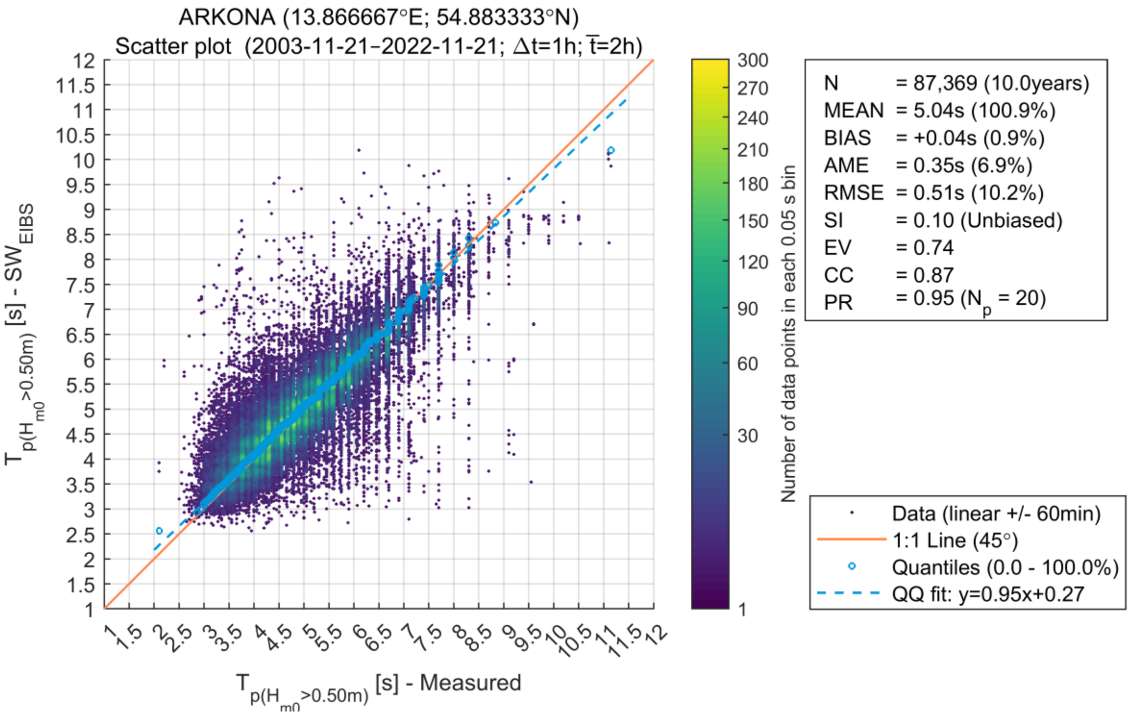

Figure 6.27 Comparison of measured and modelled T_p at Arkona

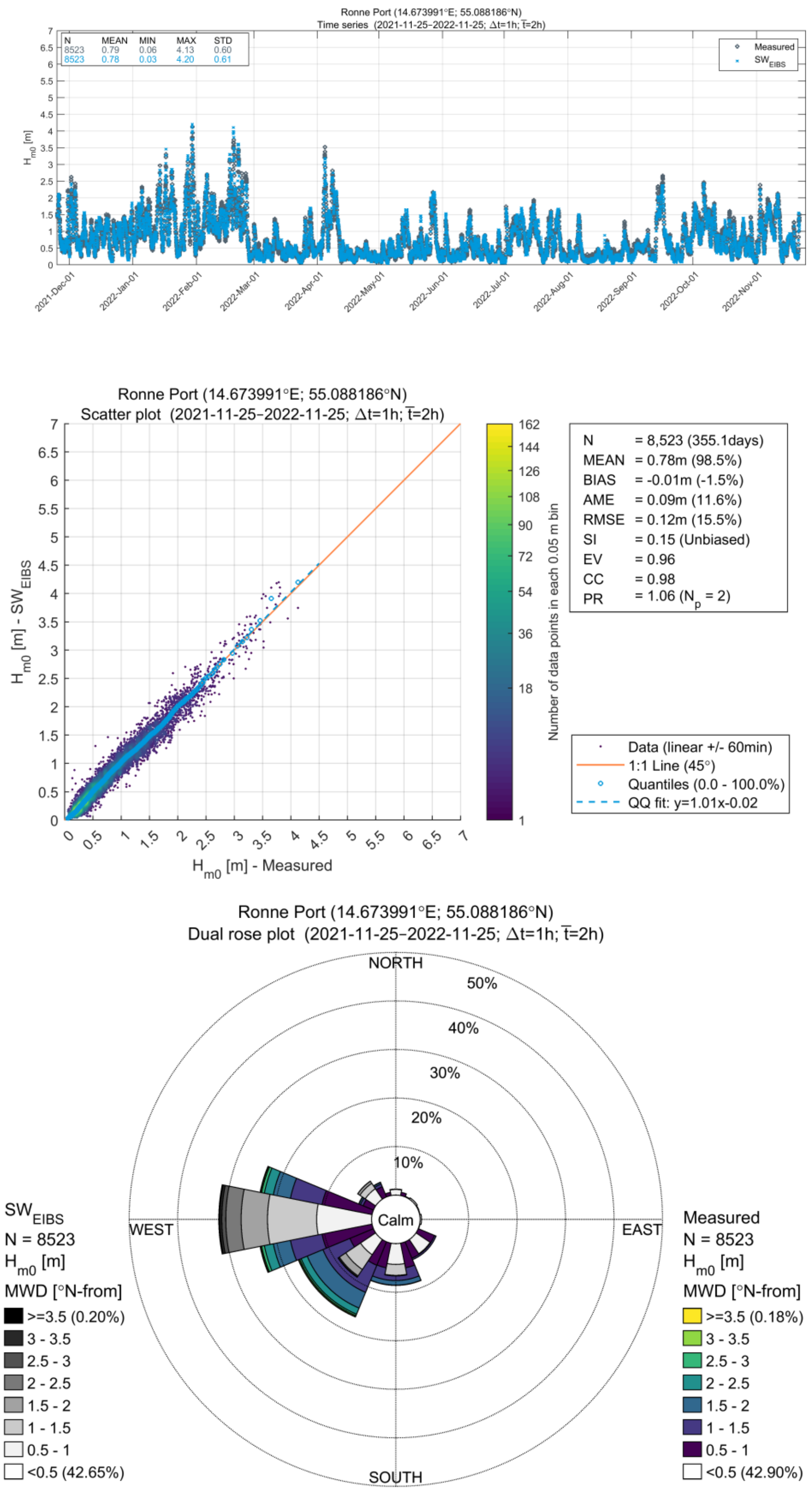

Figure 6.28 Comparison of measured and modelled H_{m0} at Ronne Port

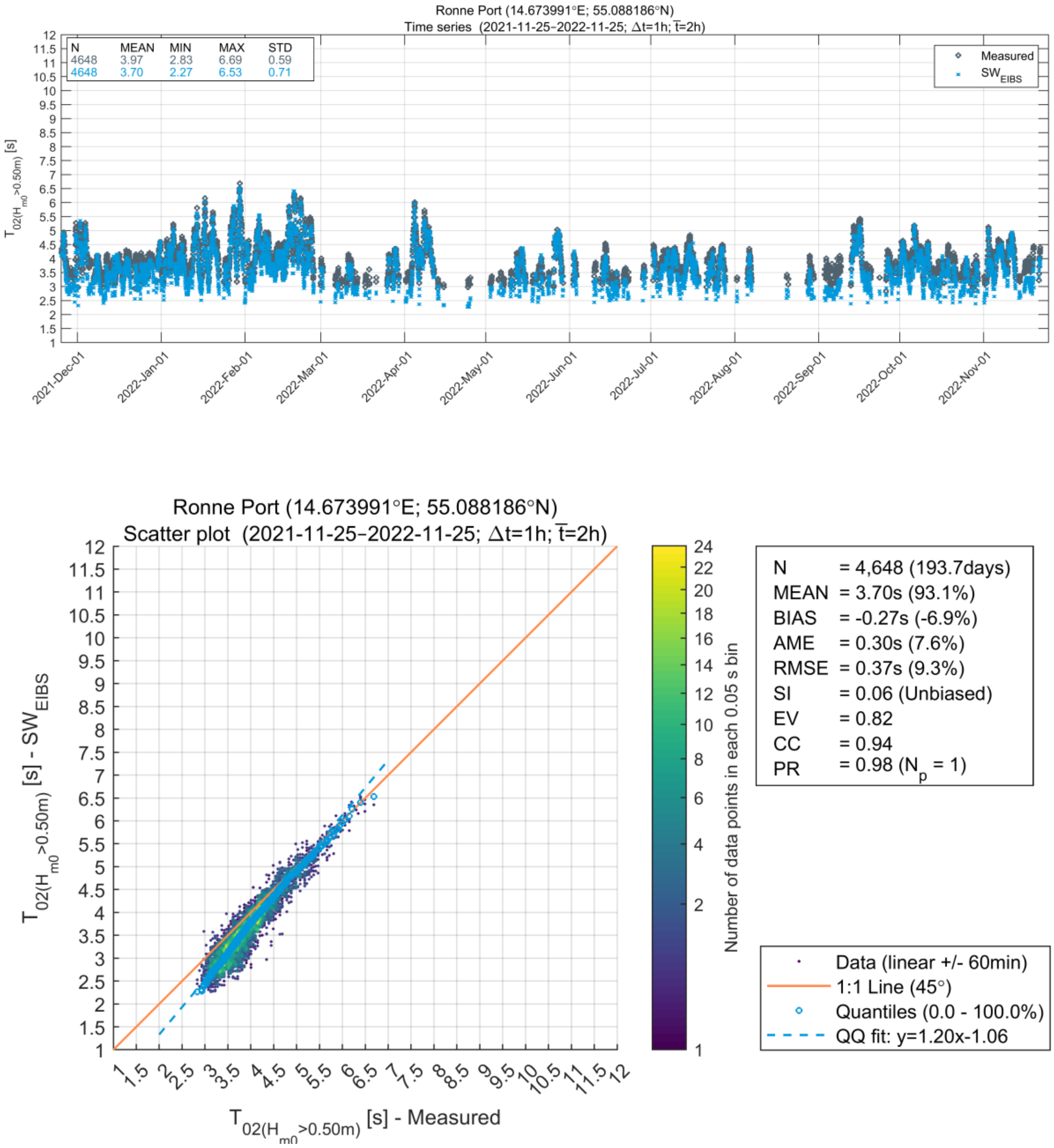

Figure 6.29 Comparison of measured and modelled T_{01} at Ronne Port

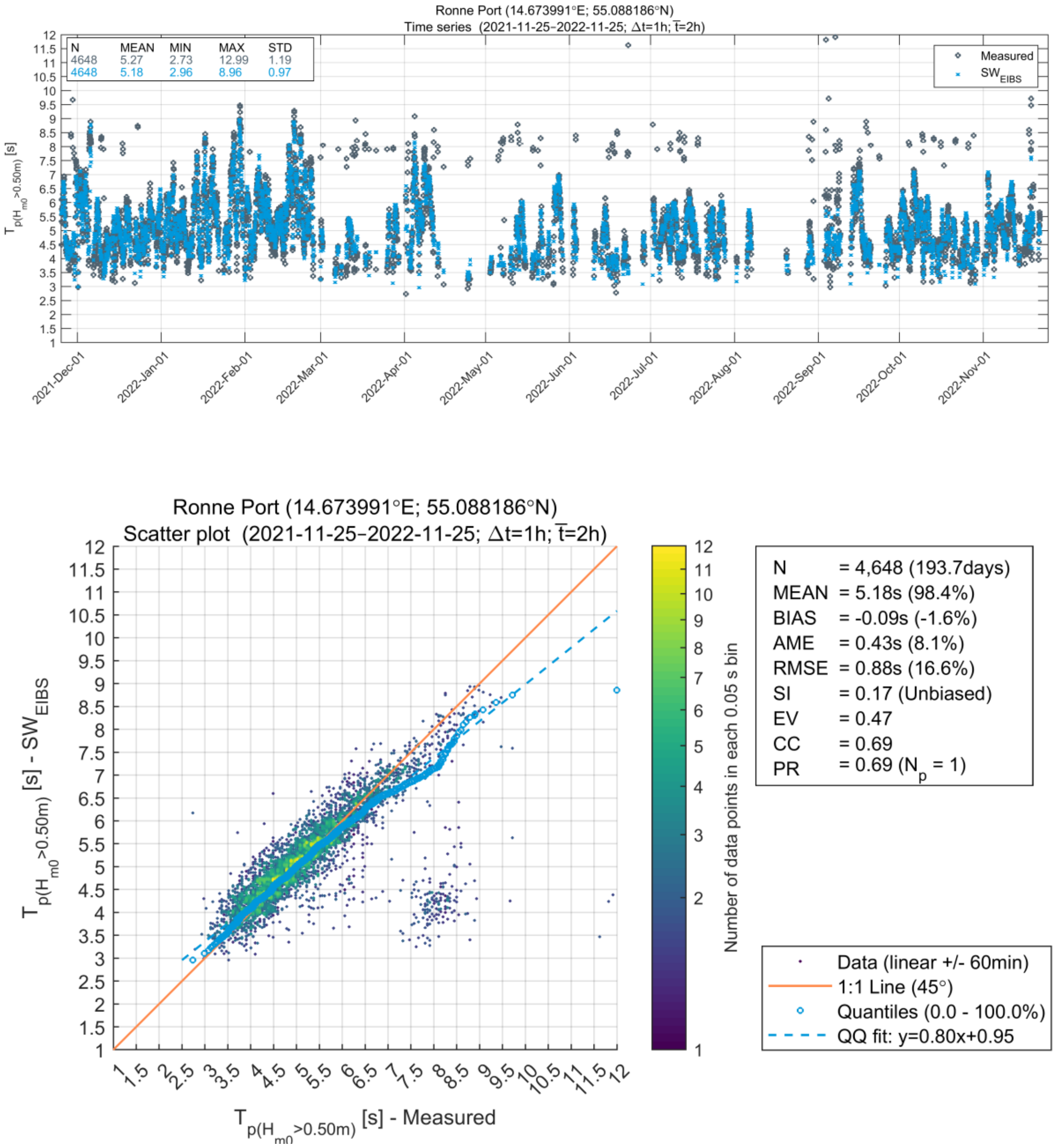

Figure 6.30 Comparison of measured and modelled T_p at Ronne Port

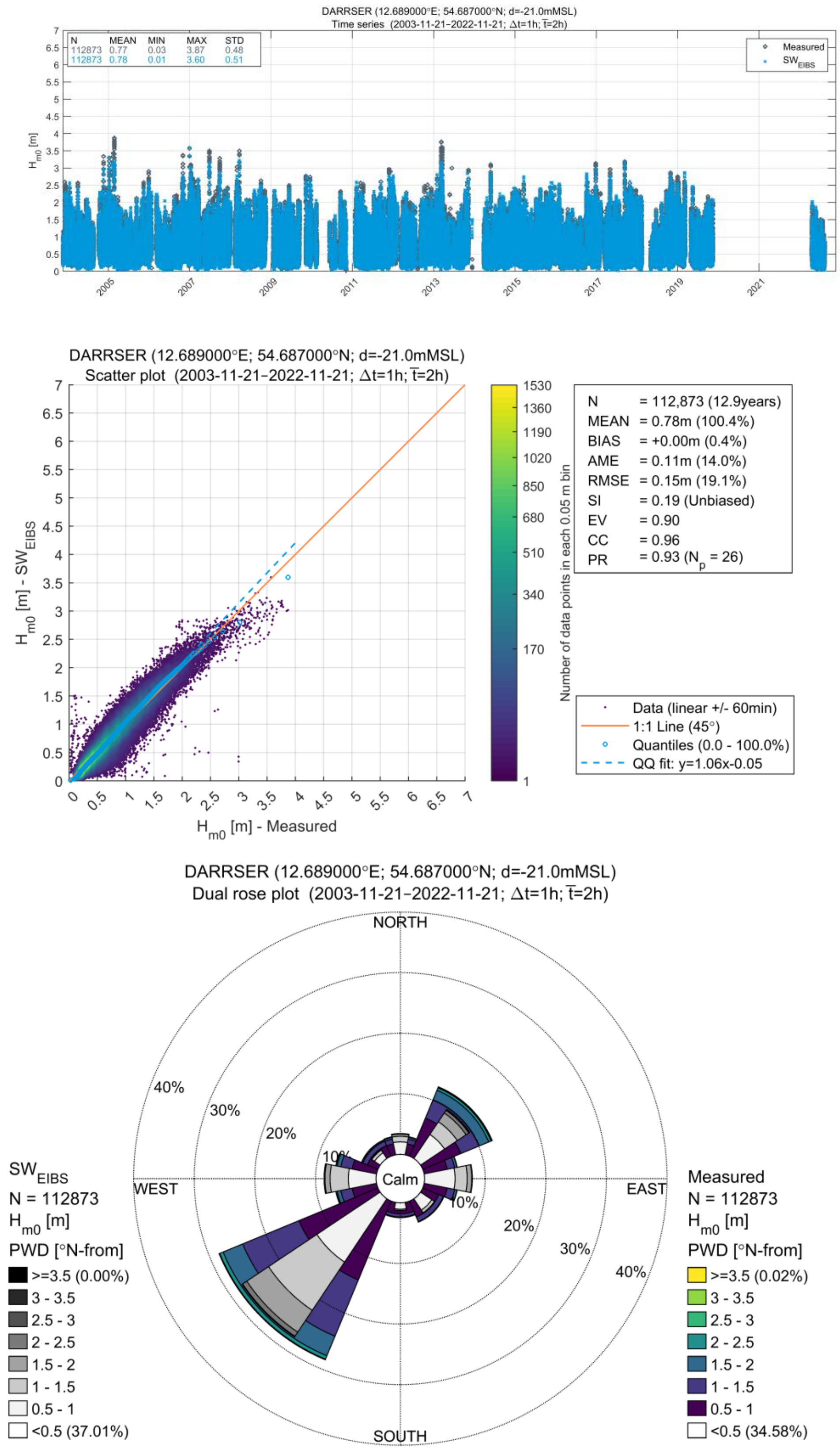

Figure 6.31 Comparison of measured and modelled H_{m0} at Darrser

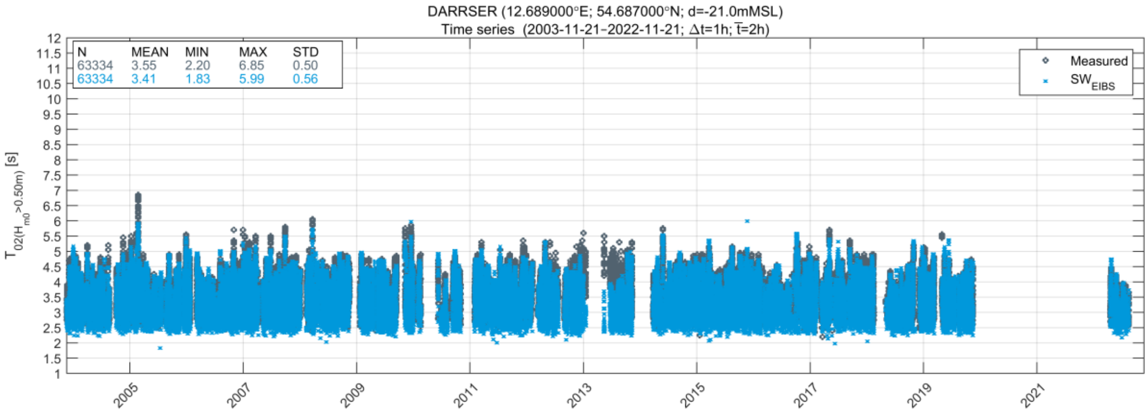

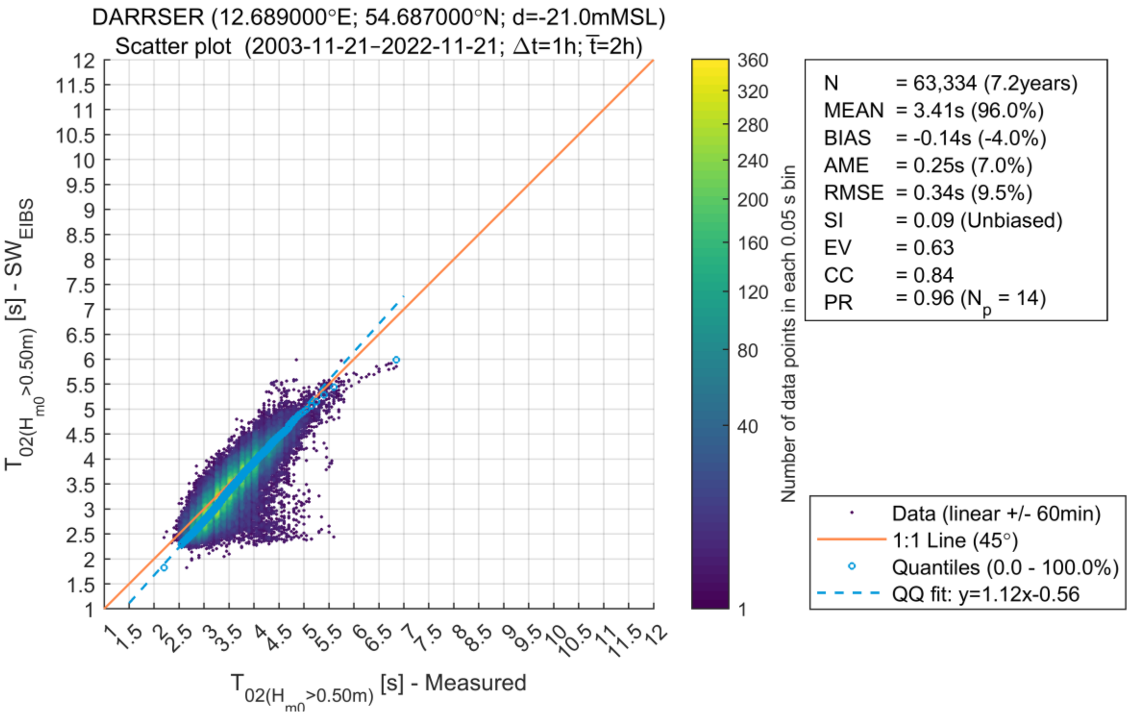

Figure 6.32 Comparison of measured and modelled T_{02} at Darrser

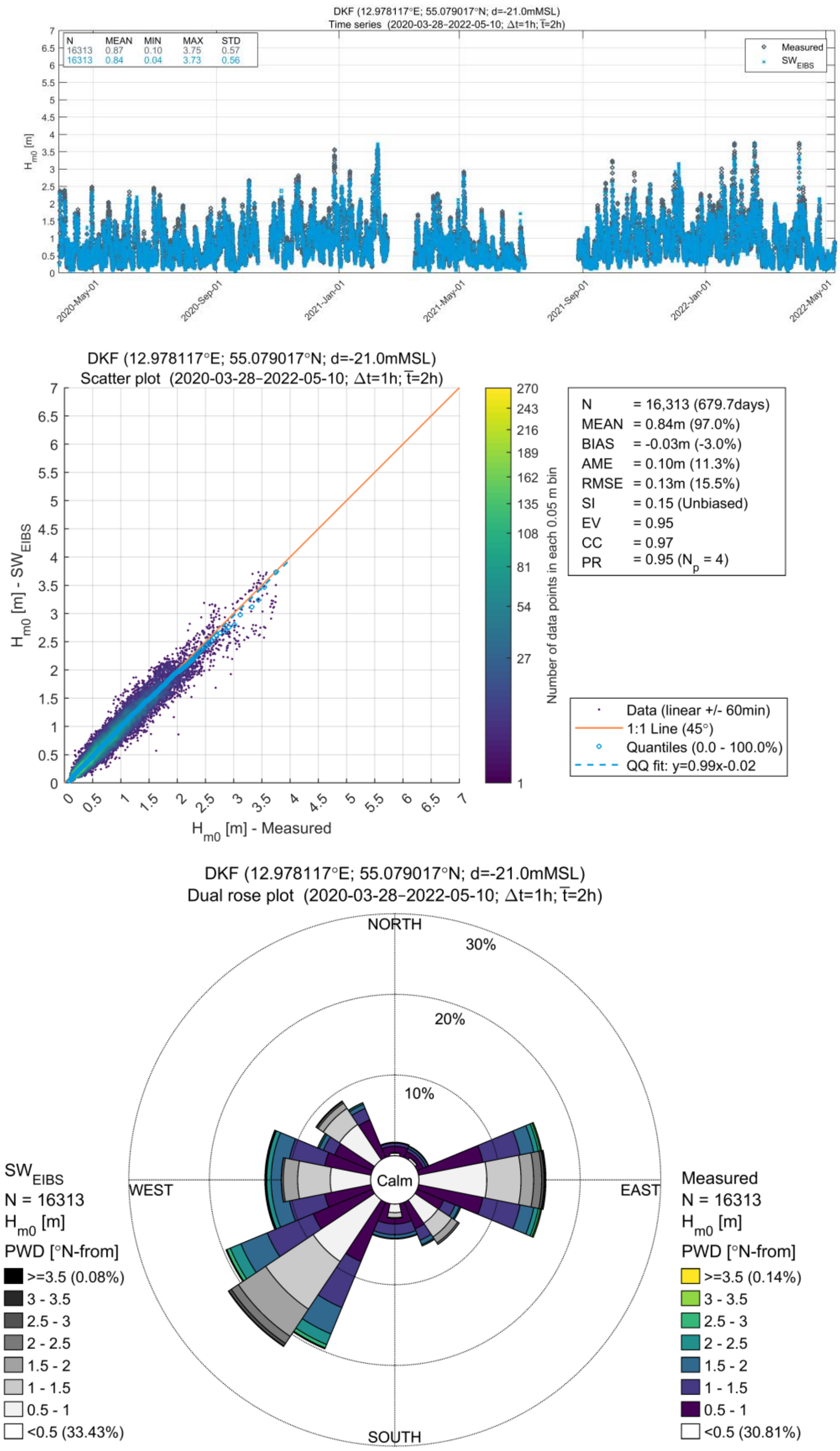

Figure 6.33 Comparison of measured and modelled H_{m0} at DKF

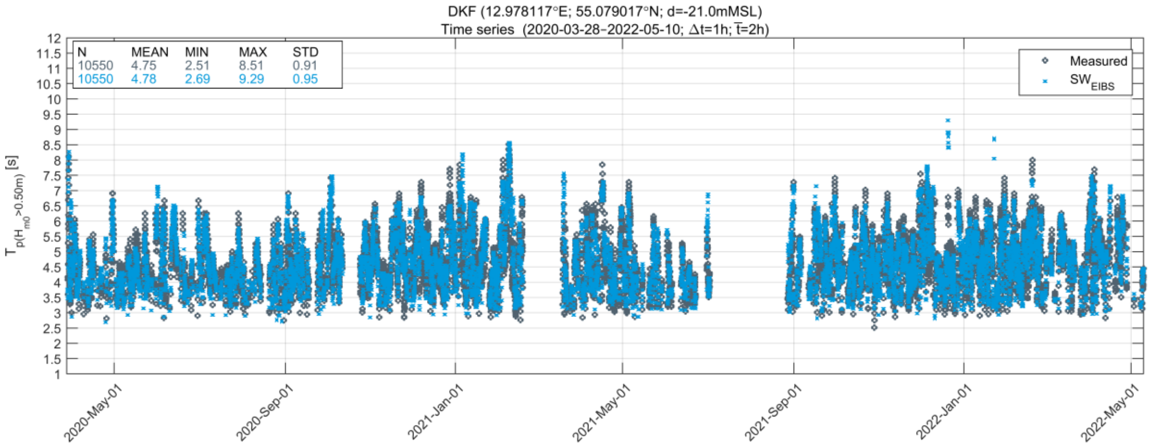

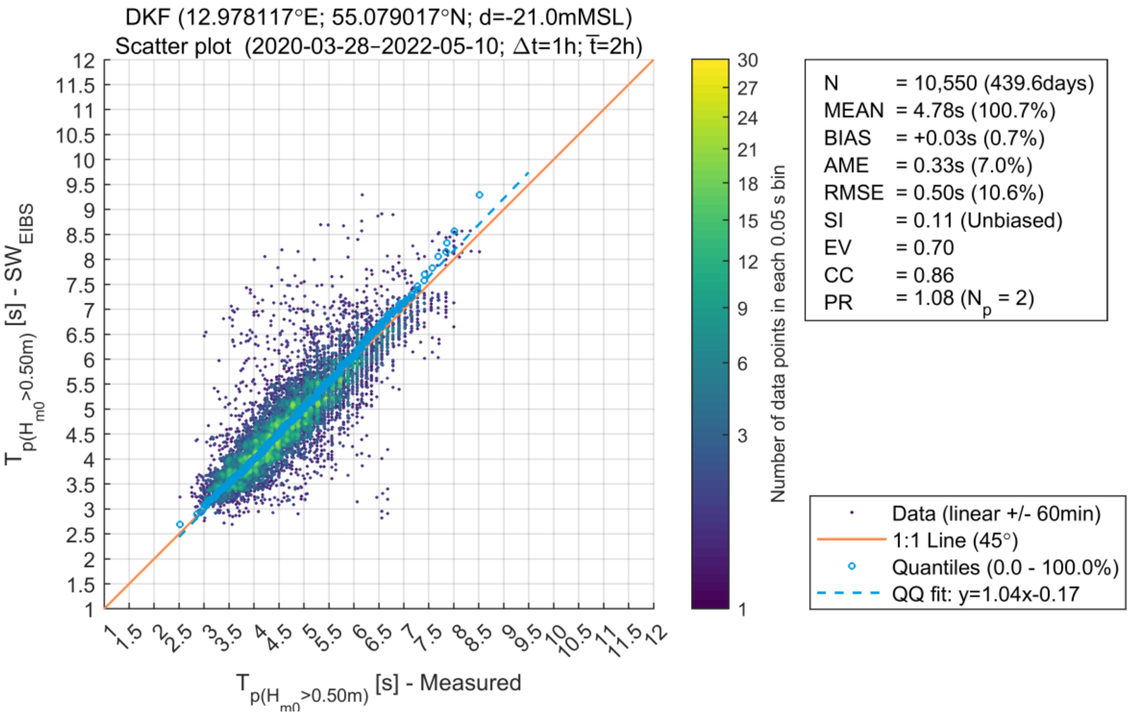

Figure 6.34 Comparison of measured and modelled T_p at DKF

Table 6.5 Statistics of wave validation (H_{m0})

Station	RMSE	SI	CC	PR
LOT3	0.15	0.16	0.98	1.00
LOT4	0.15	0.16	0.98	1.01
FINO2	0.14	0.16	0.97	0.98
Arkona	0.16	0.17	0.97	0.99
Ronne Port	0.12	0.15	0.98	1.06
Darrser	0.15	0.19	0.96	1.06
DKF	0.13	0.15	0.97	0.95
ALL (mean)	0.14	0.16	0.97	1.01

6.3.8 Validation of frequency wave spectra

Measured wave energy spectra were available from the two Wavesense 3 devices deployed at the EIBS site, and modelled wave spectra from SW_{EIBS} were saved at their locations.

The measured spectral frequencies range from 0.04 to 0.6 Hz (1.67 to 25 s), whereas the modelled spectral frequencies range from 0.058 to 1.084 Hz (0.9 to 17.4 s). Therefore, the validation considers the overlapping frequency range.

Figure 6.35 presents the comparison of frequency spectra at LOT3 and LOT4 for two events, 2022-01-17 and 2022-01-29 (storm Malik). The figures demonstrate a good ability of the model to replicate the measured spectral shapes of the two events.

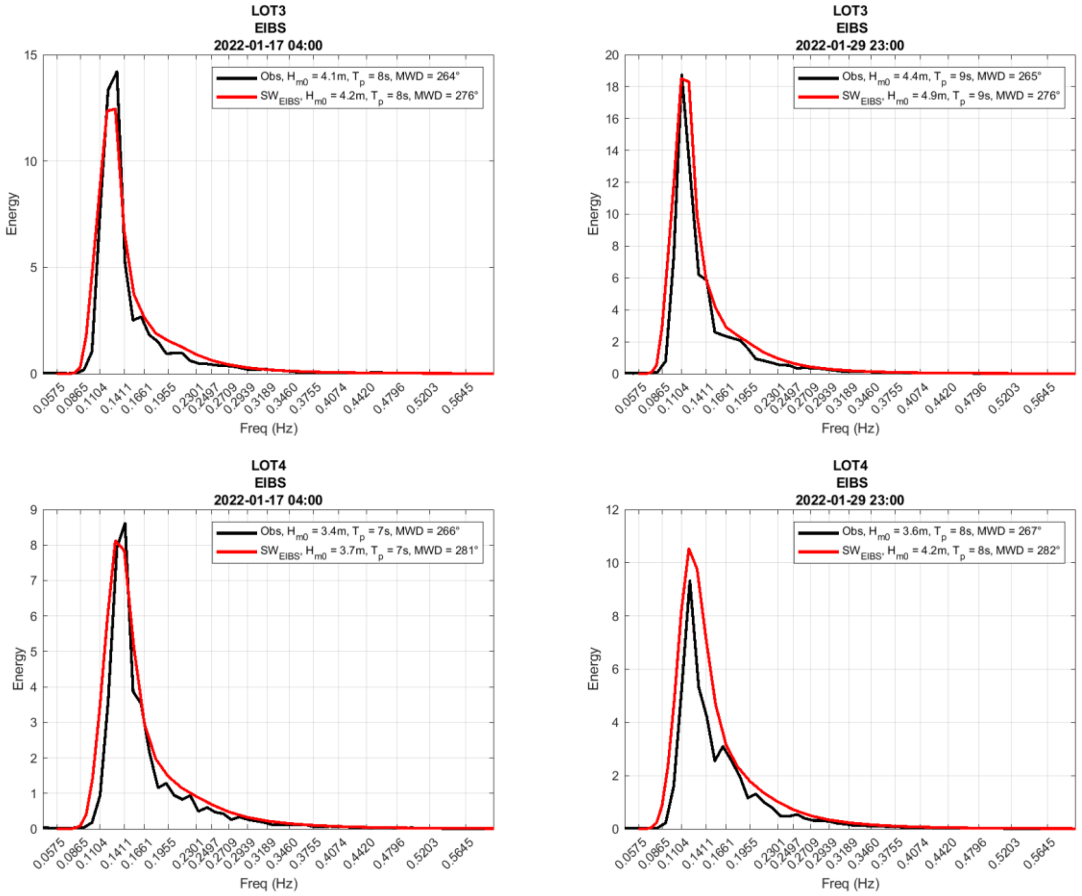

Figure 6.35 Comparison of measured and modelled spectra at LOT3 and LOT4
Black and red lines indicate observed and modelled spectra respectively on 17 January 2022 and 29 January 2022.

6.4 Assessment of wave spectra

This section contains an assessment of the applicability of theoretical spectra to describe the wave spectra for normal and extreme wave conditions. The assessment is based on the modelled frequency spectra which are validated against measurements in Section 6.3.8.

The wave conditions in the Arkona Basin are dominated by local wind. Hence, the total sea state can in most cases be described adequately by a single-peaked spectrum (such as Pierson-Moskowitz or JONSWAP). Wave spectra with more than one peak may occur mainly during non-storm conditions, when there is a comparable amount of wave energy from wind-sea and from swells partitions.

The Pierson-Moskowitz spectrum

The Pierson-Moskowitz (PM) spectrum is given by Eq. (6.1), see e.g. Section 3.5.5.1 in DNV RP-C205, [4].

$$S_{PM}(\omega) = \frac{5}{16} \cdot H_s^2 \cdot \omega_p^4 \cdot \omega^{-5} \cdot \exp\left(-\frac{5}{4}\left(\frac{\omega}{\omega_p}\right)^{-4}\right)$$
$$where: \omega_p = \frac{2\pi}{T_p} is\ the\ angular\ frequency \tag{6.1}$$

The JONSWAP spectrum

The JONSWAP (J) spectrum is given by Eq. (6.2), see Section 3.5.5.2-5 in DNV RP-C205, [4].

$$S_J(\omega) = A_\gamma \cdot S_{PM}(\omega) \cdot \gamma^{\exp\left(-0.5\left(\frac{\omega-\omega_p}{\sigma\cdot\omega_p}\right)^2\right)}$$
$$\begin{aligned} &where: \\ &\gamma = non\ dimensional\ peak\ shape\ parameter \\ &\sigma = spectral\ width\ parameter \\ &\sigma = \sigma_a \text{ for } \omega \le \omega_p \\ &\sigma = \sigma_b \text{ for } \omega > \omega_p \\ &A\gamma = \frac{0.2}{0.065 \cdot \gamma^{0.803} + 0.135} \text{ is a normalizing factor} \end{aligned} \tag{6.2}$$

Average values are $\gamma = 3.3$, $\sigma_a = 0.07$, $\sigma_b = 0.09$. If no values are given, γ may be estimated by Eq. (6.3), i.e., defining γ for each sea state (timestep) using T_p and H_{m0}. For $\gamma = 1.0$, the JONSWAP spectrum reduces to the Pierson-Moskowitz spectrum.

$$\begin{aligned} &\gamma = 5\ for\ {T_p}/{\sqrt{H_{m0}}} \le 3.6 \\ &\gamma = exp\left(5.75 - 1.15 \cdot {T_p}/{\sqrt{H_{m0}}}\right)\ for\ 3.6 < {T_p}/{\sqrt{H_{m0}}} \le 5 \\ &\gamma = 1\ for\ 5 \le {T_p}/{\sqrt{H_{m0}}} \end{aligned} \tag{6.3}$$

Recommended spectrum

Figure 6.36 presents averaged modelled frequency spectra (during 1979-2022) of SW_{EIBS} and the corresponding mean JONSWAP spectra for 0.5 m bins of H_{m0}. The figures show that the average modelled spectra match the average JONSWAP spectra well, except for H_{m0} < 0.5 m. Hence, in general, the spectrum is well represented by a single JONSWAP spectrum. For information on gamma values, it is recommended to apply the guidelines in Section 3.5.5 of RP-C205 [4], i.e. defining γ based on T_p and H_{m0}, as given in Eq. (6.3). Table 6.6 presents JONSWAP peak shape factor, γ, per H_{m0} and T_p.

Table 6.6 JONSWAP peak shape factor, γ, per H_{m0} and T_p cf. Section 3.5.5.5 in DNV [4]

γ	T_p [s]									
H_{m0} [m]	2	4	6	8	10	12	14	16	18	20
1	5.0	3.2	1.0	1.0	1.0	1.0	1.0	1.0	1.0	1.0
2	5.0	5.0	2.4	1.0	1.0	1.0	1.0	1.0	1.0	1.0
3	5.0	5.0	5.0	1.6	1.0	1.0	1.0	1.0	1.0	1.0
4	5.0	5.0	5.0	3.2	1.0	1.0	1.0	1.0	1.0	1.0
5	5.0	5.0	5.0	5.0	1.8	1.0	1.0	1.0	1.0	1.0
6	5.0	5.0	5.0	5.0	2.9	1.1	1.0	1.0	1.0	1.0
7	5.0	5.0	5.0	5.0	4.1	1.7	1.0	1.0	1.0	1.0
8	5.0	5.0	5.0	5.0	5.0	2.4	1.1	1.0	1.0	1.0
9	5.0	5.0	5.0	5.0	5.0	3.2	1.5	1.0	1.0	1.0
10	5.0	5.0	5.0	5.0	5.0	4.0	1.9	1.0	1.0	1.0

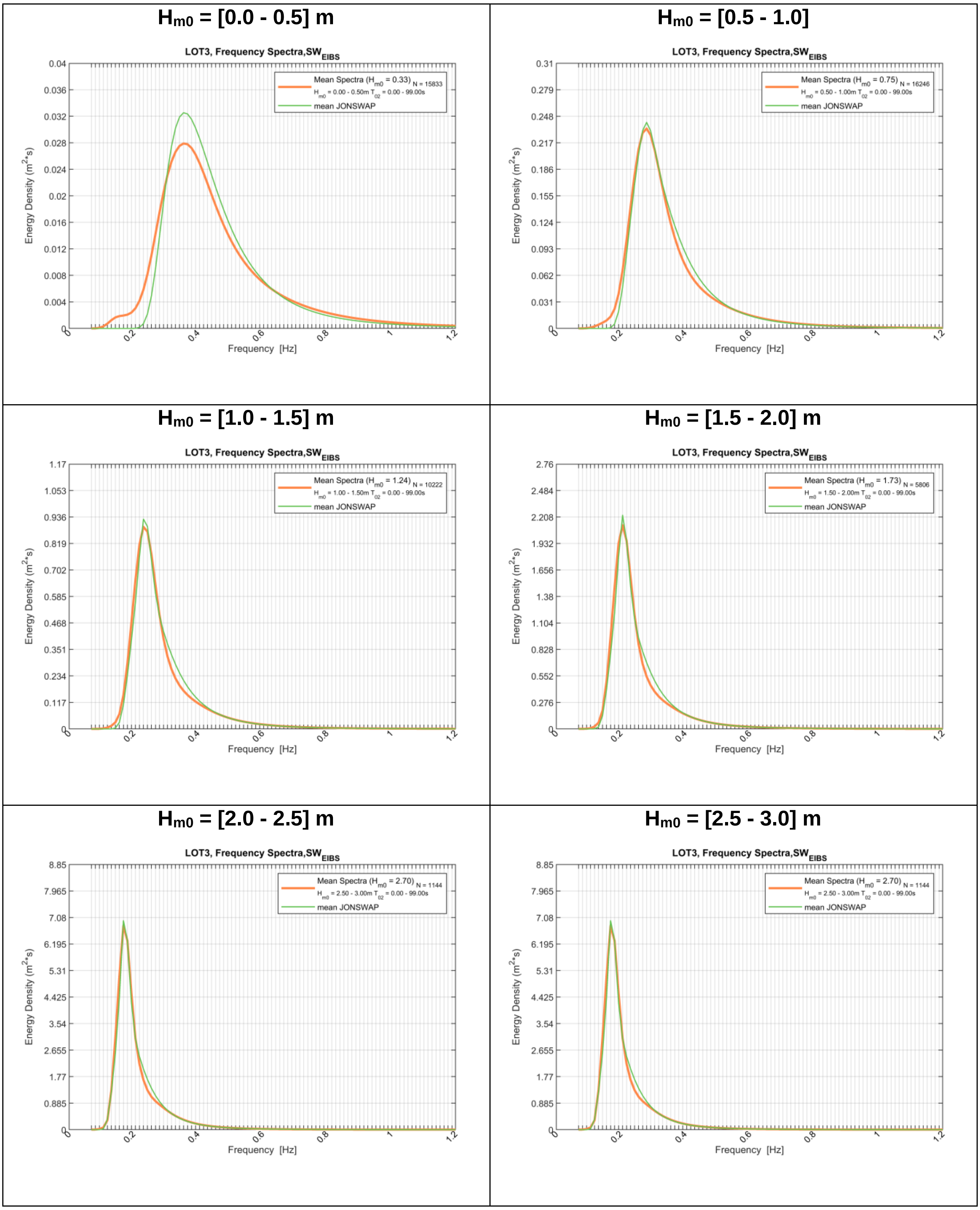

Figure continues next page.

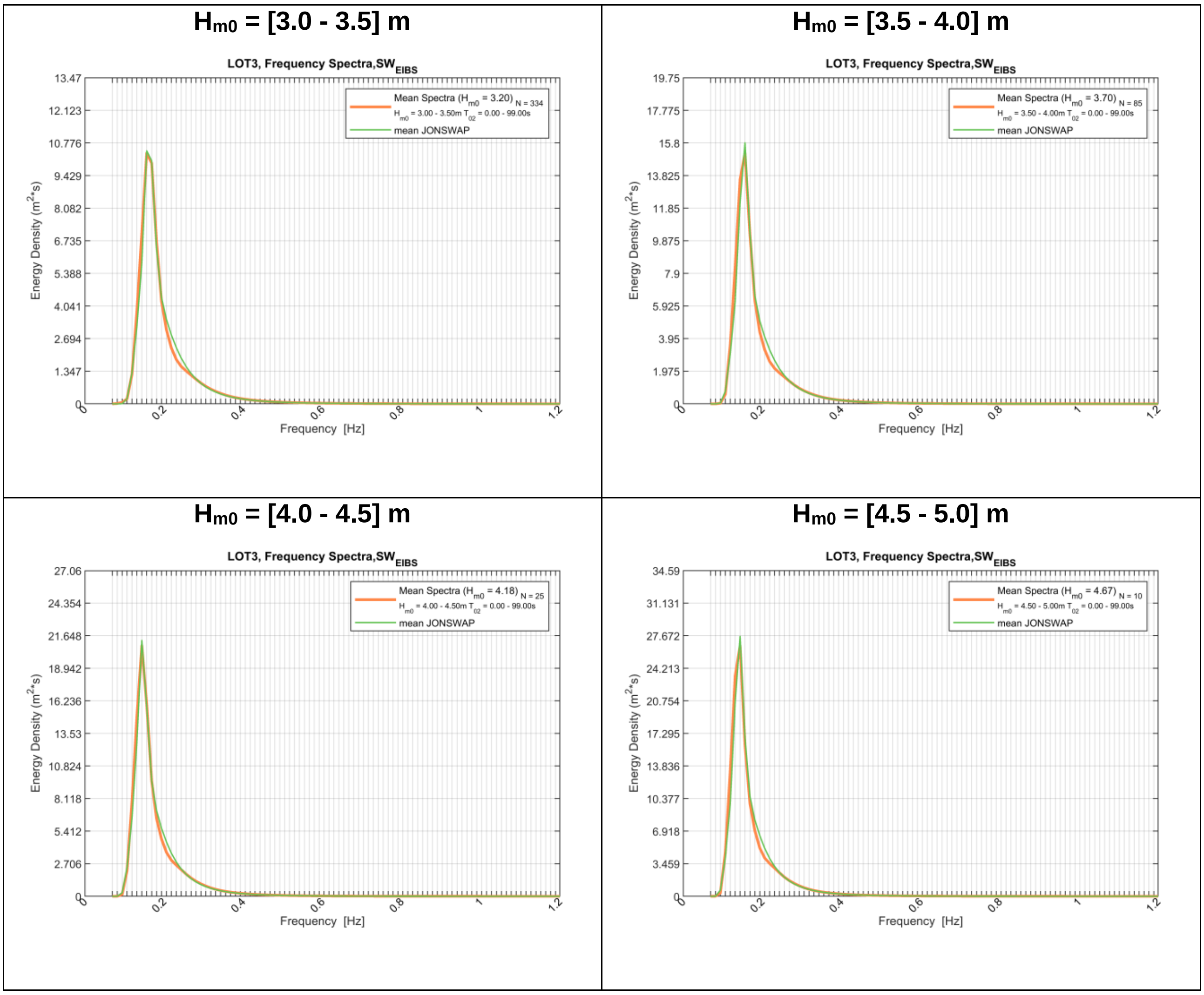

Figure 6.36 Averaged frequency spectra (during 2017-2022) of SW_{EIBS} and corresponding mean JONSWAP spectrum based on DNV [4], for 0.5 m bins (0 – 5 m) of H_{m0} at LOT3

7 Other Atmospheric Conditions

This section presents the data basis for assessing other atmospheric conditions.

Other atmospheric conditions concern air temperature, humidity, solar radiation and lightning.

7.1 Air temperature, humidity, and solar radiation

Time series data of air temperature and humidity were extracted from NORA3 model, while the solar radiation was extracted from CFSR at both LOT3 and LOT4 stations. Time series comparisons against measurements are presented in Figure 7.1 and Figure 7.2. The comparisons show a good agreement for temperature and relative humidity, while some scatter is seen for the downward solar radiation (DSWR). However, model results are in the same order of magnitude and follow a similar trend as the measurements.

Scatter plots of modelled and measured air temperature ares presented in Figure 7.3. While the comparisons show an overall good agreement the temperatures near and below 0 °C are possibly overestimated and a correction is likely necessary if data are to be used for site ice conditions assessment.

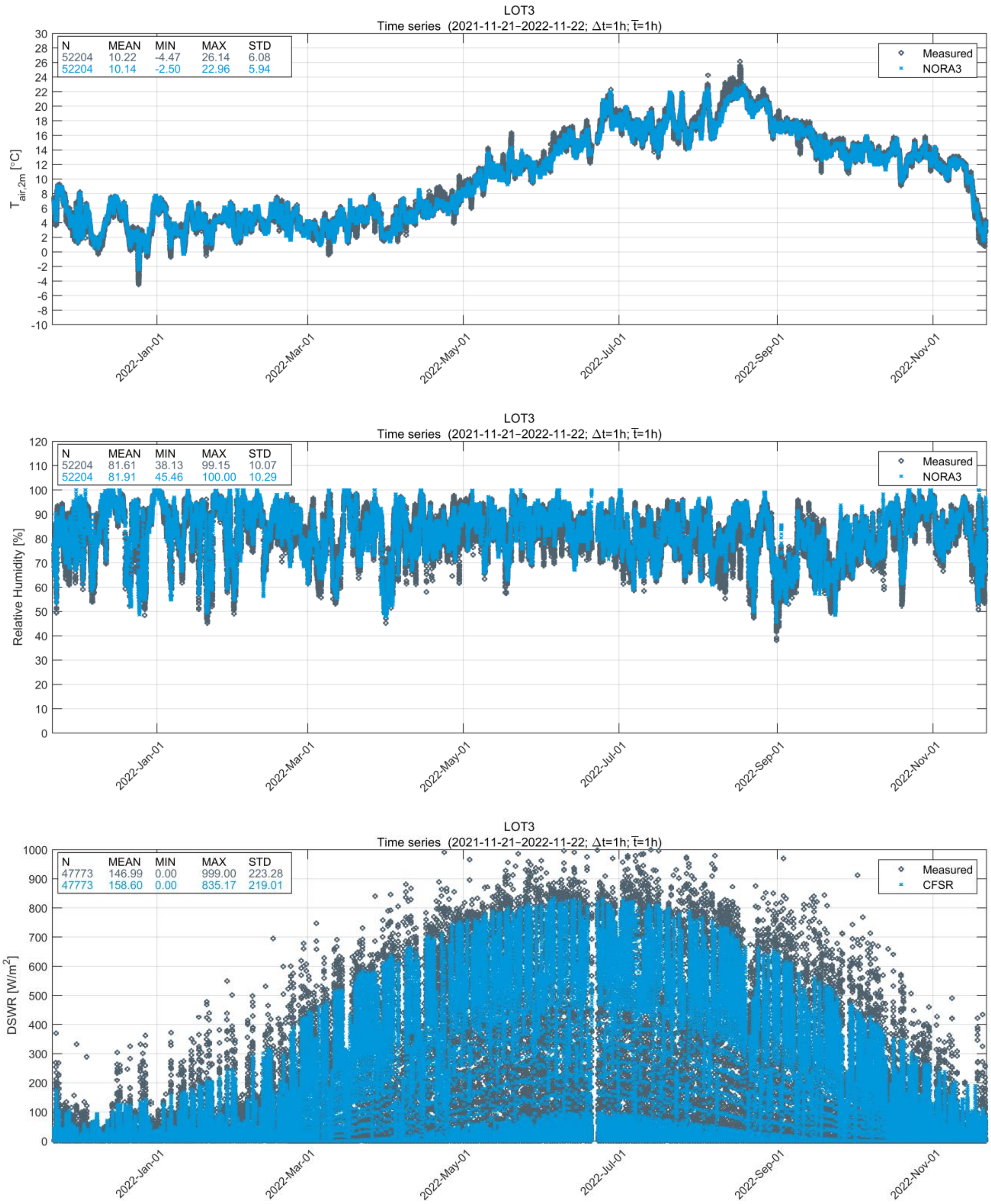

Figure 7.1 Time series comparison of atmospheric model output against measurements of air temperature at 2 m, relative humidity, and downward solar radiation at LOT3

Sensors are located at a height of 4.1 m. Atmospheric model data corresponds to 2 m height.

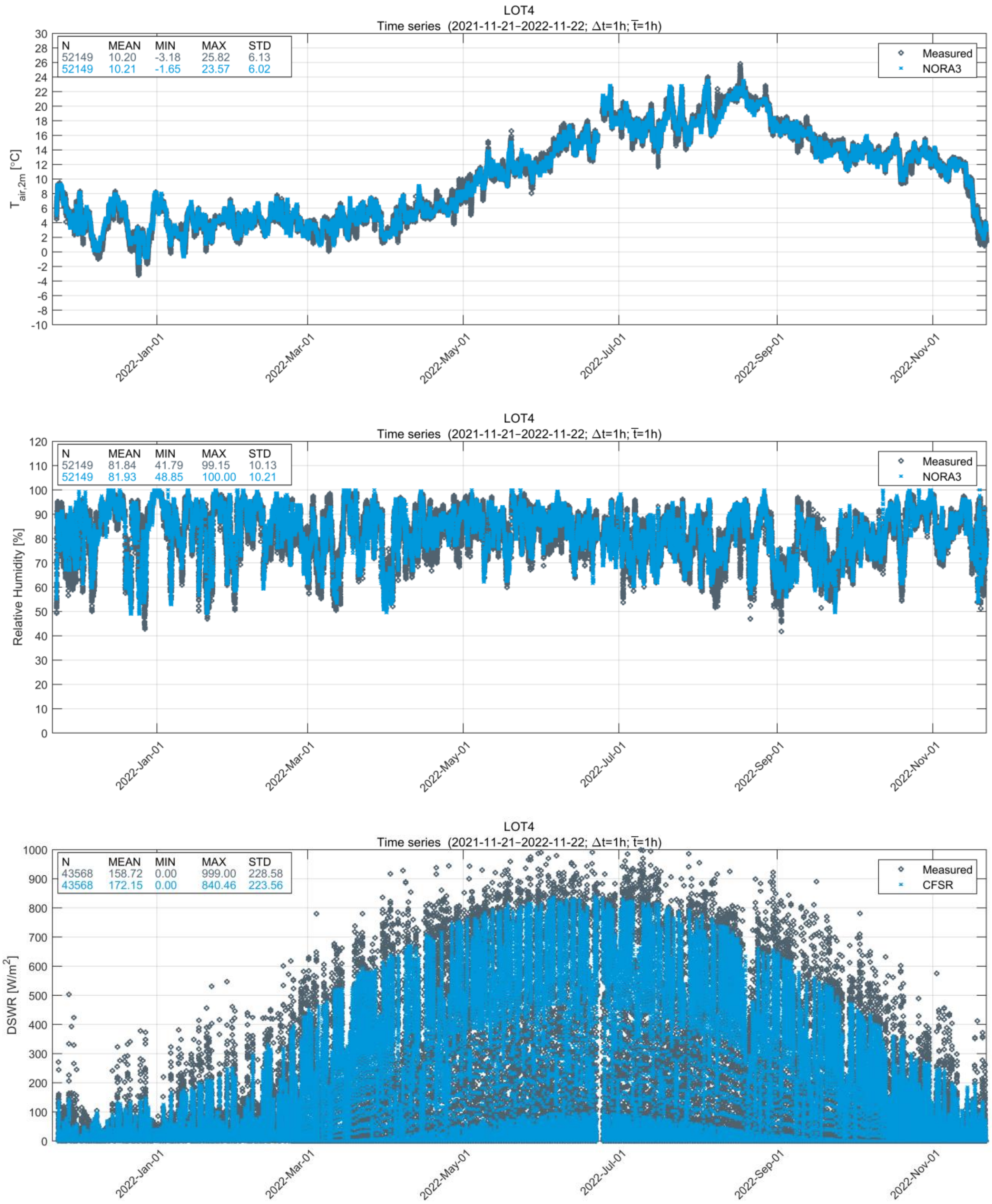

Figure 7.2 **Time series comparison of atmospheric model output against measurements of air temperature at 2 m, relative humidity, and downward solar radiation at LOT4**
Sensors are located at a height of 4.1 m. Atmospheric model data corresponds to 2 m height.

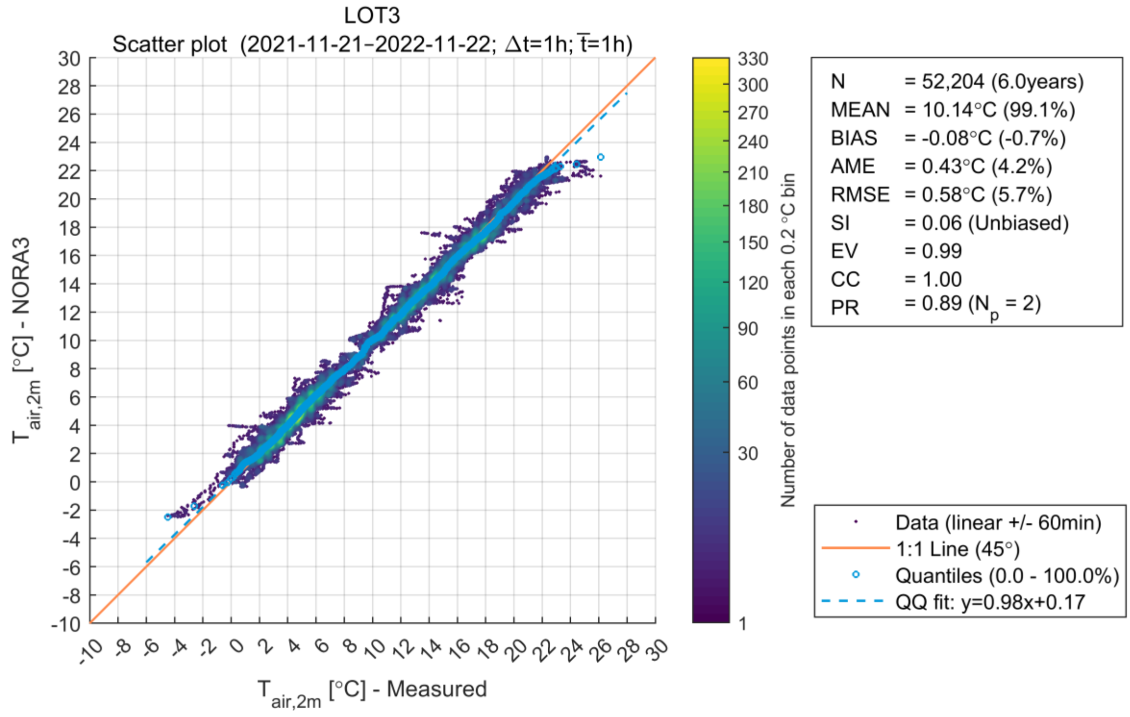

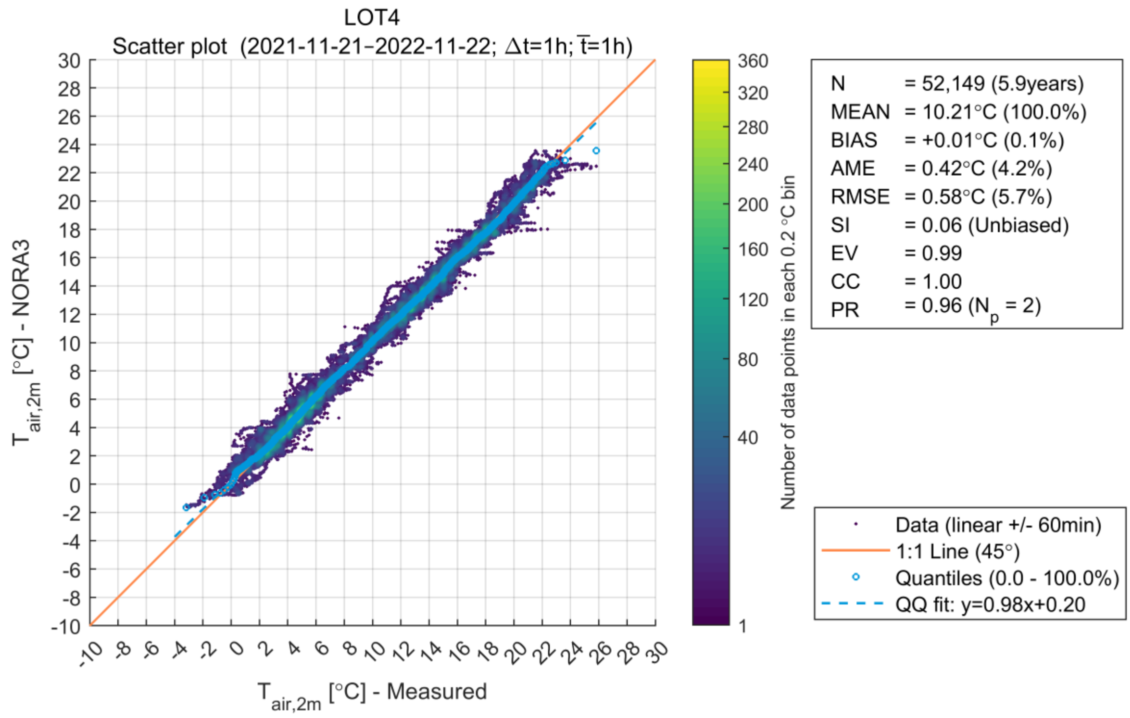

Figure 7.3 Scatter plots of atmospheric model output against measurements of air temperature at 2 m at LOT3 (top) and LOT4 (bottom)

7.2 Lightning

Lightning data was obtained from the LIS/OTD Gridded Climatology dataset [1] from NASA's Global Hydrology Resource Center (GHRC). The data consists of gridded climatology of total lightning flash rates between 1995-05-04 to 2013-12-31, recorded by the Optical Transient Detector (OTD) and Lightning Imaging Sensor (LIS).

The LIS data is available from 1995-05-04 to 2013-12-31 and only equatorward of ~38°N. The long LIS record makes the merged climatology most robust in the tropics and subtropics, while the high latitude data are entirely from OTD. The gridded climatology data include annual mean flash rate on a 0.5° grid [24]. Due to the positioning of the LIS (equatorward of about 38°), the tropic and subtopic records are the most robust, while the high latitude records are entirely from OTD. Figure 7.4 shows the average flash rate density from the high-resolution GHRC data within the western Baltic Sea. The average count around the project site is about 1.4 to 2.5 count/km^2/year.

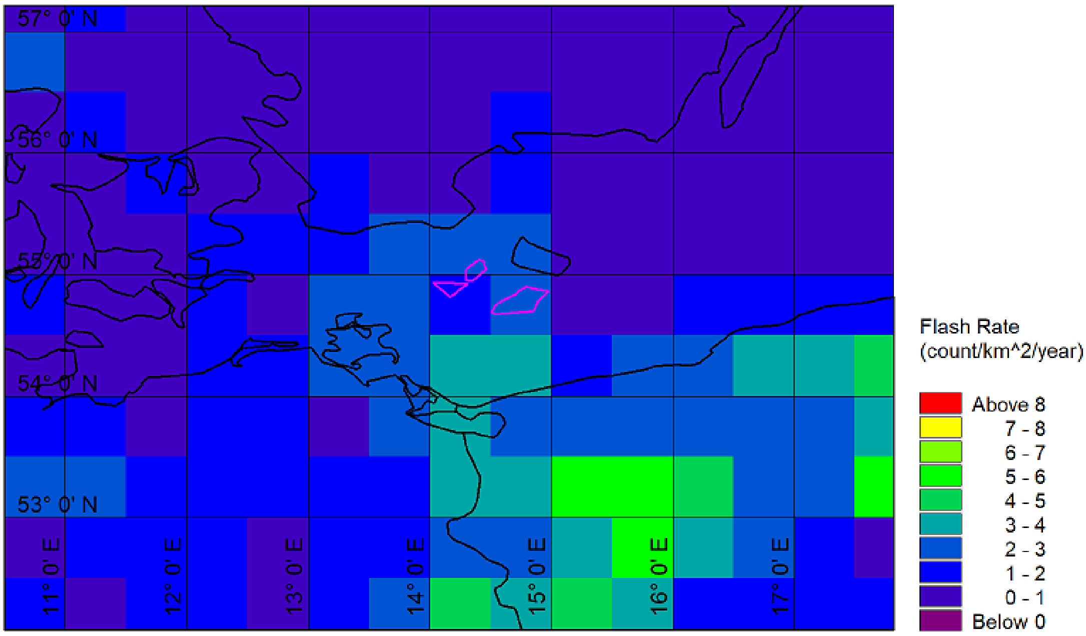

Figure 7.4 Average flash rate in count/km^2/year in the western Baltic Sea

8 Other Oceanographic Conditions

This section presents the data basis for the assessment of other ocean conditions.

Other ocean conditions concern water temperature, salinity, and density.

8.1 Water temperature, salinity, and density

Water temperature and salinity at the surface and bottom layers were adopted from the HD_{EIBS} model. The density is estimated from UNESCO PSU relation[11]. Further explanation is presented in Section 5 .

8.2 Marine Growth Assessment

Marine growth is the settlement and growth of marine organisms, including algae and animals, on submerged surfaces of ship hulls, buoys, piers and other offshore structures. Other terms for marine growth include “marine fouling” or “biofouling”. The composition and extent of marine growth varies with the biogeographical region, with an increase from high to low latitudes.

Many factors influence the amount and type of marine growth, including salinity, temperature, depth, current speed and wave exposure, in addition to biological factors such as food availability, larval supply, presence of predators, and the general biology and physiology of the fouling species. Fouling organisms will, within days to weeks, begin to colonise new hard substrates (concrete, steel) introduced in the environment. Typically, a succession in species composition will take place as the age of the deployed substrate increases. The succession is a result of organisms competing for space, and equilibrium in fouling communities will not be established in less than 4 to 10 years. Along with succession, individual organisms grow larger creating an increasing thickness of marine growth [25]. .

Two firmly attached species characterised as “hard” fouling organisms dominate in the Baltic Sea, namely the mussel *Mytilus trossolus/edulis* and the bar barnacle *Balanus improvisus*. Both species are early colonisers with free-swimming larvae in the plankton from early June to late August [27]. Initial densities of mussels and barnacles after settling can exceed 500,000/m^2 [28], and within 1-2 months, marine growth of “hard species” can attain a height of 10 mm [29]. Along with the growth of (some) individual organisms, other individuals will be overgrown, outcompeted and suffer mortality. Over the years, individual mussels grow larger, both overgrowing (and outcompeting) barnacles and developing a 2-5 stories high cover over the depth range 3-25 m. Only in the wave splash zone (0-3 m) will barnacles continue to dominate marine growth.

Individual barnacles grow to 10 mm in diameter and reach a maximum height of 6-10 mm [30]. The growth rate in *M. trossolus* is suppressed by the low salinity in the Baltic Sea [31], so while a mussel settling around June 1, in the Great Belt (at 15-18 psu) can reach 30-35 mm in early November, the shell length of a juvenile mussel in the Baltic Proper will not exceed 10-15 mm the

[11] The International thermodynamic equation of seawater, 2010: calculation and use of thermodynamic properties - UNESCO Digital Library

first year. However, given sufficient growth conditions - in terms of phytoplankton concentration and current speed - shell length may reach 55 mm, but that could take 10-15 years. In the Belt Sea, the Kattegat Sea and the North Sea dense mussel populations are vigorously predated by sea stars. However, sea stars are absent in the surface waters of the Baltic Sea due to low salinities, and the main predators are diving birds. Interestingly, diving birds avoid operating windfarms ([32] [33]), leaving only fish, such as the invasive round goby and probably also cod, as potential predators [34].

Abundance and biomass of fouling organisms (including mussels and barnacles) have been quantified on several occasions in the Baltic Sea and in the adjacent Fehmarn Belt. In the following data, including biomass, depth range of occurrence and almost absent, and reported height of “hard” and “soft” fouling, have been extracted from publications and synthesised into the most probable prediction of marine growth on submerged structures at the EIBS OWFs.

8.2.1 Marine growth in the central and western Baltic Sea

Nysted (Rødsand) offshore wind park in Fehmarn Belt established at 6-9 m depth in 2002

Common blue mussels (*Mytilus edulis*), barnacles (e.g., bay barnacle (*Balanus improvisus*)) and a few associated species of crustaceans (*Gammarus* sp., *Corophium insidiosum* and *Microdeutopus gryllotalpa*) dominated the fouling community during post-construction monitoring in 2003-2005. The rapid growth of mussels since 2003, resulting in competition for space, has almost excluded other sedentary species of invertebrates and macroalgae. A monoculture of mussels developed on shafts and stones in the foundation in 2005. The biomass of mussels on the vertical concrete shafts was comparable to the climax community developed on the nearby monitoring mast deployed in 1996 and in the same order of magnitude as the biomass of mussels on bridge piers in Øresund. The biomass of mussels on the foundations and the nearby stone reef “Schönheiders Pulle” was comparable. However, the biomass of mussels on the scour protection stones around the foundations was only one third of the biomass of mussels at Schönheiders Pulle.

The vertical zonation of the dominant species of mussels, barnacles and associated species of crustaceans was minor but related to physical (current speed) and biological factors, which affect the input of larvae and food, the growth rate of mussels and competition for space.

The biomass (and the diversity) of macroalgae (soft fouling) was low (due to the low salinity in the area), being dominated by red algae both at the turbine foundations and shafts and Schönheiders Pulle. Macroalgae were mostly confined to the scour protection stones in 2005 due to the growth and progressive expansion of mussels resulting in the overgrowth of algae. The biomass of macroalgae on the scour protection stones and on stones at Schönheiders Pulle was comparable in 2005.

In the last year of monitoring (2005), the average mussel biomass reached 10 kg dry weight/m^2. A summary of the results at Nysted is listed in Table 8.2.

Darss Sill at 20 m depth (2003-2005)

Using artificial substrates deployed at 20 m at Darss Sill, [28] followed biofouling at 3 m vertical intervals over 470 days. After 143 days and 243 days the abundance peaked at surface (5 m) of more than 500,000 individuals/m^2, mainly blue mussels (*Mytilus edulis*) and *Balanus* spp. Due to predation but also the growth of individuals caused a clear decrease to about 15,000 individuals/m^2 after 47 months. Mussels were the dominating species, accounting for more than 80% of the total biomass, followed by barnacles, which contributed almost 13% to the biomass. On a 2 m diameter model pile deployed at seabed, fouling biomass increased over a period of three years before it reached a maximum after 40 months. A semi-stable habitat started to develop in the fourth year, characterised by competition between species, struggling for space, and predation. Multiple species found space on the model pile and predators such as starfish, cod, and common shore crabs occurred regularly. The biomass of primary settlers such as mussels and barnacles decreased unless biomass patches came off and the empty space was then quickly repopulated by both taxa. Sampling data from the fouling plates showed biomass for mussels up to 1.1 kg ash-free dry weight/m^2 (surface layer after 246 days) and close to 1.9 kg ash-free dry weight/m^2 (5 m depth after 470 days). Settling density, abundance, and biomass were much higher in the mixed surface layer than at bottom layers, where values were lower.

The variation of the biomass with depth is shown in Table 8.1.

Table 8.1 Total biomass (wet weight) at the pile model (after one year of exposure) and literature values from other pile structures in the Baltic Sea (from [28])

Location and depth	Wet weight [g/m^2]
Darss, 5m	20,000
Darss, 8m	15,000
Darss, 14m	11,500
Darss 17m	4,000
Darss 19m	2,000
Nysted, Baltic, pile after 1 year [35]	3,000
Nysted, Baltic, Mast after 6 years [35]	14,500

A summary of the results at Darss is listed in Table 8.2.

Marine growth on wind farm monopiles in Kalmar Sound, Sweden

Zettler and Pollehne (2006) [28] sampled marine growth (in 2003) from monopiles of two wind farms established at Utgrunden and Yttre Stengrund located in Kalmar Sound at 20 m depth. At the time of sampling, the monopiles had been immersed for 2 and 3 years. Quantitative samples of marine growth were collected at 3 m and 5 m depth and averaged across depth, monopiles and wind farms. Control samples were collected at nearby boulders at distances of 2 and 20 m from monopiles.

Briefly, mussels completely dominated the biomass of marine growth on monopiles and boulders, while barnacles although present, had a much lower biomass, probably because of the overgrowth of mussels below splash zone.

"Soft" marine growth such as macroalgae, was practically absent on the vertical monopiles but attained higher biomass on the horizontal boulders. Whomersley and Malm [25] also quantified the condition (i.e., meat weight per mm shell length) of mussels sampled from monopiles and boulders and found significantly higher conditions in mussels from monopoles than in mussels from boulders indicating a higher availability of food (phytoplankton) on the vertical monopoles.

A summary of the results in Kalmar Sound is listed in Table 8.2.

Table 8.2 Summary of the marine growth on submerged structures in central and western Baltic

Location	Depth [m]	Mussels [gDW/m^2]	Barnacles [gDW/m^2]	Macroalgae [gDW/m^2]
Nysted (Rødsand)	-	10200±1040	1290±110	-
Darss	5	≈ 23000	≈ 1200	-
Darss	18	≈ 1000	≈ 90	
Kalmar Sound	4	1200±512	53±48	3±3

8.2.2 Marine growth on structures at EIBS OWFs

The three studies summarised above are considered relevant for projecting marine growth on submerged structures of the planned offshore wind farm site. Approximate positions where data from the fouling studies were extracted and the position of the planned offshore wind farm are shown in Figure 8.1. Observed abundance and biomass of "hard-structured" biofoulers (mussels and barnacles) in these studies define the ranges that can be expected EIBS OWFs.

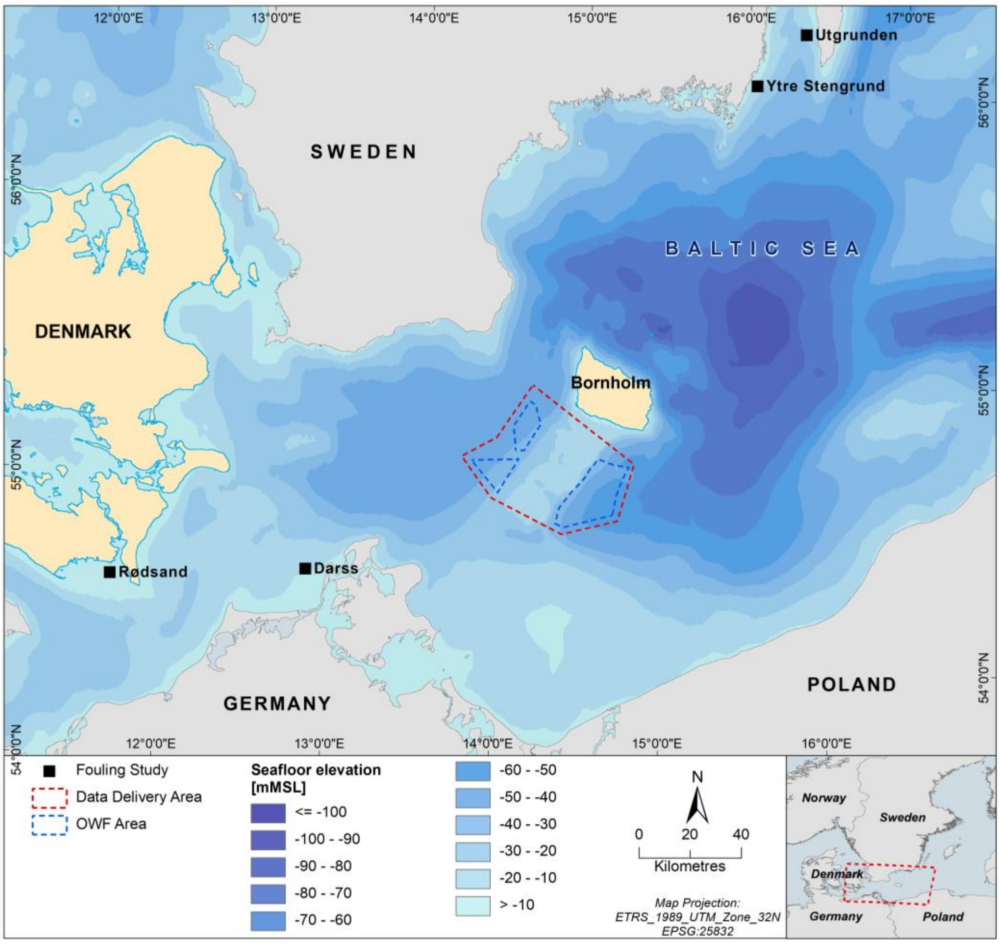

Figure 8.1 Locations where data for the fouling studies were extracted from (circles) and the position of the planned EIBS OWFs

The largest biomass of mussels was observed on panels deployed at Darss Sill which most likely can be explained by high (> 0.2 m/s) and consistent current speeds over the sill, thereby preventing food shortage in the dense mussel population. The maximum biomass of mussels at Nysted (Rødsand) wind farm was comparable to the median concentration at Darss Sill, but it took almost 3 years to approach the biomass, which was reached after 470 days at Darss Sill. The lowest biomass was found on wind farm monopiles at Utgrunden and Ytre Stengrund in the Kalmar Sound (Figure 8.2).

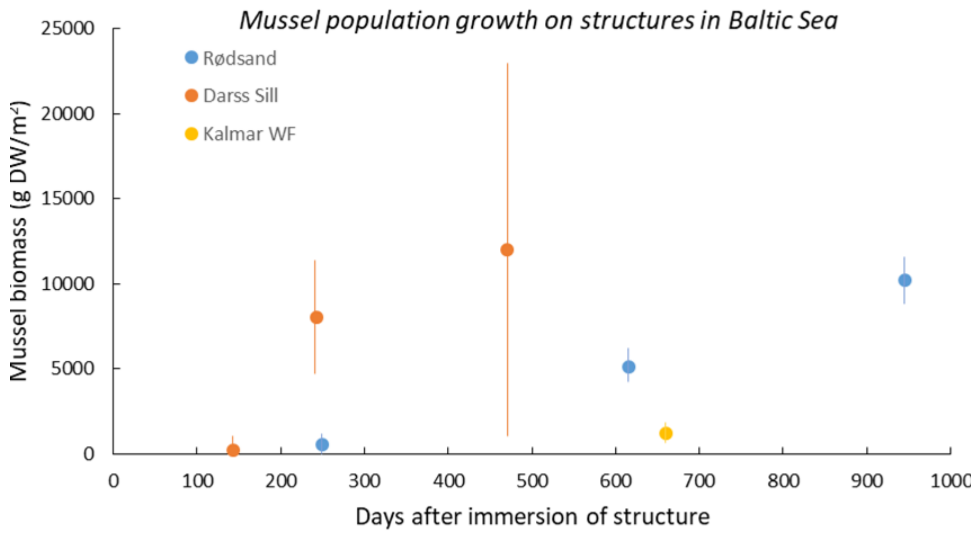

Figure 8.2 Time series of mussel biomass at three wind farm locations in the Baltic Sea
Uncertainty bars represent standard deviation (Nysted/Rødsand wind farm, Kalmar wind farms) or range over depth (Darss Sill).

At all study sites, biomass of barnacles was much lower than the biomass of mussels. Barnacles were the first to settle, but over time they were outcompeted by mussels, and they only remained in the upper splash zone (0-1 m), seemingly being a poor habitat for mussels.

Growth of marine algae (soft biofouling) was insignificant on vertical structures at the sites. Hence, with a water depth exceeding 25 m at the planned offshore wind farm, the light intensity would be insufficient to support the growth of macroalgae at structures near seabed.

Based on the above summary of the predicted marine growth on submerged structures in the Baltic the recommended thickness and density at the EIBS OWFs and what the marine growth is expected to consist of is given in Table 8.3 and adhere to DNVGL recommendations [36]. DNVGL values are recommended as the case studies are based on non-climax communities, which means that not the full growth potential has been reached. Normally 8-10 years are considered for conforming a climax community. And although DNVGL are conservative measures these are still a valid guide to adhere to.

Table 8.3 Summary of the marine growth on submerged structures at the planned EIBS OWFs

Water Depth	Description of marine growth on submerged structure	Thickness (mm) Recommendation for calculations (DNVGL-ST-0437) [36]	Density (kg/m^3) Recommendation for calculations (DNVGL-ST-0437) [36]
0-1 m:	50-60% cover with barnacles (*Balanus improvisus*) extending to a maximum height of 15 mm above structure and with a dry weight in air of 250 g/m^2 – equivalent to ca. 80-100 g/m^2 in water		
1-7 m:	80-100% cover 2-3 stories high growth of mussels	100	1325
7-10 m:	50-75% cover 2 stories high growth of mussels		
10-15 m:	30-50% cover 1-2 stories high growth of mussels		
15-20 m:	10-25% cover in one layer of mussels		
>20 m:	Scattered individuals of mussels		

9 Climate Change

This section presents a literature review to assess the impact of climate change on water level (sea level rise), winds, waves, currents and water properties. The assessment is based on an expected lifetime of 25 years of the EIBS OWFs with a construction completion in year 2030, i.e. impacts up to year 2055.

9.1 Climate change impact on water level (sea level rise)

The assessment of the sea level rise at the EIBS OWFs is based on the Sixth Assessment Report of the Intergovernmental Panel on Climate Change (IPCC) [37].

The different considered climate scenarios (Shared Socio-economic Pathways (SSPs)) are illustrated in Figure 9.1. For the present study, the most severe scenario (with respect to CO_2 emissions), SSP5-8.5, was chosen.

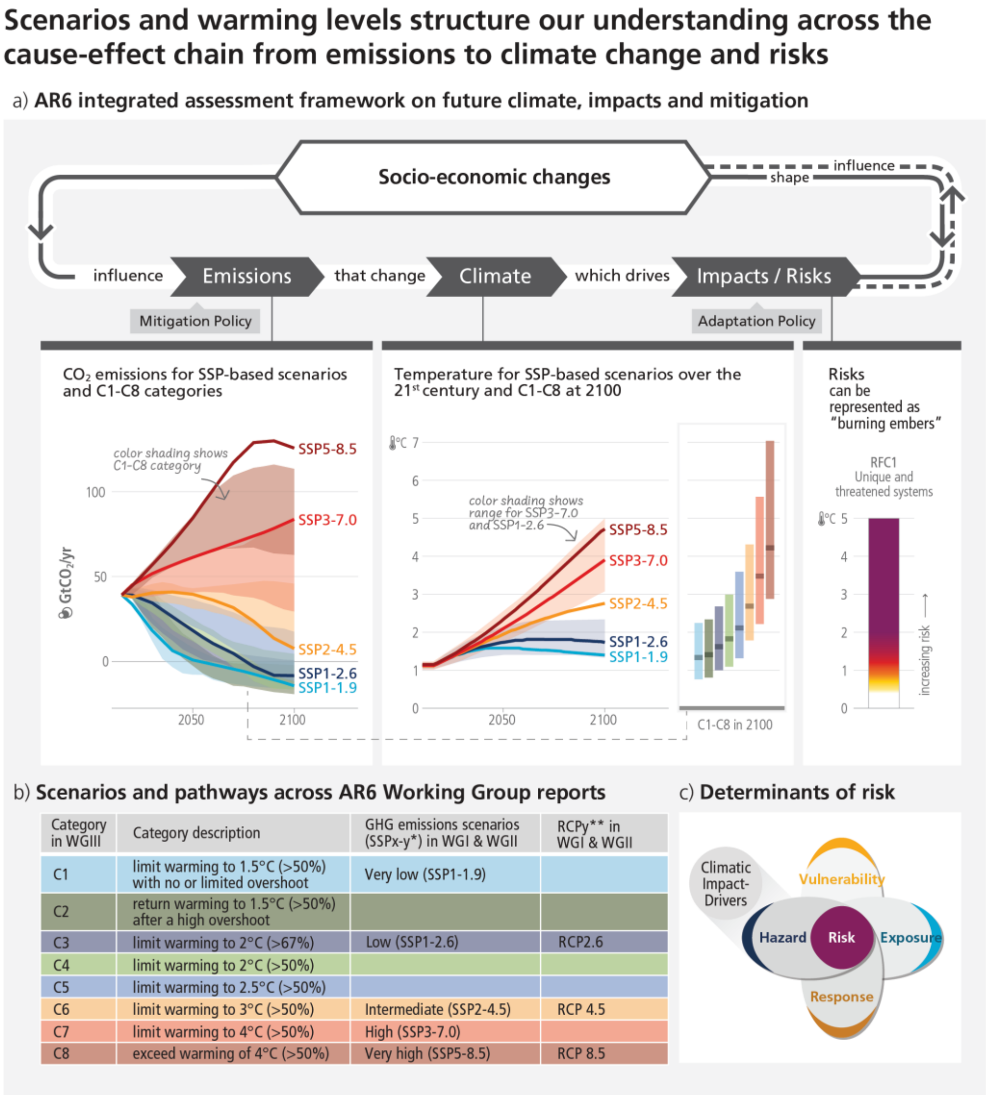

Figure 9.1 Illustration of the different Shared Socio-economic Pathways (SSP) as defined by IPCC (Cross-Section Box.2, Figure 1 from [37])
In the present study SSP5-8.5 have been applied

The end of the lifetime of the EIBS OWFs is assumed to be in year 2055, which in climate change terminology is called "Medium term".

According to IPCC (see [38]), the sea level rise in Northern Europe will amount to between 0.0m (5 percentile) and 0.5m (95 percentile) with a median of 0.25m in year 2055 (see Figure 9.2). As seen in Figure 9.3, there is a high agreement between the various climate models for the SSP5-8.5 scenario.

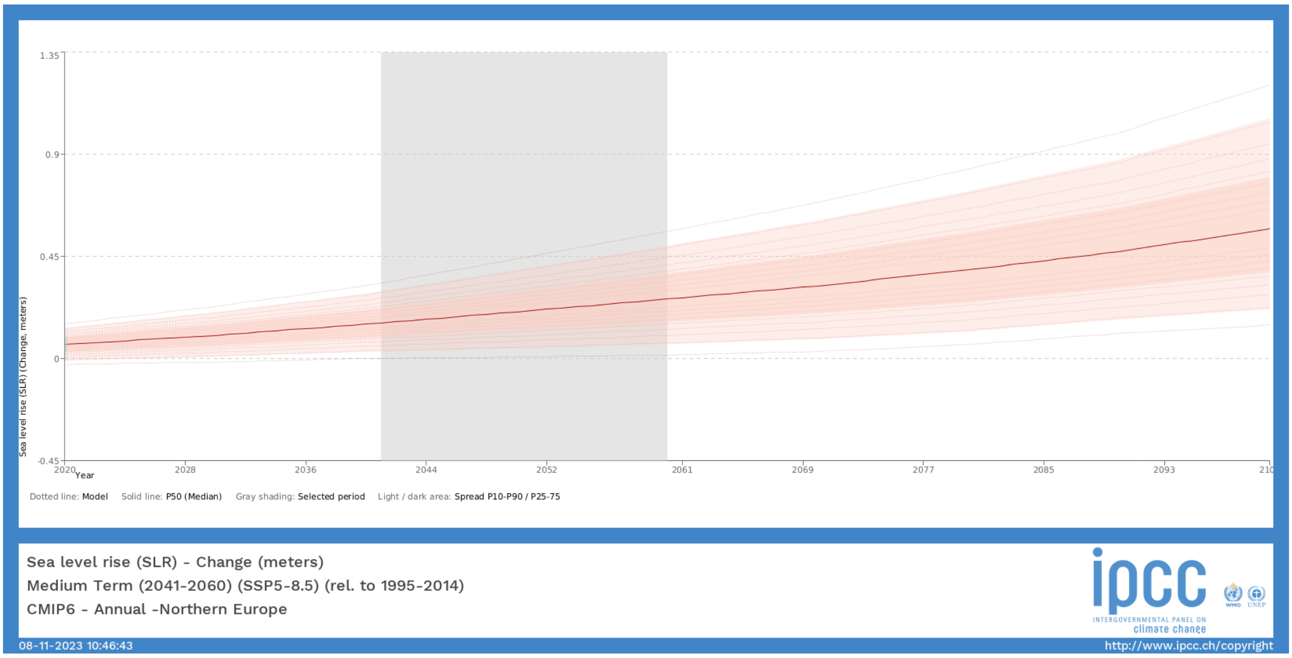

Figure 9.2 **Sea level rise (SLR) for Northern Europe for the Medium Term (2041-2060) based on Coupled Model Intercomparison Project Phase 6 (CMIP6) [38]**

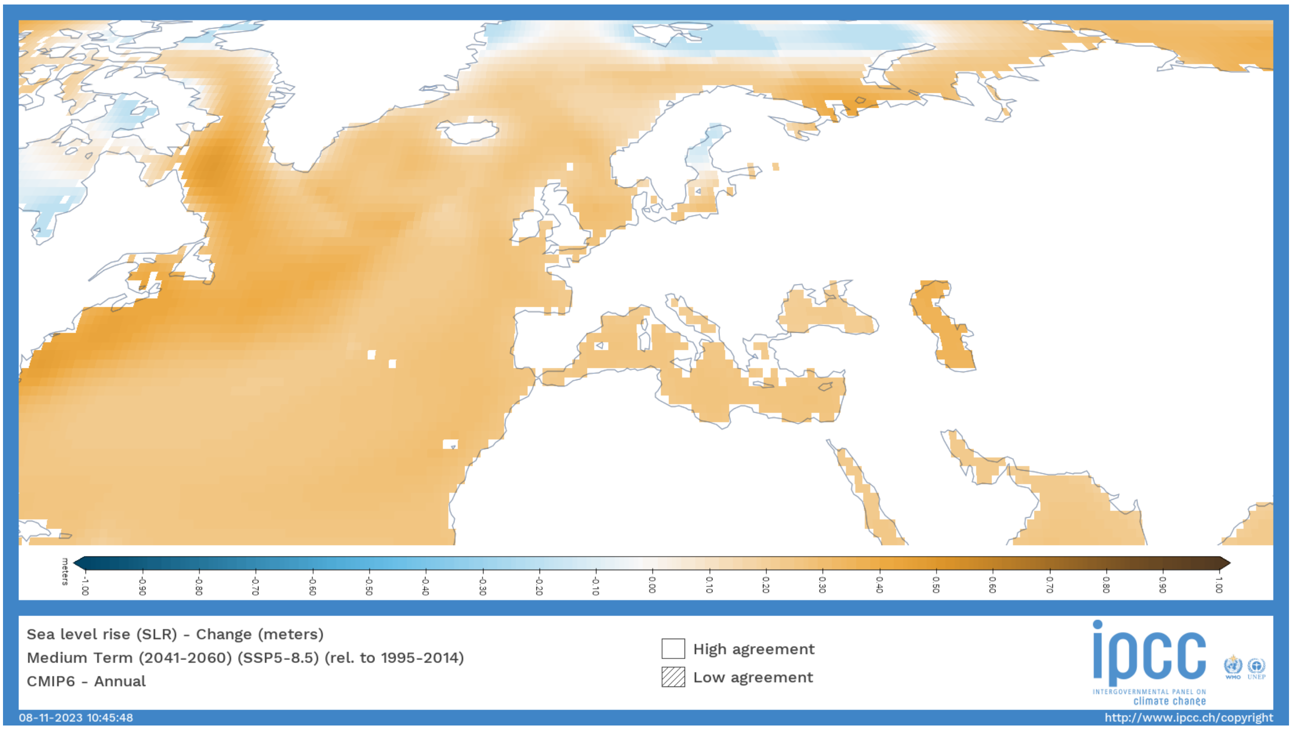

Figure 9.3 **Sea level rise variation for the Medium Term (2041-2060) based on Coupled Model Intercomparison Project Phase 6 (CMIP6) [38]**

9.2 Climate change impact on winds, waves and currents

According to IPCC (see Figure 9.4 and Figure 9.5), the change in surface wind in the Medium Term (including year 2055) as predicted by the climate models, does not show a clear trend (like does the SLR), and the climate models show a low agreement (i.e. a large scatter) in their predictions.

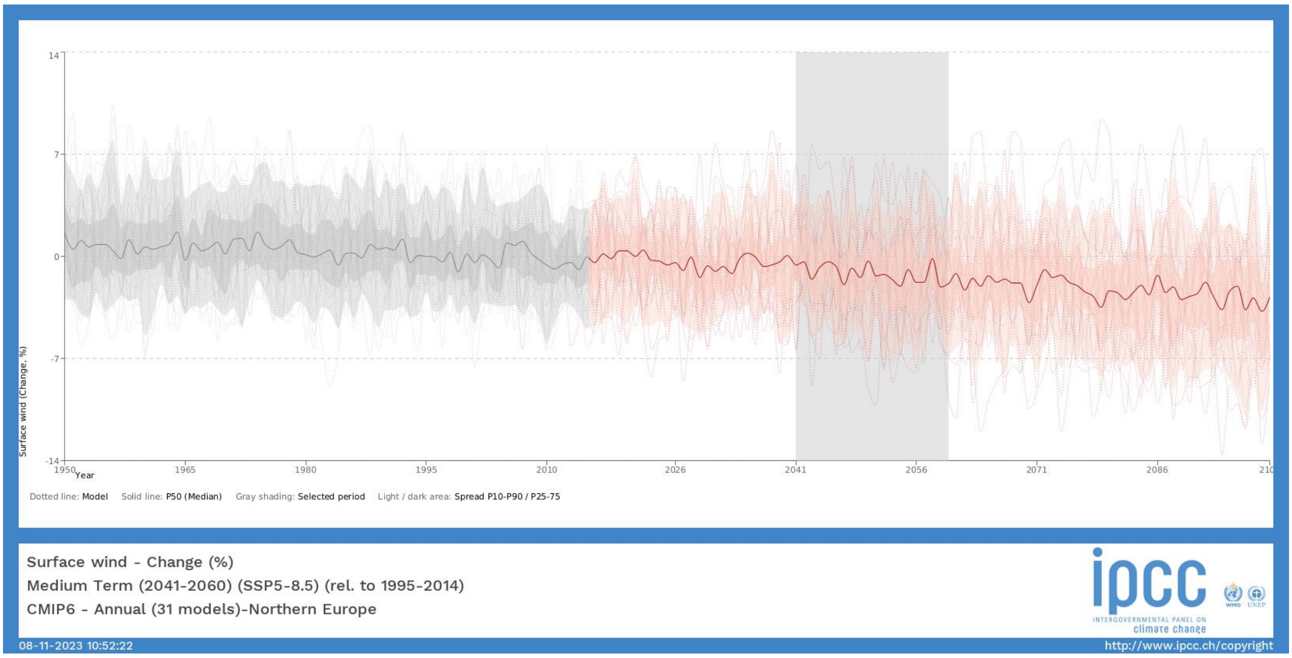

Figure 9.4 Surface wind change for Northern Europe for the Medium Term (2041-2060) based on Coupled Model Intercomparison Project Phase 6 (CMIP6) [38]

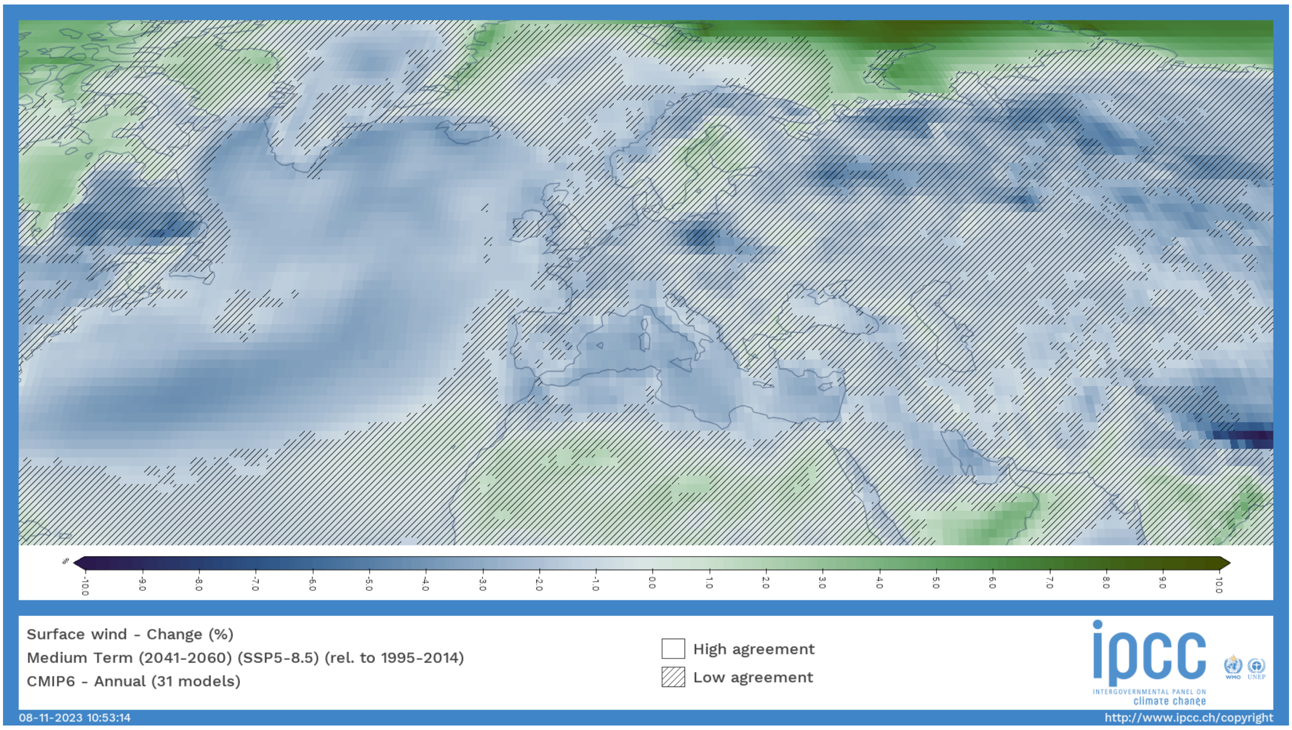

Figure 9.5 Surface wind change variation for the Medium Term (2041-2060) based on Coupled Model Intercomparison Project Phase 6 (CMIP6) [38]

This agrees with [39], which concludes: "In summary, there is no clear consensus among climate change projections in how changes in the frequency and/or intensity of extratropical cyclones will affect the Baltic Sea region. However, in future climate, the frequency of severe wind gusts in summer associated with thunderstorms may increase."

According to [39], only few wave climate projections have been carried out for the southern Baltic Sea and they are generally inconclusive.

The effect of the sea level rise on wave conditions during storm events has not been modelled in the present study. However, from another study carried out by DHI in the western Baltic Sea, changes of only a few percent of the maximum significant wave height during storm events by the end of the century taking sea level rise into account was found.

The effect of the sea level rise on current conditions during storm events have not been modelled in the present study.

Neither IPCC nor [39] mention currents explicitly. However, as mentioned in the next section (based on [39]), among climate models, no systematic changes were projected for either the saline-induced stratification or the overturning circulation in the Baltic Sea when considering all drivers of salinity changes, including wind, river runoff, and global sea level rise.

9.3 Climate change impact on water properties.

According to IPCC (see Figure 9.6 and Figure 9.7), the change in sea surface temperature in the Medium Term (including year 2055) will amount to 1.4 °C (median) with a variation between 0.3 °C (5 percentile) and 2.6 °C (95 percentile) and the climate models show a robust agreement.

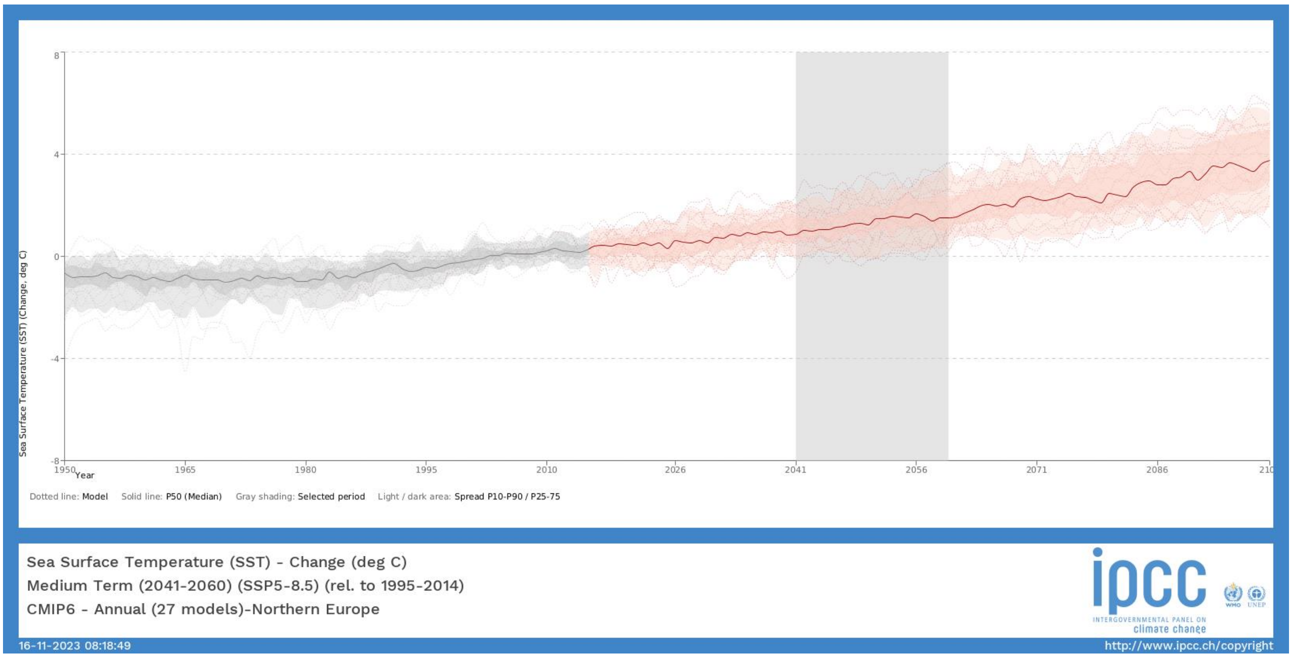

Figure 9.6 Sea surface temperature change for Northern Europe for the Medium Term (2041-2060) based on Coupled Model Intercomparison Project Phase 6 (CMIP6) [38]

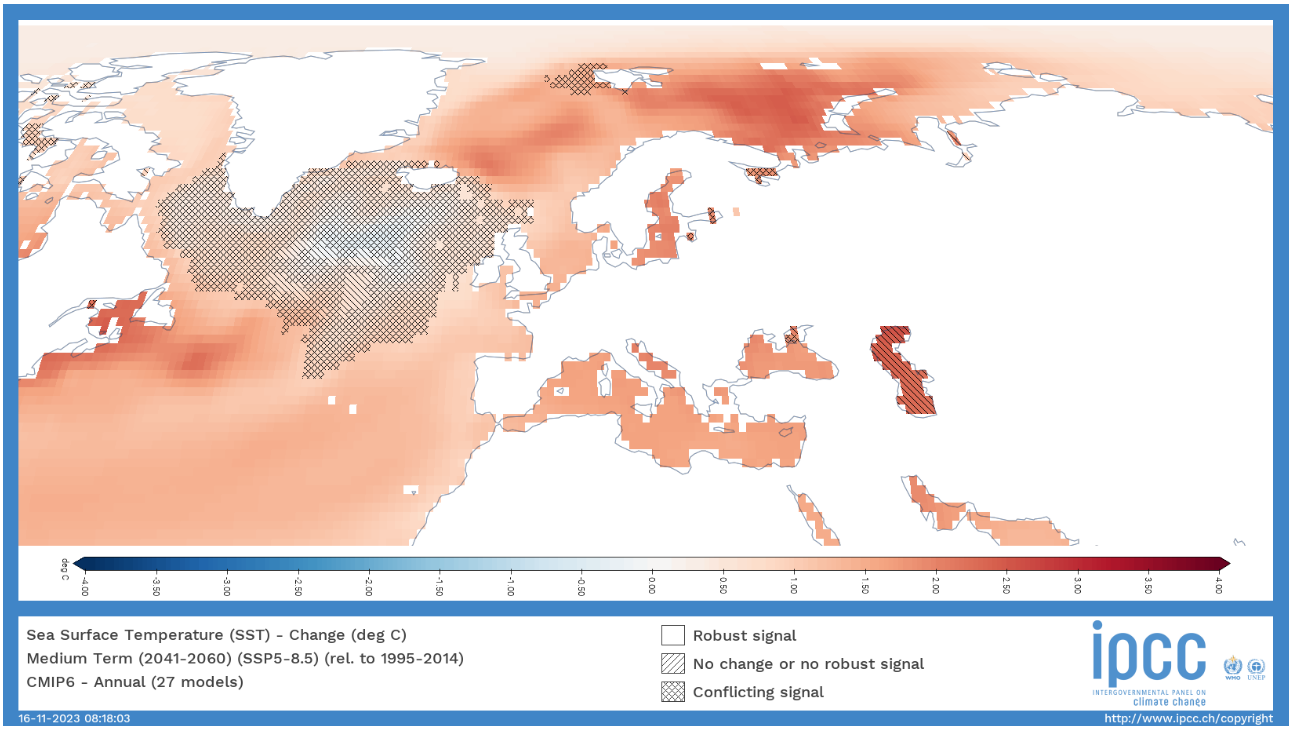

Figure 9.7 Sea surface temperature variation for the Medium Term (2041-2060) based on Coupled Model Intercomparison Project Phase 6 (CMIP6) [38]

According to [39], future changes in salinity will depend on changes in the wind patterns over the Baltic Sea region, river runoff from the Baltic Sea catchments, and mean sea level rise relative to the seabed of the sills in Danish straits. Due to the large uncertainty in projected changes in wind fields over the Baltic Sea region, freshwater supply from the catchments, and global sea level rise, salinity projections show a large variation. Ensemble studies that consider all potential drivers predict no significant changes in ensemble mean salinity [39].

Among climate models, no systematic changes were projected for either the saline-induced stratification or the overturning circulation in the Baltic Sea when considering all drivers of salinity changes, including wind, river runoff, and global sea level rise.

10 References

[1] D. J. Cecil, “LIS/OTD Gridded Lightning Climatology Data Collection,” *NASA EOSDIS Global Hydrology Resource Center Distributed Active,* no. 2, 2015.

[2] DHI, “Energy Island Baltic Sea, Metocean Site Conditions Assessment, Part B: Data Analysis,” 2023.

[3] DHI, “Energy Island Baltic Sea, Metocean Site Conditions Assessment, Part C: Hindcast revalidation note, due Jan 2024,” 2024.

[4] DNV, “DNV-RP-C205 Environmental conditions and environmental loads,” DNV AS, 2021.

[5] IEC, “Wind energy generation systems - Part 3-1: Design requirements for fixed offshore wind turbines,” IEC-61400-3:2019.

[6] Fugro, “SWLB measurements at Energy Islands, C75486_Project_Management_Plan_All_Lots F, 6 April 2022,” 2022.

[7] ISO, “Petroleum and natural gas industries — Specific requirements for offshore structures — Part 1: Metocean design and operating considerations,” *ISO 19901-1:2015,* 2015.

[8] IEC, “61400-1, Wind energy generation systems – Part 1: Design requirements, Edition 4.0, 2019-02,” 2019a.

[9] CEM, “Coastal Engineering Manual, Meteorology and Wave Climate,” 2008.

[10] WMO, “Guidelines for converting between various wind averaging periods in tropical cyclone conditions, WMO/TD,” vol. No. 1555, 2010.

[11] H. B. Ø. F. B. R. R. M. B. P. &. A. O. J. Haakenstad, “NORA3: A nonhydrostatic high-resolution hindcast of the North Sea, the Norwegian Sea, and the Barents Sea,” *Journal of Applied Meteorology and Climatology,* vol. 60, no. 10, pp. 1443-1464, 2021.

[12] A. Stigebrandt , “Processes and factors influencing the through-flow of new deepwater in the Bornholm Basin,” *Oceanologia,* 2016.

[13] K. Borenäs, R. Hietala and P. J. Lundberg, “Some estimates of the Baltic deep-water transport through the Stolpe trench.,” *Tellus A: Dynamic Meteorology and Oceanography,* p. 59, 2007.

[14] U. Gräwe, M. Naumann, V. Mohrholz and Burchard, “Anatomizing one of the largest saltwater inflows into the Baltic Sea in December 2014, J. Geophys. Res. Oceans, 120, 7676–7697,,” *Journal of Geophysical Research,* vol. 120, no. 11, pp. 7676-7697, 2015.

[15] H. U. Lass and V. Mohrholz, “On dynamics and mixing of inflowing saltwater in the Arkona Sea, J. Geophys. Res., 108, 3042,,” *Journal of Geophysical Research: Oceans,* vol. 108, no. C2, 2003.

[16] A. Lehmann, P. Lorenz and D. Jacob , “Modelling the exceptional Baltic Sea inflow events in 2002–2003.,” *Geophysical Research Letters,* vol. 31, no. L21308, 2004.

[17] H. Burchard, F. Janssen, K. Bolding, l. Umlauf and H. Rennau, “Model simulations of dense bottom currents in the Western Baltic Sea,” *Environmental Science,* 2009.

[18] H. E. Markus Meier, “Modeling the pathways and ages of inflowing salt- and freshwater in the Baltic Sea. , 74, 610.,” *Estuarine, Coastal and Shelf Science,* vol. 74, p. 610, 2007.

[19] S. Feistel, R. Feistel, D. Nehring, W. Matthaus, G. Nausch and M. Naumann, “Hypoxic and anoxic regions in the Baltic Sea, 1969 - 2015,” *Meereswissenschaftliche Berichte, Warnemünd,* vol. 100, 2016.

[20] DHI, “DKBS2: Hydrodynamic Model Setup and Validation.,” 2018.

[21] DHI, “MIKE 21 Spectral Waves FM, Spectral Wave Module, User Guide,” DHI, 2022.

[22] DHI, “MIKE 21, Spectral Wave Module, Scientific Documentation,” DHI, 2022.

[23] DHI, “DHI North Europe Hydrodynamic and Spectral Wave Model Validation,” DHI, 2023.

[24] S. Susini, M. Menendez, P. Eguia and J. M. Blanco, “Climate Change Impact on the Offshore Wind Energy Over the North Sea and the Irish Sea,” *Frontiers,* 2022.

[25] D. Whomersley and T. Malm, “Fouling assemblages on offshore wind power plants and adjacent substrata,” vol. 79, pp. 459-466, 2008.

[26] M. Lagerström, E. Ytreberg, A.-K. E. Wiklund and L. Granhag, “Antifouling paints leach copper in excess – study of metal release rates and efficacy along a salinity gradient,” *Water Research,* vol. 186, p. 116383, 2020.

[27] I. Purina and I. Barda, “Recruitment studies of the mussel Mytilus trossulus on artificial substrate near high energy shores of the north-eastern Baltic Sea,” *Environmental and Experimental Biology,* vol. 15, pp. 225-231, 2017.

[28] M. L. Zettler and F. Pollehne, “The impact of wind engine constructions on benthic growth patterns in the Western Baltic,” in *Offshore Wind Energy - Research on Environmental Impact*, 2006, pp. 201-222.

[29] A. Dziubinska and A. Szaniawska, “Short-term study on the early succession stages of fouling communities in the coastal zone of Puck Bay (southern Baltic Sea),” *International Journal Oceanography and Hydrobiology XXXIX,* vol. 4, pp. 3-16, 2010.

[30] P. R. Jonsson, A. L. Wrange, U. Lind, A. Abramova, M. Ogemark and A. Blomberg, “The Barnacle Balanus improvisus as a Marine Model - Culturing and Gene Expression,” *J. Vis. Exp.,* 2018.

[31] N. Kautsky, “Growth and Size Structure in a Baltic Mytilus edulis Population,” *Mar Biology,* vol. 68, pp. 117-133, 1982.

[32] I. K. Petersen, M. L. Mackenzie, E. Rexstad, D. Kidney and R. D. Nielsen, “Assessing cumulative impacts on long-tailed duck for the Nysted and Rødsand II offshore wind farms,” Aarhus University, Aarhus, DK, 2013.

[33] I. K. Petersen, R. D. Nielsen and M. L. Mackenzie, “Post-construction evaluation of bird abundances and distributions in the Horns Rev 2 offshore wind farm area, 2011 and 2012,” Aarhus University, Aarhus, DK, 2014.

[34] B. M. E. P. Commission., “HELCOM activities report for the year 2018: translating the commitments into actions.,” Baltic Sea Environment Proceedings no. 166, 2018.

[35] P. A. Birklund J, “Development of the fouling community on turbine foundations and scour protection in Nysted Offshroe Wind Farm,” Energy E2, 2004.

[36] DNV, “DNVGL-ST-0437, Loads and site conditions for wind turbines,” (2016).

[37] IPCC, “Sixth Assessment Report of the Intergovernmental Panel on Climate Change, Synthesis Report, Summary for Policymakers,” 2023.

[38] IPCC, “IPCC WGI Interactive Atlas,” [Online]. Available: https://interactive-atlas.ipcc.ch/.

[39] H. E. M. M. e. al, “Climate change in the Baltic Sea region: a summary,” *Earth System Dynamics,* vol. 13, no. 1, p. 457–593, 2022.

[40] S. Qvarfordt, H. Kautsky and T. Malm, “Development of fouling communities on vertical structures in the Baltic Sea,” *Estuarine, Coastal and Shelf Science,* vol. 67, pp. 618-628, 2006.

Appendix A Model Quality Indices

See next pages

DHI Model Quality Indices (QI's)

Contents

Revisions

Date	Description	Initials
2024-01-08	Version 1.3; Renamed AME to MAE.	PDG
2023-12-07	Version 1.2; Definition of PR updated.	PDG
2022-11-24	Version 1.1; Table formatting updated.	SJA
2021-08-13	Version 1.0;	PDG

Nomenclature

Abbreviation	Explanation
QI	Quality Index
POT	Peak-Over-Threshold

1 Model Quality Indices

To obtain an objective and quantitative measure of how well the model data compared to the observed data, several statistical parameters, so-called quality indices (QI's), are calculated.

Prior to the comparisons, the model data is synchronised to the time stamps of the observations so that both time series had equal length and overlapping time stamps. For each valid observation, measured at time t, the corresponding model value is found using linear interpolation between the model time steps before and after t. Only observed values that had model values within ± the representative sampling or averaging period of the observations are included (e.g., for 10-min observed wind speeds measured every 10 min compared to modelled values every hour, only the observed value every hour is included in the comparison).

The comparisons of the synchronised observed and modelled data are illustrated in (some of) the following figures:

- Time series plot including general statistics
- Scatter plot including quantiles, QQ-fit and QI's (density-colored dots)
- Histogram of occurrence vs. magnitude or direction
- Histogram of bias vs. magnitude
- Histogram of bias vs. direction
- Dual rose plot (overlapping roses)
- Peak event plot including joint (coinciding) individual peaks

The quality indices are described below, and their definitions are listed in Table 1.1. Most of the quality indices are based on the entire dataset, and hence the quality indices should be considered averaged measures and may not be representative of the accuracy during rare conditions.

The MEAN represents the mean of modelled data, while the bias is the mean difference between the modelled and observed data. MAE is the mean of the absolute difference, and RMSE is the root-mean-square of the difference. The MEAN, BIAS, MAE and RMSE are given as absolute values and relative to the average of the observed data in percent in the scatter plot.

The scatter index (SI) is a non-dimensional measure of the difference calculated as the unbiased root-mean-square difference relative to the mean absolute value of the observations. In open water, an SI below 0.2 is usually considered a small difference (excellent agreement) for significant wave heights. In confined areas or during calm conditions, where mean significant wave heights are generally lower, a slightly higher SI may be acceptable (the definition of SI implies that it is negatively biased (lower) for time series with high mean values compared to time series with lower mean values (and same scatter/spreading), although it is normalised).

EV is the explained variation and measures the proportion [0 - 1] to which the model accounts for the variation (dispersion) of the observations.

The correlation coefficient (CC) is a non-dimensional measure reflecting the degree to which the variation of the first variable is reflected linearly in the variation of the second variable. A value close to 0 indicates very limited or no (linear) correlation between the two data sets, while a value close to 1 indicates a very high or perfect correlation. Typically, a CC above 0.9 is considered a high correlation (good agreement) for wave heights. It is noted that CC is 1 (or -1) for any two fully linearly correlated variables, even if they are not 1:1. However, the slope and intercept of the linear relation may be different from 1 and 0, respectively, despite CC of 1 (or -1).

The QQ line slope and intercept are found from a linear fit to the data quantiles in a least-square sense. The lower and uppermost quantiles are not included on the fit. A regression line slope different from 1 may indicate a trend in the difference.

The peak ratio (PR) is the average ratio of the N_{peak} highest joint (coinciding) model and measured events. The peaks are found individually for each dataset through a declustering technique, such as fx two (2) Average-Annual-Peaks (AAP) and an inter-event time (IET) of 36 hours. Subsequently, the joint peaks are found by identifying events within half the IET (ie 18 hours) of each other. A general/average underestimation of the modelled peaks results in a PR < 1, while an overestimation results in a PR > 1.

An example of a peak plot is shown in Figure 1.1. 'X' represents the observed peaks (x-axis), while 'Y' represents the modelled peaks (y-axis), based on the POT methodology, both represented by circles ('o') in the plot. The joint (coinciding) peaks, defined as any X and Y peaks within ±36 hours[1] of each other (i.e., less than or equal to the number of individual peaks), are represented by crosses ('x'). Hence, the joint peaks ('x') overlap with the individual peaks ('o') only if they occur at the same time exactly. Otherwise, the joint peaks ('x') represent an additional point in the plot, which may be associated with the observed and modelled individual peaks ('o') by searching in the respective X and Y-axis directions, see example with red lines in Figure 1.1. It is seen that the 'X' peaks are often underneath the 1:1 line, while the 'Y' peaks are often above the 1:1 line.

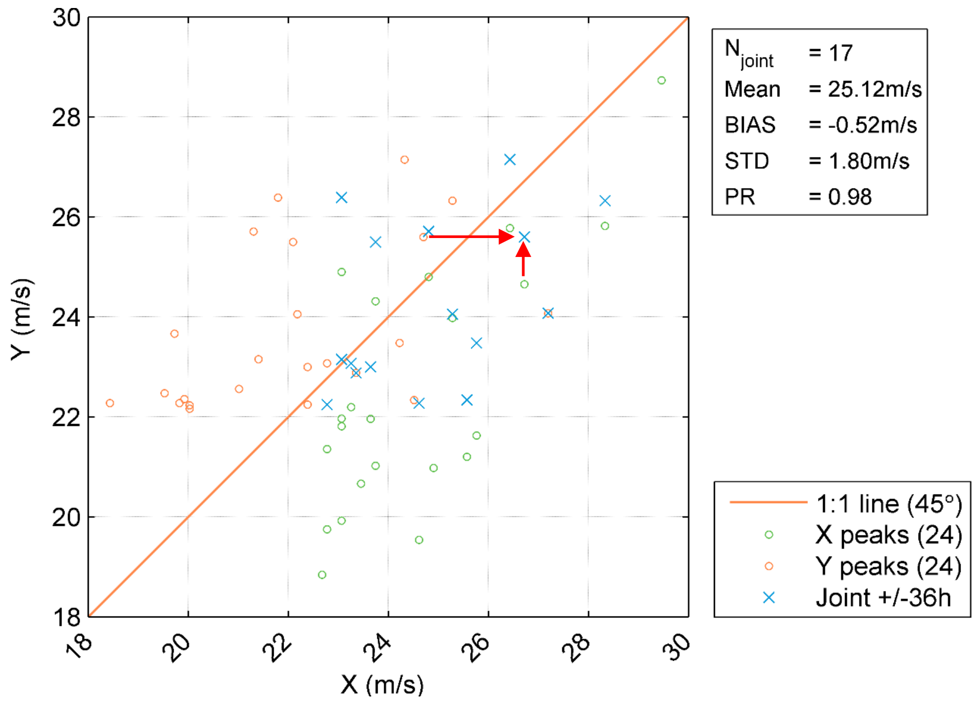

Figure 1.1 Example of peak event plot (wind speed)

1 36 hours is chosen arbitrarily as representative of an average storm duration. Often the measured and modelled peaks are within 1-2 hours of each other.

Table 1.1 Definitions of model quality indices (X = Observation, Y = Model)

Abbreviation	Description	Definition
N	Number of data (synchronised)	–
MEAN	Mean of Y data Mean of X data	$\frac{1}{N}\sum_{i=1}^{N} Y_i \equiv \overline{Y}$, $\frac{1}{N}\sum_{i=1}^{N} X_i \equiv \overline{X}$
STD	Standard deviation of Y data Standard deviation of X data	$\sqrt{\frac{1}{N-1}\sum_{i=1}^{N}(Y-\overline{Y})^2}$, $\sqrt{\frac{1}{N-1}\sum_{i=1}^{N}(X-\overline{X})^2}$
BIAS	Mean difference	$\frac{1}{N}\sum_{i=1}^{N}(Y-X)_i = \overline{Y}-\overline{X}$
MAE	Mean absolute difference	$\frac{1}{N}\sum_{i=1}^{N}(\lvert Y-X\rvert)_i$
RMSE	Root-mean-square difference	$\sqrt{\frac{1}{N}\sum_{i=1}^{N}(Y-X)_i^{\,2}}$
SI	Scatter index (unbiased)	$\frac{\sqrt{\frac{1}{N}\sum_{i=1}^{N}(Y-X-\text{BIAS})_i^{\,2}}}{\frac{1}{N}\sum_{i=1}^{N}\lvert X_i\rvert}$
EV	Explained variance	$\frac{\sum_{i=1}^{N}(X_i-\overline{X})^2-\sum_{i=1}^{N}[(X_i-\overline{X})-(Y_i-\overline{Y})]^2}{\sum_{i=1}^{N}(X_i-\overline{X})^2}$
CC	Correlation coefficient	$\frac{\sum_{i=1}^{N}(X_i-\overline{X})(Y_i-\overline{Y})}{\sqrt{\sum_{i=1}^{N}(X_i-\overline{X})^2\sum_{i=1}^{N}(Y_i-\overline{Y})^2}}$
QQ	Quantile-Quantile (line slope and intercept)	Linear least square fit to quantiles
PR	Peak ratio (of N_{peak} highest – joint – events)	$\text{PR} = \frac{\sum_{i=1}^{N_{peak}}\frac{Y_i}{X_i}}{N_{peak}}$

Appendix B Validation of Currents, Temperature, Salinity and Water Level

See next pages

Appendix B.1 Currents

LOT3: -10m

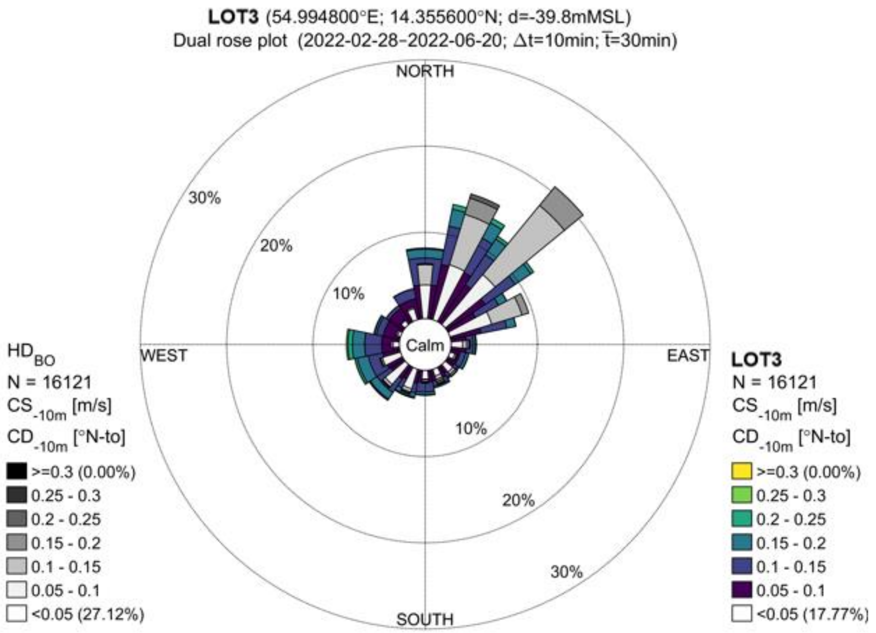

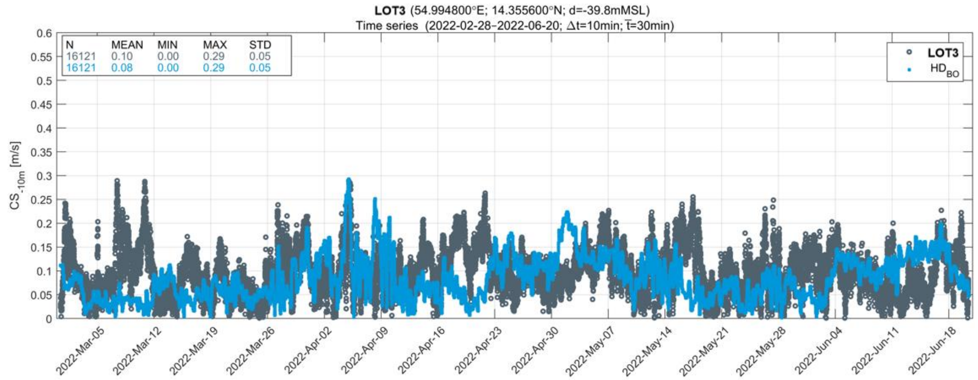

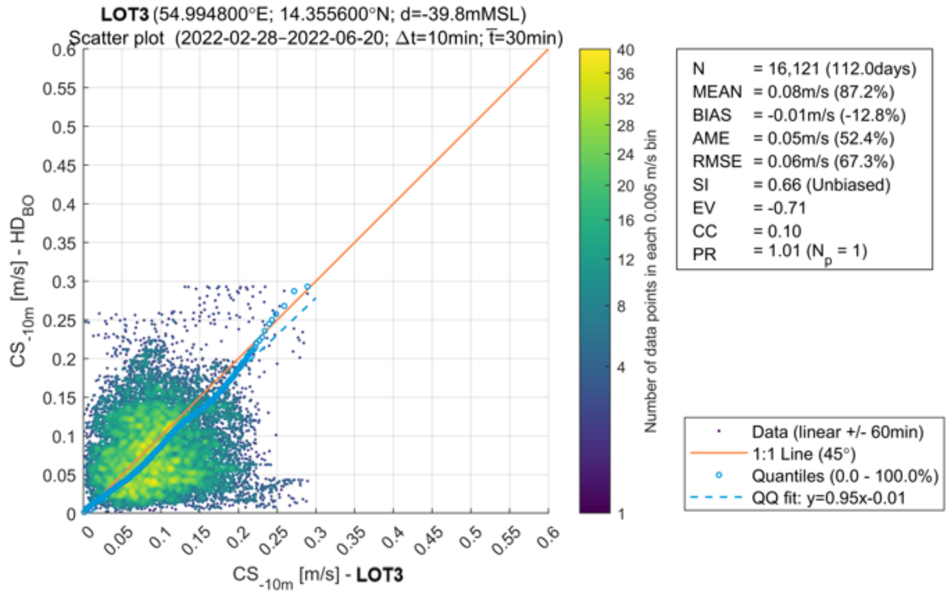

LOT3: -18m

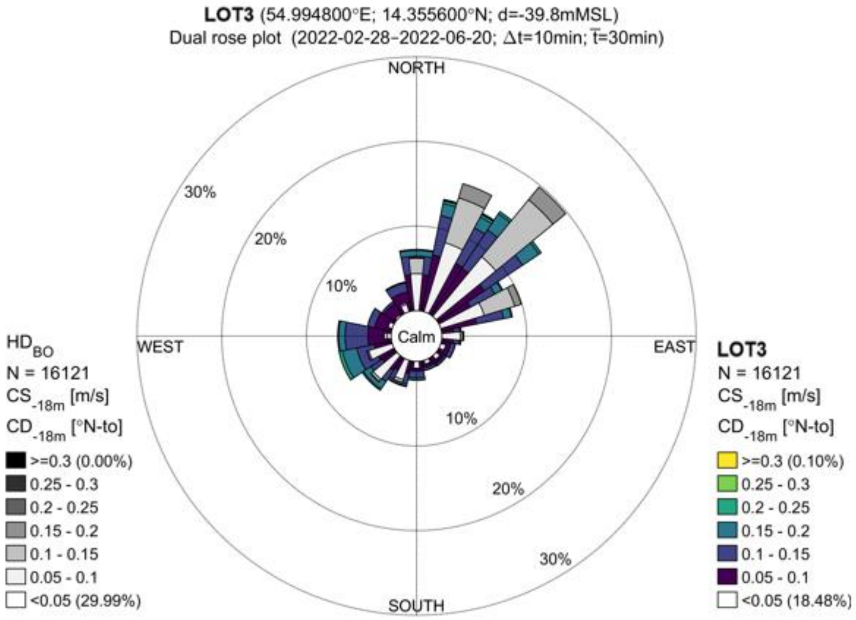
LOT3 (54.994800°E; 14.355600°N; d=-39.8mMSL)
Dual rose plot (2022-02-28–2022-06-20; Δt=10min; t̄=30min)
NORTH
SOUTH
WEST
EAST
Calm
10%
20%
30%
HDBO
N = 16121
CS-18m [m/s]
CD-18m [°N-to]
>=0.3 (0.00%)
0.25 - 0.3
0.2 - 0.25
0.15 - 0.2
0.1 - 0.15
0.05 - 0.1
<0.05 (29.99%)
LOT3
N = 16121
CS-18m [m/s]
CD-18m [°N-to]
>=0.3 (0.10%)
0.25 - 0.3
0.2 - 0.25
0.15 - 0.2
0.1 - 0.15
0.05 - 0.1
<0.05 (18.48%)

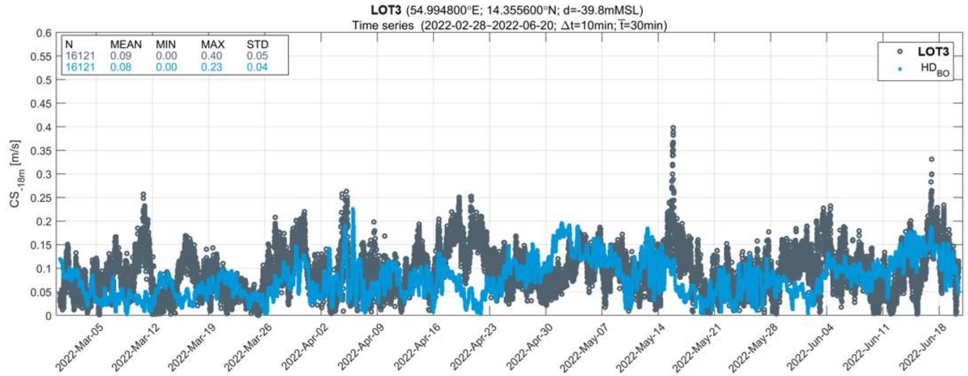
LOT3 (54.994800°E; 14.355600°N; d=-39.8mMSL)
Time series (2022-02-28–2022-06-20; Δt=10min; t̄=30min)
N MEAN MIN MAX STD
16121 0.09 0.00 0.40 0.05
16121 0.08 0.00 0.23 0.04
LOT3
HDBO
CS-18m [m/s]

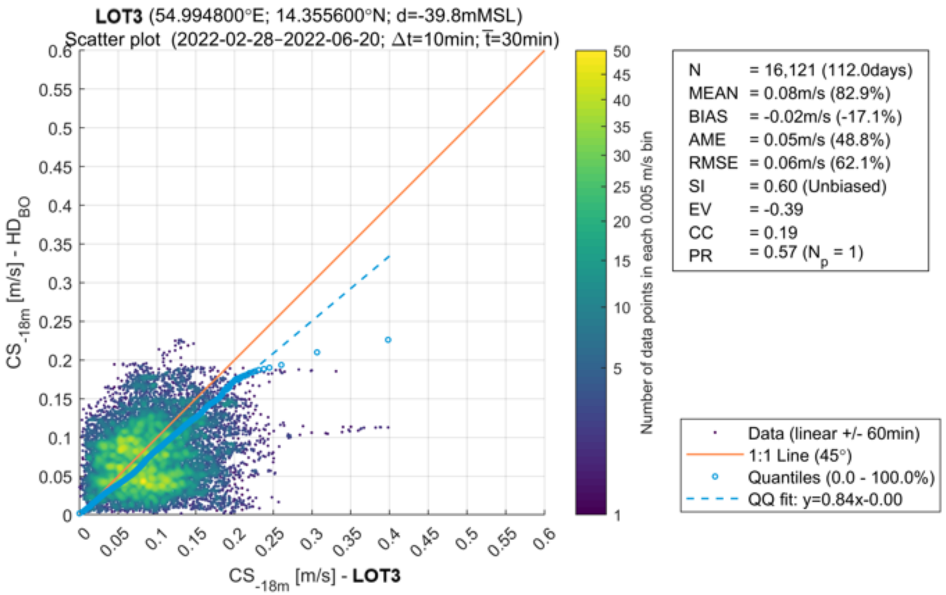
LOT3 (54.994800°E; 14.355600°N; d=-39.8mMSL)
Scatter plot (2022-02-28–2022-06-20; Δt=10min; t̄=30min)
N = 16,121 (112.0days)
MEAN = 0.08m/s (82.9%)
BIAS = -0.02m/s (-17.1%)
AME = 0.05m/s (48.8%)
RMSE = 0.06m/s (62.1%)
SI = 0.60 (Unbiased)
EV = -0.39
CC = 0.19
PR = 0.57 (Np = 1)
Number of data points in each 0.005 m/s bin
Data (linear +/- 60min)
1:1 Line (45°)
Quantiles (0.0 - 100.0%)
QQ fit: y=0.84x-0.00
CS-18m [m/s] - HDBO
CS-18m [m/s] - LOT3

LOT3: -32m

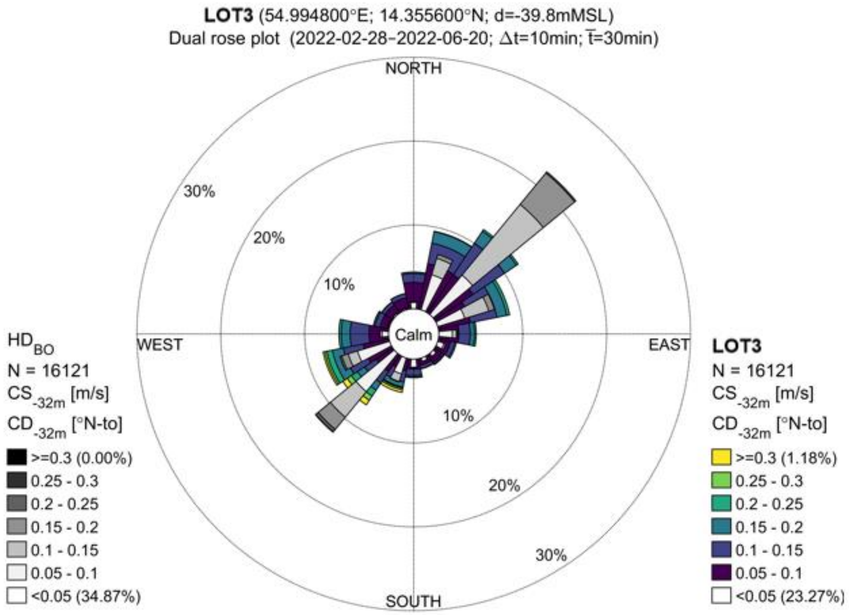
LOT3 (54.994800°E; 14.355600°N; d=-39.8mMSL)
Dual rose plot (2022-02-28-2022-06-20; Δt=10min; t̄=30min)
NORTH
SOUTH
WEST
EAST
Calm
10%
20%
30%
HDBO
N = 16121
CS-32m [m/s]
CD-32m [°N-to]
>=0.3 (0.00%)
0.25 - 0.3
0.2 - 0.25
0.15 - 0.2
0.1 - 0.15
0.05 - 0.1
<0.05 (34.87%)
LOT3
N = 16121
CS-32m [m/s]
CD-32m [°N-to]
>=0.3 (1.18%)
0.25 - 0.3
0.2 - 0.25
0.15 - 0.2
0.1 - 0.15
0.05 - 0.1
<0.05 (23.27%)

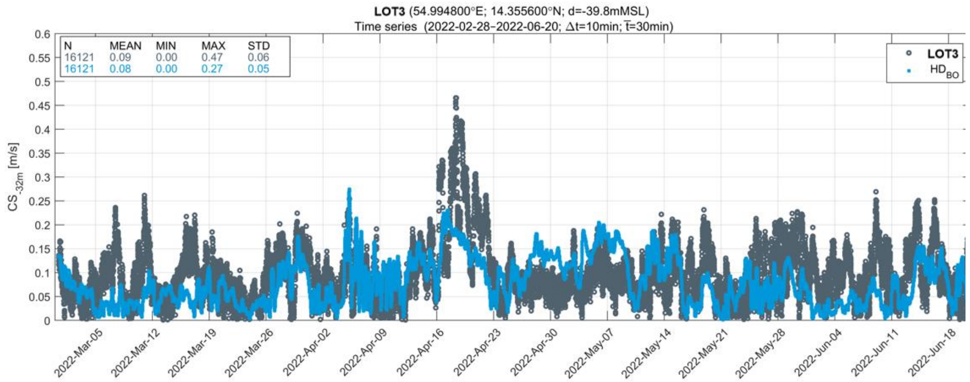
LOT3 (54.994800°E; 14.355600°N; d=-39.8mMSL)
Time series (2022-02-28-2022-06-20; Δt=10min; t̄=30min)
N MEAN MIN MAX STD
16121 0.09 0.00 0.47 0.06
16121 0.08 0.00 0.27 0.05
LOT3
HDBO
CS-32m [m/s]
2022-Mar-05
2022-Mar-12
2022-Mar-19
2022-Mar-26
2022-Apr-02
2022-Apr-09
2022-Apr-16
2022-Apr-23
2022-Apr-30
2022-May-07
2022-May-14
2022-May-21
2022-May-28
2022-Jun-04
2022-Jun-11
2022-Jun-18

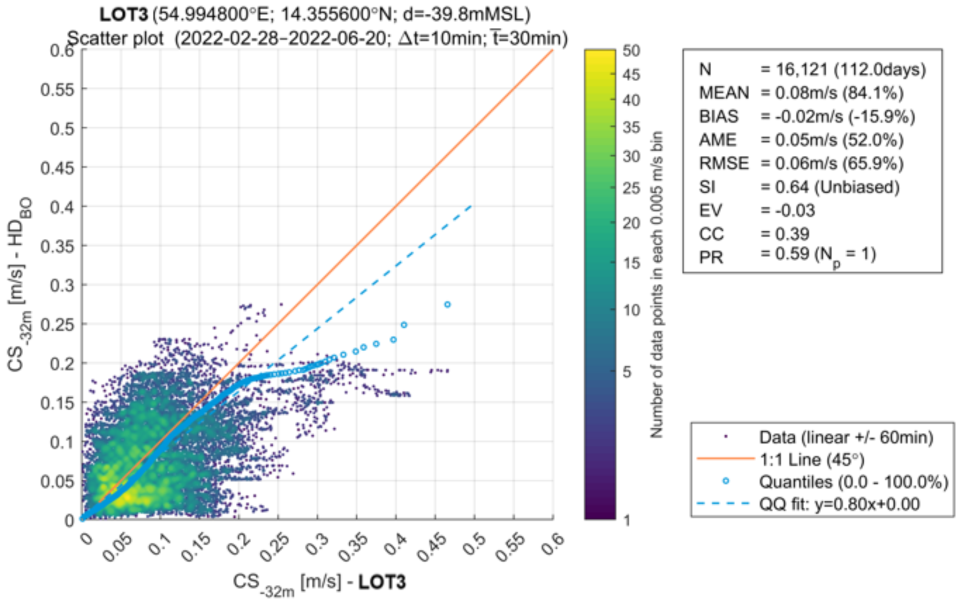
LOT3 (54.994800°E; 14.355600°N; d=-39.8mMSL)
Scatter plot (2022-02-28-2022-06-20; Δt=10min; t̄=30min)
N = 16,121 (112.0days)
MEAN = 0.08m/s (84.1%)
BIAS = -0.02m/s (-15.9%)
AME = 0.05m/s (52.0%)
RMSE = 0.06m/s (65.9%)
SI = 0.64 (Unbiased)
EV = -0.03
CC = 0.39
PR = 0.59 (Np = 1)
Number of data points in each 0.005 m/s bin
Data (linear +/- 60min)
1:1 Line (45°)
Quantiles (0.0 - 100.0%)
QQ fit: y=0.80x+0.00
CS-32m [m/s] - HDBO
CS-32m [m/s] - LOT3

LOT4: -10m

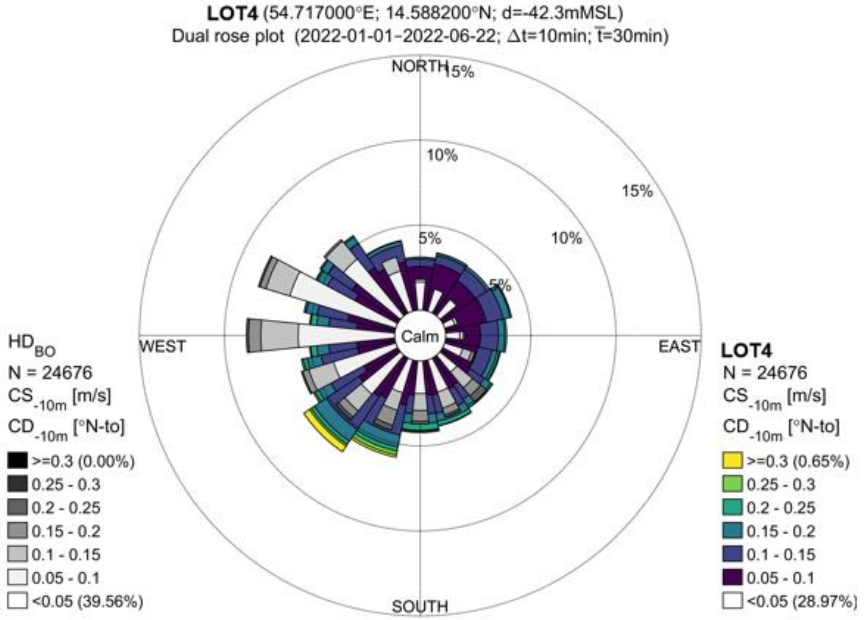

LOT4 (54.717000°E; 14.588200°N; d=-42.3mMSL)
Dual rose plot (2022-01-01-2022-06-22; Δt=10min; t̄=30min)
NORTH
SOUTH
WEST
EAST
Calm
5%
10%
15%
HDBO
N = 24676
CS-10m [m/s]
CD-10m [°N-to]
>=0.3 (0.00%)
0.25 - 0.3
0.2 - 0.25
0.15 - 0.2
0.1 - 0.15
0.05 - 0.1
<0.05 (39.56%)
LOT4
N = 24676
CS-10m [m/s]
CD-10m [°N-to]
>=0.3 (0.65%)
0.25 - 0.3
0.2 - 0.25
0.15 - 0.2
0.1 - 0.15
0.05 - 0.1
<0.05 (28.97%)

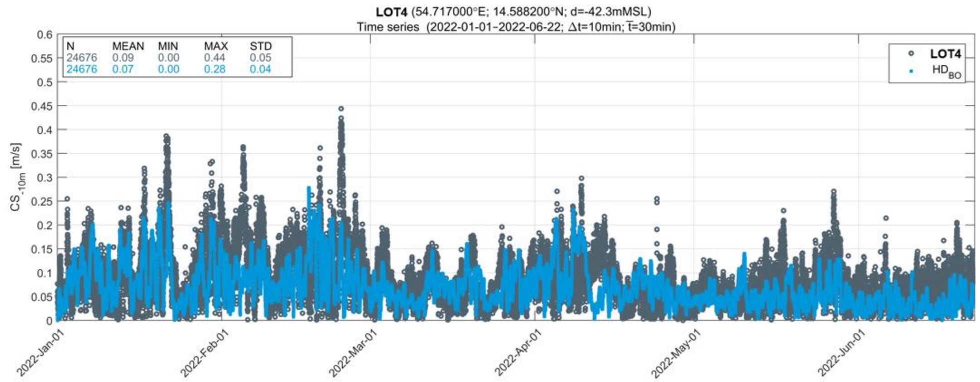

LOT4 (54.717000°E; 14.588200°N; d=-42.3mMSL)
Time series (2022-01-01-2022-06-22; Δt=10min; t̄=30min)
N MEAN MIN MAX STD
24676 0.09 0.00 0.44 0.05
24676 0.07 0.00 0.28 0.04
LOT4
HDBO
CS-10m [m/s]
2022-Jan-01
2022-Feb-01
2022-Mar-01
2022-Apr-01
2022-May-01
2022-Jun-01

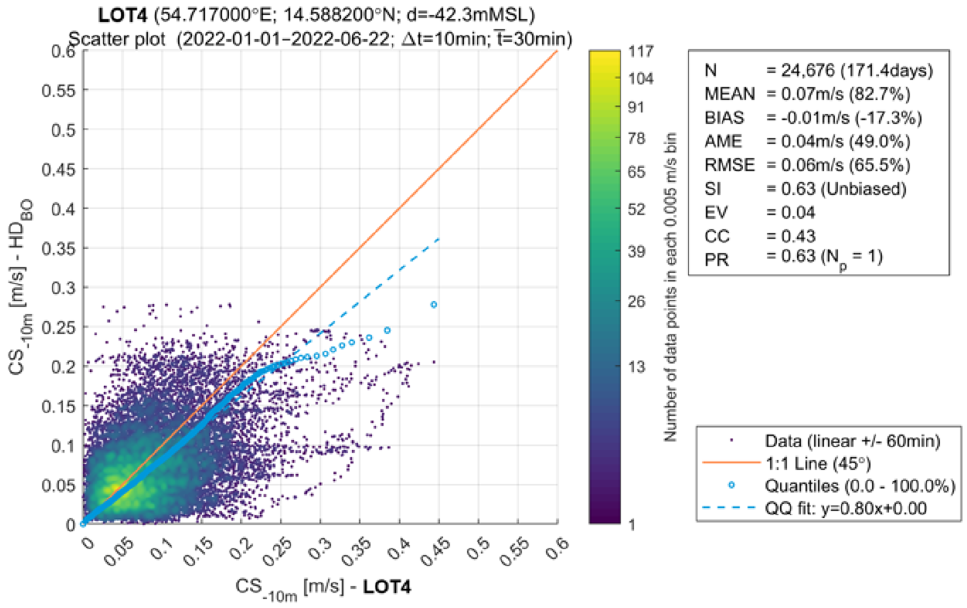

LOT4 (54.717000°E; 14.588200°N; d=-42.3mMSL)
Scatter plot (2022-01-01-2022-06-22; Δt=10min; t̄=30min)
CS-10m [m/s] - HDBO
CS-10m [m/s] - LOT4
Number of data points in each 0.005 m/s bin
N = 24,676 (171.4days)
MEAN = 0.07m/s (82.7%)
BIAS = -0.01m/s (-17.3%)
AME = 0.04m/s (49.0%)
RMSE = 0.06m/s (65.5%)
SI = 0.63 (Unbiased)
EV = 0.04
CC = 0.43
PR = 0.63 (Np = 1)
Data (linear +/- 60min)
1:1 Line (45°)
Quantiles (0.0 - 100.0%)
QQ fit: y=0.80x+0.00

LOT4: -18m

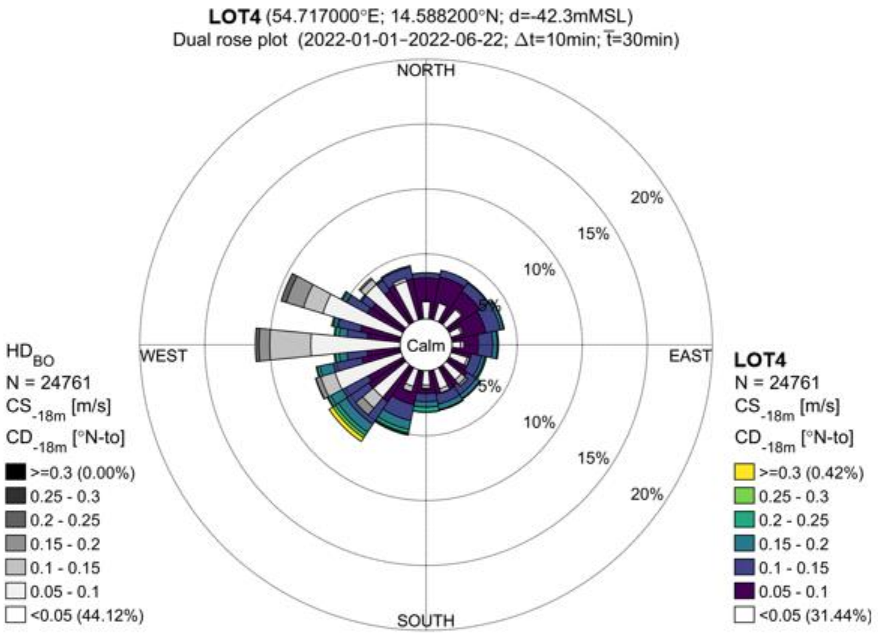
LOT4 (54.717000°E; 14.588200°N; d=-42.3mMSL)
Dual rose plot (2022-01-01-2022-06-22; Δt=10min; t̄=30min)
NORTH
SOUTH
WEST
EAST
Calm
HD_BO
N = 24761
CS_-18m [m/s]
CD_-18m [°N-to]
>=0.3 (0.00%)
0.25 - 0.3
0.2 - 0.25
0.15 - 0.2
0.1 - 0.15
0.05 - 0.1
<0.05 (44.12%)
LOT4
N = 24761
CS_-18m [m/s]
CD_-18m [°N-to]
>=0.3 (0.42%)
0.25 - 0.3
0.2 - 0.25
0.15 - 0.2
0.1 - 0.15
0.05 - 0.1
<0.05 (31.44%)

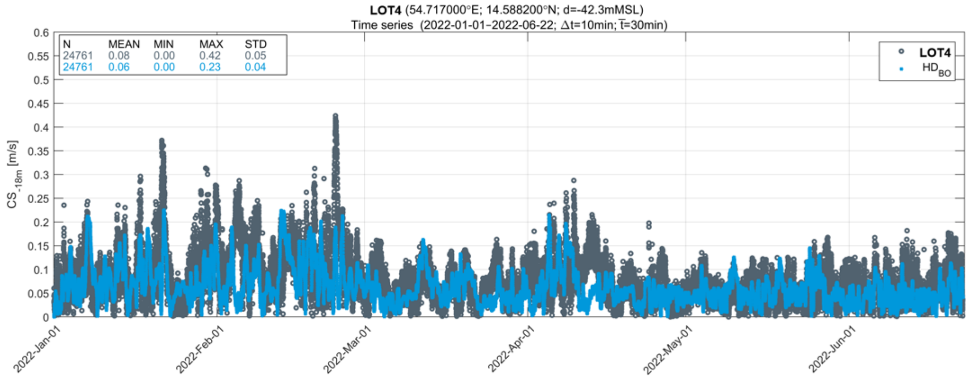
LOT4 (54.717000°E; 14.588200°N; d=-42.3mMSL)
Time series (2022-01-01-2022-06-22; Δt=10min; t̄=30min)
N MEAN MIN MAX STD
24761 0.08 0.00 0.42 0.05
24761 0.06 0.00 0.23 0.04
LOT4
HD_BO
CS_-18m [m/s]
2022-Jan-01
2022-Feb-01
2022-Mar-01
2022-Apr-01
2022-May-01
2022-Jun-01

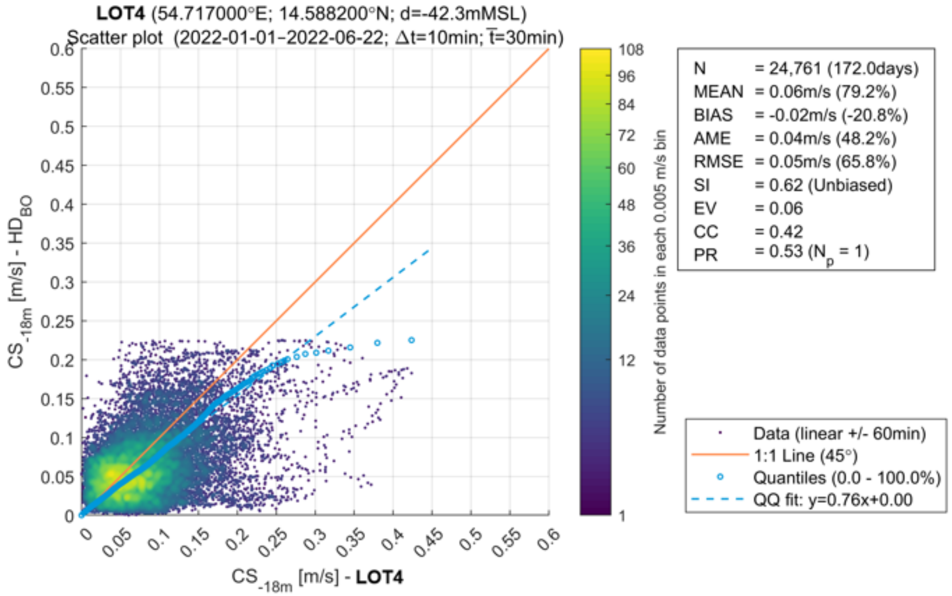
LOT4 (54.717000°E; 14.588200°N; d=-42.3mMSL)
Scatter plot (2022-01-01-2022-06-22; Δt=10min; t̄=30min)
N = 24,761 (172.0days)
MEAN = 0.06m/s (79.2%)
BIAS = -0.02m/s (-20.8%)
AME = 0.04m/s (48.2%)
RMSE = 0.05m/s (65.8%)
SI = 0.62 (Unbiased)
EV = 0.06
CC = 0.42
PR = 0.53 (N_p = 1)
Number of data points in each 0.005 m/s bin
Data (linear +/- 60min)
1:1 Line (45°)
Quantiles (0.0 - 100.0%)
QQ fit: y=0.76x+0.00
CS_-18m [m/s] - HD_BO
CS_-18m [m/s] - LOT4

LOT4: -32m

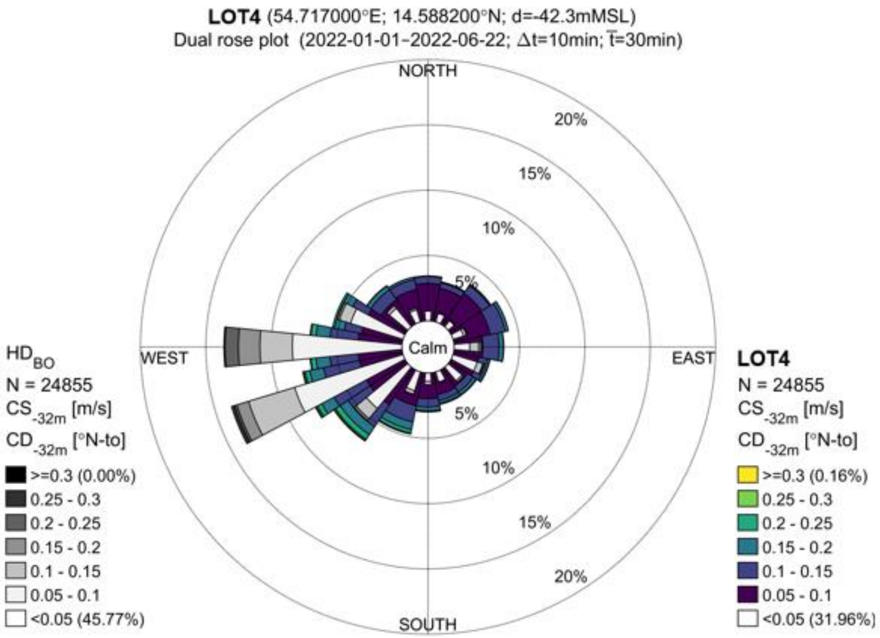

LOT4 (54.717000°E; 14.588200°N; d=-42.3mMSL)
Dual rose plot (2022-01-01–2022-06-22; Δt=10min; τ̄=30min)
NORTH
SOUTH
WEST
EAST
Calm
5%
10%
15%
20%
HD_BO
N = 24855
CS_-32m [m/s]
CD_-32m [°N-to]
>=0.3 (0.00%)
0.25 - 0.3
0.2 - 0.25
0.15 - 0.2
0.1 - 0.15
0.05 - 0.1
<0.05 (45.77%)
LOT4
N = 24855
CS_-32m [m/s]
CD_-32m [°N-to]
>=0.3 (0.16%)
0.25 - 0.3
0.2 - 0.25
0.15 - 0.2
0.1 - 0.15
0.05 - 0.1
<0.05 (31.96%)

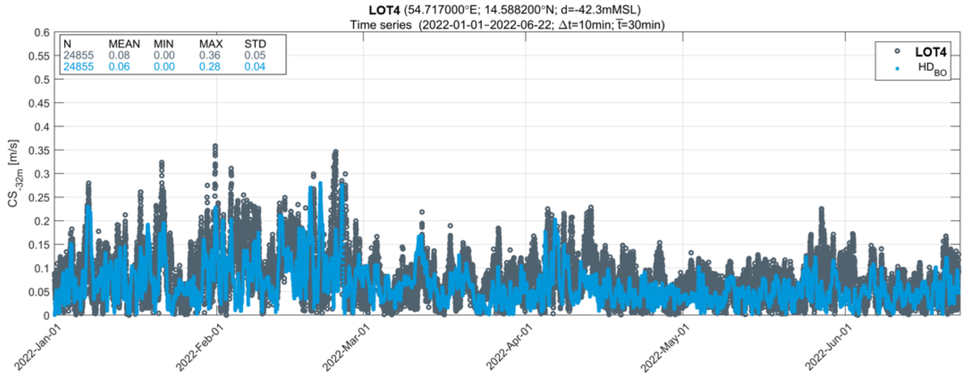

LOT4 (54.717000°E; 14.588200°N; d=-42.3mMSL)
Time series (2022-01-01–2022-06-22; Δt=10min; τ̄=30min)
N MEAN MIN MAX STD
24855 0.08 0.00 0.36 0.05
24855 0.06 0.00 0.28 0.04
LOT4
HD_BO
CS_-32m [m/s]
2022-Jan-01
2022-Feb-01
2022-Mar-01
2022-Apr-01
2022-May-01
2022-Jun-01

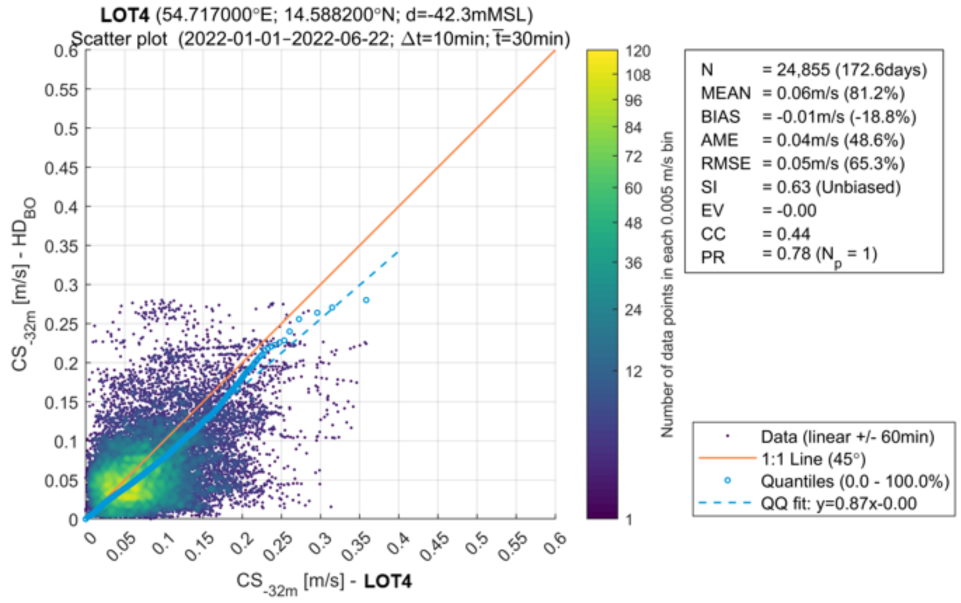

LOT4 (54.717000°E; 14.588200°N; d=-42.3mMSL)
Scatter plot (2022-01-01–2022-06-22; Δt=10min; τ̄=30min)
CS_-32m [m/s] - HD_BO
CS_-32m [m/s] - LOT4
Number of data points in each 0.005 m/s bin
N = 24,855 (172.6days)
MEAN = 0.06m/s (81.2%)
BIAS = -0.01m/s (-18.8%)
AME = 0.04m/s (48.6%)
RMSE = 0.05m/s (65.3%)
SI = 0.63 (Unbiased)
EV = -0.00
CC = 0.44
PR = 0.78 (N_p = 1)
Data (linear +/- 60min)
1:1 Line (45°)
Quantiles (0.0 - 100.0%)
QQ fit: y=0.87x-0.00

Arkona: -4m

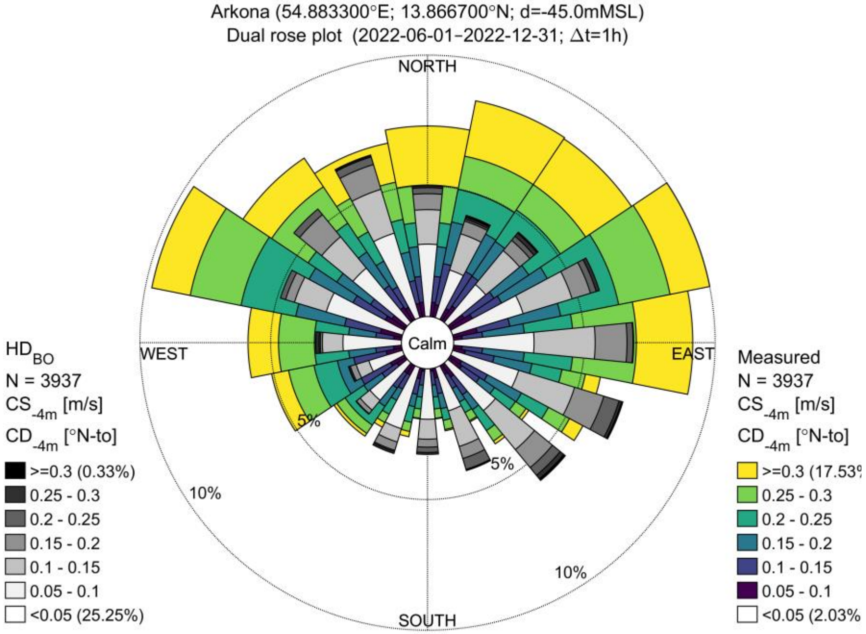
Arkona (54.883300°E; 13.866700°N; d=-45.0mMSL)
Dual rose plot (2022-06-01–2022-12-31; Δt=1h)
NORTH
WEST
EAST
SOUTH
Calm
5%
10%
HD_BO
N = 3937
CS_-4m [m/s]
CD_-4m [°N-to]
>=0.3 (0.33%)
0.25 - 0.3
0.2 - 0.25
0.15 - 0.2
0.1 - 0.15
0.05 - 0.1
<0.05 (25.25%)
Measured
N = 3937
CS_-4m [m/s]
CD_-4m [°N-to]
>=0.3 (17.53%
0.25 - 0.3
0.2 - 0.25
0.15 - 0.2
0.1 - 0.15
0.05 - 0.1
<0.05 (2.03%

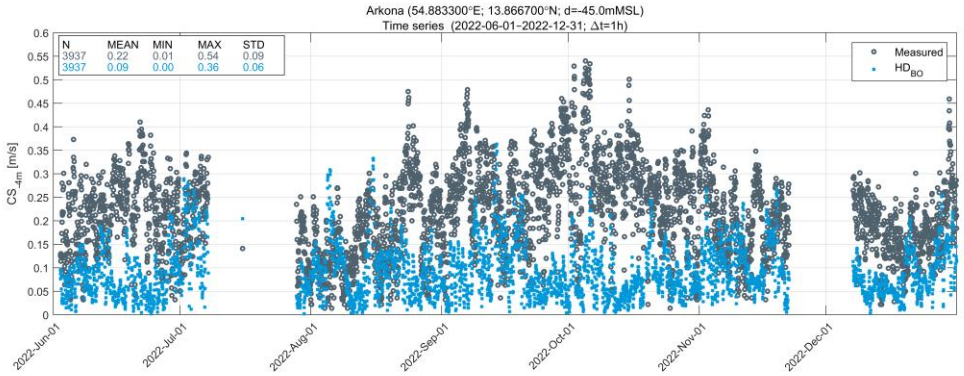
Arkona (54.883300°E; 13.866700°N; d=-45.0mMSL)
Time series (2022-06-01–2022-12-31; Δt=1h)
N MEAN MIN MAX STD
3937 0.22 0.01 0.54 0.09
3937 0.09 0.00 0.36 0.06
Measured
HD_BO
CS_-4m [m/s]
2022-Jun-01
2022-Jul-01
2022-Aug-01
2022-Sep-01
2022-Oct-01
2022-Nov-01
2022-Dec-01

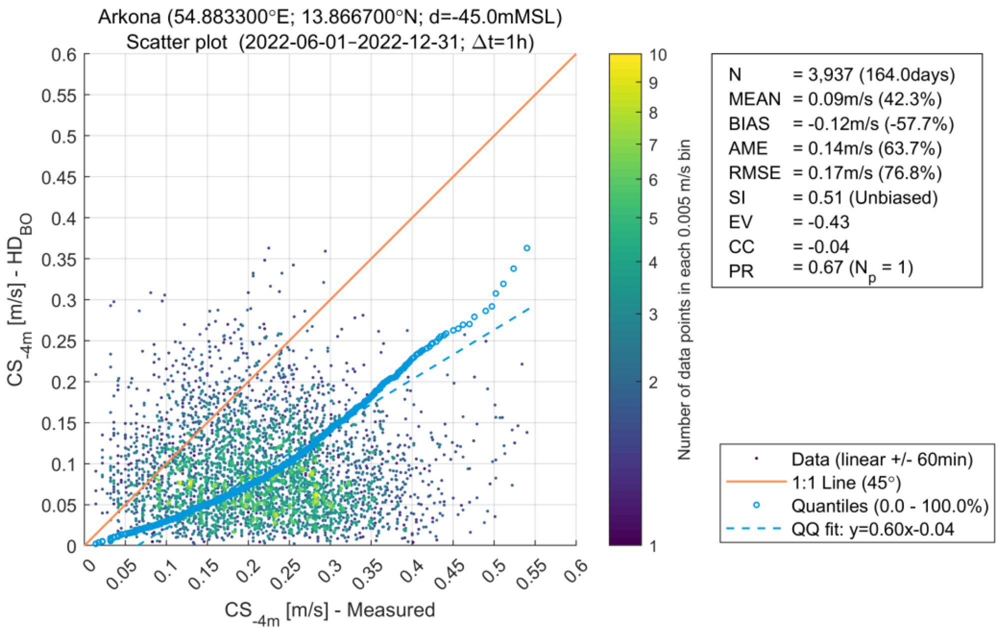
Arkona (54.883300°E; 13.866700°N; d=-45.0mMSL)
Scatter plot (2022-06-01–2022-12-31; Δt=1h)
CS_-4m [m/s] - HD_BO
CS_-4m [m/s] - Measured
Number of data points in each 0.005 m/s bin
N = 3,937 (164.0days)
MEAN = 0.09m/s (42.3%)
BIAS = -0.12m/s (-57.7%)
AME = 0.14m/s (63.7%)
RMSE = 0.17m/s (76.8%)
SI = 0.51 (Unbiased)
EV = -0.43
CC = -0.04
PR = 0.67 (N_p = 1)
Data (linear +/- 60min)
1:1 Line (45°)
Quantiles (0.0 - 100.0%)
QQ fit: y=0.60x-0.04

Arkona: -10m

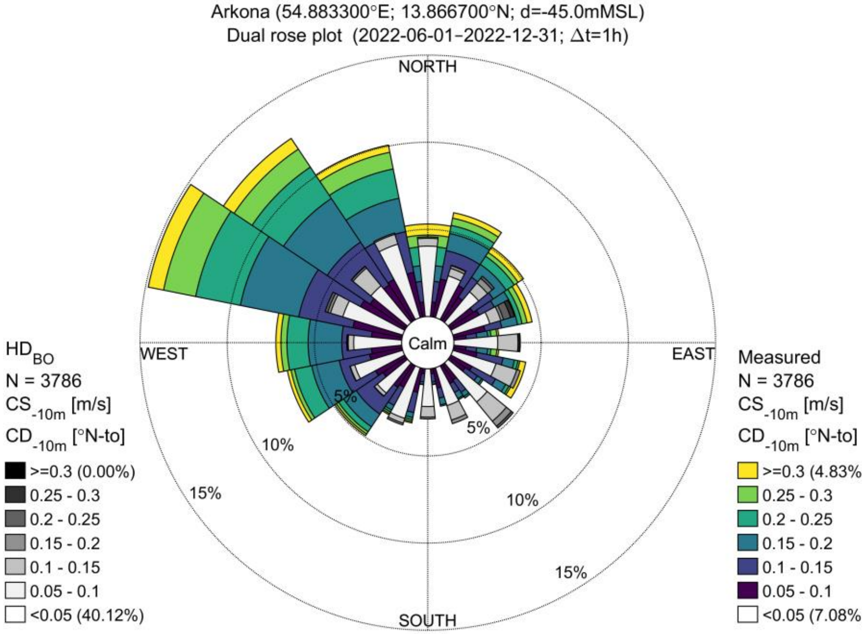
Arkona (54.883300°E; 13.866700°N; d=-45.0mMSL)
Dual rose plot (2022-06-01–2022-12-31; Δt=1h)
NORTH
WEST
EAST
SOUTH
Calm
5%
10%
15%
HD_BO
N = 3786
CS_-10m [m/s]
CD_-10m [°N-to]
>=0.3 (0.00%)
0.25 - 0.3
0.2 - 0.25
0.15 - 0.2
0.1 - 0.15
0.05 - 0.1
<0.05 (40.12%)
Measured
N = 3786
CS_-10m [m/s]
CD_-10m [°N-to]
>=0.3 (4.83%
0.25 - 0.3
0.2 - 0.25
0.15 - 0.2
0.1 - 0.15
0.05 - 0.1
<0.05 (7.08%

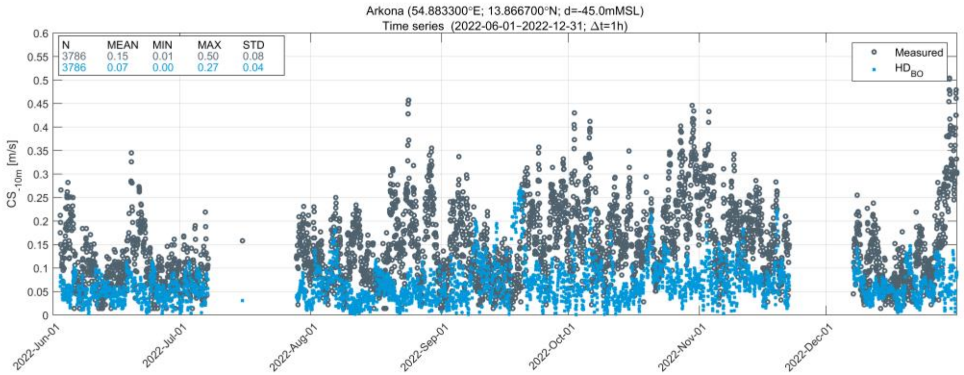
Arkona (54.883300°E; 13.866700°N; d=-45.0mMSL)
Time series (2022-06-01–2022-12-31; Δt=1h)
N MEAN MIN MAX STD
3786 0.15 0.01 0.50 0.08
3786 0.07 0.00 0.27 0.04
Measured
HD_BO
CS_-10m [m/s]
2022-Jun-01
2022-Jul-01
2022-Aug-01
2022-Sep-01
2022-Oct-01
2022-Nov-01
2022-Dec-01

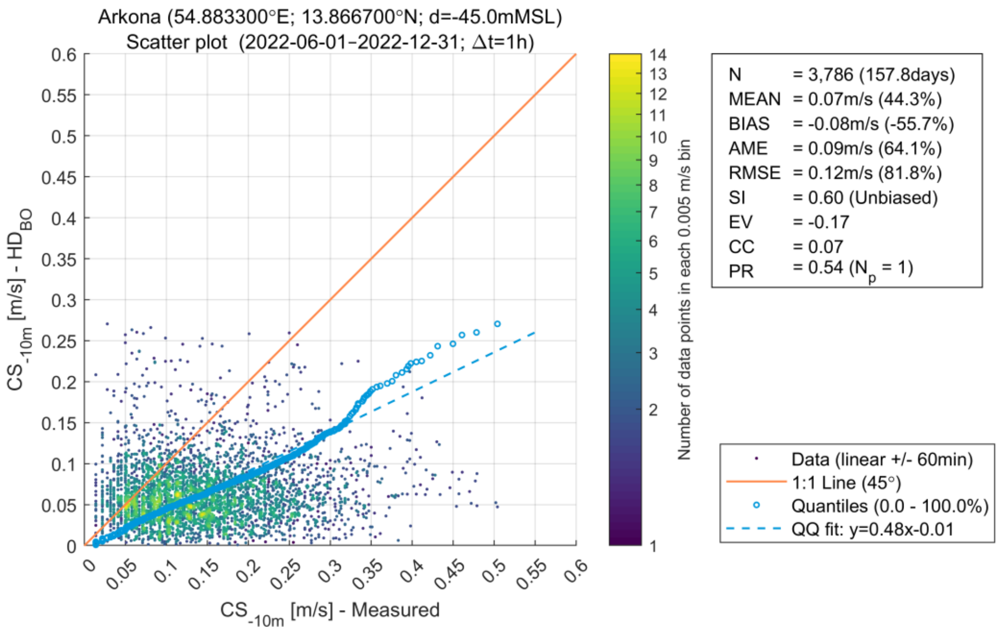
Arkona (54.883300°E; 13.866700°N; d=-45.0mMSL)
Scatter plot (2022-06-01–2022-12-31; Δt=1h)
CS_-10m [m/s] - HD_BO
CS_-10m [m/s] - Measured
Number of data points in each 0.005 m/s bin
N = 3,786 (157.8days)
MEAN = 0.07m/s (44.3%)
BIAS = -0.08m/s (-55.7%)
AME = 0.09m/s (64.1%)
RMSE = 0.12m/s (81.8%)
SI = 0.60 (Unbiased)
EV = -0.17
CC = 0.07
PR = 0.54 (N_p = 1)
Data (linear +/- 60min)
1:1 Line (45°)
Quantiles (0.0 - 100.0%)
QQ fit: y=0.48x-0.01

Arkona: -20m

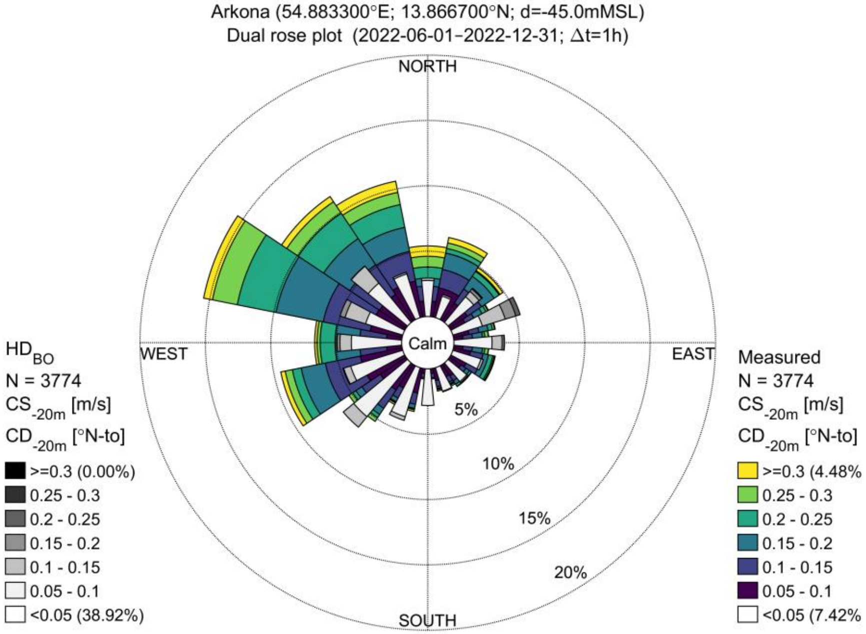
Arkona (54.883300°E; 13.866700°N; d=-45.0mMSL)
Dual rose plot (2022-06-01–2022-12-31; Δt=1h)
NORTH
WEST
EAST
SOUTH
Calm
5%
10%
15%
20%
HD_BO
N = 3774
CS_-20m [m/s]
CD_-20m [°N-to]
>=0.3 (0.00%)
0.25 - 0.3
0.2 - 0.25
0.15 - 0.2
0.1 - 0.15
0.05 - 0.1
<0.05 (38.92%)
Measured
N = 3774
CS_-20m [m/s]
CD_-20m [°N-to]
>=0.3 (4.48%
0.25 - 0.3
0.2 - 0.25
0.15 - 0.2
0.1 - 0.15
0.05 - 0.1
<0.05 (7.42%

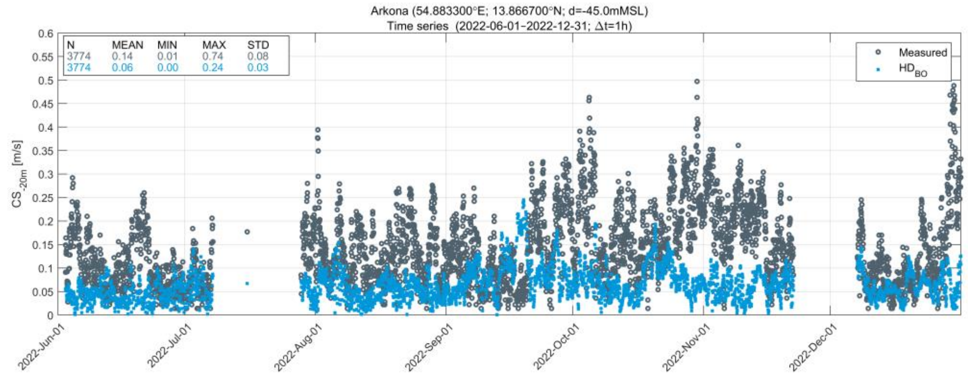
Arkona (54.883300°E; 13.866700°N; d=-45.0mMSL)
Time series (2022-06-01–2022-12-31; Δt=1h)
N MEAN MIN MAX STD
3774 0.14 0.01 0.74 0.08
3774 0.06 0.00 0.24 0.03
Measured
HD_BO
CS_-20m [m/s]
2022-Jun-01
2022-Jul-01
2022-Aug-01
2022-Sep-01
2022-Oct-01
2022-Nov-01
2022-Dec-01

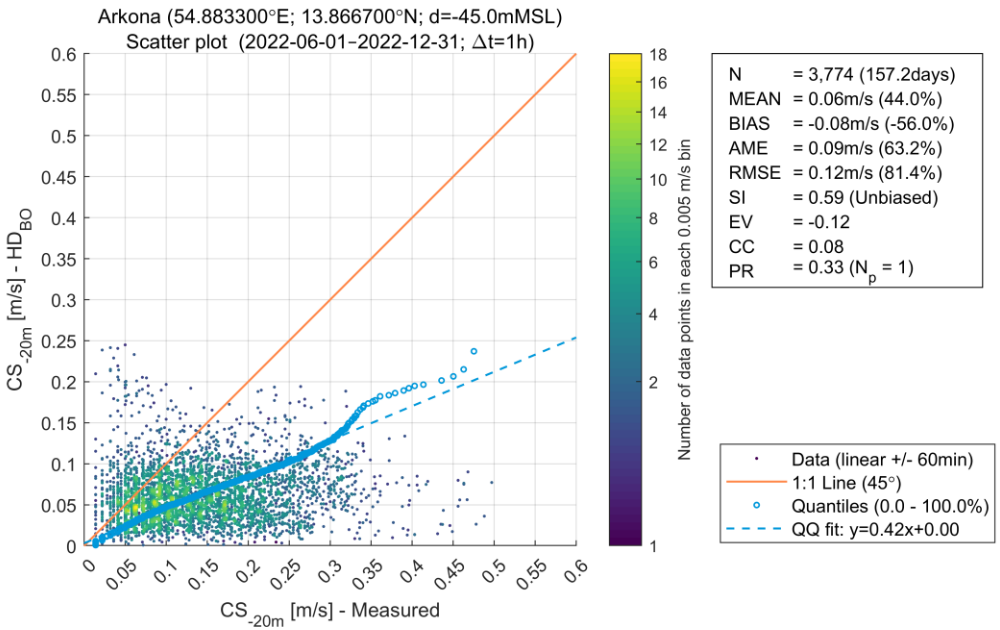
Arkona (54.883300°E; 13.866700°N; d=-45.0mMSL)
Scatter plot (2022-06-01–2022-12-31; Δt=1h)
CS_-20m [m/s] - HD_BO
CS_-20m [m/s] - Measured
Number of data points in each 0.005 m/s bin
N = 3,774 (157.2days)
MEAN = 0.06m/s (44.0%)
BIAS = -0.08m/s (-56.0%)
AME = 0.09m/s (63.2%)
RMSE = 0.12m/s (81.4%)
SI = 0.59 (Unbiased)
EV = -0.12
CC = 0.08
PR = 0.33 (N_p = 1)
Data (linear +/- 60min)
1:1 Line (45°)
Quantiles (0.0 - 100.0%)
QQ fit: y=0.42x+0.00

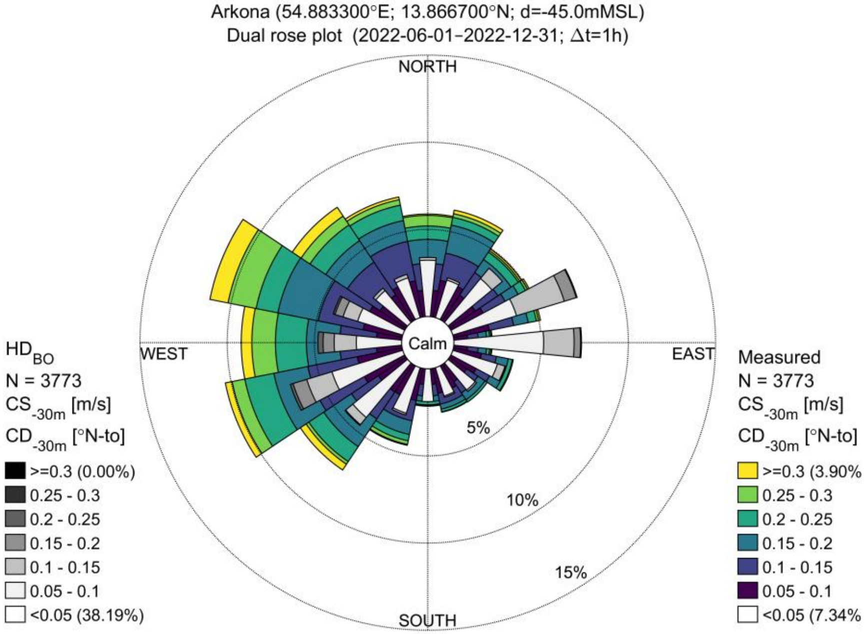

Arkona (54.883300°E; 13.866700°N; d=-45.0mMSL)
Dual rose plot (2022-06-01–2022-12-31; Δt=1h)
NORTH
WEST
EAST
SOUTH
Calm
5%
10%
15%
HD_BO
N = 3773
CS_-30m [m/s]
CD_-30m [°N-to]
>=0.3 (0.00%)
0.25 - 0.3
0.2 - 0.25
0.15 - 0.2
0.1 - 0.15
0.05 - 0.1
<0.05 (38.19%)
Measured
N = 3773
CS_-30m [m/s]
CD_-30m [°N-to]
>=0.3 (3.90%
0.25 - 0.3
0.2 - 0.25
0.15 - 0.2
0.1 - 0.15
0.05 - 0.1
<0.05 (7.34%

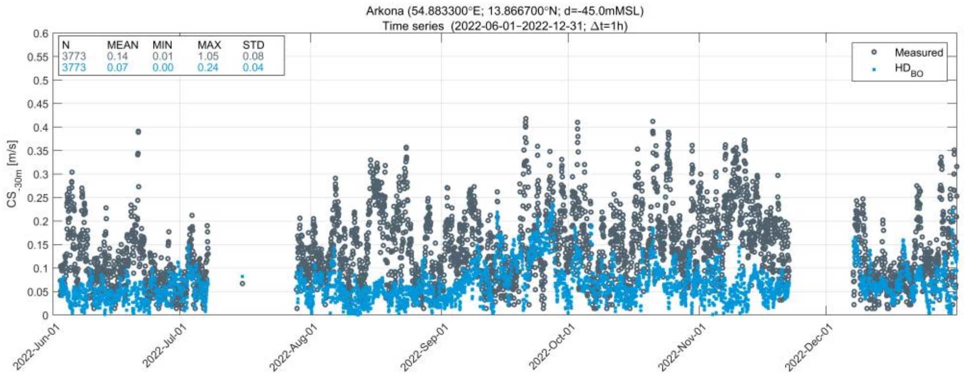

Arkona (54.883300°E; 13.866700°N; d=-45.0mMSL)
Time series (2022-06-01–2022-12-31; Δt=1h)
N MEAN MIN MAX STD
3773 0.14 0.01 1.05 0.08
3773 0.07 0.00 0.24 0.04
Measured
HD_BO
CS_-30m [m/s]
2022-Jun-01
2022-Jul-01
2022-Aug-01
2022-Sep-01
2022-Oct-01
2022-Nov-01
2022-Dec-01

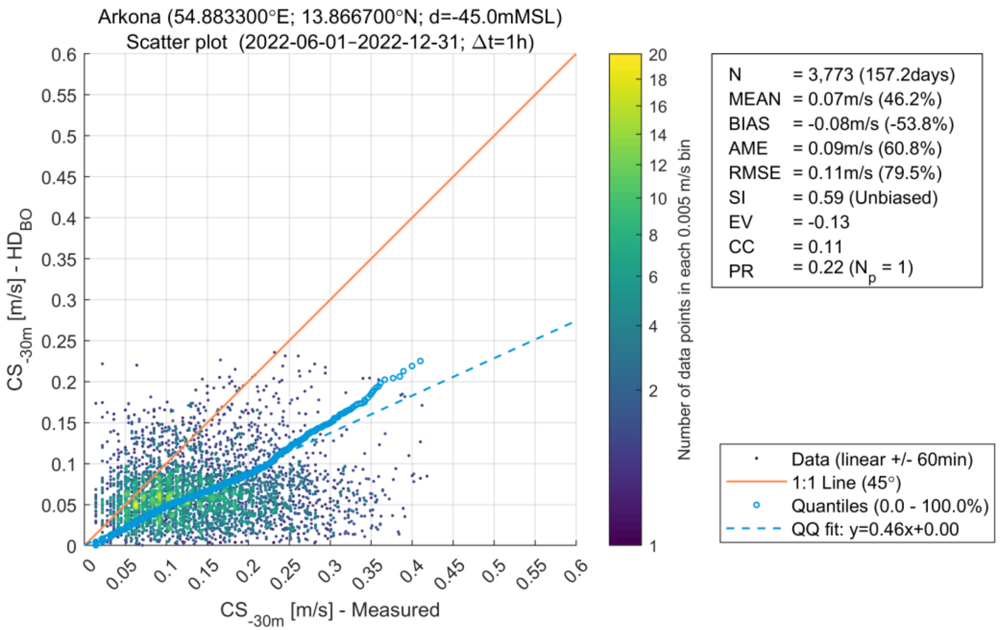

Arkona (54.883300°E; 13.866700°N; d=-45.0mMSL)
Scatter plot (2022-06-01–2022-12-31; Δt=1h)
CS_-30m [m/s] - HD_BO
CS_-30m [m/s] - Measured
Number of data points in each 0.005 m/s bin
N = 3,773 (157.2days)
MEAN = 0.07m/s (46.2%)
BIAS = -0.08m/s (-53.8%)
AME = 0.09m/s (60.8%)
RMSE = 0.11m/s (79.5%)
SI = 0.59 (Unbiased)
EV = -0.13
CC = 0.11
PR = 0.22 (N_p = 1)
Data (linear +/- 60min)
1:1 Line (45°)
Quantiles (0.0 - 100.0%)
QQ fit: y=0.46x+0.00

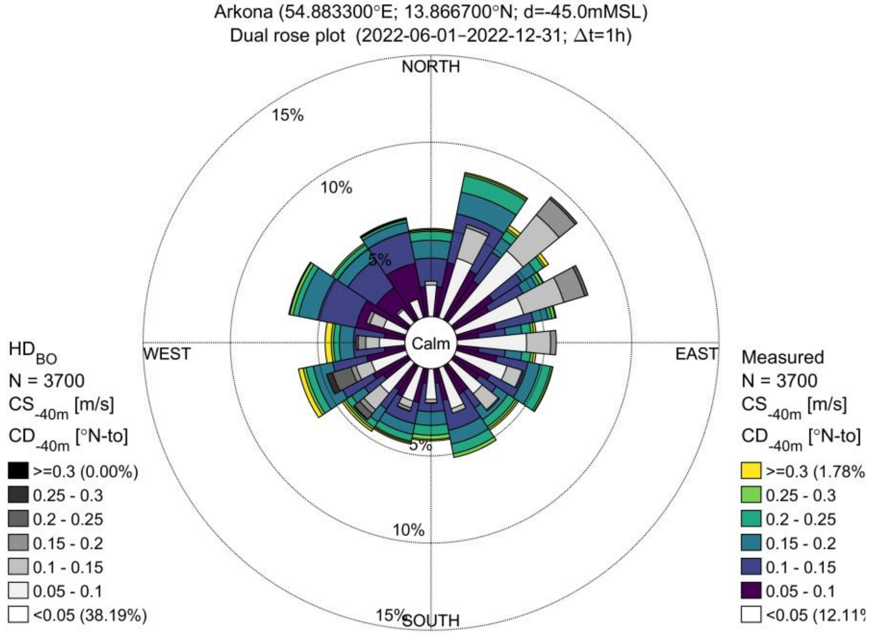
Arkona (54.883300°E; 13.866700°N; d=-45.0mMSL)
Dual rose plot (2022-06-01–2022-12-31; Δt=1h)
NORTH
SOUTH
WEST
EAST
Calm
5%
10%
15%
HD_BO
N = 3700
CS -40m [m/s]
CD -40m [°N-to]
>=0.3 (0.00%)
0.25 - 0.3
0.2 - 0.25
0.15 - 0.2
0.1 - 0.15
0.05 - 0.1
<0.05 (38.19%)
Measured
N = 3700
CS -40m [m/s]
CD -40m [°N-to]
>=0.3 (1.78%
0.25 - 0.3
0.2 - 0.25
0.15 - 0.2
0.1 - 0.15
0.05 - 0.1
<0.05 (12.11%

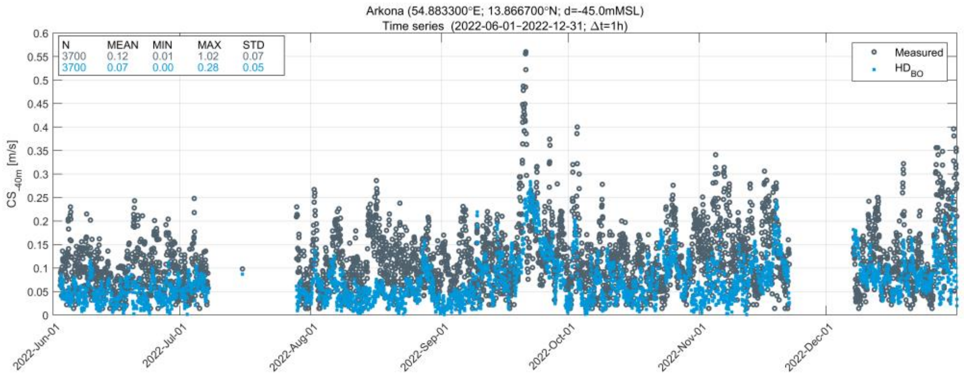
Arkona (54.883300°E; 13.866700°N; d=-45.0mMSL)
Time series (2022-06-01–2022-12-31; Δt=1h)
N MEAN MIN MAX STD
3700 0.12 0.01 1.02 0.07
3700 0.07 0.00 0.28 0.05
Measured
HD_BO
CS -40m [m/s]
2022-Jun-01
2022-Jul-01
2022-Aug-01
2022-Sep-01
2022-Oct-01
2022-Nov-01
2022-Dec-01

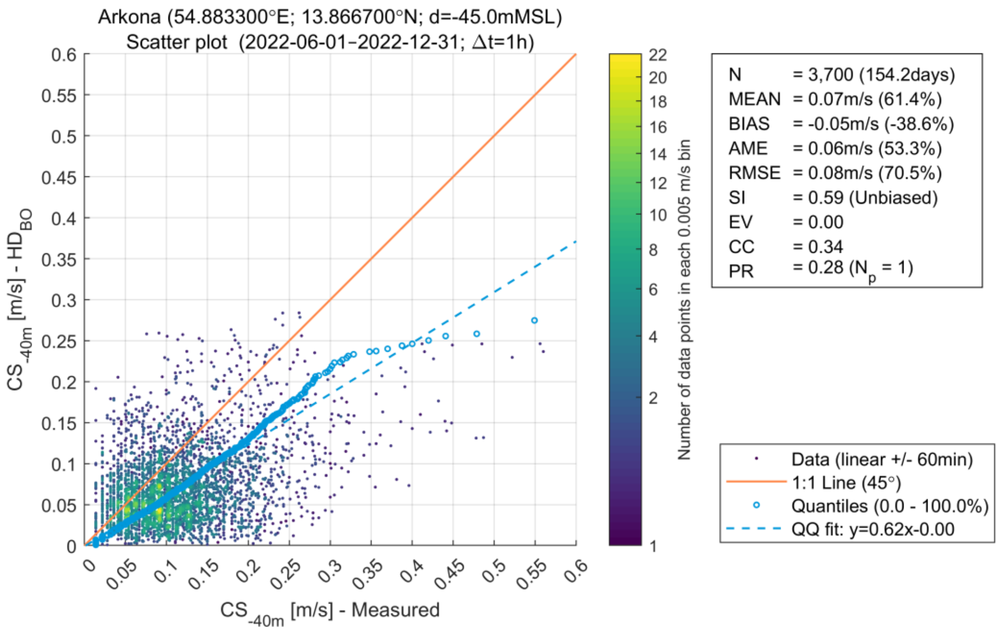
Arkona (54.883300°E; 13.866700°N; d=-45.0mMSL)
Scatter plot (2022-06-01–2022-12-31; Δt=1h)
CS -40m [m/s] - HD_BO
CS -40m [m/s] - Measured
Number of data points in each 0.005 m/s bin
N = 3,700 (154.2days)
MEAN = 0.07m/s (61.4%)
BIAS = -0.05m/s (-38.6%)
AME = 0.06m/s (53.3%)
RMSE = 0.08m/s (70.5%)
SI = 0.59 (Unbiased)
EV = 0.00
CC = 0.34
PR = 0.28 (N_p = 1)
Data (linear +/- 60min)
1:1 Line (45°)
Quantiles (0.0 - 100.0%)
QQ fit: y=0.62x-0.00

FINO2: -2m

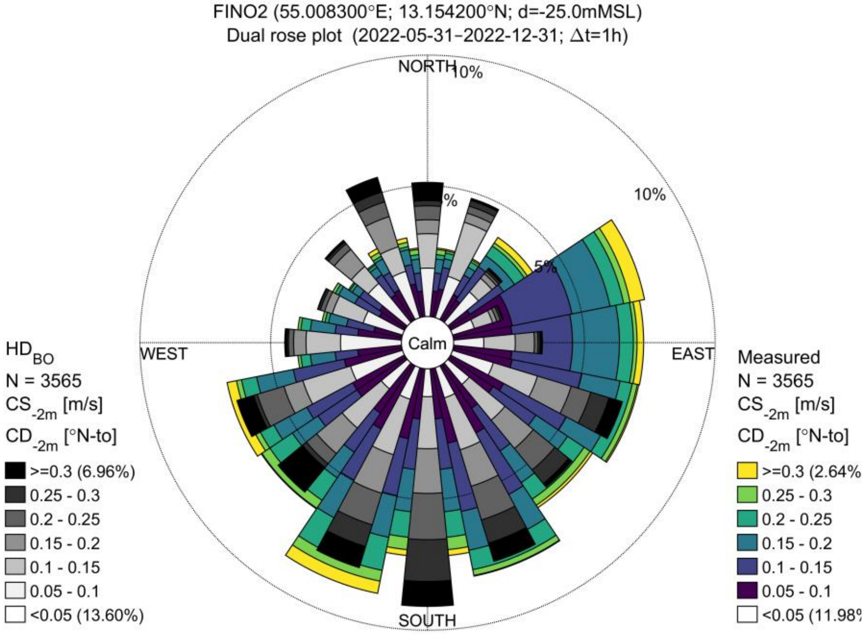
FINO2 (55.008300°E; 13.154200°N; d=-25.0mMSL)
Dual rose plot (2022-05-31–2022-12-31; Δt=1h)
NORTH
SOUTH
WEST
EAST
Calm
5%
10%
HD$_{BO}$
N = 3565
CS$_{-2m}$ [m/s]
CD$_{-2m}$ [°N-to]
>=0.3 (6.96%)
0.25 - 0.3
0.2 - 0.25
0.15 - 0.2
0.1 - 0.15
0.05 - 0.1
<0.05 (13.60%)
Measured
N = 3565
CS$_{-2m}$ [m/s]
CD$_{-2m}$ [°N-to]
>=0.3 (2.64%
0.25 - 0.3
0.2 - 0.25
0.15 - 0.2
0.1 - 0.15
0.05 - 0.1
<0.05 (11.98

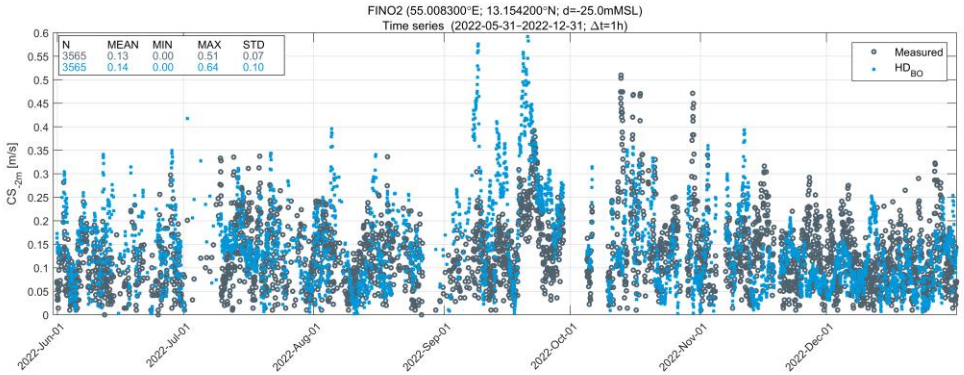
FINO2 (55.008300°E; 13.154200°N; d=-25.0mMSL)
Time series (2022-05-31–2022-12-31; Δt=1h)
N MEAN MIN MAX STD
3565 0.13 0.00 0.51 0.07
3565 0.14 0.00 0.64 0.10
Measured
HD$_{BO}$
CS$_{-2m}$ [m/s]
2022-Jun-01
2022-Jul-01
2022-Aug-01
2022-Sep-01
2022-Oct-01
2022-Nov-01
2022-Dec-01

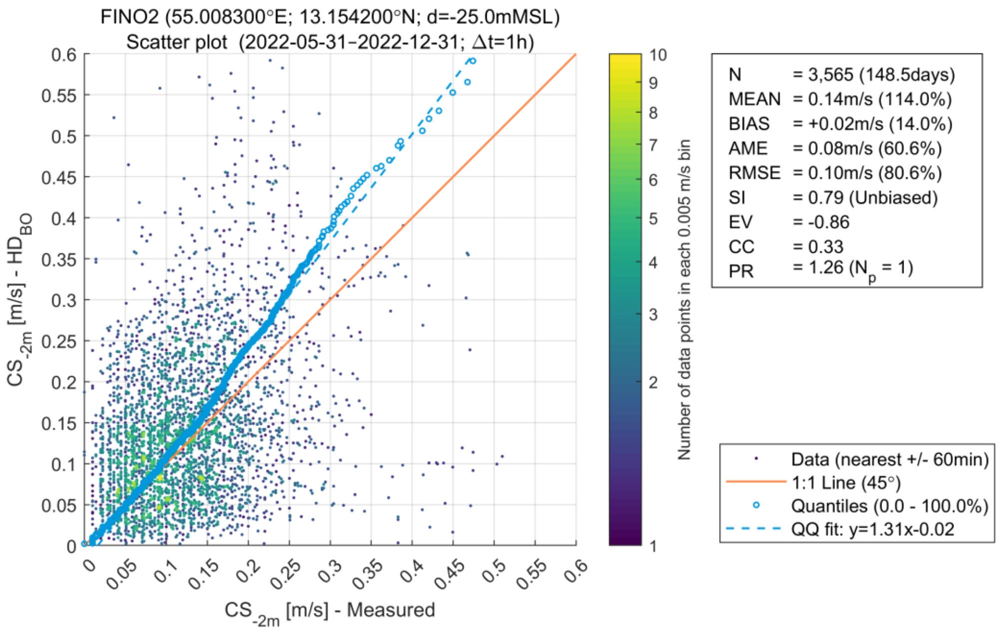
FINO2 (55.008300°E; 13.154200°N; d=-25.0mMSL)
Scatter plot (2022-05-31–2022-12-31; Δt=1h)
CS$_{-2m}$ [m/s] - HD$_{BO}$
CS$_{-2m}$ [m/s] - Measured
Number of data points in each 0.005 m/s bin
N = 3,565 (148.5days)
MEAN = 0.14m/s (114.0%)
BIAS = +0.02m/s (14.0%)
AME = 0.08m/s (60.6%)
RMSE = 0.10m/s (80.6%)
SI = 0.79 (Unbiased)
EV = -0.86
CC = 0.33
PR = 1.26 (N$_p$ = 1)
Data (nearest +/- 60min)
1:1 Line (45°)
Quantiles (0.0 - 100.0%)
QQ fit: y=1.31x-0.02

FINO2: -10m

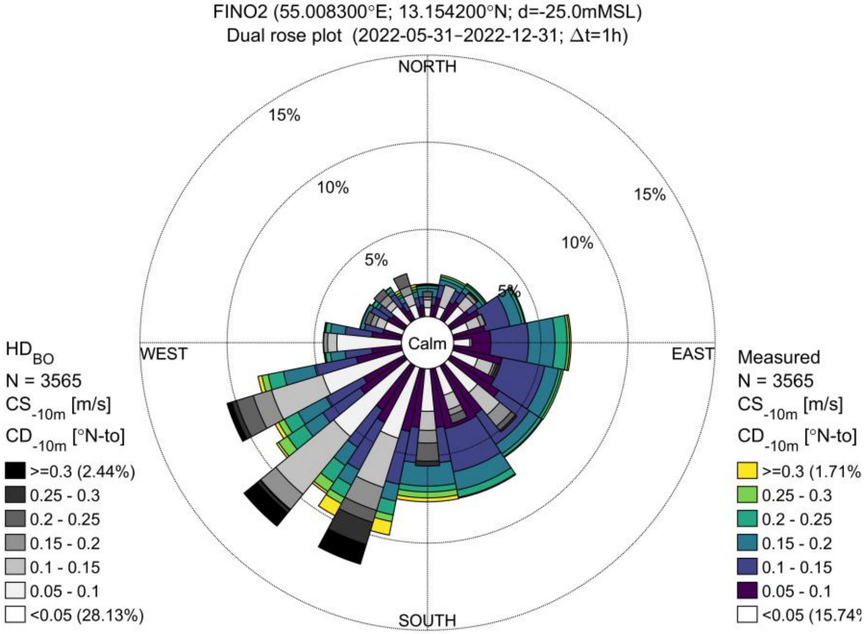
FINO2 (55.008300°E; 13.154200°N; d=-25.0mMSL)
Dual rose plot (2022-05-31-2022-12-31; Δt=1h)
NORTH
SOUTH
WEST
EAST
Calm
HD_BO
N = 3565
CS_-10m [m/s]
CD_-10m [°N-to]
>=0.3 (2.44%)
0.25 - 0.3
0.2 - 0.25
0.15 - 0.2
0.1 - 0.15
0.05 - 0.1
<0.05 (28.13%)
Measured
N = 3565
CS_-10m [m/s]
CD_-10m [°N-to]
>=0.3 (1.71%
0.25 - 0.3
0.2 - 0.25
0.15 - 0.2
0.1 - 0.15
0.05 - 0.1
<0.05 (15.74

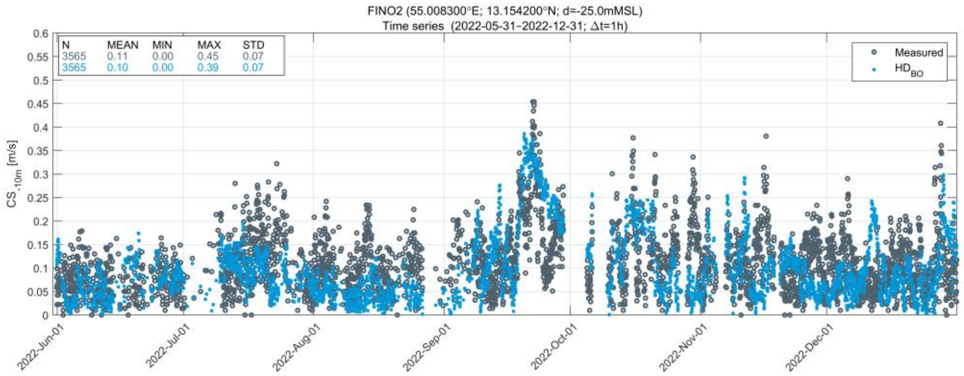
FINO2 (55.008300°E; 13.154200°N; d=-25.0mMSL)
Time series (2022-05-31-2022-12-31; Δt=1h)
N MEAN MIN MAX STD
3565 0.11 0.00 0.45 0.07
3565 0.10 0.00 0.39 0.07
Measured
HD_BO
CS_-10m [m/s]

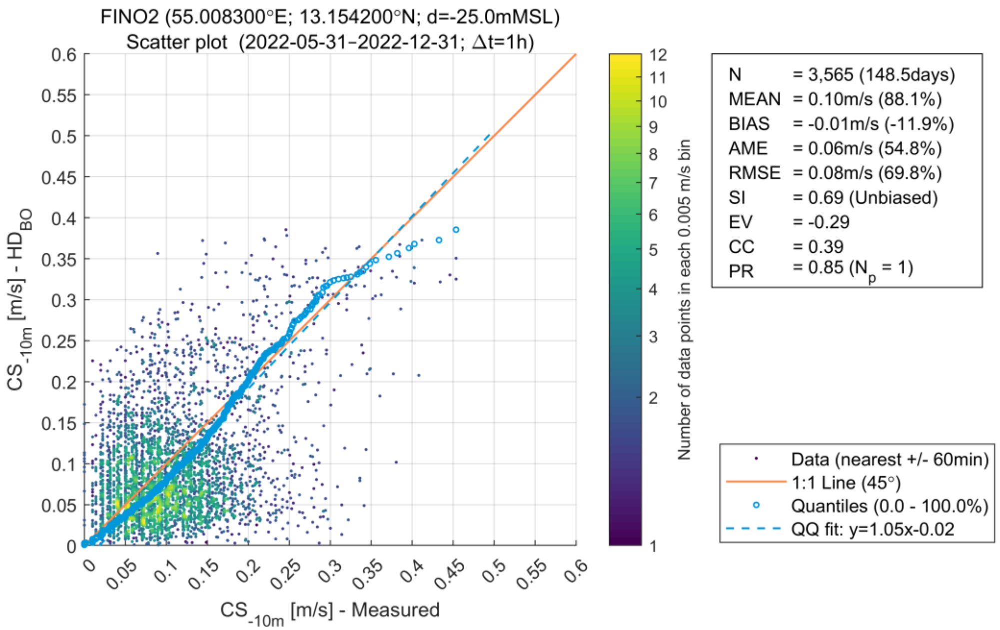
FINO2 (55.008300°E; 13.154200°N; d=-25.0mMSL)
Scatter plot (2022-05-31-2022-12-31; Δt=1h)
CS_-10m [m/s] - HD_BO
CS_-10m [m/s] - Measured
Number of data points in each 0.005 m/s bin
N = 3,565 (148.5days)
MEAN = 0.10m/s (88.1%)
BIAS = -0.01m/s (-11.9%)
AME = 0.06m/s (54.8%)
RMSE = 0.08m/s (69.8%)
SI = 0.69 (Unbiased)
EV = -0.29
CC = 0.39
PR = 0.85 (N_p = 1)
Data (nearest +/- 60min)
1:1 Line (45°)
Quantiles (0.0 - 100.0%)
QQ fit: y=1.05x-0.02

FINO2: -20m

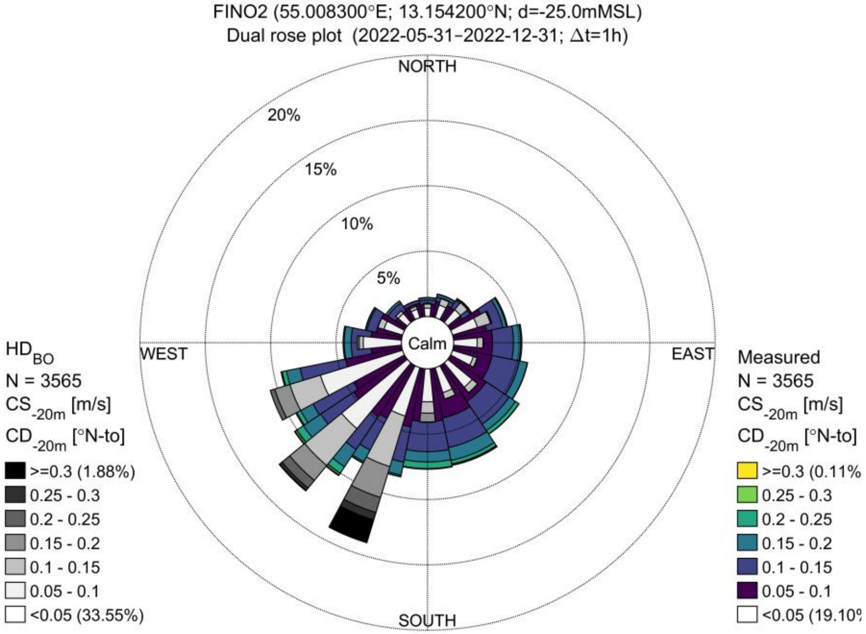

FINO2 (55.008300°E; 13.154200°N; d=-25.0mMSL)
Dual rose plot (2022-05-31-2022-12-31; Δt=1h)
NORTH
SOUTH
WEST
EAST
Calm
5%
10%
15%
20%
HDBO
N = 3565
CS-20m [m/s]
CD-20m [°N-to]
>=0.3 (1.88%)
0.25 - 0.3
0.2 - 0.25
0.15 - 0.2
0.1 - 0.15
0.05 - 0.1
<0.05 (33.55%)
Measured
N = 3565
CS-20m [m/s]
CD-20m [°N-to]
>=0.3 (0.11%
0.25 - 0.3
0.2 - 0.25
0.15 - 0.2
0.1 - 0.15
0.05 - 0.1
<0.05 (19.10%

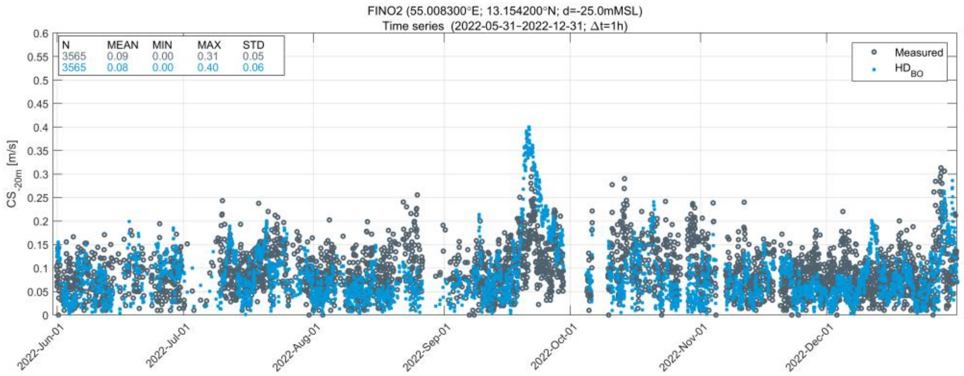

FINO2 (55.008300°E; 13.154200°N; d=-25.0mMSL)
Time series (2022-05-31-2022-12-31; Δt=1h)
N MEAN MIN MAX STD
3565 0.09 0.00 0.31 0.05
3565 0.08 0.00 0.40 0.06
Measured
HDBO
CS-20m [m/s]
2022-Jun-01
2022-Jul-01
2022-Aug-01
2022-Sep-01
2022-Oct-01
2022-Nov-01
2022-Dec-01

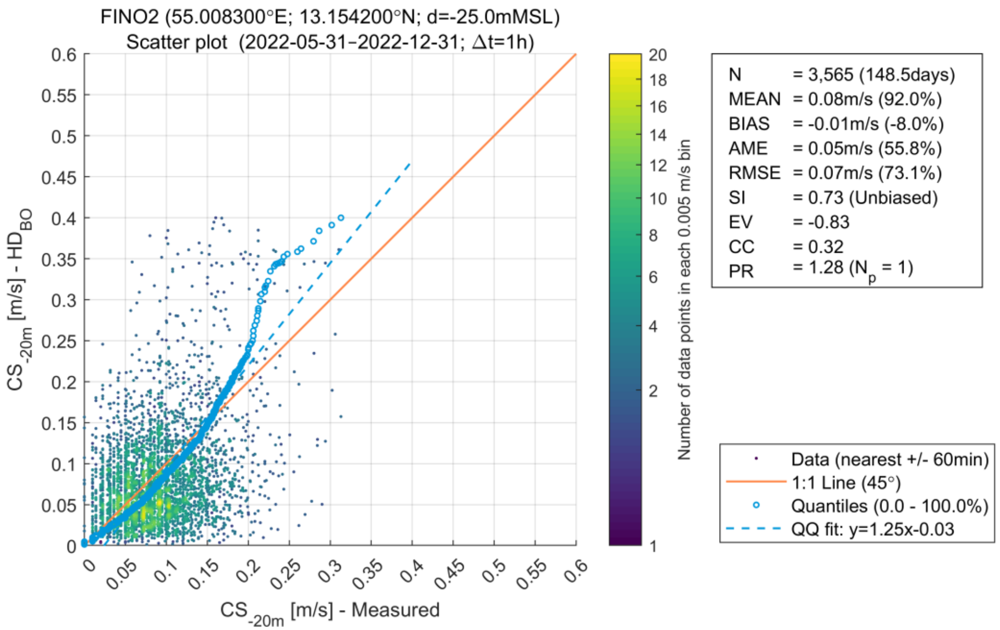

FINO2 (55.008300°E; 13.154200°N; d=-25.0mMSL)
Scatter plot (2022-05-31-2022-12-31; Δt=1h)
CS-20m [m/s] - HDBO
CS-20m [m/s] - Measured
Number of data points in each 0.005 m/s bin
N = 3,565 (148.5days)
MEAN = 0.08m/s (92.0%)
BIAS = -0.01m/s (-8.0%)
AME = 0.05m/s (55.8%)
RMSE = 0.07m/s (73.1%)
SI = 0.73 (Unbiased)
EV = -0.83
CC = 0.32
PR = 1.28 (Np = 1)
Data (nearest +/- 60min)
1:1 Line (45°)
Quantiles (0.0 - 100.0%)
QQ fit: y=1.25x-0.03

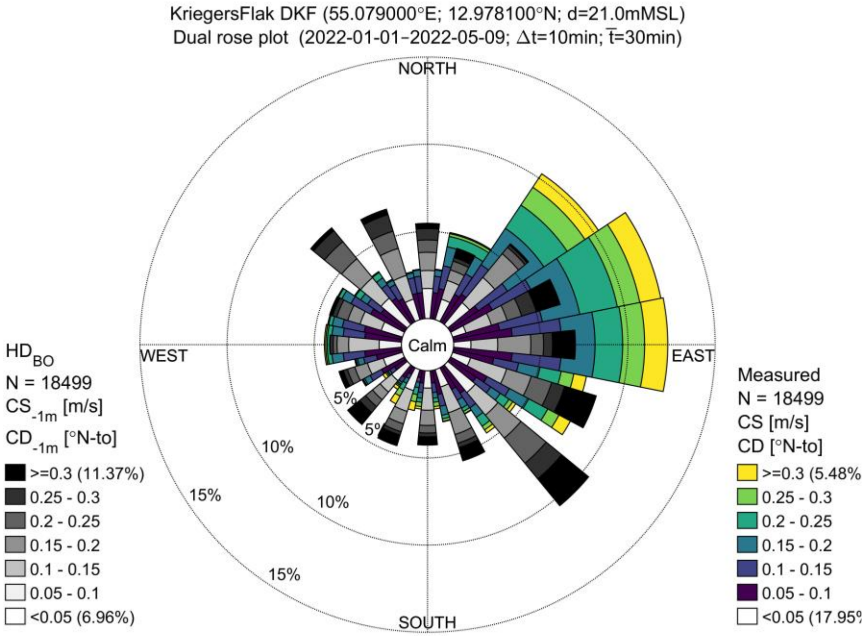
KriegersFlak DKF (55.079000°E; 12.978100°N; d=21.0mMSL)
Dual rose plot (2022-01-01-2022-05-09; Δt=10min; t̄=30min)
NORTH
WEST
EAST
SOUTH
Calm
5%
10%
15%
HD_BO
N = 18499
CS -1m [m/s]
CD -1m [°N-to]
>=0.3 (11.37%)
0.25 - 0.3
0.2 - 0.25
0.15 - 0.2
0.1 - 0.15
0.05 - 0.1
<0.05 (6.96%)
Measured
N = 18499
CS [m/s]
CD [°N-to]
>=0.3 (5.48%
0.25 - 0.3
0.2 - 0.25
0.15 - 0.2
0.1 - 0.15
0.05 - 0.1
<0.05 (17.95

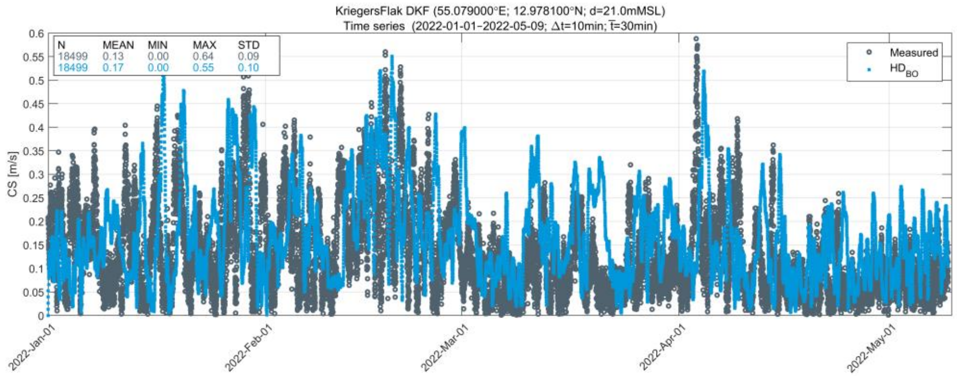
KriegersFlak DKF (55.079000°E; 12.978100°N; d=21.0mMSL)
Time series (2022-01-01-2022-05-09; Δt=10min; t̄=30min)
N MEAN MIN MAX STD
18499 0.13 0.00 0.64 0.09
18499 0.17 0.00 0.55 0.10
Measured
HD_BO
CS [m/s]
2022-Jan-01
2022-Feb-01
2022-Mar-01
2022-Apr-01
2022-May-01

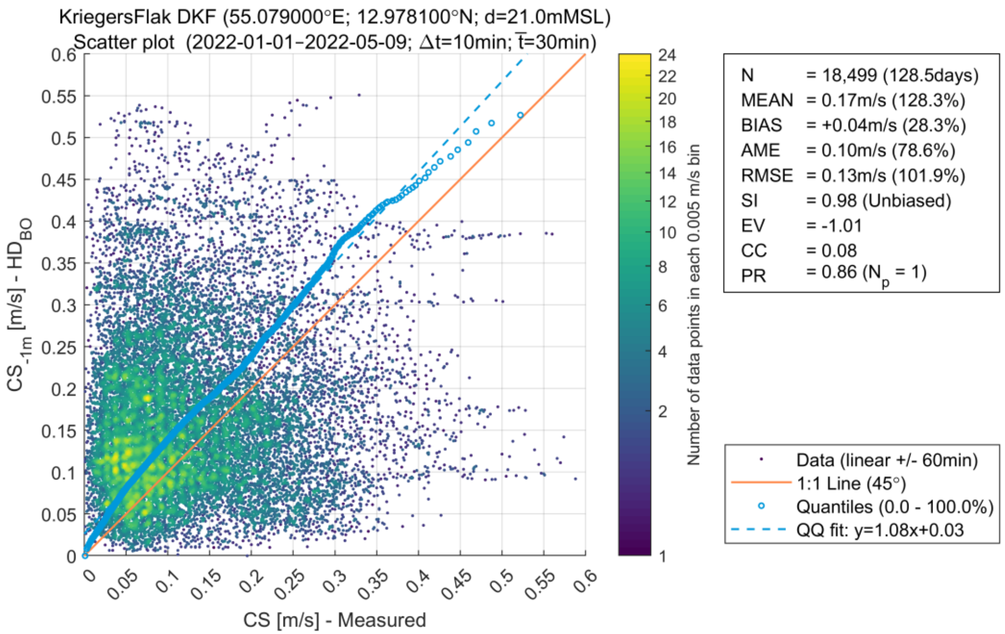
KriegersFlak DKF (55.079000°E; 12.978100°N; d=21.0mMSL)
Scatter plot (2022-01-01-2022-05-09; Δt=10min; t̄=30min)
CS -1m [m/s] - HD_BO
CS [m/s] - Measured
Number of data points in each 0.005 m/s bin
N = 18,499 (128.5days)
MEAN = 0.17m/s (128.3%)
BIAS = +0.04m/s (28.3%)
AME = 0.10m/s (78.6%)
RMSE = 0.13m/s (101.9%)
SI = 0.98 (Unbiased)
EV = -1.01
CC = 0.08
PR = 0.86 (N_p = 1)
Data (linear +/- 60min)
1:1 Line (45°)
Quantiles (0.0 - 100.0%)
QQ fit: y=1.08x+0.03

Appendix B.2 Temperature and Salinity

LOT4: surface

Temperature

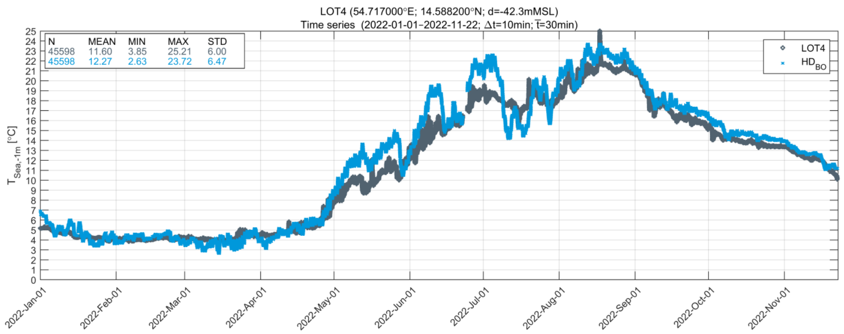

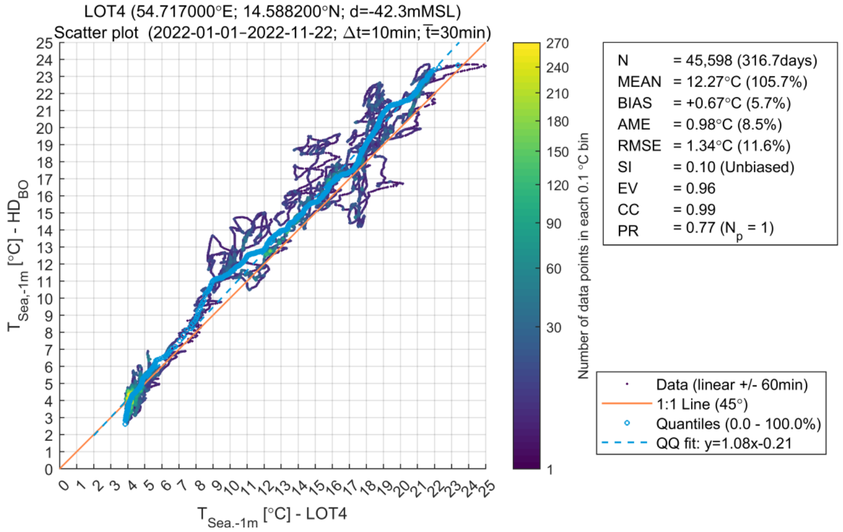

Salinity

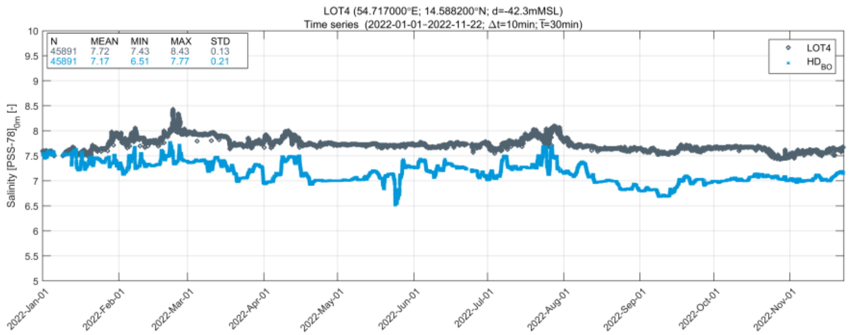

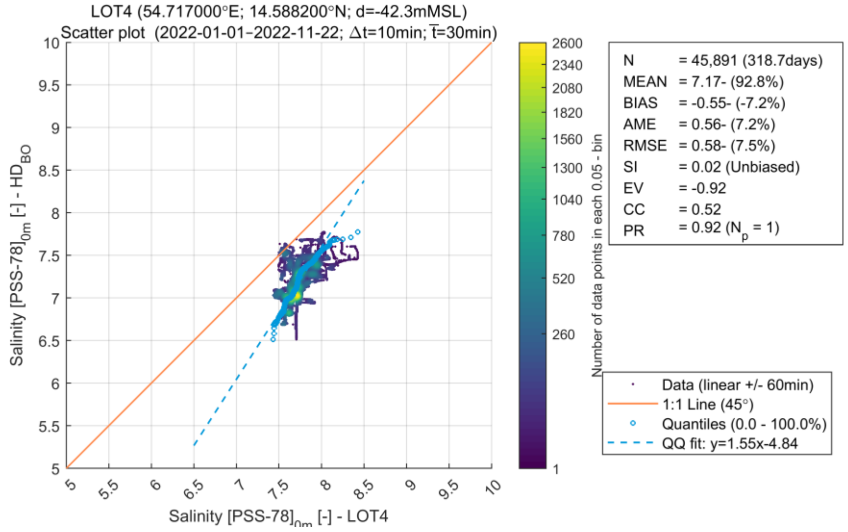

LOT4: -9m

Temperature

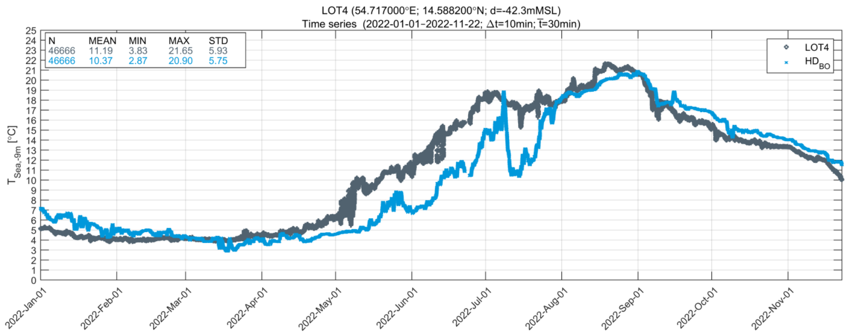

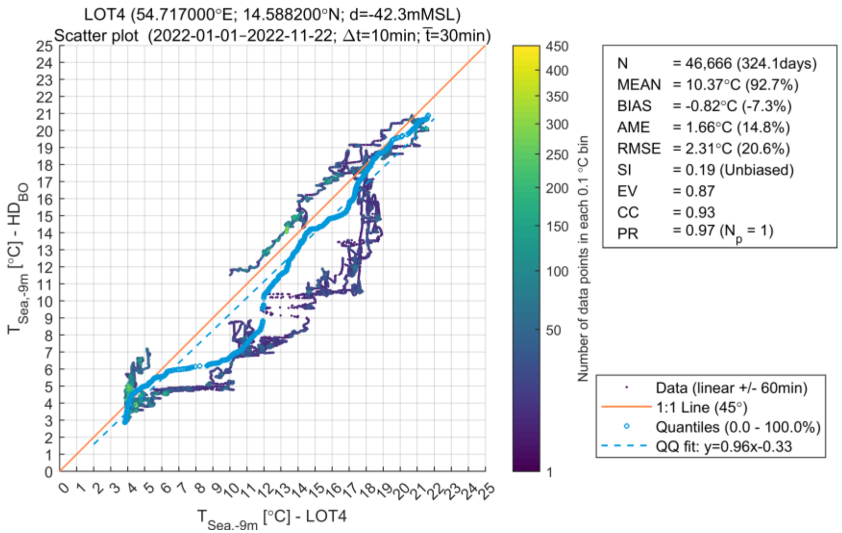

Salinity

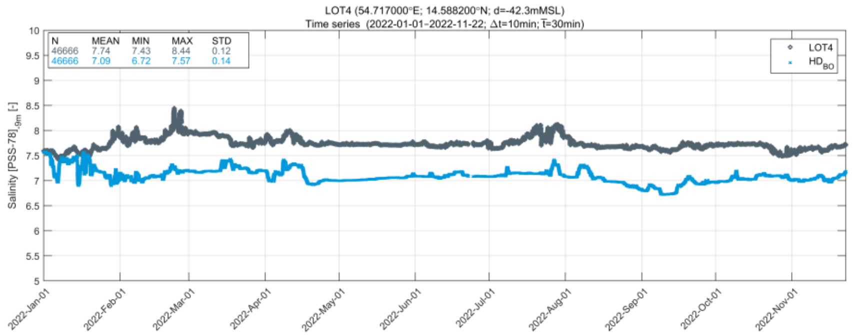

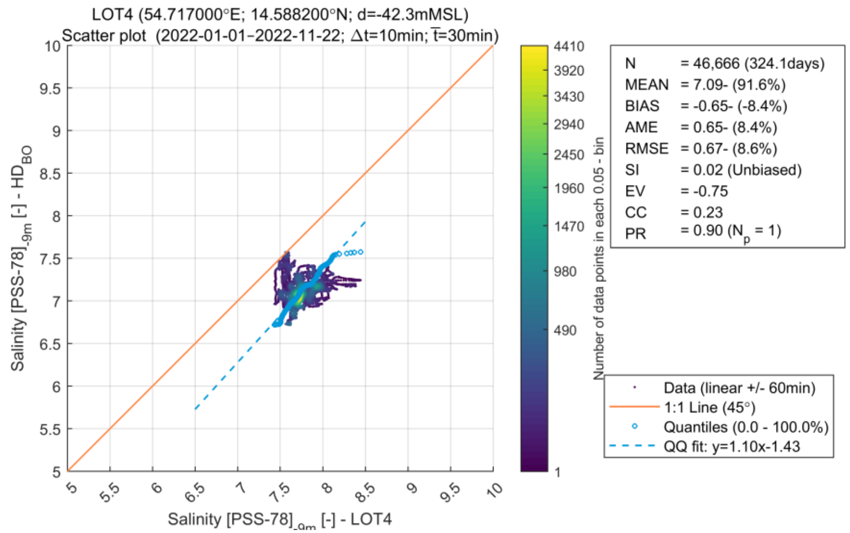

LOT4: -18m

Temperature

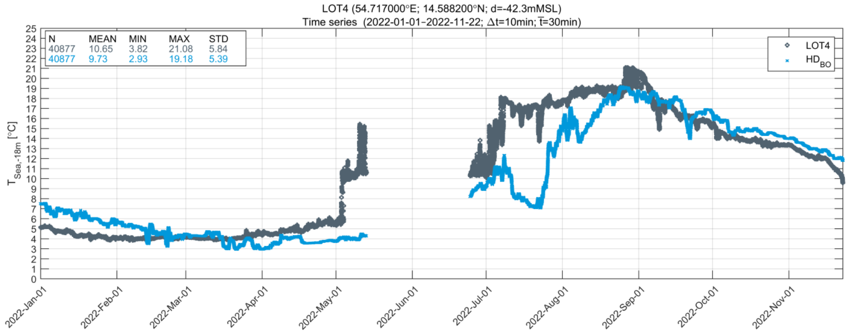

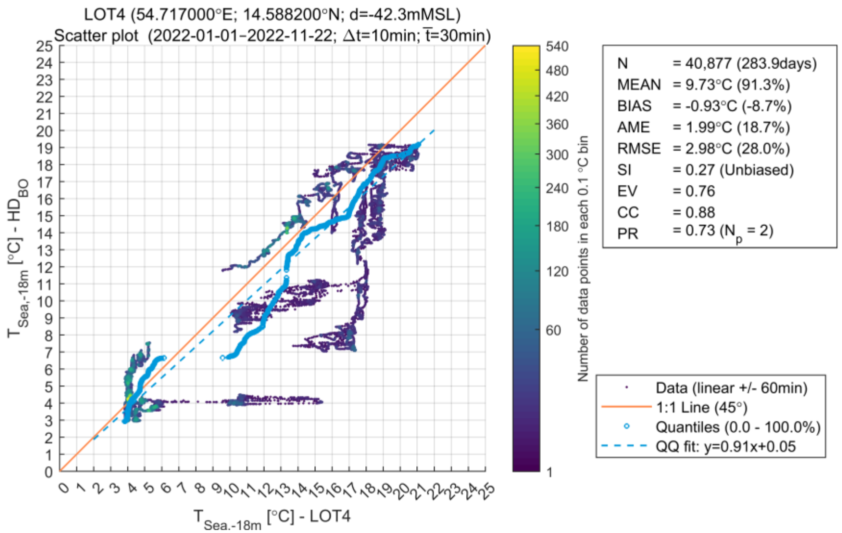

Salinity

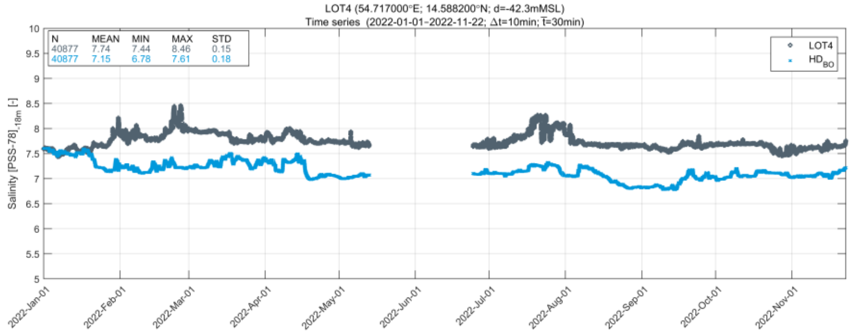

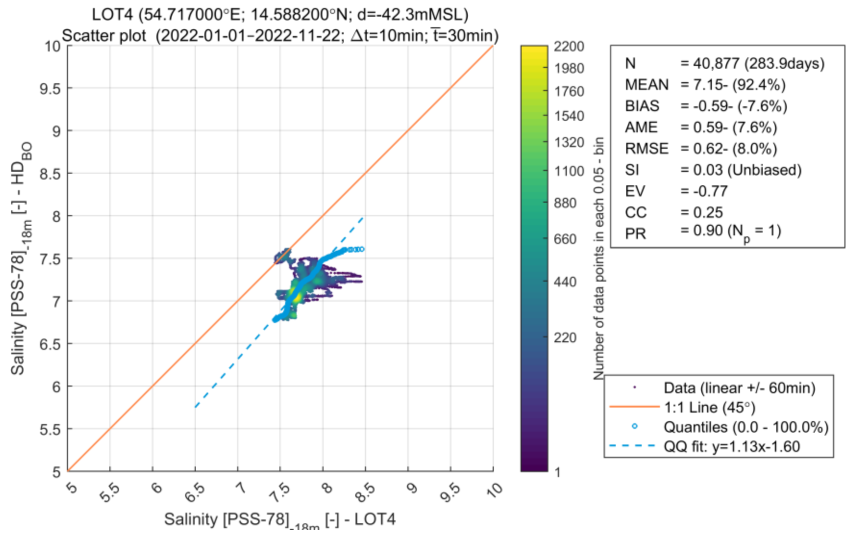

LOT4: -25m

Temperature

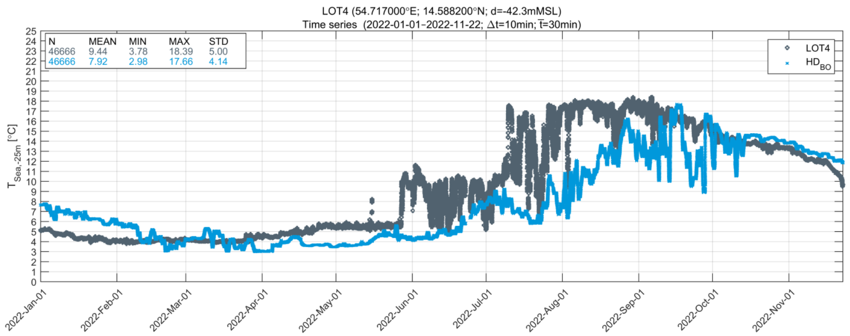

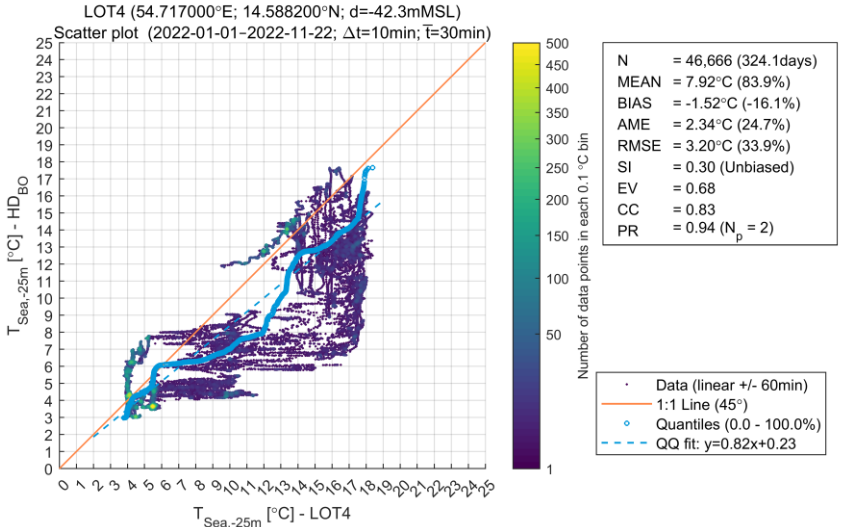

Salinity

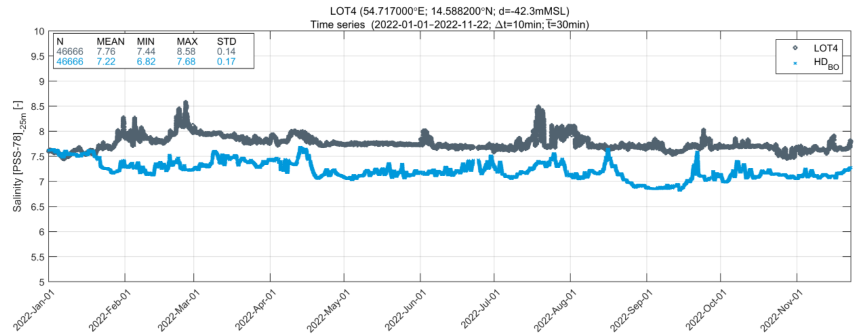

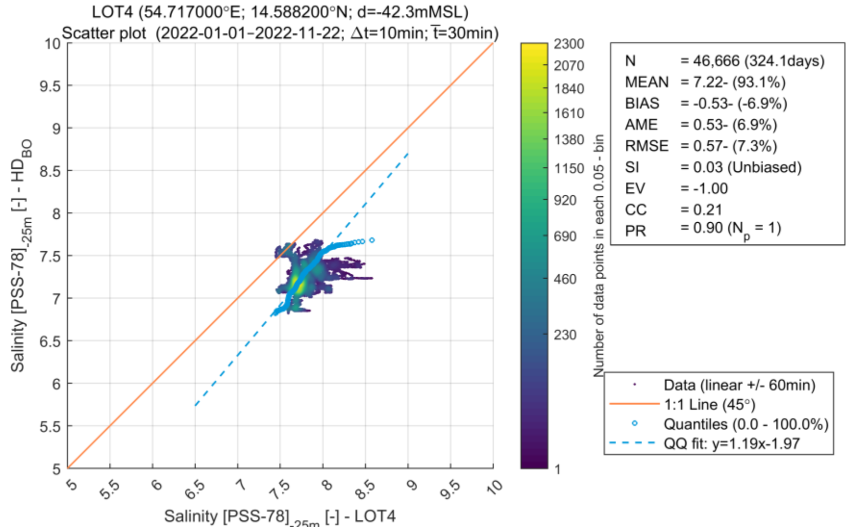

LOT4: -33m

Temperature

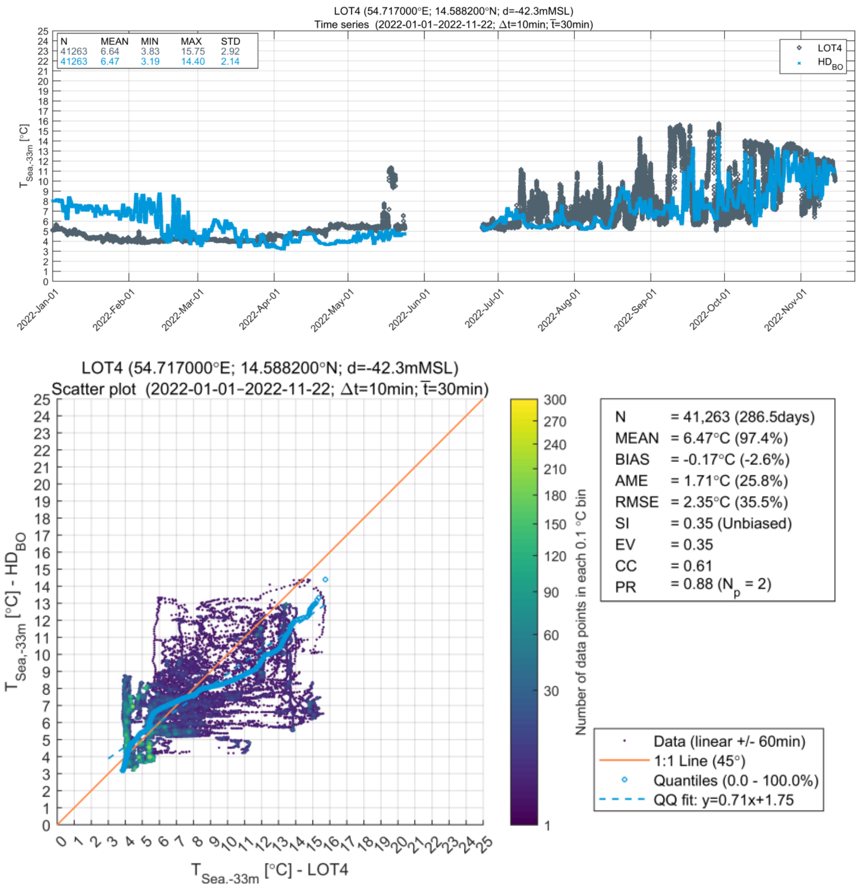

Salinity

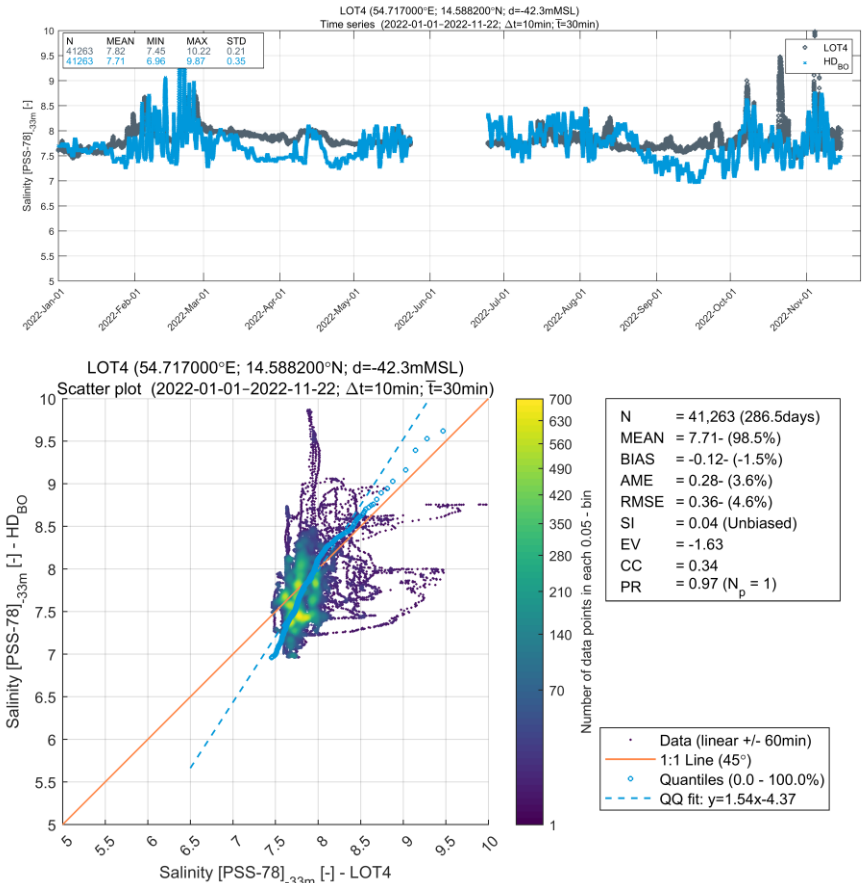

Arkona: -2m

Temperature

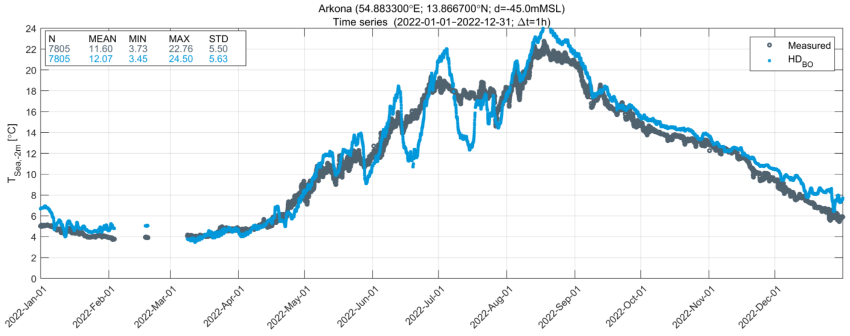

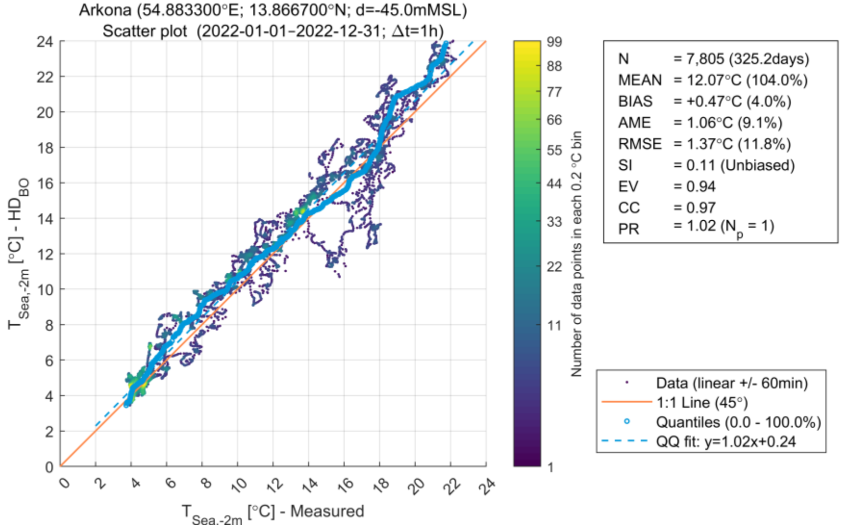

Salinity

Arkona: -5m

Temperature

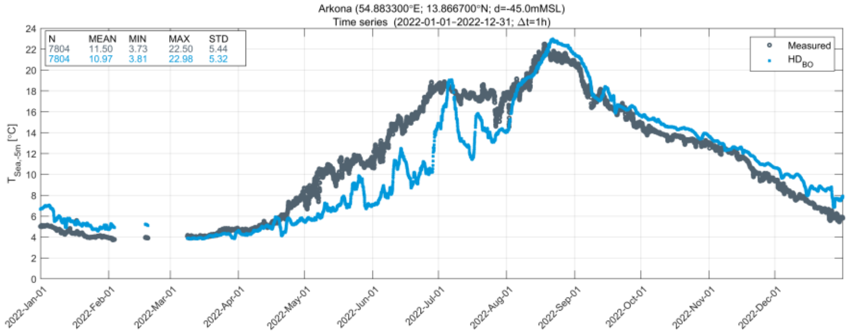

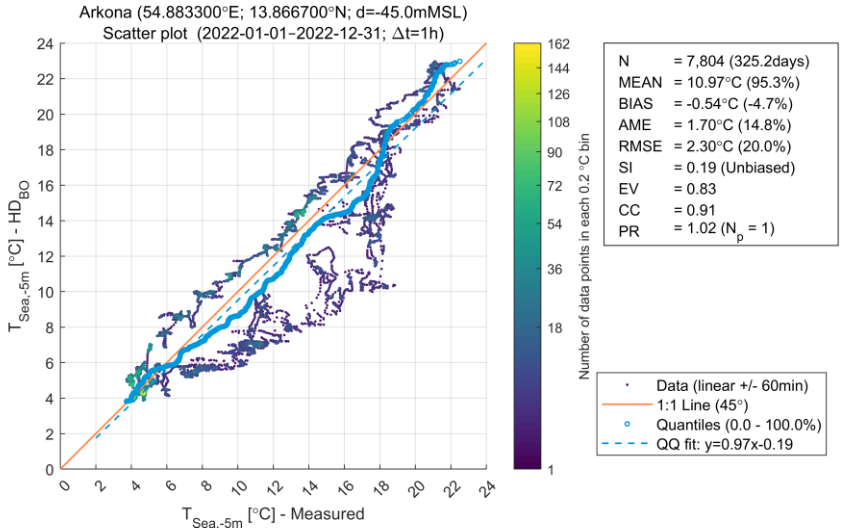

Salinity

Arkona: -7m

Temperature

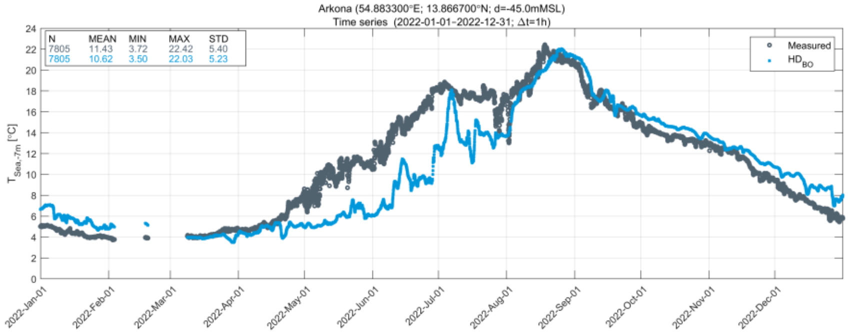

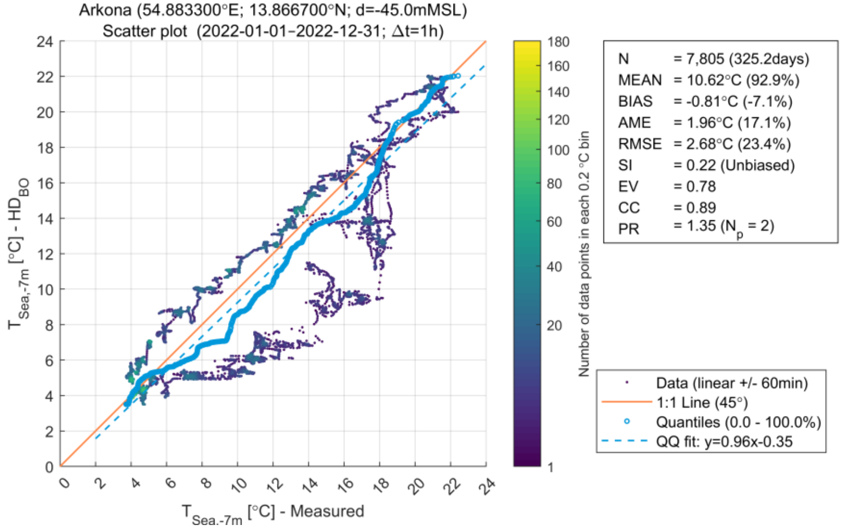

Salinity

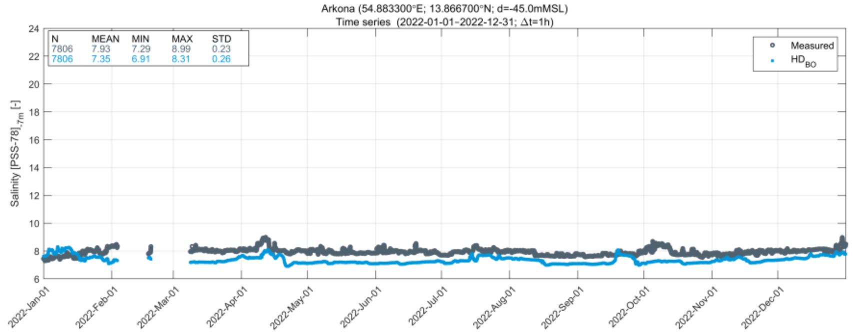

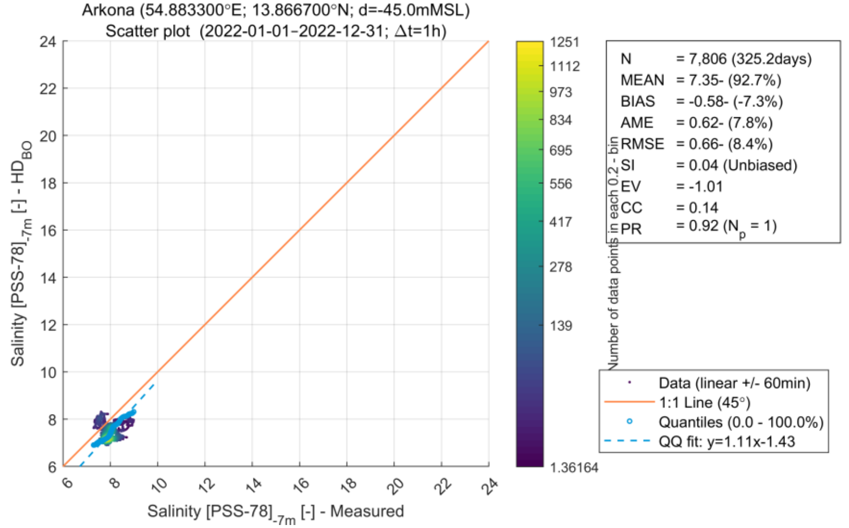

Arkona: -25m

Temperature

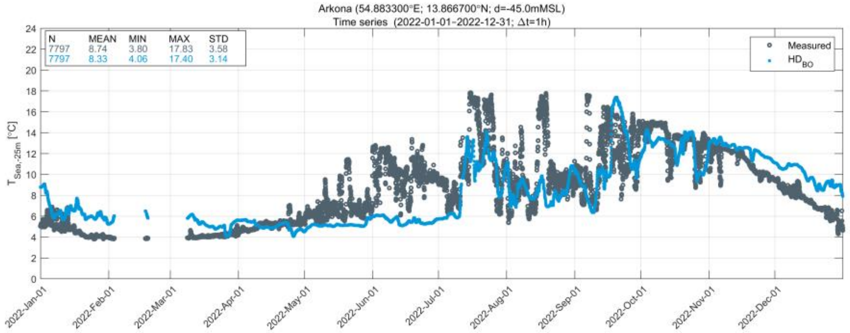

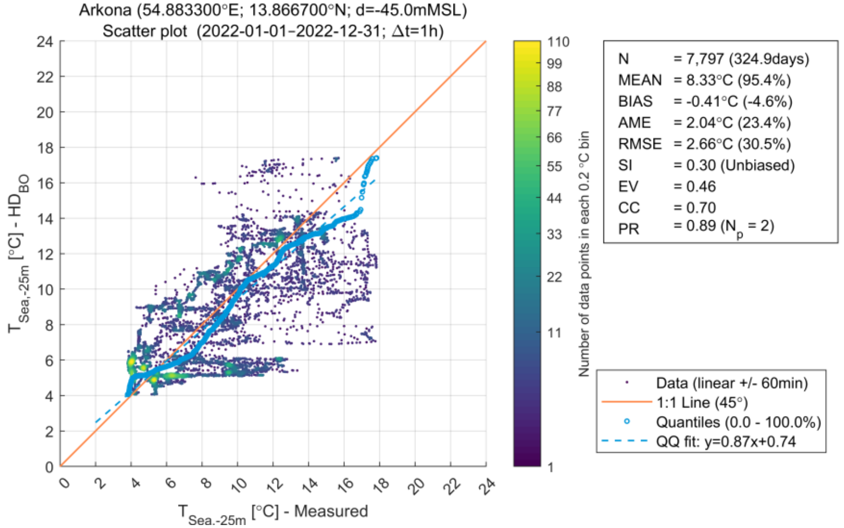

Salinity

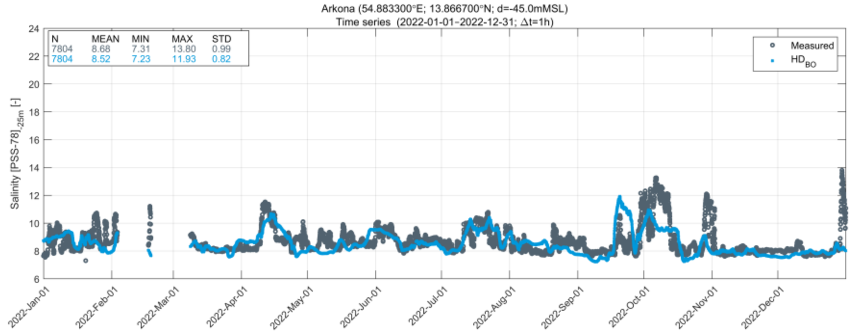

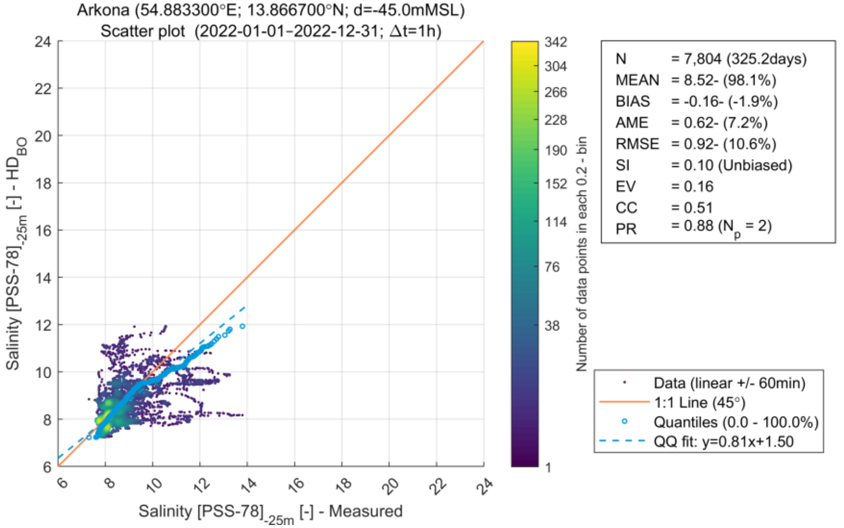

Arkona: -40m

Temperature

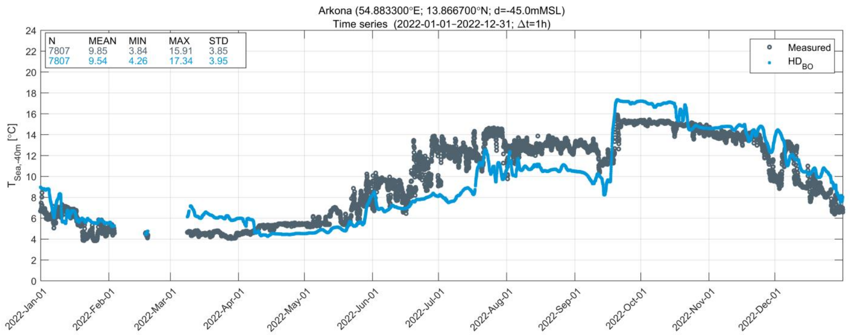

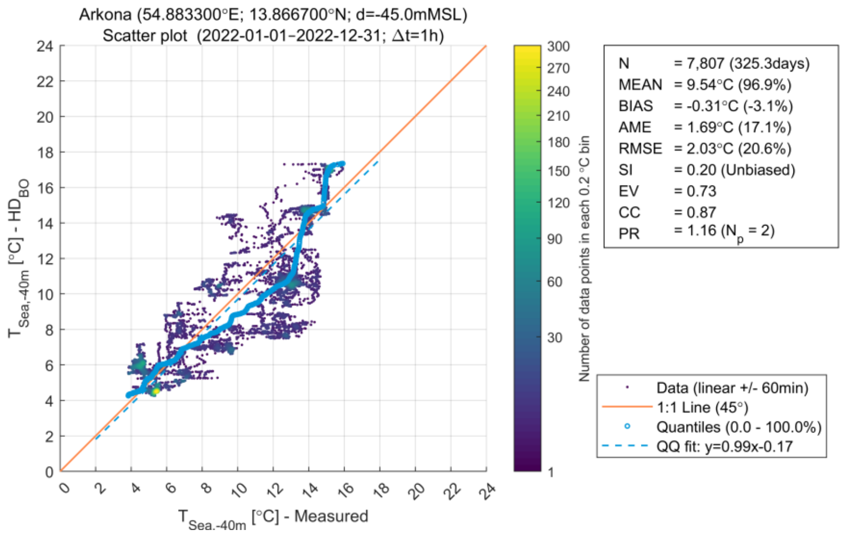

Salinity

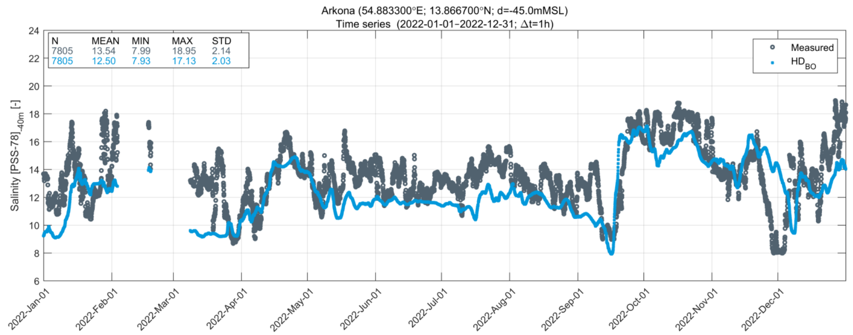

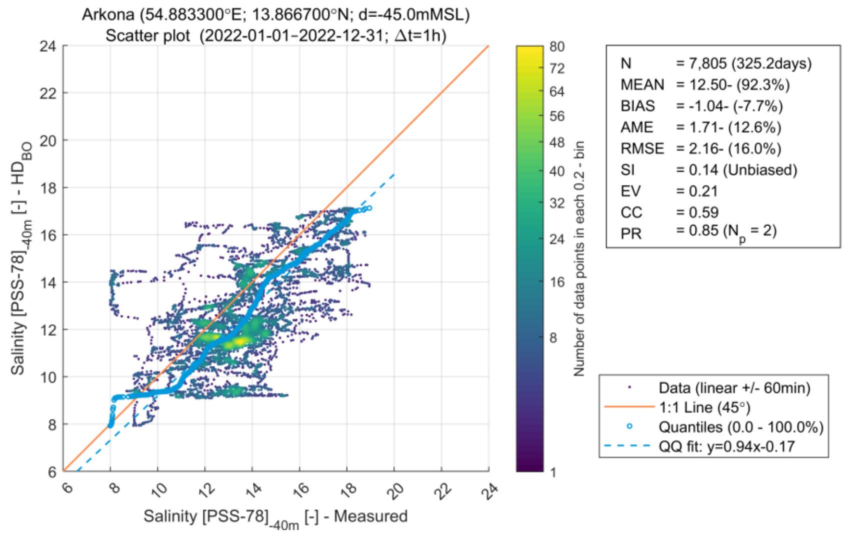

FINO2: -2m

Temperature

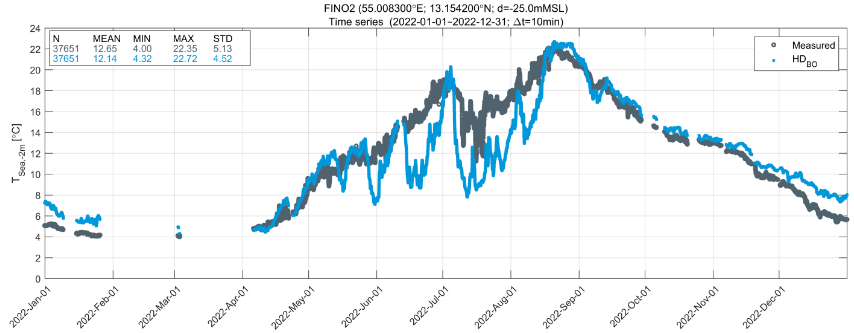

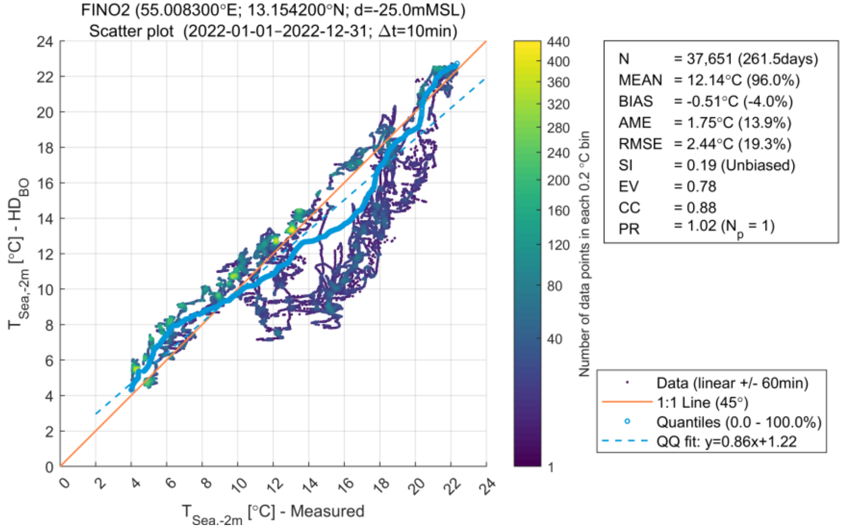

Salinity

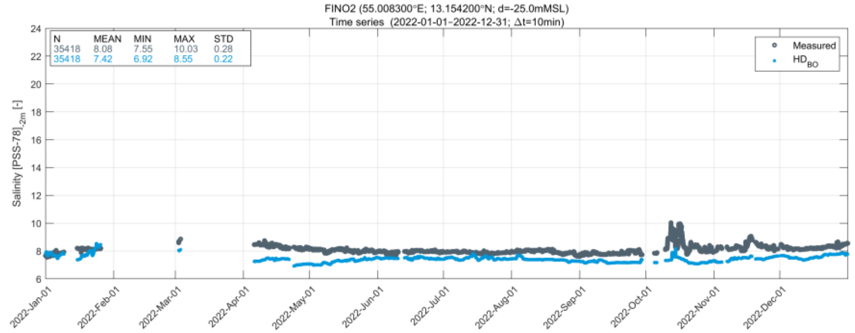

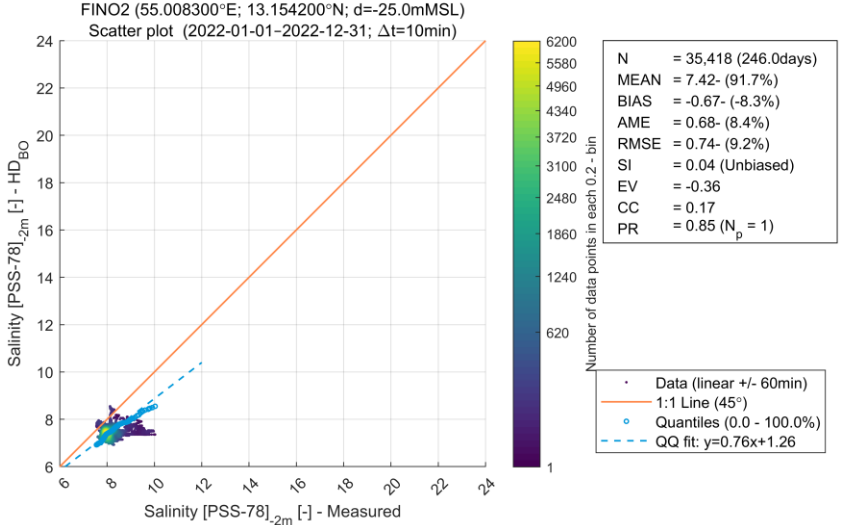

FINO2: -10m

Temperature

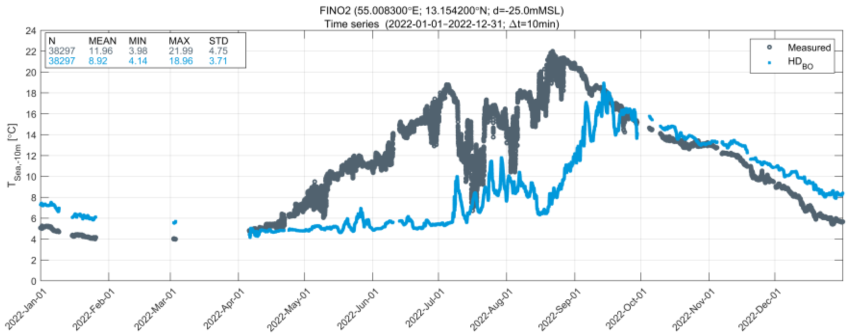

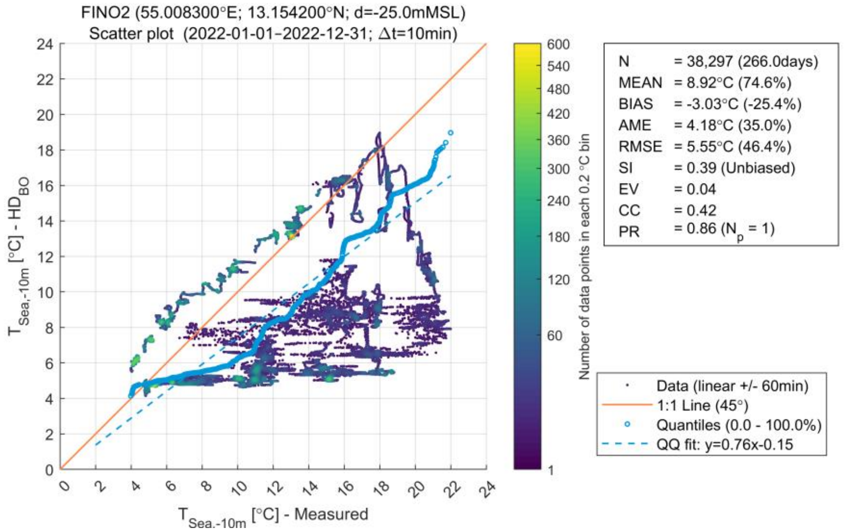

Salinity

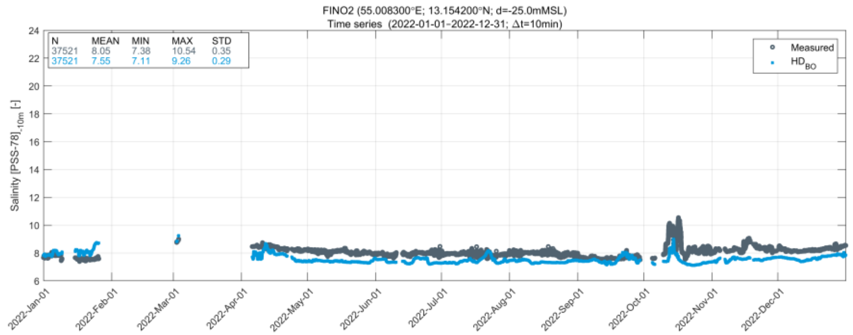

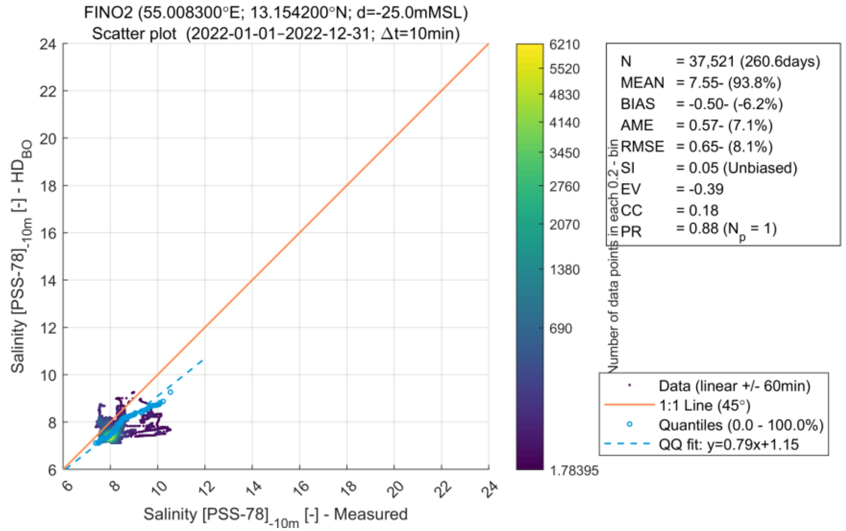

FINO2: -20m

Temperature

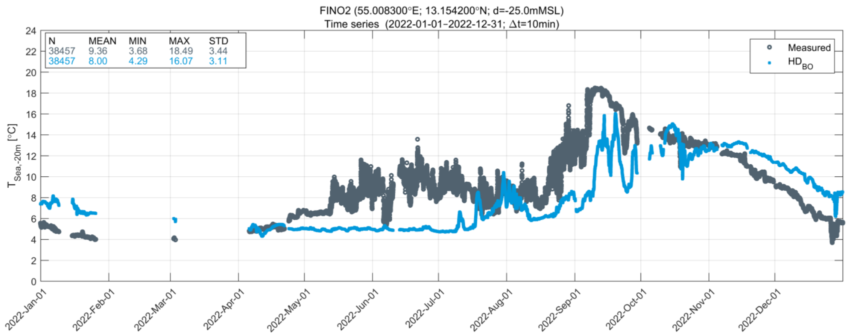

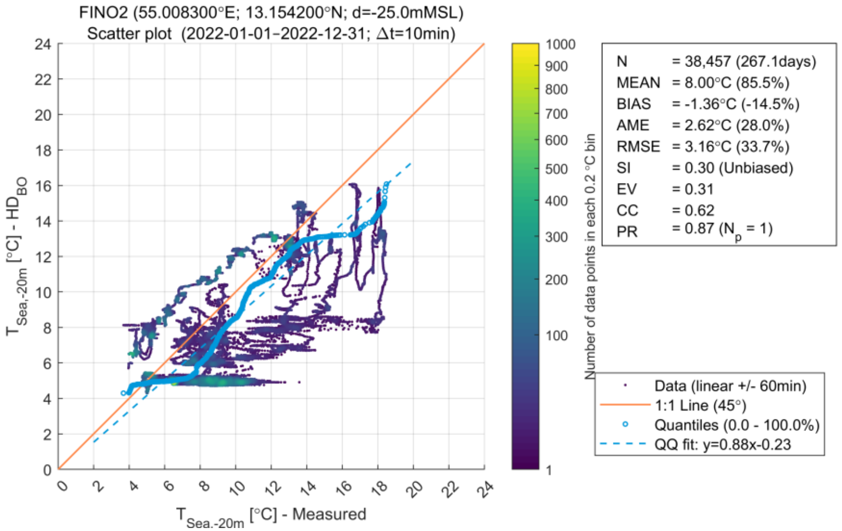

Salinity

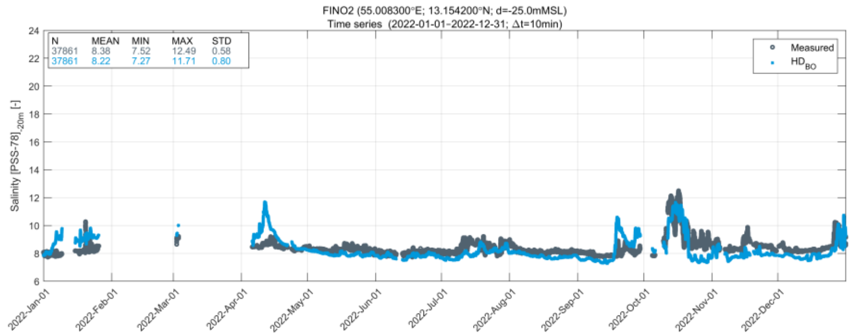

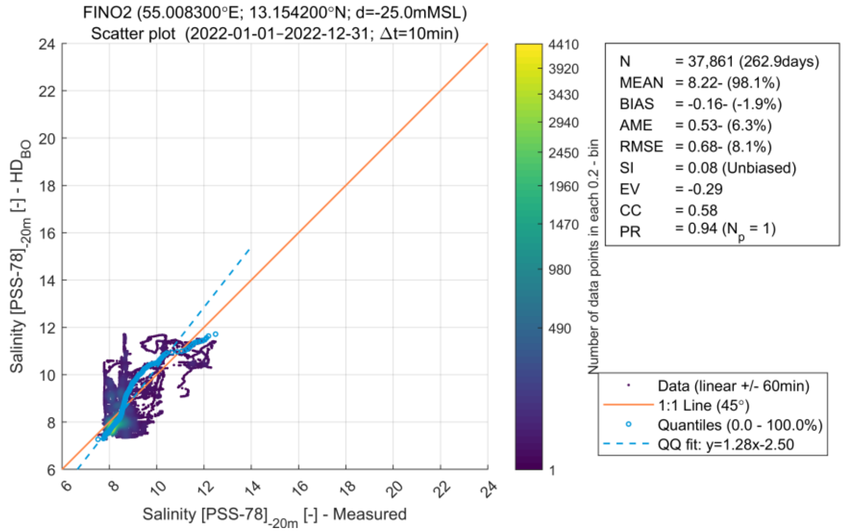

LOT3

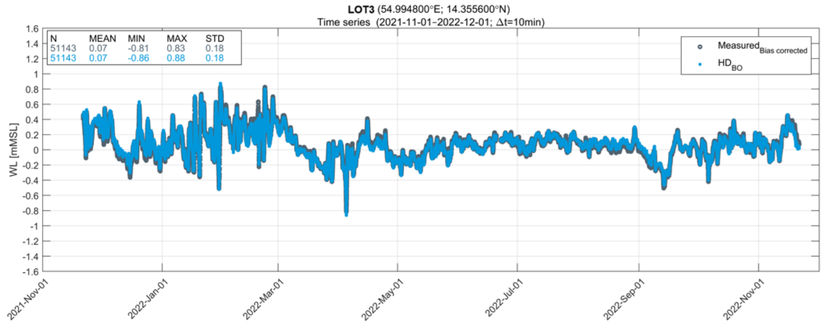
LOT3 (54.994800°E; 14.355600°N)
Time series (2021-11-01-2022-12-01; Δt=10min)
N MEAN MIN MAX STD
51143 0.07 -0.81 0.83 0.18
51143 0.07 -0.86 0.88 0.18
Measured Bias corrected
HD BO
WL [mMSL]

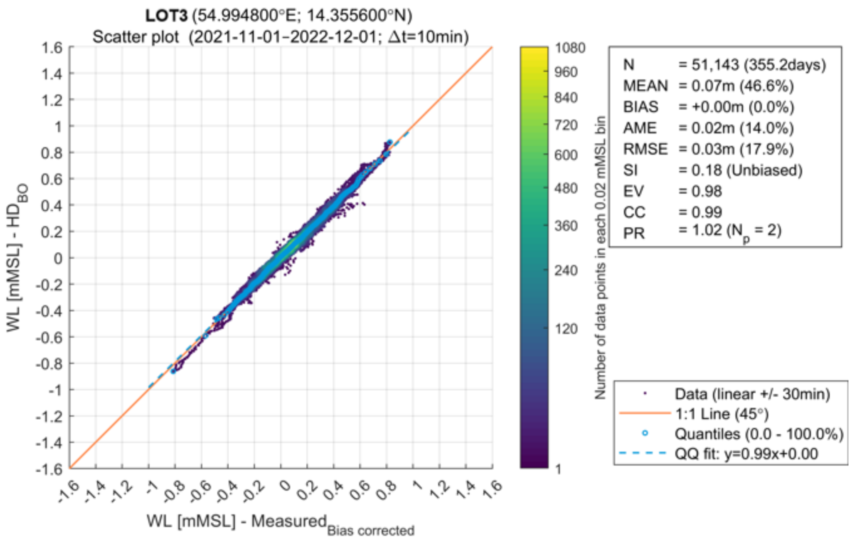
LOT3 (54.994800°E; 14.355600°N)
Scatter plot (2021-11-01-2022-12-01; Δt=10min)
N = 51,143 (355.2days)
MEAN = 0.07m (46.6%)
BIAS = +0.00m (0.0%)
AME = 0.02m (14.0%)
RMSE = 0.03m (17.9%)
SI = 0.18 (Unbiased)
EV = 0.98
CC = 0.99
PR = 1.02 (Np = 2)
Data (linear +/- 30min)
1:1 Line (45°)
Quantiles (0.0 - 100.0%)
QQ fit: y=0.99x+0.00
Number of data points in each 0.02 mMSL bin
WL [mMSL] - HD BO
WL [mMSL] - Measured Bias corrected

LOT4a

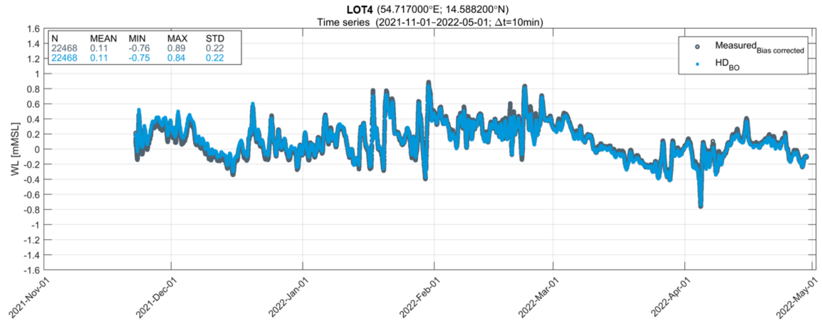
LOT4 (54.717000°E; 14.588200°N)
Time series (2021-11-01-2022-05-01; Δt=10min)
N MEAN MIN MAX STD
22468 0.11 -0.76 0.89 0.22
22468 0.11 -0.75 0.84 0.22
Measured Bias corrected
HD BO
WL [mMSL]

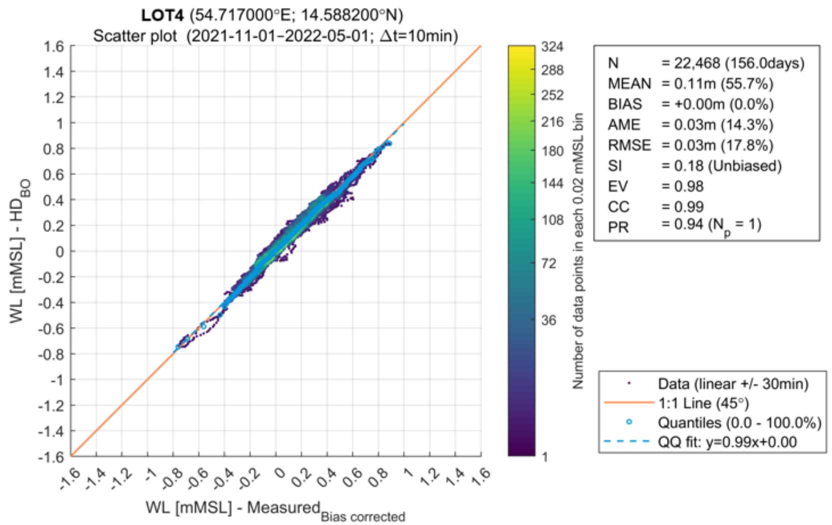
LOT4 (54.717000°E; 14.588200°N)
Scatter plot (2021-11-01-2022-05-01; Δt=10min)
N = 22,468 (156.0days)
MEAN = 0.11m (55.7%)
BIAS = +0.00m (0.0%)
AME = 0.03m (14.3%)
RMSE = 0.03m (17.8%)
SI = 0.18 (Unbiased)
EV = 0.98
CC = 0.99
PR = 0.94 (Np = 1)
Data (linear +/- 30min)
1:1 Line (45°)
Quantiles (0.0 - 100.0%)
QQ fit: y=0.99x+0.00
Number of data points in each 0.02 mMSL bin
WL [mMSL] - HD BO
WL [mMSL] - Measured Bias corrected

LOT4b

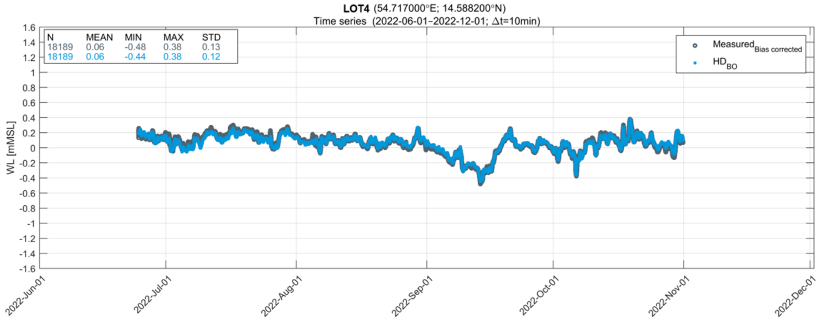
LOT4 (54.717000°E; 14.588200°N)
Time series (2022-06-01-2022-12-01; Δt=10min)
N MEAN MIN MAX STD
18189 0.06 -0.48 0.38 0.13
18189 0.06 -0.44 0.38 0.12
Measured Bias corrected
HD BO
WL [mMSL]
2022-Jun-01
2022-Jul-01
2022-Aug-01
2022-Sep-01
2022-Oct-01
2022-Nov-01
2022-Dec-01

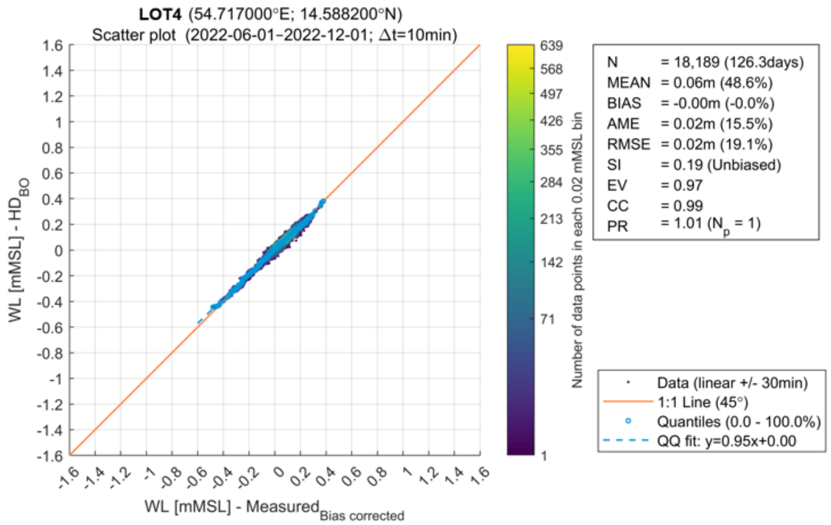
LOT4 (54.717000°E; 14.588200°N)
Scatter plot (2022-06-01-2022-12-01; Δt=10min)
N = 18,189 (126.3days)
MEAN = 0.06m (48.6%)
BIAS = -0.00m (-0.0%)
AME = 0.02m (15.5%)
RMSE = 0.02m (19.1%)
SI = 0.19 (Unbiased)
EV = 0.97
CC = 0.99
PR = 1.01 (N p = 1)
Number of data points in each 0.02 mMSL bin
Data (linear +/- 30min)
1:1 Line (45°)
Quantiles (0.0 - 100.0%)
QQ fit: y=0.95x+0.00
WL [mMSL] - HD BO
WL [mMSL] - Measured Bias corrected

Tejn

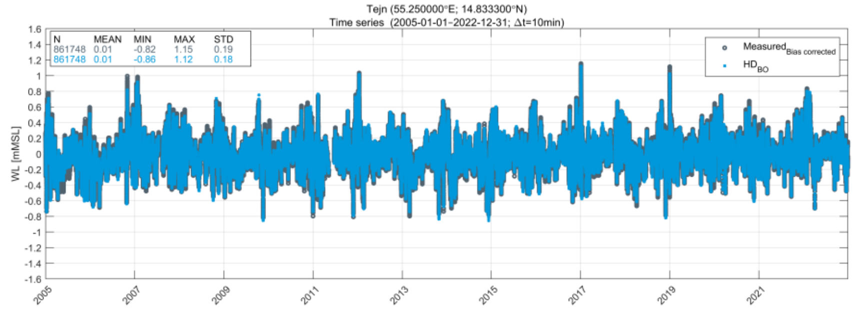
Tejn (55.250000°E; 14.833300°N)
Time series (2005-01-01-2022-12-31; Δt=10min)
N MEAN MIN MAX STD
861748 0.01 -0.82 1.15 0.19
861748 0.01 -0.86 1.12 0.18
Measured Bias corrected
HD BO
WL [mMSL]

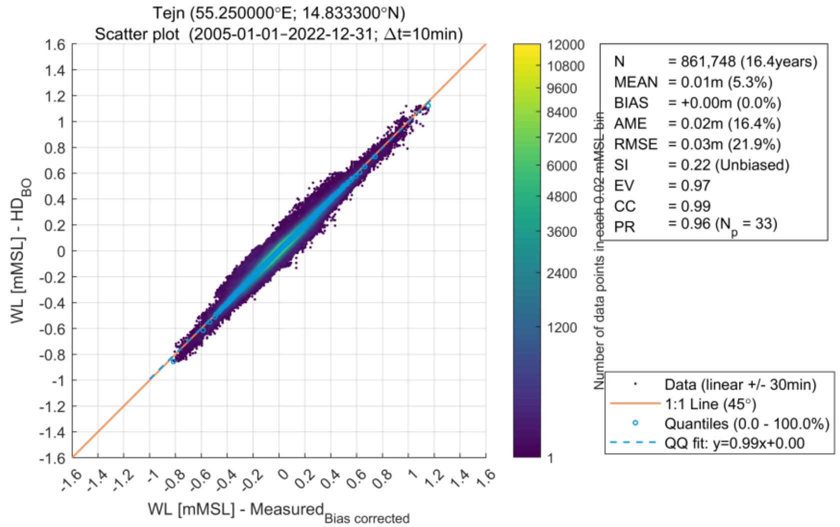
Tejn (55.250000°E; 14.833300°N)
Scatter plot (2005-01-01-2022-12-31; Δt=10min)
N = 861,748 (16.4years)
MEAN = 0.01m (5.3%)
BIAS = +0.00m (0.0%)
AME = 0.02m (16.4%)
RMSE = 0.03m (21.9%)
SI = 0.22 (Unbiased)
EV = 0.97
CC = 0.99
PR = 0.96 (N p = 33)
Number of data points in each 0.02 mMSL bin
Data (linear +/- 30min)
1:1 Line (45°)
Quantiles (0.0 - 100.0%)
QQ fit: y=0.99x+0.00
WL [mMSL] - HD BO
WL [mMSL] - Measured Bias corrected

Karlshamn

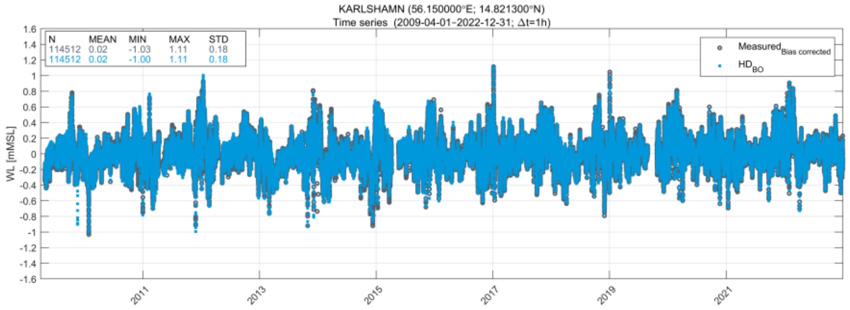

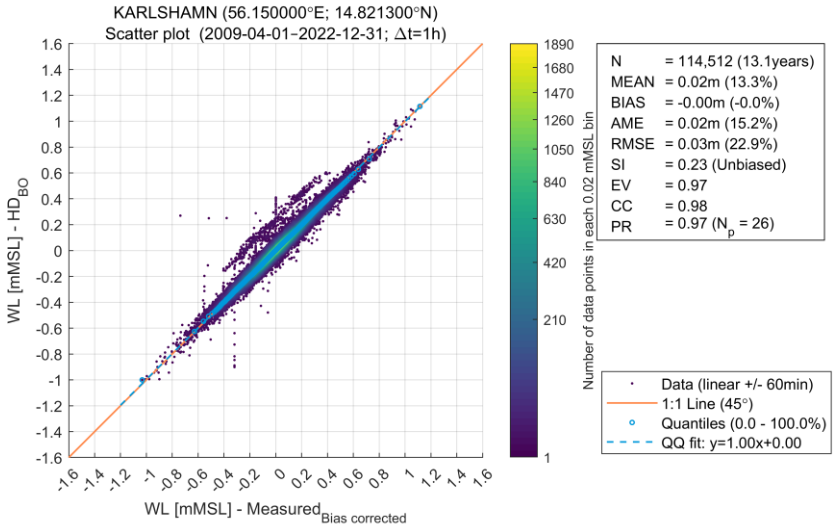

Klagshamn

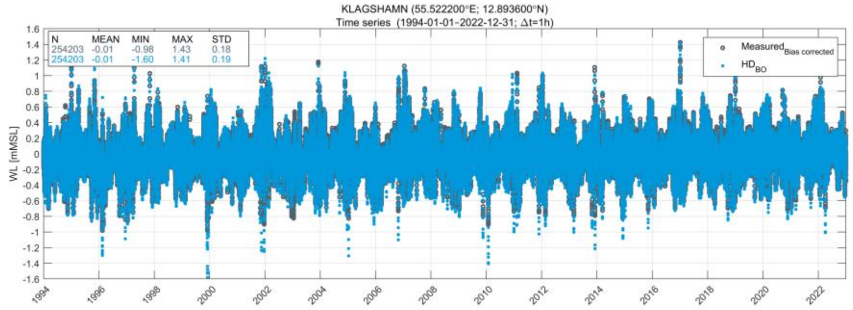

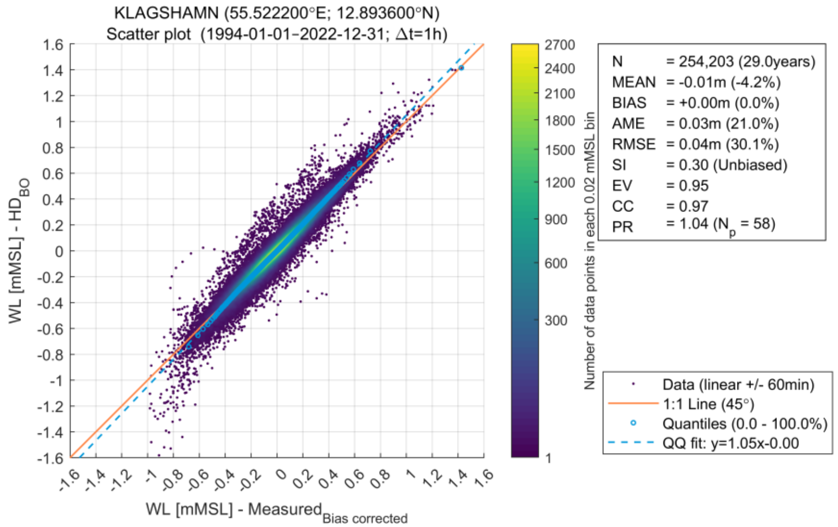

Kungholmsfort

Simrishamn

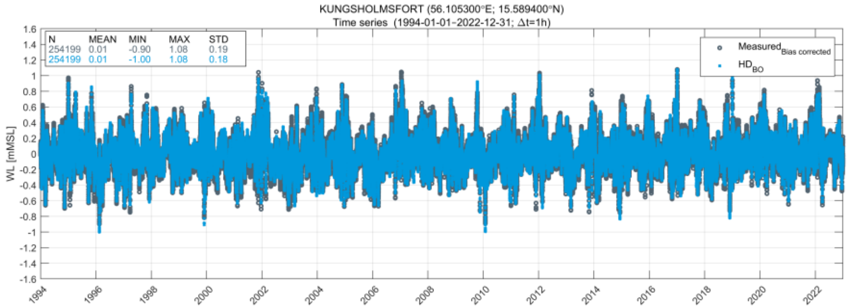

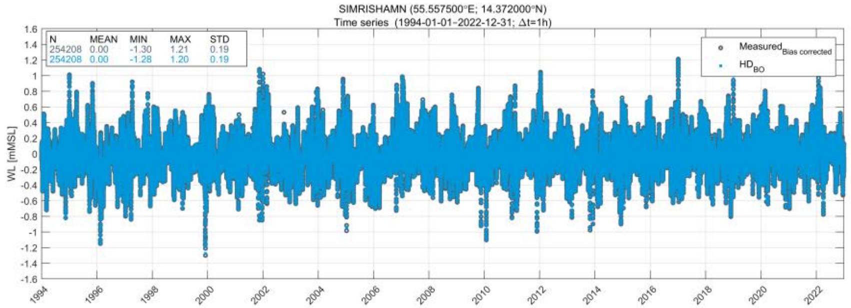

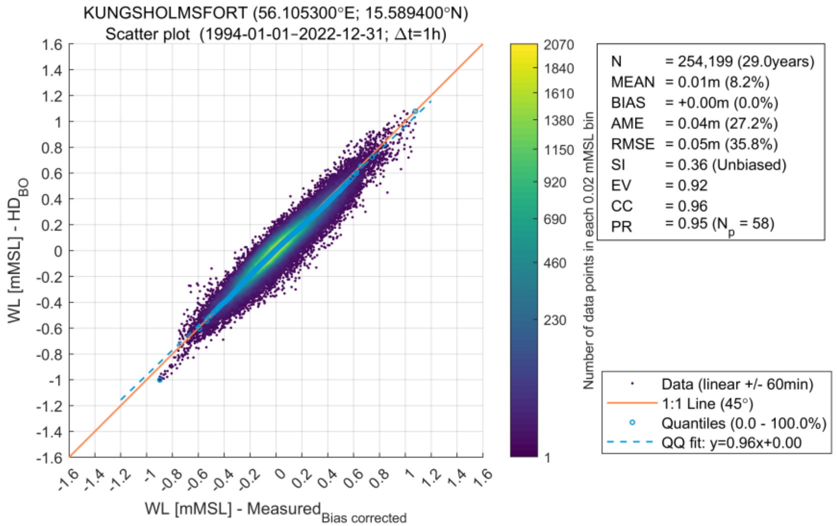

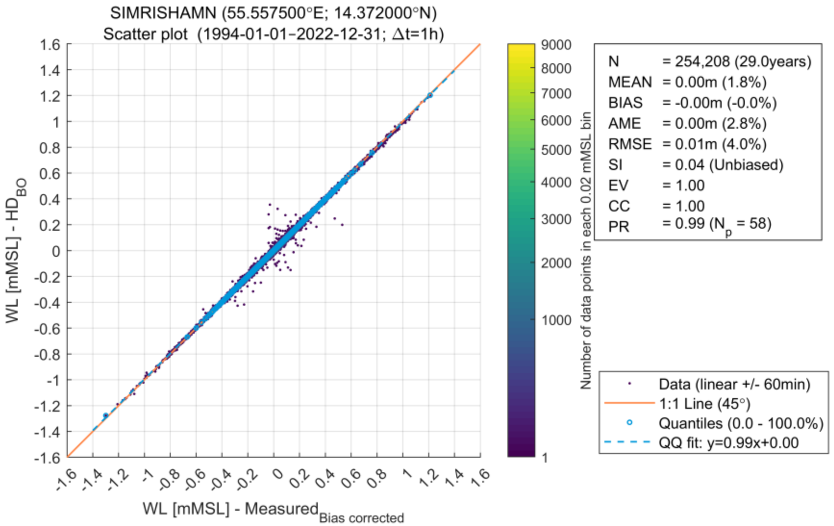

Ystad

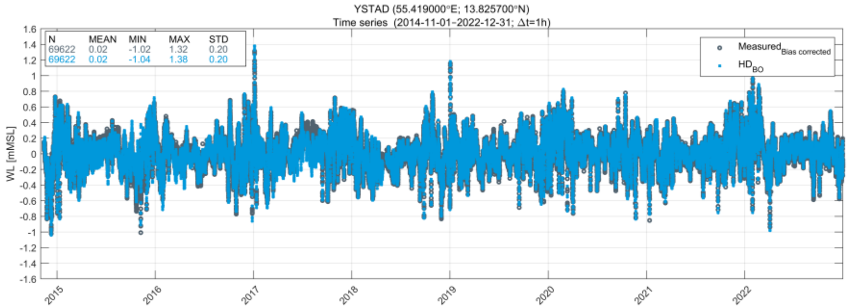

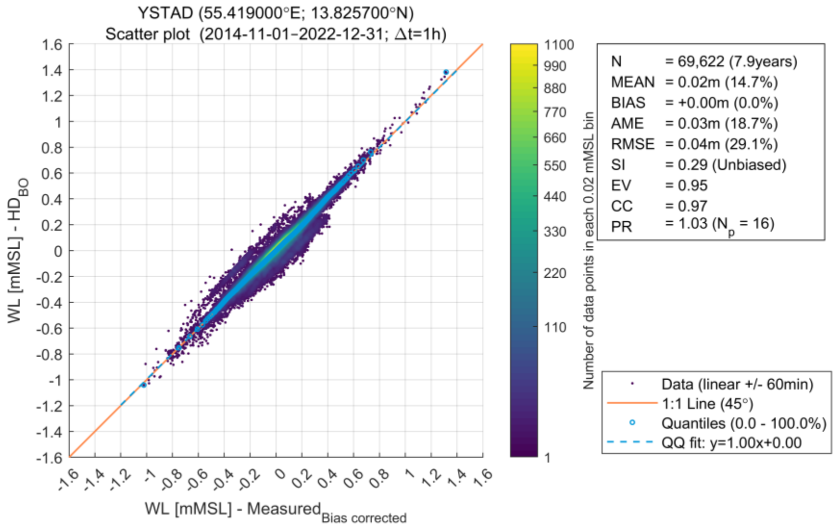

Skanor

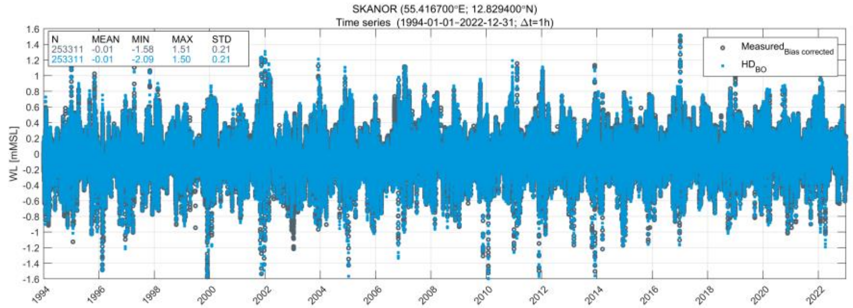

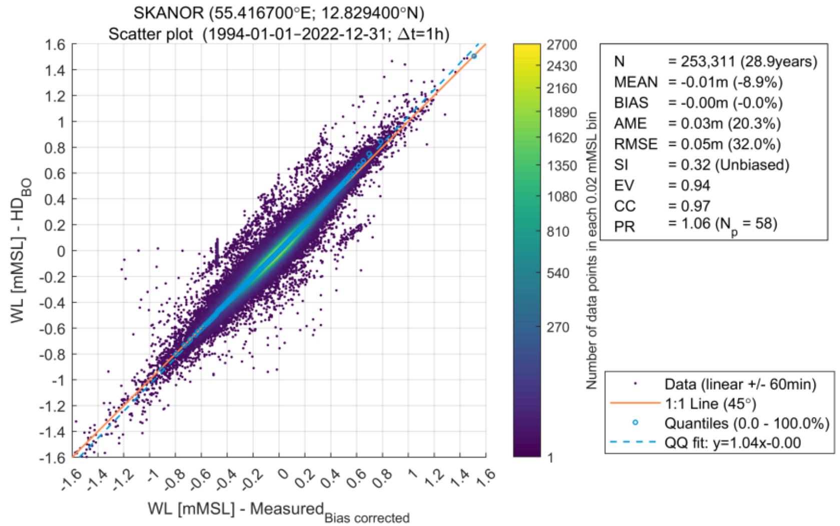

Rødvig Havn

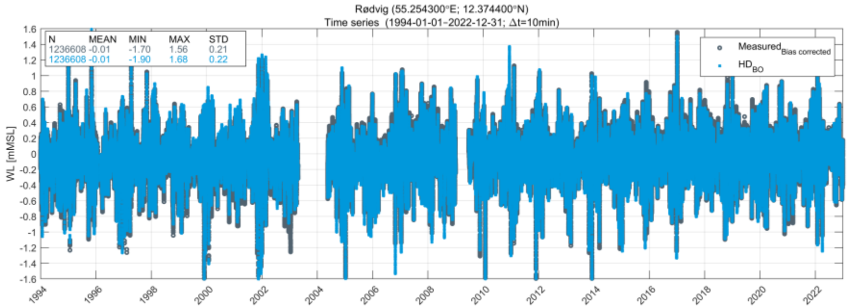

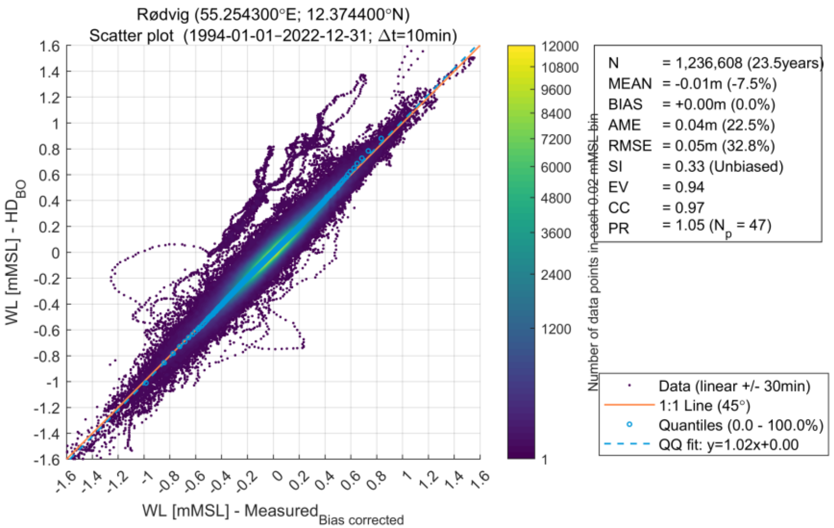

Rønne Havn

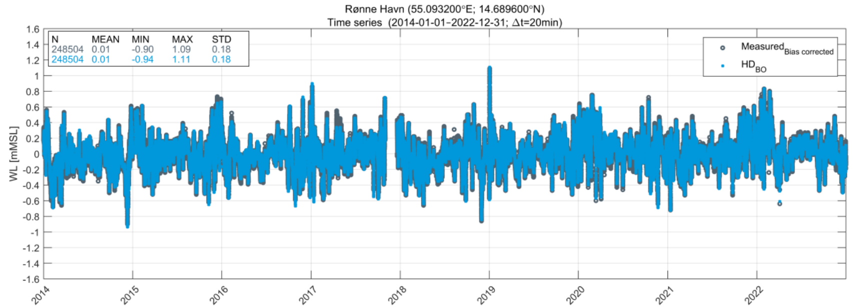

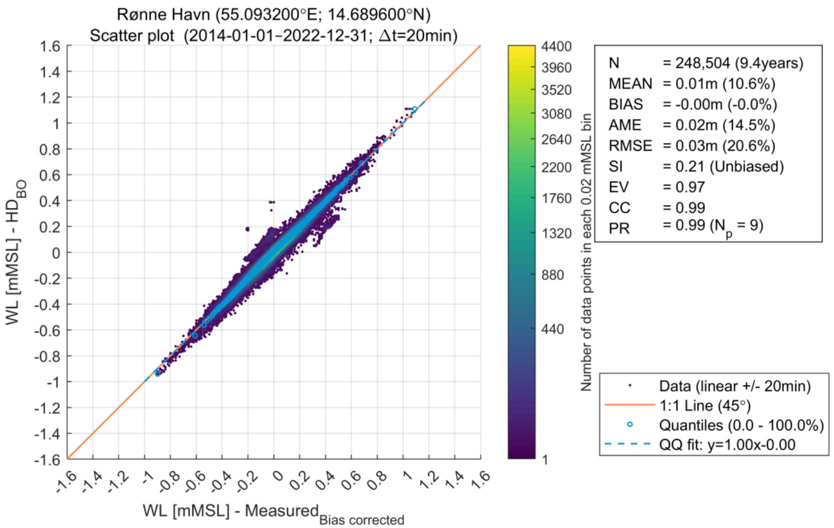

Drogden Fyr

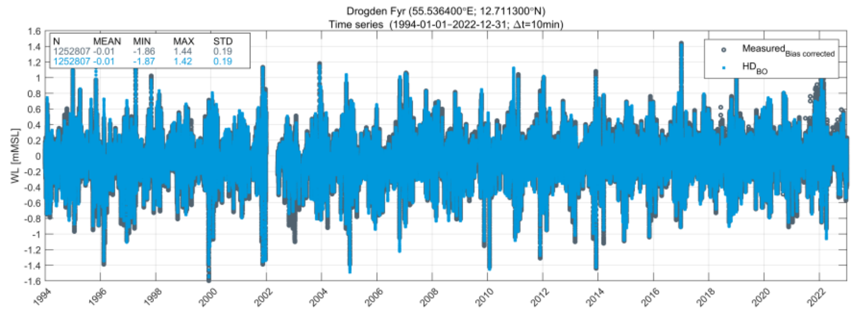

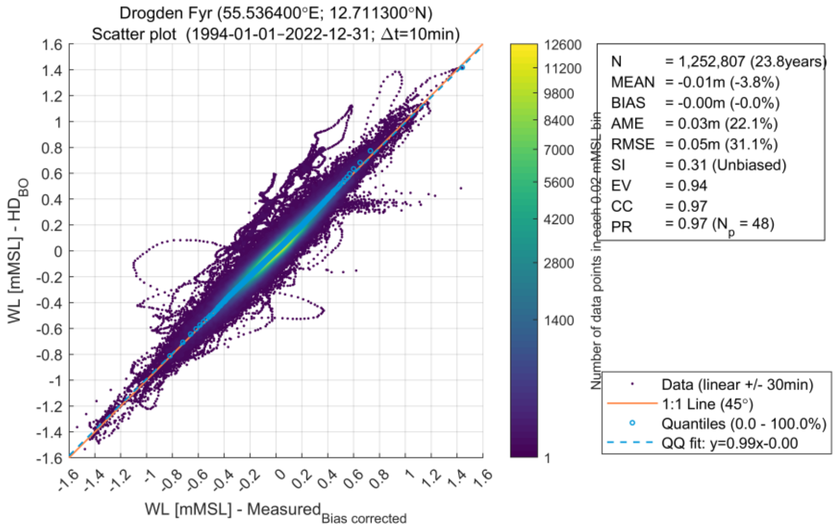

Ustka

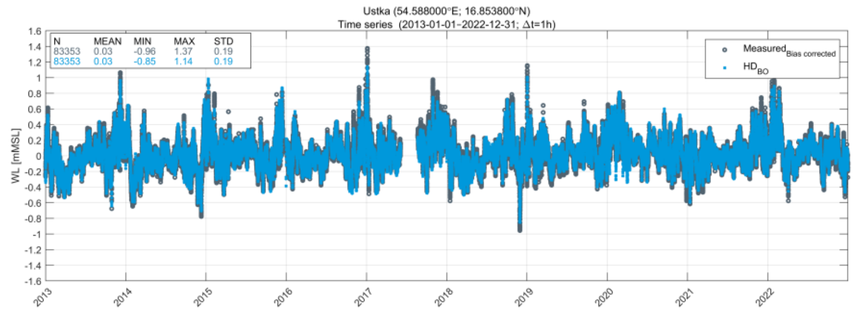

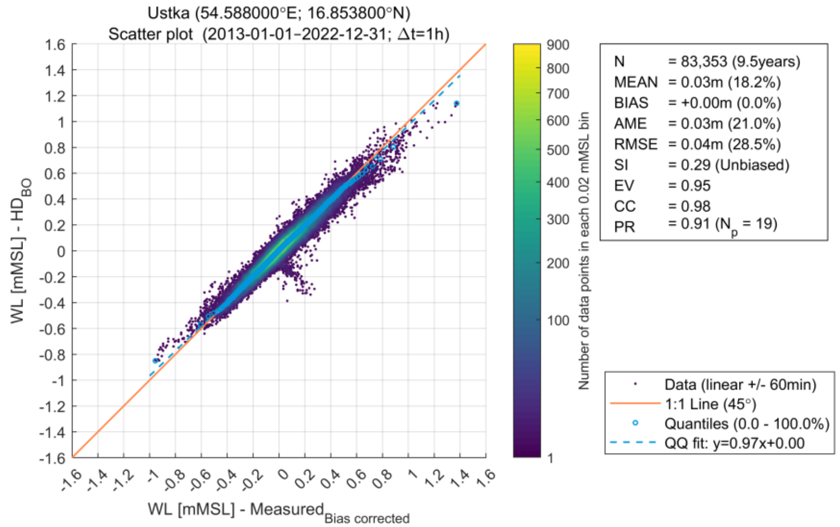

Gedser

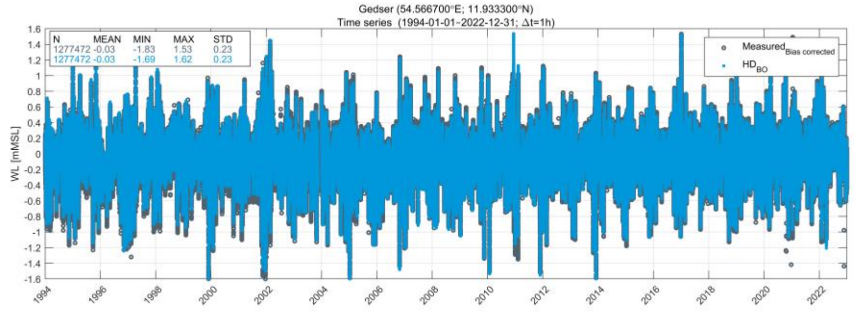

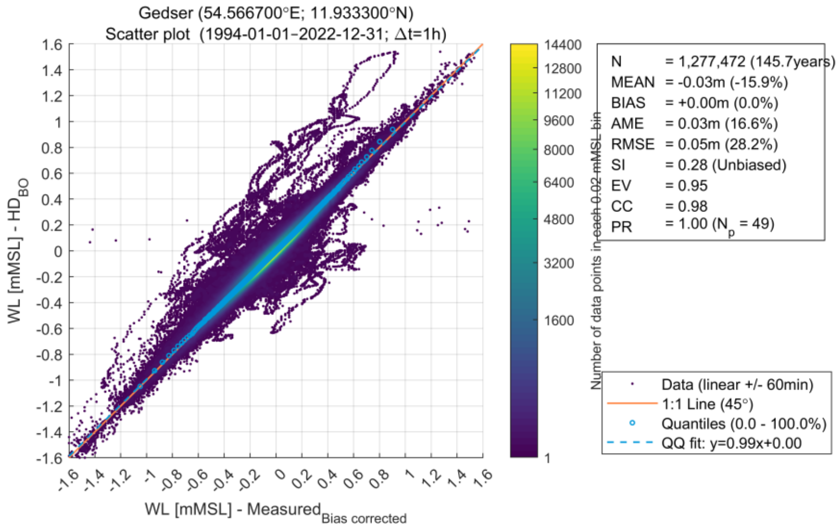

Darlowo